Developing Hydrocarbon Stapled Peptides for Inhibiting Estrogen Receptor/Coactivator Interactions

BY
THOMAS EDWARD SPELTZ
B.S./M.S. DePaul University 2010/2011

DISSERTATION

Submitted as partial fulfillment of the requirements for the degree of Doctor of Philosophy in Medicinal Chemistry in the Graduate College of the University of Illinois at Chicago, 2018

Chicago, Illinois

Defense Committee:

Terry Moore, Chair and Advisor
Gregory Thatcher
Pavel Petukhov
Justin Mohr, Chemistry
Joanna Burdette

DEDICATION

This thesis is dedicated to my wife, Maggie, your unwavering support has allowed me to accomplish this research.

ACKNOWLEDGEMENTS

Above all, thank you Terry Moore. As a mentor, you have exceeded all expectations imaginable. The time I have spent in your lab has been the most enriching of my life. Thanks to you my entire graduate experience will be treasured.

I would not have been able to accomplish this work without the intellectual and scientific contributions of my peers and collaborators. In addition to designing the molecular dynamics experiments to interrogate the gamma-methylated stapled peptides in chapter 2 and the peptide folding energetics in chapter 3, Chris Mayne taught me how to set up, perform, and analyze molecular dynamics simulations. I was able to use this approach to facilitate the discovery of R4K1. Sean Fanning solved crystal structures of at least 10 different peptide/estrogen receptor complexes and took the time to teach me how to efficiently express and purify estrogen receptor. Geoffrey Greene and John Katzenellenbogen readily provided plasmids of estrogen receptor for recombinant expression. Kathryn Carlson taught me how to perform the TR-FRET assay and made her time available for consultation to help me work out kinks in the assay. Hyun Lee performed valuable SPR experiments and taught me how to effectively use the Biacore. Gerd Prehna assisted with the development and design of biochemical assays. In addition to performing all cellular experiments to test R4K1, Jeanne Danes computed the % localization of FITC-R4K1 in MCF-7 cells. To my prelim and thesis committee advisors, Jonna Frasor, Stephen DiMagno, Gregory Thatcher, Pavel Petukhov, Justin Mohr, and Joanna Burdette, thank you for sharing your wisdom and establishing an open environment for me to seek guidance and advice. I would also like to thank Dr. Richard van Breemen and Pasha Petukov for sponsoring and supporting my career progression

throughout my T32 funded training. To all members of the Department of Medicinal Chemistry and Pharmacognosy, especially my labmates~ Atul, Ben, Brian, Zamia, Kornelia, Phil, Kirthi, Zohra, Ewelina, and Tahnee, thank you for making everyday a joy.

The research presented in this thesis was supported by the Office of the Director, National Institutes of Health (OD) and National Center for Complementary and Integrative Health (NCCIH) (5T32AT007553) through a T32 pre-doctoral training fellowship and W. E. van Doren scholarships (2015, 2016, and 2017) from the Department of Medicinal Chemistry and Pharmacognosy in the College of Pharmacy at UIC.

TES

AUTHORS CONTRIBUTIONS

Chapter 1 is original work with text and figure improvement editing by Terry Moore. Minor portions are derived from the introduction sections of *Angewandte Chemie* and *ACS Chemical Biology* publications. Chapter 2 is derived from a manuscript published in *Angewandte Chemie*. The written portion includes original work and written and/or edited portions by Terry Moore and Chris Mayne. The estrogen receptor and steroid receptor coactivator proteins were expressed, labeled, and purified with assistance from Kathryn Carleson. The plasmids for expressing the receptor and steroid receptor coactivator were provided by John Katzenellenbogen. The crystal structures were solved by Sean Fanning with assistance from Colin Fowler. The molecular dynamics simulations were performed by Chris Mayne. Chris Mayne prepared the crystal structure figures used in the manuscript. The surface plasmon resonance assay was performed by Hyun Lee. Gerd Prehna assisted with protein purification and Ben Ramirez helped with the collection of NMR data for the peptides. Chapter 3 is a manuscript that is currently in submission. The written portion includes original work and written and/or edited portions by Terry Moore and Chris Mayne. Chris Mayne performed the bias exchange umbrella sampling molecular dynamics simulations and prepared the figure portions that display the computational results. Chris wrote the experimental section for the computational studies also prepared the figures that depict the crystal structures. Sean Fanning solved the crystal structures and wrote the experimental section for X-ray structure solution. Zamia Siddiqui performed the proteolytic assays and temperature dependent circular dichroism experiment. Chapter 4 is derived from a manuscript published in *ACS Chemical Biology*. The written portion includes original work and written and/or edited portions by Terry

Moore and Jonna Frasor. The confocal microcopy experiments and related figure preparation were carried out in a joint effort between myself and Jeanne Danes, with assistance from Peter Toth. Jeanne Danes performed the calculation to determine % FITC-peeptide localization. The lactate dehydrogenase assay, RNA isolation and qPCR, western blots, and proliferation assays were performed by Jeanne Danes. The RNAseq experiment was performed by the genomics core facility, RRC at UIC, with specific consultation and experimental procedures provided by Zarema Arbieva, Nina Los, and Mark Maienschein-Cline. Joshua Stender performed the original bioinformatic analysis to generate the differential expression data set and prepared the expression heatmap. Chapter 5 is original work and will eventually be submitted as a manuscript. The D538G/C417 and Y537S/C417 mutant estrogen receptor plasmids were provided by John Katzenellenbogen. The D538G and Y537S plasmids were provided by Geoffrey Greene. Chapter 6 is original work. The natural product libraries screened were provided by Brian Murphey and Jimmy Orjala. Casey Murphey assisted with preparing fraction plates for screening. Taxon identification and “known chemistry” for Orjala hits were provided by Daniel May. Throughout these projects, summer rotation students Tahnee Muller, Kirthi Bellamkondra, and Zohra Sattar provided support in peptide synthesis and purification.

TABLE OF CONTENTS

CHAPTER

TABLE OF CONTENTS (continued)

TABLE OF CONTENTS (continued)

LIST OF TABLES

LIST OF TABLES (continued)

LIST OF FIGURES

LIST OF FIGURES (continued)

LIST OF FIGURES (continued)

LIST OF FIGURES (continued)

LIST OF FIGURES (continued)

LIST OF FIGURES (continued)

LIST OF FIGURES (continued)

LIST OF FIGURES (continued)

LIST OF FIGURES (continued)

LIST OF ABBREVIATIONS

4OHT	4-hydroxytamoxifen
AIB-1	amplified in breast cancer-1
ATP	adenosine triphosphate
BEUS	bias exchange umbrella sampling
boc	tert-butyloxycarbonyl
CBI	coactivator binding inhibitor
CD	circular dichroism
CHA	cyclohexyl alanine
CHARMM	chemistry at Harvard macromolecular mechanics
CMAP	correction map
COLVARs	collective variables
CREB cAMP	response element-binding protein
CRISPR	clustered regularly interspaced short palindromic repeats
ctDNA	circulating tumor deoxyribonucleic acid
DCM	dichloromethane
DIPEA	diisoproylethylamine
DMF	dimethylformamide
DMSO	dimethylsulfoxide
DNA	deoxyribonucleic acid
dsDNA	double strand deoxyribonucleic acid
E2	17β-estradiol
EDTA	ethylenediaminetetraacetic acid

EGR3	early growth response 3
ER	estrogen receptor alpha
ER+	estrogen receptor alpha positive
ERE	estrogen response element
ERα	estrogen receptor alpha
ESI	electrospray ionization
FBS	fetal bovine serum
FDR	false discovery rate
FITC	fluorescein isothiocyanate
Fmoc	9-fluorenylmethoxycarbonyl
Fmoc-cl	9-fluorenylmethoxycarbonyl chloride
GADPH	Glyceraldehyde 3-phosphate dehydrogenase
HBS-EP	HEPES buffered saline EDTA surfactant P20
HBTU	hexafluorophosphate benzotriazole tetramethyl uronium
HCl	hydrochloric acid
HCTU	hexafluorophosphate chlorobenzotriazole tetramethyl uronium
HOBt	hydroxybenzotriazole
HPLC	high performance liquid chromatography
HRMS	high resolution mass spectrometry
ICAM1	Intercellular Adhesion Molecule 1
IGFBP4	Insulin-like growth factor-binding protein 4
IT-TOF	ion trap time of flight

LCMS	liquid chromatography mass spectrometry
LDH	lactate dehydrogenase
MBHA	Methylbenzhydrylamine
MCF-7	cell line derived from breast ductal carcinoma
MD	molecular dynamics
MeCN	acetonitrile
MHz	megahertz
mRNA	messenger ribonucleic acid
mtt	4-methyltrityl
NAMD	nanoscale molecular dynamics
NBFIX	non-bonded fix
NFκB	nuclear factor kappa-light-chain-enhancer of activated B cells
NMP	N-methylpyrrolidinone
NMR	nuclear magnetic resonance
NPT	number of particles, pressure, and temperature
NR-box	nuclear receptor box
Opip	2-phenylisopropyl ester
PARP	poly adenosine diphosphate-ribose polymerase
PEG	polyethylene glycol
PELP1	Proline-, glutamic acid- and leucine-rich protein 1
PME	particle mesh Ewald
PMF	potential of mean force

PPI	protein-protein interaction
ppm	parts per million
PR	progesterone receptor
PS2	trefoil factor 1
PTGES	prostaglandin E synthase
PyClock	6-Chloro-benzotriazole-1-yloxy-tris-pyrrolidinophosphonium hexafluorophosphate
ReIB	rel related gene
RIP140	receptor-interacting protein 140
RIPA	radioimmunoprecipitation assay buffer
RNA	ribonucleic acid
RNA-seq	ribonucleic acid sequencing
RPMI	Roswell Park Memorial Institute
RT-qPCR	real-time polymerase chain reaction
RU	response unit
S5	(S)-2-amino-2-methylhept-6-enoic acid
SA	streptavidin
SEM	standard error of mean
SERD	selective estrogen receptor degrader
SERM	selective estrogen receptor modulator
SPR	surface plasmon resonance
SRC2	steroid receptor coactivator-2

SRC-3	steroid receptor coactivator-3
STR	short tandem repeats
T47D	cell line derived from breast ductal carcinoma
t-BuLi	tertbutyl lithium
TFA	trifluoroacetic acid
THF	tetrahydrofuran
TIP3P	transferable intermolecular potential with 3 points
TNFα	tumor necrosis factor alpha
TR-FRET	time-resolved fluorescence resonance energy transfer
TsOH	toluenesulfonic acid
VMD	visual molecular dynamics
WHAM	weighted histogram analysis method

SUMMARY

Chapter 1 provides a brief mechanistic overview of ligand activated steroid receptor coactivator recruitment. FDA approved strategies for treating estrogen receptor positive breast cancer are described and previous discoveries regarding coactivator binding inhibitors are referenced with an emphasis on the development of linear and constrained peptides. The concept of stapled peptides is described. Chapter 2 details the synthetic preparation, biochemical activity, and structural characterization of gamma-methylated stapled peptides. The benefits of preparing stapling amino acids that better mimic functional groups of natural amino acids is established. Chapter 3 details the molecular dynamics guided design of lactam/olefin bicyclic stapled peptides. A predictive correlation between the computational method and helical stability is noted. Chapter 4 describes the design and activity of R4K1, a cell permeable stapled that inhibits estrogen receptor mediated gene transcription and cell proliferation in estrogen receptor positive breast cancer cell lines. Chapter 5 describes the synthetic preparation of high affinity stapled peptides for targeting mutant forms of estrogen receptor. Novel gamma-functionalized stapling amino acids were used to prepare stapled peptides with enhanced selectivity for estrogen receptor D538G over the wild-type isoform. Chapter 6 presents the findings of a high-throughput screen of natural products for the discovery of novel coactivator binding inhibitors.

1. Introduction

1.1 Estrogen receptor-positive breast cancer and clinical approaches for treatment.

In 2018 an estimated 250,000 women in the United States will be diagnosed with breast cancer.[1] Roughly 175,000 of those women will harbor cancers that show an increased expression of estrogen receptor alpha, from now on referred to as estrogen receptor or ER.[2-3] In estrogen receptor-positive (ER+) cancers, the activity of ER is often associated with uncontrolled tumor formation. Depending on the stage of the cancer at diagnosis, treatment of estrogen receptor-positive breast cancer may involve a combination of surgical procedures to remove identifiable tumors, radiation therapy, and/or adjuvant pharmaceutical therapy consisting of different combinations of 71 approved drugs that fall into the categories of general chemotherapy, targeted therapy, and/or hormone therapy.[4] Targeted therapies include monoclonal antibodies, tyrosine kinase inhibitors, cyclin dependent kinase inhibitors, mammalian target of rapamycin inhibitors, and Poly adenosine diphosphate-ribose polymerase (PARP) inhibitors. Hormone therapy is effective in treating estrogen receptor-positive breast cancer and consists of two fundamental strategies; 1) to block the natural production of estrogen using aromatase inhibitors and 2) to antagonize estrogen receptor function using small molecules that inhibit estradiol induced stimulation.[5] These therapeutic strategies have proven effective at either preventing or delaying the onset of recurrent breast cancer for a large percentage of women; however, over half of ER+ cancers may develop tumors that no longer respond to any of these therapies.[6] Because resistance to endocrine therapy can develop, there is a significant need for new therapies, exemplified by the >200 ongoing clinical trials to examine other targeted therapies.[7] Because the estrogen

receptor remains highly expressed in recurrent/resistant disease, it may be possible to develop therapies that inhibit the function of ER in a fundamentally different way that is complimentary to currently approved hormone therapies.

1.2 The estrogen receptor/coactivator interaction

The estrogen receptor is a hormone-activated nuclear receptor involved in biological pathways that require significant gene regulation. For instance, a typical genome profiling experiment will yield hundreds of genes either up- or down-regulated by estrogen receptor.[8-9] Estrogen receptor plays a critical role in the proliferative and differential actions of the female reproductive tract and mammary glands.[10] Importantly, ER is correlated with disease progression in over 70% of all breast cancers.[3] The correlation between estrogen receptor expression and breast cancer situates estrogen receptor as both a biological marker and therapeutic target. Over the past 50 years, hormone therapy has been developed and applied to prevent the aberrant activity of estrogen receptor in breast cancer progression.

The canonical pathway of estrogen receptor-mediated gene transcription (**Figure 1.1A**) is initiated by binding of an agonist such as estradiol to the ligand binding domain of ER. Upon ligand binding, the ER dimerizes, enters the nucleus, binds to specific promoter sequences of DNA known as estrogen response elements (EREs), and recruits p160 proteins. These coactivating proteins have enzymatic activity and serve as scaffolding proteins to recruit p300/CREB, which assist in modifying histone proteins and DNA to prepare genes downstream of EREs for RNA polymerase-mediated transcription. [11 12]

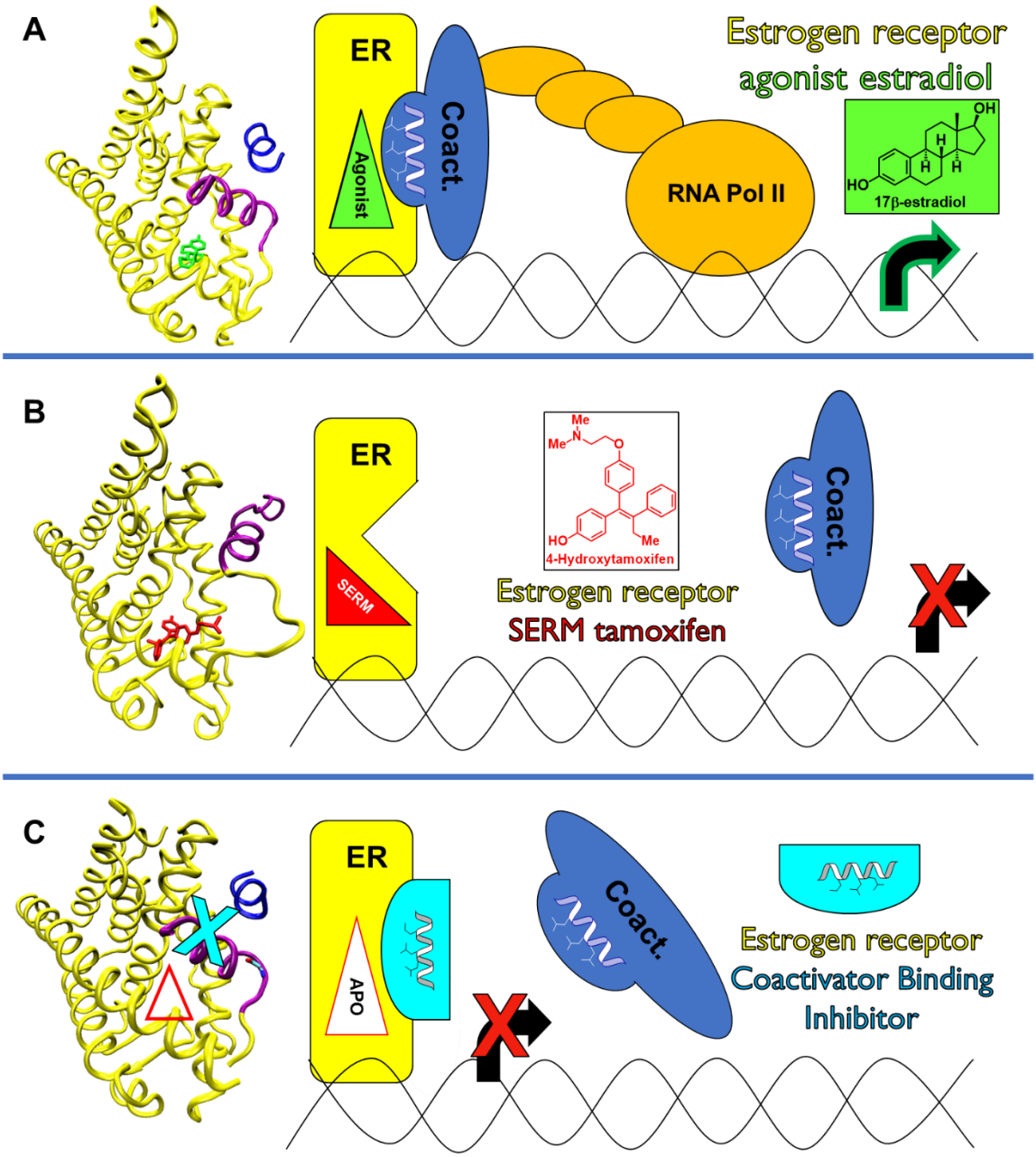

Figure 1.1 Mechanistic determinants for different classes of estrogen receptor ligands. **A.** Agonist conformation induced by estradiol enhances coactivator recruitment. **B.** Antagonist 4-hydroxytamoxifen prevents coactivator recruitment. **C.** Coactivator binding inhibitor (CBI) blocks coactivator recruitment through direct binding displacement.

1.3 Hormone therapy and endocrine resistance

Hormone therapy for ER+ breast cancer relies on two strategies to prevent the activation of ER. The first strategy is to eliminate natural production of estrogen so that ER can never be activated. This can be accomplished either surgically, by performing oophorectomy, or pharmacologically, by using gonadotropin-releasing hormone agonists and/or aromatase inhibitors. A second form of hormone therapy relies on using small molecules that bind to ER in place of estradiol and induce conformations that are unfavorable for recruiting p160 proteins (**Figure 1.1B**) or induce unstable conformations of ER that lead to protein degradation. Hormone therapy is effective in preventing and delaying the onset of recurrent cancer when used as a preventive in at-risk patients, as adjuvant therapy after initial cancer diagnosis, and as a treatment for metastatic breast cancer. Unfortunately, many women will develop tumors that become unresponsive to approved hormone therapies even though the tumors still express estrogen receptor.[6]

A significant effort has been applied to elucidate the biological mechanisms that lead to endocrine therapy resistance (see reviews).[13-14] While some mechanisms are independent from the estrogen receptor pathway, overexpression and mis-regulation of coactivators, as well as mutations in the estrogen receptor ligand binding domain, are linked to resistance. For instance, steroid receptor coactivator-3 (SRC-3), also known as amplified in breast cancer-1 (AIB-1) is overexpressed in breast cancers and SRC-3 overexpression is correlated with resistance to tamoxifen.[15-17] In addition to overexpression of coactivators, underexpression of corepressors is also seen in endocrine-resistant breast cancer.[18] Recent genomic studies have identified mutations within the ligand binding domain of metastatic breast cancer that have been shown to

confer constitutive activity, in that ER mutants do not require estradiol to initiate gene expression.[19-22] Additionally, common mutations D538G and Y537S appear less responsive to currently approved agonists in biochemical and cellular assays.[23-24] One mechanistic implication of the presence of D538G and Y537S mutations is that they stabilize helix 12 in a conformation that recruits p160 coactivator proteins independent of an agonist ligand.[25]

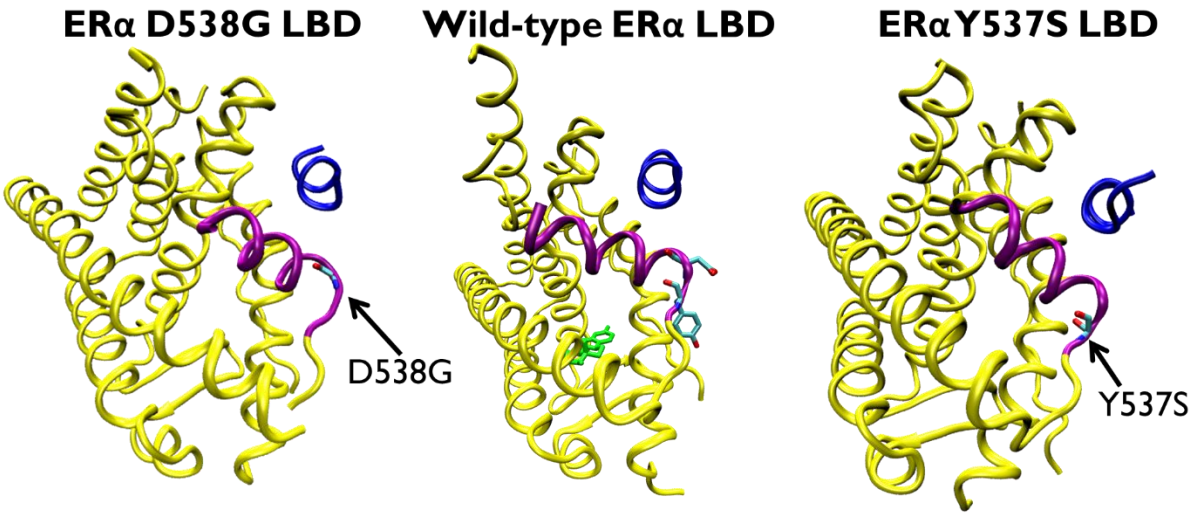

Figure 1.2 Structural location of estrogen receptor ligand-binding domain mutations Y537S and D538G.

1.4 Estrogen Receptor Coactivator Binding Inhibitors

Fundamentally different from clinically approved hormone therapies, coactivator binding inhibitors (CBIs) have been proposed as an alternative method to inhibit estrogen receptor activity (**Figure 1.1C**).[26] CBIs are proposed to inhibit the genomic activity of estrogen receptor by blocking coactivator recruitment to activated, potentially DNA-bound receptor. This can be accomplished using small molecules [27-29] or peptides [30-32] that have

high binding affinity for the surface groove on the estrogen receptor that is normally used for coactivator binding. The biological significance of the ER/SRC3 interaction is well established,[33] and the protein-protein interaction surface has been structurally characterized using x-ray crystallography and cryo-electron microscopy.[34, 11] Importantly, steroid receptor coactivators bind to the agonist conformation of estrogen receptor through a conserved helical "LxxLL" motif.[35-36] On this basis, several research groups have developed small molecules, peptidomimetics and stabilized alpha helical peptides (**Figure 1.3**, compounds **1.1-1.5**) to bind on this surface groove of ER to inhibit ER/SRC3 interactions. While biochemical inhibition of ER/SRC interactions has been shown, an extremely limited number of biological experiments have linked phenotypic responses of CBIs in more advanced cell culture or animal models to the mechanism of inhibiting the ER/SRC3 interaction.[37]

High-throughput screens have been used to generate hits for structural classes that are capable of inhibiting ER/SRC3 interactions. One example series is the discovery and optimization of guanylhydrazones and quinizolinones (**Figure 1.3,** compounds **1.6** and **1.9**).[27, 38] More effective strategies have relied on better mimicking the "LxxLL" structure motif and include biphenyl[28] and oligobenzamide[37] proteomimetics. The oligobenzamide ERX-11 (**Figure 1.3,** compound **1.8**) is perhaps the best characterized CBI. Based on mechanistic studies, ERX-11 was described as a coregulator inhibitor as the molecule appeared to block both coactivator and corepressor binding to the AF-2 domain of estrogen receptor. ERX-11 was shown to block ER-regulated gene transcription, induce apoptosis in ER+ cell lines, and inhibit growth of estrogen receptor-positive cancer in mouse xenograft models.

The development of peptide-based CBIs has steadily progressed since the helical "LxxLL" coactivator binding motif **(Figure 1.3**, compound **1.1**) was first characterized.[39, 16] Initial attempts to enhance binding affinity and promote cellular activity of CBI peptides incorporated macrocyclic constraints to the primary sequence of LxxLL-containing nuclear receptor interacting segments of steroid receptor coactivator sequences in the form of disulfides[40], thio-ether[41], and lactam bonds[42]. Spatola and coworkers[32] developed high-affinity CBI peptides by substituting leucine residues of the "LxxLL" motif with bulky hydrophobic amino acids such as neopentyl glycine and tert-butyl glycine. From this series, a crystal structure was also reported for a disulfide helix- stabilized CBI. Geistlinger, et al. prepared a library of an *i, i+4* lactam-cyclized SRC3 peptide with 21 natural and non-natural amino acids replacing each leucine of the LxxLL motif.[42] Peptides in the library showed varying levels of selectivity between ER alpha, ER beta, and human thyroid receptor; however, no cellular experiments were carried out. To generate a bioactive SRC3 peptide, Brunsveld prepared Arg_9-conjugated SRC sequences. [31] An SRC3 sequence with nine arginine residues conjugated to the *C*-terminus was found to penetrate cells and recruit estrogen receptor to the nucleoli. More recently, Phillips et al. reported crystal structures of "hydrocarbon-stapled" peptides (see below) with high affinity for estrogen receptor alpha and beta. [30] Although the highest affinity peptide, SP2, had a K_D of 75 nM, no biological evaluation was reported.

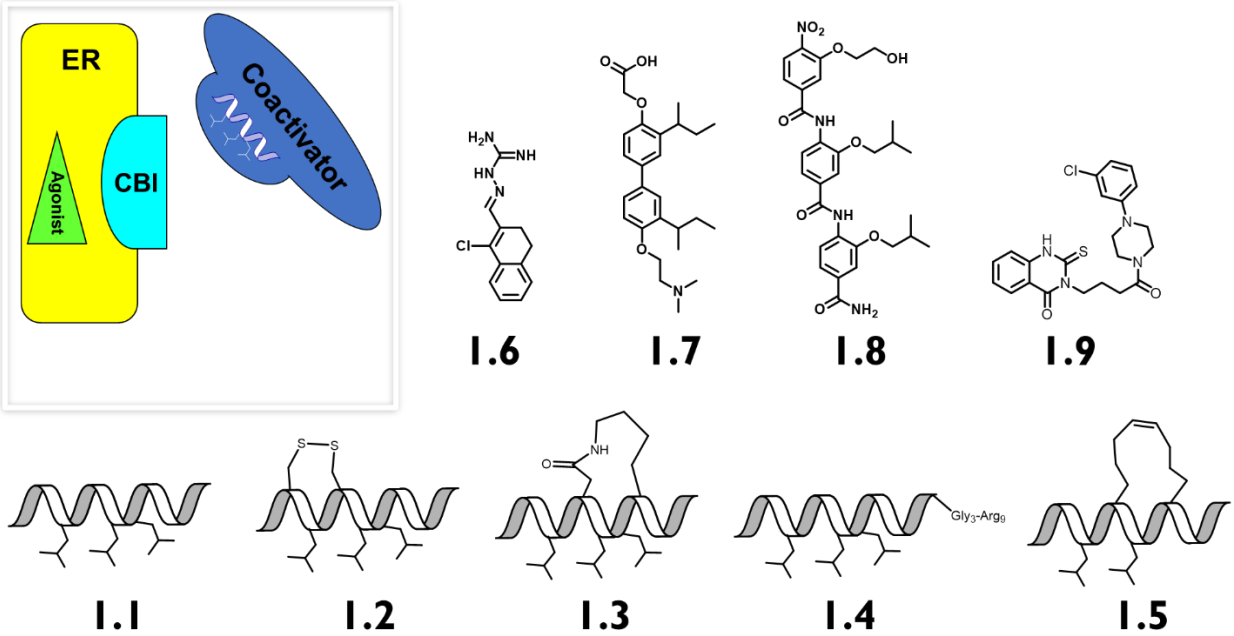

Figure 1.3 Small molecule and peptide-based coactivator binding inhibitors

1.5 Hydrocarbon stapled peptides

A powerful method for blocking α-helical protein-protein interactions—like the ER/coactivator interaction—employs "stapled" peptides, which are peptides that are constrained by linking sidechains through olefin metathesis.[43] Optimized by Verdine and coworkers,[43] stapled peptides have been used to inhibit many different α-helical protein-protein interactions.[30, 44-52] Stapled peptides confer several benefits, including conformational stability, proteolytic stability,[53] and, in some cases, cell permeability,[54-55] and they are being tested in the clinic for acute myeloid leukemia, peripheral T-cell lymphoma, and myelodysplastic syndrome (ClinicalTrials.gov ID: NCT02909972 and NCT02264613).

The recommended strategy for preparing stapled peptides is to conduct a "stapling scan."[56-58] Similar to an alanine scan, the purpose of this strategy is to substitute the

stapling amino acids at sequential positions along the entire sequence to determine optimum stapling positions. Aside from enhancing proteolytic stability and/or cell permeability, the unnatural stapling amino acids may have negative or positive contributions to binding affinity. Increases in affinity may result from additional buried hydrophobic surface area, whereas decreases in affinity are likely a result of unfavorable steric clashes. If a crystal structure of the target interaction has been solved, structure-based design can be used to speculate potentially favorable stapling sites. The commonly used, commercially available stapling amino acids are α,α-disubstituted, containing an α-methyl group and an alkene terminated sidechain of 3, 5, or 8 carbons.[59] Helical enhancement has been used as a readout on model peptides to determine desirable stereochemical combinations of linkers for *i* to *i+3, i+4*, or *i+7* sites (**Figure 1.4**). The alpha methyl group has been shown to help facilitate the ring closing metathesis reaction; however, stapled peptides can be prepared lacking the methyl group.[60] In addition, the amino acid B_5 has been used to create double stapled peptides.[61]

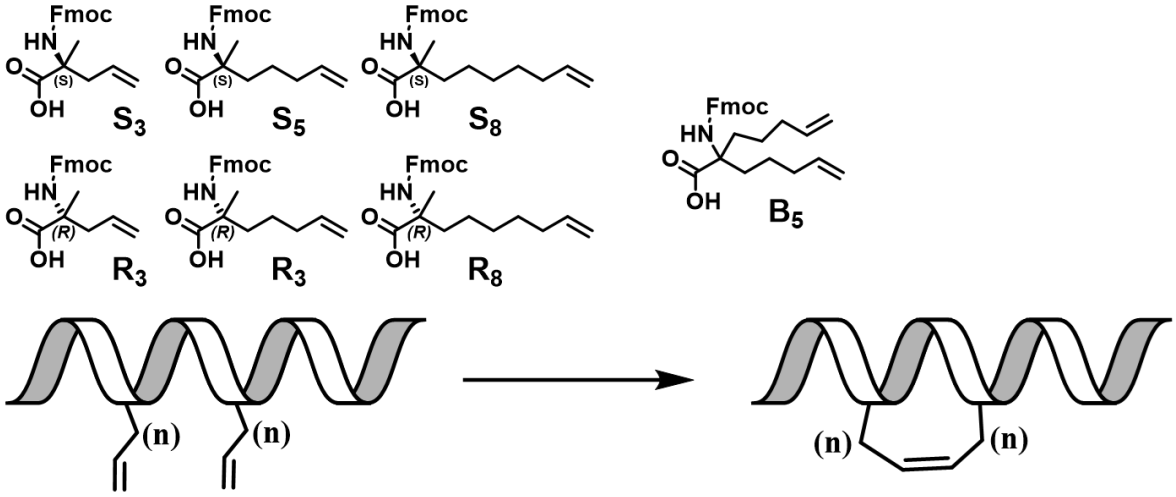

Figure 1.4 Commercially available stapling amino acids and model stapled peptide

As new potential targets are identified, and the number of stapled peptides grow, the benefits and drawbacks are becoming apparent. Perhaps the most contested[62] and important factor moving forward is cell penetration, as the mechanisms of uptake are still not fully understood and there are controversial guidelines for defining the primary and secondary sequence requirements. Recently, there have been two critical studies regarding cell penetration of stapled peptides. Chu and Moellering et al. compared ~200 different stapled peptides ranging in formal charge and single vs stitched staple design.[63] Stapled peptides showed increased penetration relative to linear peptides, with stitched peptides (double-stapled peptides incorporating residue **B5**, **Figure 1.4**) showing greater penetration than singly stapled peptides. Peptides with a positive formal charge at pH 7.5 had increased cellular uptake with results showing a Gaussian distribution centered at +4. Mechanistically, they found stapled peptide uptake was dependent on ATP and enhanced by the presence of negatively charged proteoglycans on the cell surface. Using a library of BIM BH3 stapled peptides, Bird et al. performed an in-depth analysis to optimize properties such as isoelectric point, helicity, and hydrophobicity for cell permeability.[55] The study found uptake was correlated to hydrophobicity (as measured by HPLC retention time) and helicity. Further conclusions showed that peptides with extremely high helicity and positive charge could result in non-specific membrane lysis.

The potential for stapled peptides to disrupt protein-protein interactions is enticing; however, the barriers to overcome for developing stapled peptides are indeed great. Fortunately, two decades of research into outlining strategies for producing effective stapled peptide have opened the door to targeting helix-promoted protein-protein interactions throughout many disciplines. Recently, stapled peptides have been reported

to inhibit respiratory syncytial virus and middle east respiratory syndrome coronavirus by disrupting the fusion mechanism of class I viral fusion proteins,[64-65] stabilize the antimicrobial peptide polybia-MP1,[66] inhibit allergic airway inflammation as an intervention for asthmatic patients,[67] enhance the drug like properties of glucagon-like peptide 2,[68] selectively target Mcl-1 over related Bcl-2 family paralogs for selective cytotoxicity to Mcl-1-dependent cancer cells,[69] and exploit synthetic lethality by targeting the chromosome transmission fidelity 4 protein hub.[70] Regarding breast cancer research, stapled peptides have been designed to disrupt ER/SRC interactions, [30, 71-72] inhibit the WASF3-CYFIP1 complex for suppressing breast cancer metastasis,[73] and potentiate anti-tumor activity by disrupting the brefeldin A-inhibited guanine nucleotide-exchange protein 3-prohibitin 2 complex.[74] Future challenges associated with targeting ER/SRC interactions include achieving sufficient binding affinity to compete with overexpressed levels of coactivator protein and optimization of cell permeability.

2. γ-Methylated Hydrocarbon Stapled Peptides for the Estrogen Receptor/Coactivator Interaction[†]

2.1 Introduction

To synthesize hydrocarbon stapled peptides, two or more strategically chosen residues of a native peptide sequence are replaced with non-natural α-methyl-α-alkenyl amino acids. Ring-closing metathesis forms a macrocycle between the *i* and *i+3, i+4,* or *i+7* positions.[75] Because the constraint may interfere with the ability of the peptide to bind to its receptor, stapled peptides are typically designed so the constraint is placed on a *non-interacting* face of an α-helix.[56] Recently, others have reported successfully replacing *interacting* helical residues with a staple.[30, 76-80] Although it lacks the branching functionality of valine, leucine, and isoleucine, the staple has the ability to bind to protein surfaces. As we show in this work, incorporating hydrophobic functionality at the constraint may more accurately mimic native sequences to increase affinity, and it may also further stabilize bioactive conformations.

Phillips et al. reported an early example of replacing interacting residues with a hydrocarbon staple.[30] The crystal structure of stapled peptide PFE-SP2 bound to estrogen receptor α (ERα) showed that an *i, i+4* hydrocarbon staple can replace isoleucine and leucine residues on the binding face of a steroid receptor coactivator 2

[†]Portions of this chapter are reproduced with permission from Speltz, T. E.; Fanning, S. W.; Mayne, C. G.; Fowler, C.; Tajkhorshid, E.; Greene, G. L.; Moore, T. W. Stapled Peptides with γ-Methylated Hydrocarbon Chains for the Estrogen Receptor/Coactivator Interaction. *Angew. Chem. Int. Ed.* **2016**, 55, 4252. License number 4284860114129.

(SRC2) peptide. This replacement yields an increase in α-helicity and affinity. SRC2 interacts with the surface of ERα over two turns of an α-helix using an ILXXLL motif (X is any amino acid).[39] This protein-protein interaction has been well-investigated, if recalcitrant,[26, 35, 81-82] to treat endocrine therapy-resistant breast cancers. Recently identified ERα mutants that are constitutively active and implicated in metastases have brought renewed focus to this therapeutically important interaction. [19-22]

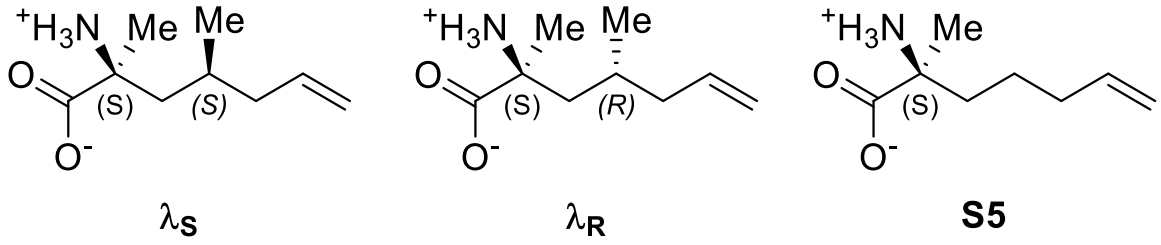

Figure 2.1. Chemical structure of branched stapling amino acids

2.2 Design and synthesis of gamma-methylated stapled peptides

We designed stapled peptides that incorporate branched stapling residues as functionalized constraints. Specifically, we designed amino acids based on stapling amino acid S5 that incorporate a methyl group in the γ-position to mimic branched hydrophobic amino acids Ile689 and Leu693 of the I_{689}LXXLL_{694} motif of SRC2. Because S5 contains an α-methyl group for helical stability, incorporation of a γ-methyl group establishes 1,5-interactions, which, when appropriately positioned, could bolster helical conformations imposed by the constraint. We synthesized requisite amino acids λ_R and λ_S by joining one of Schöllkopf's bis-lactim ethers with enantio-enriched branched alkenyl sidechains, which were synthesized using Evans' *N*-acyloxazolidinone chemistry (Figures 2.1-2.3).[83-84] These amino acids, in combination with S5 (Figure 2.1), were incorporated into

residues 687–697 of SRC2. Solid phase peptide synthesis and ring closing metathesis were carried out as previously reported, and four stapled peptides containing $\lambda_{R/S}$ and/or S5 were successfully synthesized (Figure 2.7A). The *Z*-alkene configuration was consistent with ^{1}H NMR H-C=C-H coupling constants of 10–11 Hz (Figures 2.11-2.14). SRC2-P6 failed to undergo ring-closing metathesis, even under forcing conditions, suggesting that substituting the *i+4* stapling residue with *R*-γ-substitutions results in *syn*-pentane interactions that are non-productive for ring-closing.

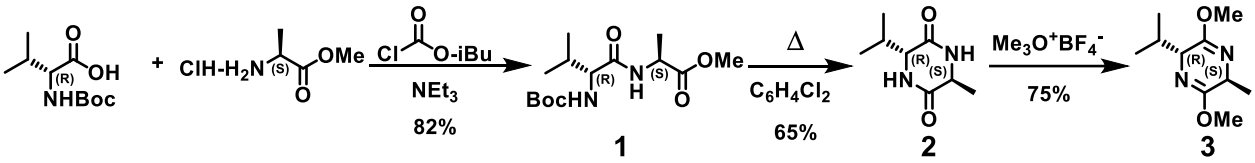

Figure 2.2. Synthesis of Schöllkopf bislactim ether

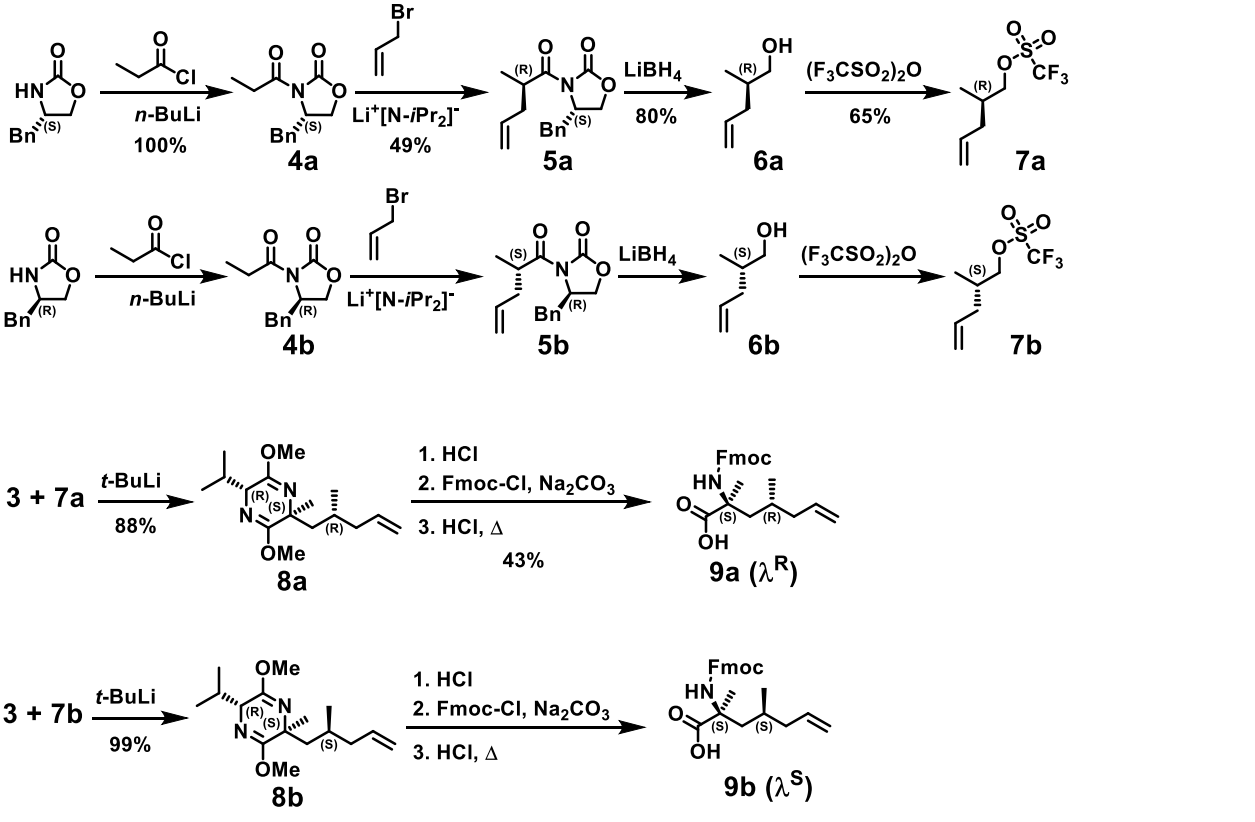

Figure 2.3. Synthesis of gamma-methylated stapling amino acids

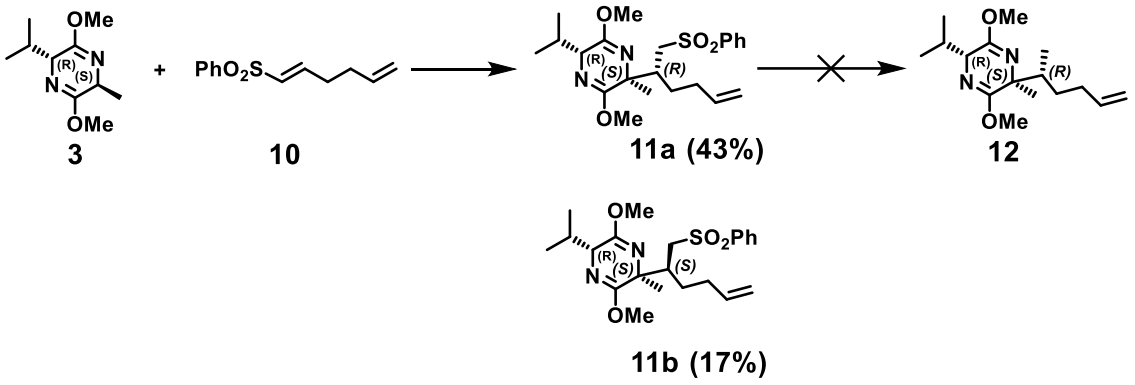

Figure 2.4. Synthetic approach for beta-methylated stapling amino acids

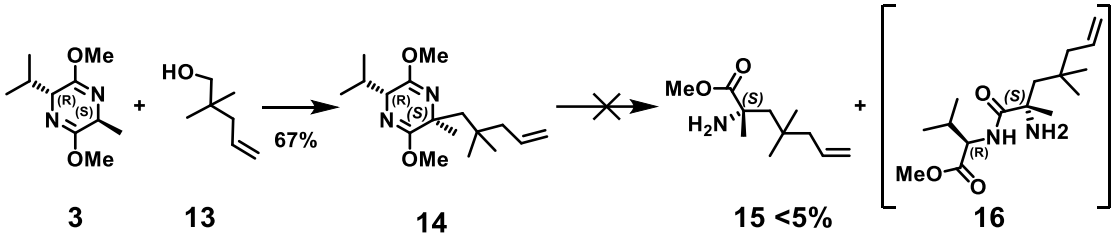

Figure 2.5. Synthetic approach for gamma-dimethyl stapling amino acids

To prepare isoleucine-mimicking stapling amino acids, we applied a synthetic scheme which required a sodium-mercury amalgam reduction of phenylsulfone **11a** (Figure 2.4). The alkylation of bislactim ether **3** with phenylsulfone **10** afforded **11a** in 5:2 mixture of diastereomers (*R* and *S* substituted phenylsulfone). The diastereomers were easily separated by flash chromatography and the identity of the minor product was resolved using X-ray crystallography (Figure 2.6, Tables 2.3-2.10). The stereoselectivity of similar reactions was reported to be >90% which suggests possible room for improvement.[85] The sodium-mercury amalgam reduction of **11a** gave poor yields of a 2:1 mixture of product **12** and an inseparable side-product which showed loss of alkene. A different synthetic scheme may be necessary to prepare beta-functionalized stapling amino acids, as many metal-based sulfone eliminations show large percentages of

undesirable reduction or rearrangements when substrates contain alkenes.[86-87] A test reaction (not reported) of the acid-catalyzed cleavage of product **12** showed incomplete hydrolysis to individual amino methylesters. A steric effect that inhibits hydrolysis of the Schöllkopf intermediate was also observed in the attempted cleavage of the germinal dimethyl gamma-substituted compound **14** (Figure 2.5). Compound **15** was never isolated as a pure compound, and the impurity was the dipeptide **16**. Attempted cleavage conditions included 0.25-1.0 M HCl, TsOH, or TFA. These results suggest that even if the synthesis of **12** was optimized, the next step may then prove unsuccessful.

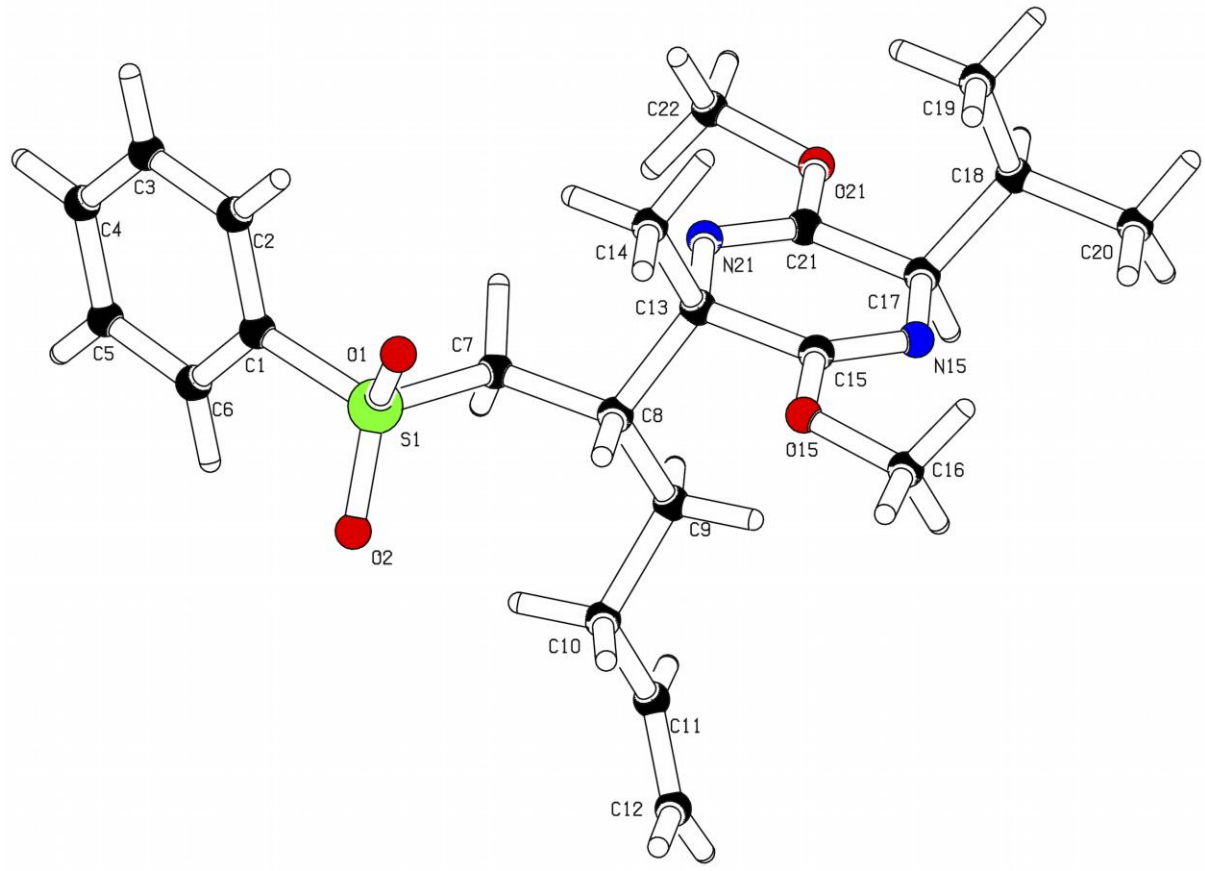

Figure 2.6. Crystal structure of bislactim ether **11b**

2.3 Biochemical analysis of gamma-methylated stapled peptides

A time-resolved fluorescence resonance energy transfer (TR-FRET) assay (Figure 2.7B) was used to measure interaction of a steroid receptor coactivator 3 (SRC3) fragment with ERα ligand-binding domain.[88] In this assay, the wild-type peptide has an IC_{50} of 1100 nM. The unfunctionalized stapled peptide SRC2-SP4 has an IC_{50} of 390 nM. This peptide is analogous to PFE-SP2, described by Phillips et al., but has a wild-type Q→R substitution, which increases the affinity two-fold. Epimers SRC2-SP2 and -SP3 were the most active, showing a 12-fold increase in potency compared to wild-type. SRC2-SP1, designed to incorporate a branched stapling residue to replace conserved Leu693, displayed minimal activity. In addition to the TR-FRET assay, surface plasmon resonance (see Figure 2.15) was used to obtain dissociation constants for SRC2-SP1 (530 nM), SRC2-SP2 (42 nM), and SRC2-SP3 (39 nM).

Circular dichroism (CD) analysis of the peptides (Figure 2.7C) indicates the wild-type sequence is disordered and that the stapled peptide SRC2-SP4 adopts an alpha helical conformation in solution. The CD spectrum for SRC2-SP1 shows that a λ_R substitution at Leu693 negatively impacts α-helicity; however, a λ_S substitution at Ile689 (SRC2-SP3) maintains helicity as does a λ_R substitution at Ile689 (SRC2-SP2), albeit to a lesser extent. The observation that addition of methyl groups may positively impact affinity while having a slightly negative effect on helicity may imply that constructive interactions with the surface of the receptor are more important for affinity than locking in a helical conformation.

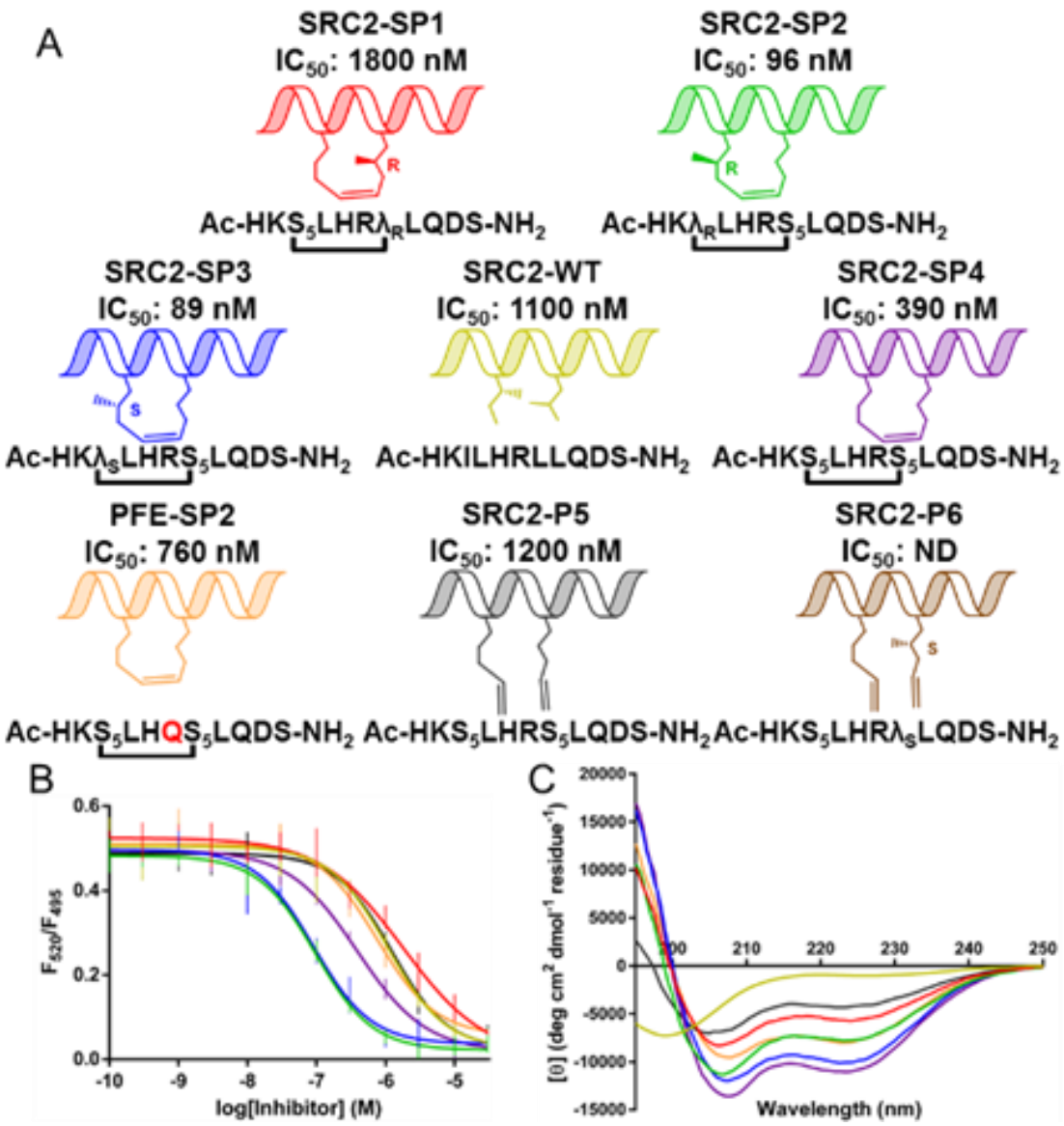

Figure 2.7. Structure and biophysical characterization of gamma-methylated stapled peptides. (A) Peptides (B) Time-resolved fluorescence resonance energy transfer dose-response curves for inhibition of ERα/SRC3. (C) Circular dichroism measurements were taken in 45 mM phosphate buffer pH 7.4 with 10% MeOH. SRC2-WT (yellow), SRC2-SP1 (red), SRC2-SP2 (green), SRC2-SP3 (blue), SRC2-SP4 (magenta), PFE-SP2 (orange), SRC2-P5 (gray), SRC2-P6 (brown).

2.4 Crystal structure analysis of gamma-methylated stapled peptides

We obtained co-crystal structures of SRC2-SP1, -SP2, -SP3, -SP4, and -P5 bound to the ligand binding domain of constitutively active Y537S ERα mutant. In all cases, the peptides bind in a similar α-helical conformation,[89] occupy the hydrophobic groove, and make contacts with the so-called "charge clamp:" flanking Lys and Glu residues that align complimentarily with the inherent dipole of the coactivator helix. The most notable difference is that the stapled peptides display a 1.2 Å shift towards the Glu end of the charge clamp, as compared to wild-type (Figure 2.8A-C). The γ-CH_3 of SRC2-SP1 occupies the same region as Leu693 (Figure 2.8A), and it occupies a pseudo-equatorial conformation to alleviate unfavorable *syn*-pentane strain between the α- and γ-methyl groups (Figure 2.8D). The resulting orientation of the γ-methyl increases contact with Ile358 of ERα, which may disrupt its interaction with the Lys end of the charge clamp. Minimizing *syn*-pentane interactions at this position also substantially alters the χ_1 torsion angle (−44°), at Leu693 relative to the more helical stapled peptides (i.e., χ_1 = +61° for SRC2-SP3; see Figure 2.8A). Analogous to SRC2-SP1, minimization of *syn*-pentane interactions is seen with the γ-methyl group of SRC2-SP3, but, instead of opposing the predominant conformation, the *S*-γ-methyl reinforces a high-affinity conformation (Figure 2.8D). Additionally, the γ-methyl occupies the same region as Ile689 in the wild-type sequence (Figure 2.8C). The γ-methyl of SRC2-SP2 also occupies this same space (Figure 2.8D), even though the methyl groups are opposite in configuration. The change in the χ_2 torsions between these two peptides is ~120°, which can explain how this is possible (Figure 2.8D).

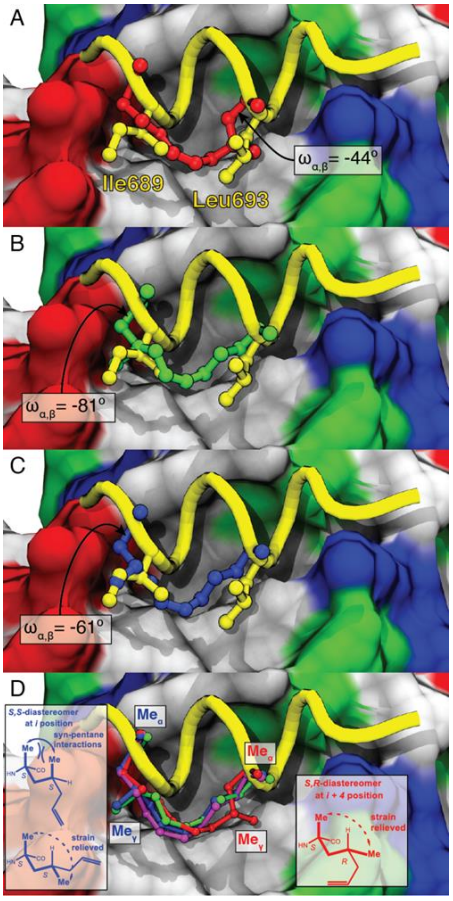

Figure 2.8. X-ray co-crystal structures of peptides bound to ERα (surface: red = acidic, blue = basic, white = nonpolar, green = polar). (A) SRC2-SP1 (red, PDB 5DXB), (B) SRC2-SP2 (green, PDB 5HYR), and (C) SRC2-SP3 (blue, PDB 5DX3) superimposed onto SRC2-WT (yellow, PDB 3ERD). Torsion angles ($\omega_{\alpha,\beta}$) about the Cα-Cβ bond at position Leu693 are shown. (D) Hydrocarbon staples of SRC2-SP1 (red), SRC2-SP3 (blue), and SRC2-SP4 (magenta, PDB 5DXE) superimposed onto the backbone of SRC2-WT (shown as a yellow tube). SRC2-SP1, SRC2-SP2, and SRC2-SP3 adopt conformations to alleviate syn-pentane interactions between the α- and γ-methyls. The sidechains of non-cyclic SRC2-P5 also bind along the hydrophobic shelf (see supporting information).

2.5 Molecular dynamics studies of gamma-methylated stapled peptides.

We carried out molecular dynamics (MD) studies on SRC2-SP1, -SP2, -SP3, and -SP4 bound to ERα using the NAMD2[90] simulation package with trajectory analysis performed in VMD.[91] The structural ensembles confirmed the strong influence of *syn*-pentane interactions to the conformations adopted by the staple. In particular, the dihedral angles between position 693 in SRC2-SP1 and SRC2-SP2, -SP3, and -SP4 are opposite in sign, with substantially more fluctuation at this position in SRC2-SP1 (see Figure 2.9A). In agreement with the x-ray structure, the simulations suggest that SRC2-SP2 adopts a pseudo-eclipsed conformation of –90° at position 689. ERα accommodates the branching methyl of the λ_S residue at position 689, but the λ_R residue at position 693 introduces a steric clash with Ile358 of the protein and induces a substantial shift in peptide positioning (Figure 2.9C). We also carried out MD studies on SRC2-SP1–4 in solution in the absence of ERα. These data confirm that the observed χ_1 torsion angles in solution correlate well with the observed angles in the crystal structure, with the caveat that SRC2-SP4 shows stable conformations at both –60º and –90º in solution (see supporting information).

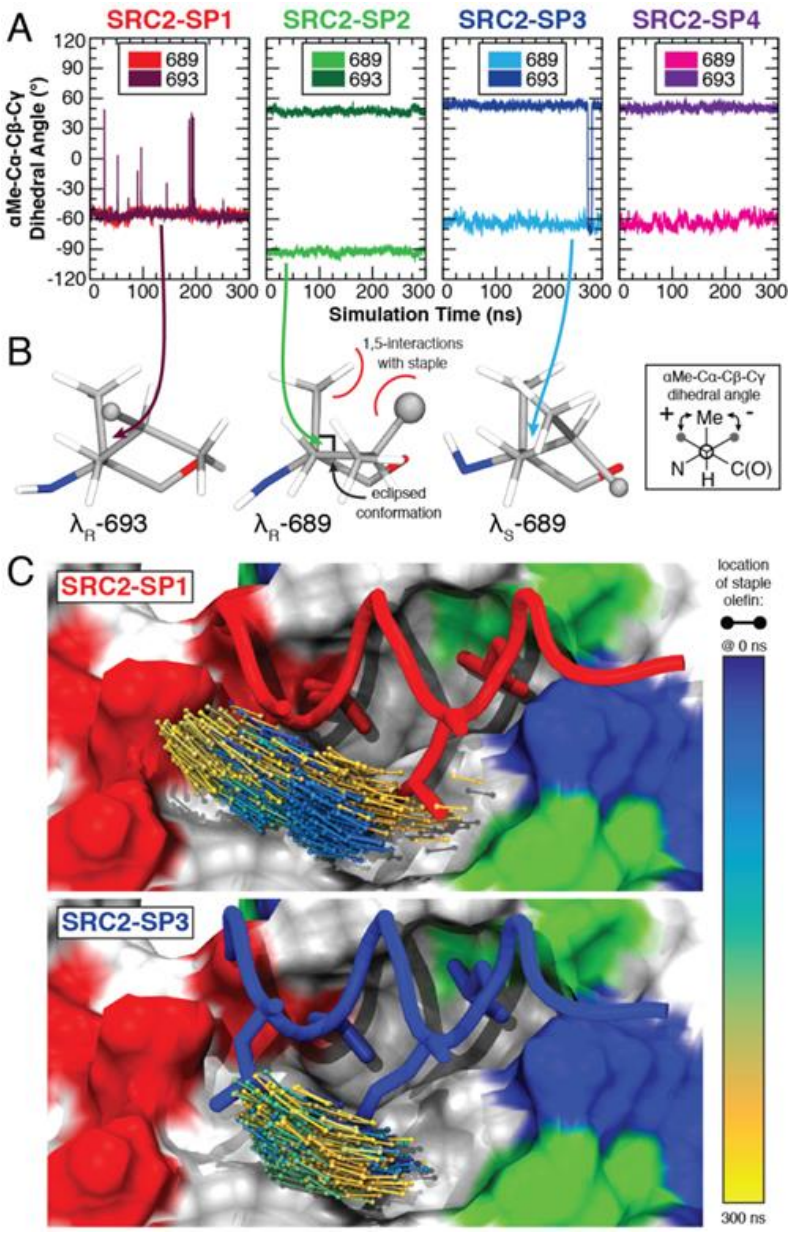

Figure 2.9. MD simulations of peptides bound to ERα. (A) The dihedral angle about the χ_1 bond reveals different conformations of staple residues 689 and 693 for peptides SRC2-SP1, SRC2-SP2 and SRC2-SP3. (B) The structural conformations of the γ-methyl substituted residue are shown for the last frame of the simulation. (C) The position of the staple shifts substantially during the course of the simulation for SRC2-SP1 and is relatively stable for SRC2-SP3.

2.6 Conclusion

In conclusion, we have created a stapling amino acid, λ_S, that both mimics native branched side chains and stabilizes a helical conformation. In this study, we have used this amino acid and its epimer, λ_R, to prepare highly potent inhibitors of the ERα/SRC interaction. We have shown that incorporation of a γ-methyl in the *R*- or *S*-configuration at the *i* position of an *i, i+4* stapled peptide is a tolerated modification that allows the hydrocarbon staple to effectively mimic branched hydrophobic residues, although the *S*-methyl results in a conformation with higher helical content than the *R* does. The *S*-methyl reinforces an α-helical conformation through minimization of *syn*-pentane interactions. Incorporation of a γ-methyl group at the *i+4* position in either configuration appears to have a destabilizing effect on α-helicity. Although the design here is for interacting residues, incorporation of γ-methyl groups may be applicable to non-interacting stapled residues, as well. In this regard, the simulated and observed staple geometry of methyl substitutions has provided a blueprint for installing γ-methyls and other substituents in stapling amino acids for related protein-protein interactions.

2.7 Peptide synthesis, characterization, and biochemical testing

2.7.1. General information

Fmoc-S5-OH and Grubbs' 1st generation catalyst were purchased from Sigma-Aldrich. Commercially available Fmoc amino acids were purchased from Novabiochem, Oakwood, or Sigma-Aldrich. HBTU, HCTU, dimethylformamide (DMF), trifluoroacetic acid (TFA), triisopropylsilane, piperidine, 1,2-dichloroethane, Rink Amide MBHA resin, acetic anhydride, *N*-methylpyrrolidinone (NMP) and *N,N*-diisopropylethylamine were

purchased from Fisher and subsidiaries and were used as supplied. The peptide PFE-SP2 was purchased from Anaspec, Inc.

2.7.2 Peptide synthesis

Solid phase peptide synthesis was carried out as described by Kim, Grossman and Verdine.[92] Standard Fmoc solid phase peptide synthesis was carried out on a 30 μmol scale using HBTU as the activating reagent. The peptide couplings of λ_R and λ_S were carried out over a single two hour coupling cycle using 3 eq. of the Fmoc protected amino acids. When incorporating λ_R or λ_S, the ring closing metathesis failed to progress to completion after two 2-hour room temperature cycles of 20% Grubbs' 1st generation catalyst loading. Up to two additional cycles of ring closing metathesis at 65 ^{o}C were performed to effect completion of the ring-closing metathesis reaction.

2.7.3 Peptide purification

The crude peptides were purified by semi-preparative HPLC (Solvent System MeCN:H_2O with 0.1% formic acid; 0-4 min, 10% MeCN; 4-22 min 10-45% MeCN; 22-24 min, 45-80% MeCN; 24-30 min, 80% MeCN; 30-31 min 80-10% MeCN. Column: Phenomenex Luna 5 μm C18(2), 100 Å, 250 x 10 mm). Fractions containing pure peptide were lyophilized and weighed to 0.01 mg on an analytical balance before being dissolved in DMSO. The purity of the peptides was established using HPLC on a Shimadzu LC-20AB (Solvent system MeCN:H_2O with 0.1% formic acid; 0-4 min, 10% MeCN; 4-14 min, 10-70% MeCN; 14-17 min, 70% MeCN. Column: Phenomenex Luna C8, 5 μ, 100 Å, 50 x 4.6 mm). A Shimadzu LCMS-2020 mass spectrometer with electrospray ionization was used to verify the molecular weight of purified peptides.

2.7.4 ^{1}H NMR of Peptides

Lyophilized peptides were dissolved in CD_3OD at a concentration of ~2 mg/mL. ^{1}H NMR spectra were obtained on a Bruker 600 MHz.DRX NMR spectrometer using XWINNMR version 3.5 at the University of Illinois Center for Structural Biology. Chemical shifts (δ) are given in ppm and coupling constants (*J*) are reported in Hz.

2.7.5 Circular Dichroism

Circular dichroism (CD) data were collected using a Jasco J-815 CD Spectrometer. Peptides were diluted to 50 μM in 45 mM phosphate buffer pH 7.4 with 10% methanol. Spectra were acquired at 20 ºC, over the range of 260–190 nm using the following instrument settings: 0.5 nm pitch, 1 nm band width, 1 second response, 20 nm/min scan speed, 0.2 cm cell length, and 3 accumulations. The baseline from a blank sample of 45 mM phosphate buffer pH 7.4 with 10% methanol was subtracted from each data set, and the data were minimally smoothed using the same level of adaptive smoothing.

2.7.6 Time-resolved fluorescence resonance energy transfer (TR-FRET) assay

The assay protocol was adopted from an established procedure.[88] Briefly, the peptides were incubated with 4 nM ERα-417 (amino acids 304–554; C381,530S; site-specifically labeled at C417 with biotin-maleimide), 1 nM streptavidin-terbium chelate (LanthaScreen® Tb-Streptavidin; ThermoFisher Scientific catalog number: PV3965), 50 nM steroid receptor coactivator 3 (residues 627–829; labeled nonspecifically with 5-iodoacetamidofluorescein), and 4 μM estradiol in 80 μL of TR-FRET buffer (20 mM Tris-HCl, 10% glycerol, 50 mM NaCl, 0.01% Nonidet® P 40 substitute at pH 7.5) with a DMSO concentration of 3%. After incubating for 45 minutes at room temperature, TR-FRET

readings were taken on a Biotek Synergy H4 hybrid reader using the software Gen5 v. 1.11.5. The excitation band used was 360/40 nm with a 100 µs delay and a 500 µs collection time with emission readings at 495/5 nm and 520/25 nm. The experiment was performed in triplicate using Corning black, polystyrene, flat bottom, non-binding surface area, 96-well half area assay plates. Graphpad Prism v. 6.01 was used to generate best-fit curves of the data (ratio of emission at 520 nm / emission at 495 nm; background emission of control with no estradiol and DMSO blank was subtracted) to sigmoidal, 4PL, where X is log (concentration of inhibitor).

2.7.7 Surface plasmon resonance

Purified ERα-417 (amino acids 304–554; C381,530S; site-specifically labeled at C417 with biotin-maleimide) was diluted to 0.5 mg/mL with HBS-EP buffer (10 mM HEPES, pH 7.4, 150 mM NaCl, 3 mM EDTA, and 0.05% surfactant P20) and injected for 5 min at a 7 µL/min flow rate on a Series S sensor chip SA for immobilization at 25 °C with running buffer HBS-EP using a Biacore T200 instrument. Blank surfaces were used as controls on flow channels 1 and 3. ERα was immobilized to flow channels 2 and 4, and immobilization levels were ~3100 RU and 2700 RU, respectively. Stapled peptide solutions at a series of increasing concentrations were applied to all four channels at a 30 µL/min flow rate with assay buffer (10 mM HEPES, pH 7.5, 0.15 M NaCl, 0.1% Chaps, and 2% DMSO, supplemented with 50 nM estradiol), and real-time response units (RU) were monitored. Sensorgrams were analyzed using the Biacore T200 evaluation software 3.0. All data were referenced by blank channel responses at each concentration, and the K_D values were determined by fitting the reference subtracted data to a steady-state

affinity equation. Kinetic fittings were done by 1 to 1 binding equation embedded in the Biacore T200 evaluation software 3.0.

2.7.8 X-ray crystallography

X-ray crystallography for estrogen receptor complexes was carried out by Sean Fanning. The exact protocol is published and freely available.

2.7.9 Molecular dynamic simulations

Chris Mayne performed molecular dynamic simulations. The exact protocol is published and freely available. (DOI: 10.1002/anie.201510557)

2.8 Synthesis of amino acids Fmoc-λ_R and Fmoc-λ_S

2.8.1 General information

^{1}H and ^{13}C NMR spectra were recorded on a Bruker 400 MHz spectrometer. Peak positions are given in parts per million (δ). Molecular weight was determined using a Shimadzu LCMS-2020 mass spectrometer with electrospray ionization. High-resolution mass spectrometry (HRMS) spectra were recorded on a Shimadzu LCMS-IT-TOF, and the mass-to-charge ratio of the compounds was within 0.05% of calculated values. Flash chromatography was performed using silica gel (230-400 mesh).

2.8.2 Synthetic procedures

Boc-d-valine-l-alanine methylester (1) – Triethylamine (6.86 g, 68 mmol, 1.0 eq) was added to a solution of Boc-D-valine (14.8 g, 68 mmol, 1.0 eq) in dichloromethane (200 mL) cooled below 4 ºC. Isobutyl chloroformate (9.30 g, 68 mmol, 1.0 eq) was added to the solution of triethylamine and Boc-D-valine over 30 minutes, and the resulting mixture

was stirred for an additional 30 minutes. A solution of L-alanine methyl ester (9.50 g, 68 mmol, 1.0 eq) and triethylamine (6.86 g, 68 mmol, 1.0 eq) in dichloromethane (200 mL) was stirred for 30 minutes and then added to the mixture of triethylamine, Boc-D-valine, and isobutyl chloroformate over 2 hours while maintaining the temperature below 4 ºC. The resulting mixture was stirred at room temperature for 16 hours. The reaction mixture was washed with water (3 × 300 mL) and brine (200 mL). The organic layer was dried with $MgSO_4$ and concentrated under vacuum to give 19.6 g of crude product, which was recrystallized from 1:1 water:ethanol to give 16.9 g of a white solid (82%).

^{1}H-NMR (400 MHz, $CDCl_3$): δ = 6.65 (d, *J* = 7.1 Hz, 1 H), 5.10 (d, *J* = 8.6 Hz, 1 H), 4.58 (quin, *J* = 7.2 Hz, 1 H), 3.98 (br. s., 1 H), 3.73 (s, 3 H), 2.16 (dq, *J* = 13.1, 6.7 Hz, 1 H), 1.43 (s, 9 H), 1.40 (d, *J* = 7.1 Hz, 3 H), 0.95 (d, *J* = 6.8 Hz, 3 H), 0.90 (d, *J* = 6.8 Hz, 3 H)

^{13}C-NMR (101 MHz, $CDCl_3$): δ = 173.0, 171.3, 155.7, 79.3, 59.4, 52.1, 47.7, 30.8, 28.0, 18.9, 17.8, 17.5

LCMS-ESI $[M+H]^+$ 303.25

(3*R*,6*S*)-3-isopropyl-6-methylpiperazine-2,5-dione (**2**) - Boc-D-Val-L-Ala-methyl ester (13.8 g, 45 mmol) was dissolved in 1,2-dichlorobenzene (140 mL) and heated to 175–180 ºC for 24 hrs. Methanol that formed was removed by distillation. The reaction mixture was placed in a 0 ºC freezer overnight, and a crystalline solid was collected by filtration and washed with methyl tert-butyl ether to yield 5.00 g of a white solid (64.5%). If needed, the product can be recrystallized from ethanol:water to remove impurities.

^{1}H-NMR (400 MHz, DMSO-d_6): δ = 8.09 (s, 1 H), 8.12 (s, 1 H), 3.92 (q, *J* = 6.5 Hz, 1 H), 3.54 (br. s., 1 H), 2.21–2.04 (m, 1 H), 1.25 (d, *J* = 6.8 Hz, 3 H), 0.93 (d, *J* = 6.8 Hz, 3 H), 0.86 (d, *J* = 6.6 Hz, 3 H)

^{13}C-NMR (101 MHz, DMSO-d_6): δ = 168.9, 167.4, 60.2, 49.0, 32.2, 18.6, 18.5, 17.2

LCMS-ESI $[M+H]^+$ 171.05

(2*R*,5*S*)-2-isopropyl-3,6-dimethoxy-5-methyl-2,5-dihydropyrazine (3) – Trimethyloxonium tetrafluoroborate (10.0 g, 67.6 mmol, 2.3 eq) and (3*R*,6*S*)-3-isopropyl-6-methylpiperazine-2,5-dione (5.00 g, 29.4 mmol, 1.0 eq) were well mixed in a round bottom flask. Dry dichloromethane (75 mL) was added, and the solution was vigorously stirred for two days. Additional trimethyloxonium tetrafluoroborate (1.5 g, 10.1 mmol, 0.34 eq) was added, and the mixture was stirred for one more day. The acidic reaction mixture was quenched by pipetting it into a solution of ice cold sodium bicarbonate (75 mL saturated). During the quenching process aq. 1 M NaOH was added as needed to the sodium bicarbonate solution to maintain a pH > 7. After quenching, dichloromethane (3 × 50 mL) was used to extract organic material from the aq. solution. The organic layer was washed with water (2 × 50 mL) and brine (1 × 50 mL), dried over $MgSO_4$ and concentrated to an oil under vacuum. The impure product was purified by flash column chromatography (4:1 hexane:ether) to give 4.35 g of a clear oil (75%).

^{1}H-NMR (400 MHz, $CDCl_3$): δ = 4.00 (dq, *J* = 7.1, 3.5 Hz, 1 H), 3.95 (q, *J* = 3.5 Hz, 1 H), 3.69 (s, 3 H), 3.67 (s, 3 H), 2.25 (spt of d, *J* = 6.8, 3.3 Hz 1 H), 1.35 (d, *J* = 7.1 Hz, 3 H), 1.04 (d, *J* = 7.1 Hz, 3 H), 0.70 (d, *J* = 6.8 Hz, 3 H)

^{13}C-NMR (101 MHz, $CDCl_3$): δ = 164.9, 163.4, 60.9, 52.4, 52.3, 51.4, 31.8, 21.3, 19.0, 16.6

LCMS-ESI $[M+H]^+$ 199.13

Specific Rotation $[\alpha]_D^{RT}$ -43.9 (*c*, 1.95 $CHCl_3$)

(*S*)-4-benzyl-3-propionyloxazolidin-2-one (4a) – To a solution of (*S*)-4-benzyloxazolidin-2-one (3.20 g, 18.1 mmol, 1.00 eq) in THF (65 mL) at −78 ºC was added 1.6 M *n*-butyllithium in hexane (12.4 mL, 19.9 mmol, 1.10 eq) dropwise over 20 minutes. The temperature of the solution was maintained at −78 °C prior to and during the addition of base. Propionyl chloride (1.84 g, 19.9 mmol, 1.10 eq) was added over 10 minutes and the solution was stirred at −78 °C for 2.5 hrs. The reaction was warmed to room temperature and quenched with saturated ammonium chloride (10 mL). The THF was removed under vacuum and the residual oil was taken up into dichloromethane (100 mL), washed with water (1 × 50 mL), washed with 10% sodium hydroxide (1 × 50 mL), washed with water (2 × 50 mL), washed with brine (1 × 50 mL), dried over $MgSO_4$, and concentrated to a white powder (4.20 g, 99.8%).

^{1}H-NMR (400 MHz, $CDCl_3$): δ = 7.38–7.31 (m, 2 H), 7.30–7.26 (m, 1 H), 7.21 (d, *J* = 6.8 Hz, 2 H), 4.68 (dddd, *J* = 9.9, 6.9, 3.4, 3.2 Hz, 1 H), 4.21 (dd, *J* = 9.0, 7.8 Hz, 1 H), 4.17 (dd, *J* = 9.1, 3.3 Hz, 1 H), 3.31 (dd, *J* = 13.3, 3.2 Hz, 1 H), 3.00 (dq, *J* = 17.9, 7.6 Hz, 1 H), 2.93 (dq, *J* = 17.9, 7.3 Hz, 1 H), 2.77 (dd, *J* = 13.4, 9.6 Hz, 1 H), 1.21 (t, *J* = 7.3 Hz, 3 H)

^{13}C-NMR (101 MHz, $CDCl_3$): δ = 174.0, 153.4, 135.3, 129.3, 128.8, 127.2, 66.1, 55.1, 37.8, 29.1, 8.2

LCMS-ESI $[M+H]^+$ 234.15

Specific Rotation $[\alpha]_D^{RT}$ +59 (*c*, 7.6 $CHCl_3$)

(*R*)-4-benzyl-3-propionyloxazolidin-2-one (4b) – This compound was prepared similarly to the procedure described for **4a**, but with (*R*)-4-benzyloxazolidin-2-one as starting material.

^{1}H-NMR (400 MHz, $CDCl_3$) δ = 7.37−7.31 (m, 2 H), 7.31−7.25 (m, 1 H), 7.24−7.19 (m, 2 H), 4.68 (dddd, *J* = 10.6, 7.1, 3.2, 3.0 Hz, 1 H), 4.22 (dd, *J* = 9.0, 6.8 Hz, 3 H), 4.17 (dd, *J* = 9.1, 3.3 Hz, 1 H), 3.31 (dd, *J* = 13.4, 3.0 Hz, 1 H), 2.99 (dq, *J* = 17.9, 7.3 Hz, 1 H), 2.93 (dq, *J* = 17.9, 7.3 Hz, 1 H), 2.78 (dd, *J* = 13.3, 9.7 Hz, 1 H), 1.21 (t, *J* = 7.3 Hz, 3 H)

^{13}C-NMR (101 MHz, $CDCl_3$) δ 174.0, 153.4, 135.3, 129.3, 128.9, 127.2, 66.1, 55.1, 37.8, 29.1, 8.2

LCMS-ESI $[M+H]^+$ 234.15

Specific Rotation $[\alpha]_D^{RT}$ -49 (*c*, 4.9 $CHCl_3$)

Reference Procedure: Evans and DiMare.[93]

(*S*)-4-benzyl-3-((*R*)-2-methylpent-4-enoyl)oxazolidin-2-one (5a) – To a solution of 0.94 M lithium diisopropyl amide (20 mL, 18.9 mmol, 1.10 eq) in THF/hexanes at −78 ºC was

added a solution of **4a** (4.00 g, 17.1 mmol, 1.00 eq) in THF (25 mL) over 30 minutes. After allowing the solution to stir for 15 minutes at −78 ºC, allyl bromide (3.64 g, 51.4 mmol, 3.00 eq) was added dropwise over 30 minutes. Stirring was continued for 30 minutes at −78 ºC followed by an additional stirring for 2.5 hrs at 0 ºC in an ice bath. Upon the disappearance of starting material, the reaction mixture was warmed to room temperature and quenched with saturated ammonium chloride (20 mL). Volatile reaction components were removed under vacuum. The residue was dissolved in DCM (100 mL), washed with water (2 × 75 mL), washed with brine (75 mL), dried with magnesium sulfate and concentrated to a golden oil (4.93 g). The product was purified by flash column chromatography (elution at 1:4 hexane:ethyl acetate) resulting in 2.30 g of a white solid (49%) after removal of solvent.

^{1}H-NMR (400 MHz, $CDCl_3$): δ = 7.37–7.31 (m, 2 H), 7.31–7.27 (m, 1 H), 7.25–7.21 (m, 2 H), 5.84 (ddt, *J* = 17.0, 10.0, 7.1 Hz, 1 H), 5.16–5.04 (m, 2 H), 4.69 (dddd, *J* = 10.6, 6.8, 3.3, 3.1 Hz, 1 H), 4.23–4.13 (m, 2 H), 3.88 (sxt, *J* = 6.8 Hz, 1 H), 3.30 (dd, *J* = 13.4, 3.3 Hz, 1 H), 2.71 (dd, *J* = 13.4, 9.9 Hz, 1 H), 2.54 (dtt, *J* = 14.1, 6.8, 1.3 Hz, 1 H), 2.26 (dtt, *J* = 14.1, 7.1, 1.0 Hz, 1 H), 1.20 (d, *J* = 6.8 Hz, 3 H)

^{13}C-NMR (101MHz, $CDCl_3$): δ = 176.4, 153.1, 135.3, 135.2, 129.4, 128.9, 127.3, 117.2, 66.0, 55.3, 38.0, 37.9, 37.1, 16.4

LCMS-ESI $[M+H]^+$ 274.20

Specific Rotation $[\alpha]_D^{RT}$ +33.6 (*c*, 5.9 $CHCl_3$)

(*R*)-4-benzyl-3-((*S*)-2-methylpent-4-enoyl)oxazolidin-2-one (5b) – This compound was prepared similarly to the procedure described for **5a** by using the oppositely configured starting material.

^{1}H-NMR (400 MHz, $CDCl_3$): δ = 7.37–7.31 (m, 2 H), 7.31–7.27 (m, 1 H), 7.26–7.19 (m, 2 H), 5.84 (ddt, *J* = 17.0, 10.1, 7.0 Hz, 1 H), 5.15–5.04 (m, 2 H), 4.69 (dddd, *J* = 10.0, 6.9, 3.4, 3.2 Hz, 1 H), 4.24−4.13 (m, 2 H), 3.88 (sxt, *J* = 6.8 Hz, 1 H), 3.30 (dd, *J* = 13.1, 3.3 Hz, 1 H), 2.71 (dd, *J* = 13.1, 9.9 Hz, 1 H), 2.53 (dtt, *J* = 14.0, 6.8, 1.3 Hz, 1 H), 2.25 (dtt, *J* = 14.0, 7.3, 1.3 Hz, 1 H), 1.20 (d, *J* = 6.8 Hz, 3 H)

^{13}C-NMR (101 MHz, $CDCl_3$): δ = 176.5, 153.1, 135.4, 135.2, 129.4, 128.9, 127.3, 117.1, 66.0, 55.3, 38.1, 37.9, 37.1, 16.4

LCMS-ESI $[M+H]^+$ 274.20

Specific Rotation $[\alpha]_D^{RT}$ -36.1 (*c*, 5.1 $CHCl_3$)

Reference Procedure: Evans, Ennis, and Mathre. [84]

(*R*)-2-methylpent-4-en-1-ol (6a) – Compound **5a** (0.820 g, 3.0 mmol, 1.0 eq) was dissolved in diethylether (25 mL) and cooled to 0 ºC in an ice/salt bath. To this solution was added ethanol (0.207 g, 4.5 mmol, 1.5 eq) followed by $LiBH_4$ (4 × 25 mg portions, 4.6 mmol, 1.5 eq). The solution was stirred for 1 hr at 0 ºC and then stirred for an additional 3 hrs at room temperature. The reaction was quenched with 1 M NaOH (25 mL). The organic layer was separated, and the aqueous layer was extracted with diethyl ether (2 × 25 mL). The combined organic layers were washed with ammonium chloride (1 × 50 mL),

water (2 × 50 mL), brine (1 × 50 mL), dried over $MgSO_4$ and concentrated to an oily-solid. The residue was subjected to flash column chromatography (1:1 hexane: ethyl acetate) to afford **6a** (0.240 g, 80%).

^{1}H-NMR (400 MHz, $CDCl_3$): δ = 5.78 (ddt, *J* = 17.2, 10.1, 7.1 Hz, 1 H), 5.06–4.96 (m, 2 H), 3.47 (ddd, *J* = 10.6, 6.6, 5.8 Hz, 1 H), 3.41 (ddd, *J* = 10.6, 6.6, 5.6 Hz, 1 H), 2.22 (br. t, *J* = 5.8 Hz, 1 H), 2.16 (dtt, *J* = 14.0, 6.6, 1.3 Hz, 1 H), 1.90 (dtt, *J* = 14.0, 6.6, 1.3 Hz, 1 H), 1.77−1.64 (octet, *J* = 6.6 Hz, 1 H), 0.90 (d, *J* = 6.8 Hz, 3 H)

^{13}C-NMR (101 MHz, $CDCl_3$): δ = 136.9, 115.9, 67.6, 37.7, 35.5, 16.3

Specific Rotation $[\alpha]_D^{RT}$ +1.5 (*c*, 19.9 $CHCl_3$)

(*S*)-2-methylpent-4-en-1-ol (6b) – This compound was prepared similarly to the procedure described for **6a** by using the oppositely configured starting material.

^{1}H-NMR (400 MHz, $CDCl_3$): δ = 5.83 (ddt, *J* = 17.1, 10.0, 7.1 Hz, 1 H), 5.10–4.98 (m, 2 H), 3.53 (dd, *J* = 10.4, 6.3 Hz, 1 H), 3.47 (dd, *J* = 10.6, 6.3 Hz, 1 H), 2.18 (dtt, *J* = 14.0, 6.6, 1.3 Hz, 1 H), 1.96 (dtt, *J* = 14.0, 6.8, 1.3 Hz, 1 H), 1.75 (octet, *J* = 6.6 Hz, 1 H), 1.43 (br. s, 1H), 0.94 (d, *J* = 6.8 Hz, 3 H)

^{13}C-NMR (101 MHz, $CDCl_3$): δ = 136.9, 115.8, 67.5, 37.7, 35.5, 16.2

Specific Rotation $[\alpha]_D^{RT}$ -1.9 (*c*, 16.5 $CHCl_3$)

Reference Procedure: Meiries, Bartoli, Decostanzi, Parrain, and Commeiras. [21]

(2*S*,5*R*)-5-isopropyl-3,6-dimethoxy-2-methyl-2-((*R*)-2-methylpent-4-en-1-yl)-2,5-dihydropyrazine (8a) – This compound was prepared similarly to the procedure described for **8b** by using the oppositely configured starting material.

^{1}H-NMR (400 MHz, $CDCl_3$): δ = 5.77–5.63 (m, 1 H), 4.97 (t, *J* = 1.3 Hz, 1 H), 4.95–4.92 (m, 1 H), 3.97 (d, *J* = 3.3 Hz, 1 H), 3.67 (s, 3 H), 3.66 (s, 3 H), 2.28 (dtt, *J* = 10.4, 6.9, 3.3 Hz, 1 H), 2.01–1.89 (m, 2 H), 1.85–1.76 (m, 1 H), 1.44–1.32 (m, 2 H), 1.31 (s, 3 H), 1.09 (d, *J* = 6.8 Hz, 3 H), 0.83 (d, *J* = 6.6 Hz, 3 H), 0.69 (d, *J* = 6.8 Hz, 3 H)

^{13}C-NMR (101 MHz, $CDCl_3$): δ = 165.7, 161.3, 137.5, 115.6, 61.1, 58.6, 52.1, 52.0, 47.2, 41.9, 31.0, 29.8, 29.7, 21.2, 19.4, 16.9

HRMS $[M+H]^+$ calcd for $C_{16}H_{29}N_2O_2$, 281.2224; found, 281.2223

Specific Rotation $[\alpha]_D^{RT}$ + 49.1 (*c*, 1.03 $CHCl_3$)

(2*S*,5*R*)-5-isopropyl-3,6-dimethoxy-2-methyl-2-((*S*)-2-methylpent-4-en-1-yl)-2,5-dihydropyrazine (8b) – **Step 1**:The alcohol **6b** (0.764 g, 7.63 mmol) was dissolved in dichloromethane (16 mL) and cooled to −78 ºC. Pyridine (0.665 g, 8.40 mmol) was added in one portion followed by the dropwise addition of trifluoromethanesulfonic anhydride (2.26 g, 8.022 mmol). After addition, the solution was stirred for 10 minutes at −78 ºC and transferred to an ice bath, where stirring was continued for an additional 30 minutes. At this point hexane (32 mL) was added followed by 1 M sulfuric acid (32 mL). The organic layer was set aside, and the aqueous layer was extracted with dichloromethane (50 mL). The combined organic layers were filtered through a plug of silica, and additional dichloromethane (75 mL) was used to flush residual triflate through the silica, leaving

behind an orange residue. The organic layer was dried over $MgSO_4$ and concentrated under vacuum to yield 0.950 g (4.0 mmol), which was used directly in step 2. **Step 2:** The bislactim ether **3** (0.792 g, 4.0 mmol) was dissolved in THF (16 mL) and cooled to −78 ºC. *tert*-BuLi in hexane (3.69 mL, 4.8 mmol) was added dropwise over 45 minutes, and stirring was continued for an additional hour at −78 ºC. While maintaining the temperature at −78 ºC, the triflate of **6b** formed in Step 1 (0.950 g, 4.0 mmol) dissolved in THF (2 mL) was added dropwise over 30 minutes. Stirring was continued overnight as the solution was allowed to warm to room temperature slowly. The reaction was quenched with conc. ammonium chloride (5 mL), and volatile organics were removed under vacuum. The mixture was diluted with water (25 mL) and extracted with diethyl ether (3 × 30 mL). The organic layer was washed with water (1 × 50 mL) and brine (1 × 50 mL), dried over $MgSO_4$ and concentrated under vacuum to give an oil. The oil was purified by flash column chromatography (9:1 hexane: ethyl acetate) to afford 1.12 g of **8b** (99.9% based on **3**).

^{1}H-NMR (400 MHz, $CDCl_3$): δ = 5.81–5.67 (m, 1 H), 5.02–4.91 (m, 2 H), 3.98 (d, *J* = 3.3 Hz, 1 H), 3.67 (s, 3 H), 3.66 (s, 3 H), 2.28 (dtt, *J* = 10.3, 6.9, 3.4 Hz, 1 H), 2.03 (qd, *J* = 6.9, 5.8 Hz, 1 H), 1.85 (dt, *J* = 14.1, 7.2 Hz, 1 H), 1.76–1.69 (m, 1 H), 1.62 (dd, *J* = 13.6, 4.0 Hz, 1 H), 1.44–1.34 (m, 1 H), 1.31 (s, 3 H), 1.09 (d, *J* = 6.8 Hz, 3 H), 0.75 (d, *J* = 6.8 Hz, 3 H), 0.69 (d, *J* = 6.8 Hz, 3 H)

^{13}C-NMR (101 MHz, $CDCl_3$): δ = 166.0, 161.5, 137.5, 115.6, 61.1, 57.9, 52.1, 52.0, 47.3, 42.8, 31.0, 29.9, 29.3, 19.5, 19.4, 16.9

HRMS $[M+H]^+$ calcd for $C_{16}H_{29}N_2O_2$, 281.2224; found, 281.2229

Specific Rotation $[\alpha]_D^{RT}$ +28.1 (*c*, 1.45 $CHCl_3$)

Reference Procedure: Schöllkopf, Groth, and Deng. [94]

(2*S*,4*R*)-2-((((9H-fluoren-9-yl)methoxy)carbonyl)amino)-2,4-dimethylhept-6-enoic acid (9a; Fmoc-λ_R) – Compound **8a** (0.280 g, 1.0 mmol, 1.0 eq) was added to a solution of 0.3 M HCl (8.3 mL, 2.5 eq) and stirred overnight at room temperature. The solution was stirred for 4 additional days, and additional THF (1 mL) was added on the morning of each day. Upon disappearance of starting material, the reaction was basified to pH 8 by the dropwise addition of 1 M ammonium hydroxide, extracted with ethyl acetate (3 × 20 mL), and concentrated under vacuum. Undesired valine methyl ester was removed by vacuum. The residual oil was taken up in dioxane (3.25 mL) and aq. 10% sodium carbonate (3.25 mL, 3 eq) at 0 ºC. Fmoc-Cl (0.258 g, 1.0 eq) was added slowly, and the reaction mixture was allowed to warm to room temperature and stir overnight. The next day the reaction mixture was diluted with water (10 mL), extracted with dichloromethane (3 × 20 mL), washed with water (30 mL), washed with brine (30 mL), dried with $MgSO_4$ and concentrated. The residue was taken up in 1:1 dioxane : 2.5 M HCl (6 eq. HCl), and the solution was heated at reflux for 3 days. Upon disappearance of the methyl ester (as observed by LC-MS) the reaction solvent was removed under vacuum, and the crude product was purified by flash column chromatography (0–2.5% CH_3OH in CH_2Cl_2), resulting in 0.169 g of a crystalline solid **9a** (43%).

^{1}H-NMR (400 MHz, CD_3OD): δ = 7.81–7.75 (m, 1 H), 7.66–7.62 (m, 1 H), 7.40–7.35 (m, 2 H), 7.31–7.26 (m, 2 H), 5.80–5.63 (m, 1 H), 5.01–4.92 (m, 1 H), 4.31 (br. s, 2 H), 4.22–

4.16 (m, 1 H), 2.10–2.01 (m, 1 H), 1.96–1.70 (m, 3 H), 1.63–1.54 (m, 1 H), 1.50 (br. s, 3 H), 0.90 (d, *J* = 6.3 Hz, 3 H)

^{13}C-NMR (101 MHz, CD_3OD): δ = 177.9, 156.9, 145.4, 142.7, 138.3, 128.9, 128.3, 126.3, 121.0, 116.8, 67.6, 60.4, 48.5, 43.8, 43.5, 30.4, 24.4, 21.5

HRMS $[M+H]^+$ calcd for $C_{24}H_{28}NO_4$, 394.2013; found, 394.2000

Specific Rotation $[\alpha]_D^{RT}$ +5.8 (*c*, 8.5 $CHCl_3$)

(2*S*,4*S*)-2-((((9H-fluoren-9-yl)methoxy)carbonyl)amino)-2,4-dimethylhept-6-enoic acid (**9b; Fmoc-λ$_S$) –** This compound was prepared similarly to the procedure described for **8a**, but used the oppositely configured starting material.

^{1}H-NMR (400 MHz, $CDCl_3$): δ = 7.82–7.71 (m, 2 H), 7.68–7.58 (m, 2 H), 7.42–7.32 (m, 2 H), 7.31–7.22 (m, 2 H), 5.83–5.62 (m, 1 H), 5.03–4.93 (m, 2 H), 4.92 (br. s, 2 H), 4.38–4.24 (m, 2 H), 4.23–4.11 (m, 1 H), 2.15–2.00 (m, 2 H), 1.95–1.83 (m, 1 H), 1.74 (dd, *J* = 14.0, 7.7 Hz, 1 H), 1.66–1.56 (m, 1 H), 1.49 (br. s, 3 H), 0.86 (d, *J* = 6.3 Hz, 3 H)

^{13}C-NMR (101 MHz, $CDCl_3$): δ = 178.2, 156.8, 145.4, 142.7, 138.3, 128.9, 128.3, 126.3, 121.1, 116.7, 67.6, 60.2, 48.6, 43.9, 43.6, 30.2, 24.6, 20.9

HRMS $[M+H]^+$ calcd for $C_{24}H_{28}NO_4$, 394.2013; found, 394.2002

Specific Rotation $[\alpha]_D^{RT}$ +6.03 (*c*, 23.0 $CHCl_3$)

(2*S*,5*R*)-5-isopropyl-3,6-dimethoxy-2-methyl-2-((*R*)-1-(phenylsulfonyl)hex-5-en-2-yl)-2,5-dihydropyrazine (11a) - The bislactim ether **3** (0.476 g, 2.4 mmol) was dissolved in THF (10 mL) and cooled to −78 ºC. *tert*-BuLi in hexane (2.03 mL, 2.64 mmol) was added dropwise over 45 minutes, and stirring was continued for an additional hour at −78 ºC. While maintaining the temperature at −78 ºC, the phenylsulfone **10** (0.533 g, 2.4 mmol) dissolved in THF (2 mL) was added dropwise over 30 minutes. Stirring was continued for 35 min. The reaction was quenched with conc. ammonium chloride (2 mL) at -78 ºC, and allowed to warm to room temperature. The mixture was diluted with water (25 mL) and extracted with diethyl ether (3 × 30 mL). The organic layer was washed with water (1 × 50 mL) and brine (1 × 50 mL), dried over $MgSO_4$ and concentrated under vacuum to give an oil. The oil was purified by flash column chromatography (0-20% hexane: ethyl acetate) to afford 0.46 g of **11a** (43%). A compound confirmed to be the diastereoisomer **11b** (2*S*,5*R*)-5-isopropyl-3,6-dimethoxy-2-methyl-2-((*S*)-1-(phenylsulfonyl)hex-5-en-2-yl)-2,5 eluted first and was also recovered 0.18 g (17%).

11a ^{1}H-NMR (400 MHz, $CDCl_3$): δ = 7.87 - 7.92 (m, 2 H), 7.63 - 7.68 (m, 1 H), 7.54 - 7.59 (m, 2 H), 5.79 (ddt, *J*=17.0, 10.3, 6.6, 6.6 Hz, 1 H), 4.92 - 5.04 (m, 2 H), 3.87 (d, *J*=3.5 Hz, 1 H), 3.61 (s, 3 H), 3.42 (s, 3 H), 2.91 - 2.96 (m, 2 H), 2.17 - 2.35 (m, 3 H), 2.06 - 2.16 (m, 1 H), 1.85 - 1.95 (m, 1 H), 1.56 (dd, *J*=9.6, 4.8 Hz, 1 H), 1.27 (s, 3 H), 1.03 (d, *J*=6.8 Hz, 3 H), 0.64 (d, *J*=6.8 Hz, 3 H)

LCMS-ESI $[M+H]^+$ 421.25

11b ^{1}H-NMR (400 MHz, $CDCl_3$): δ = 7.94 - 7.99 (m, 2 H), 7.62 - 7.68 (m, 1 H), 7.55 - 7.61 (m, 2 H), 5.66 (ddt, *J*=17.0, 10.3, 6.6, 6.6 Hz, 1 H), 4.86 - 4.96 (m, 2 H), 3.91 (d, *J*=3.3 Hz, 1 H), 3.74 (dd, *J*=15.5, 3.2 Hz, 1 H), 3.65 (s, 3 H), 3.55 (s, 3 H), 2.90 (dd, *J*=15.4, 5.8

Hz, 1 H), 2.51 - 2.58 (m, 1 H), 2.23 (td, *J*=6.8, 3.5 Hz, 1 H), 1.89 - 2.01 (m, 2 H), 1.18 - 1.25 (m, 4 H), 1.04 - 1.13 (m, 4 H), 0.64 (d, *J*=6.8 Hz, 3 H)

11b ^{13}C-NMR (101 MHz, $CDCl_3$): δ = 164.4, 162.4, 140.3, 138.2, 133.5, 129.2, 128.1, 114.6, 60.9, 60.5, 57.2, 52.2, 52.1, 40.1, 31.9, 31.0, 30.8, 26.9, 19.3, 16.9

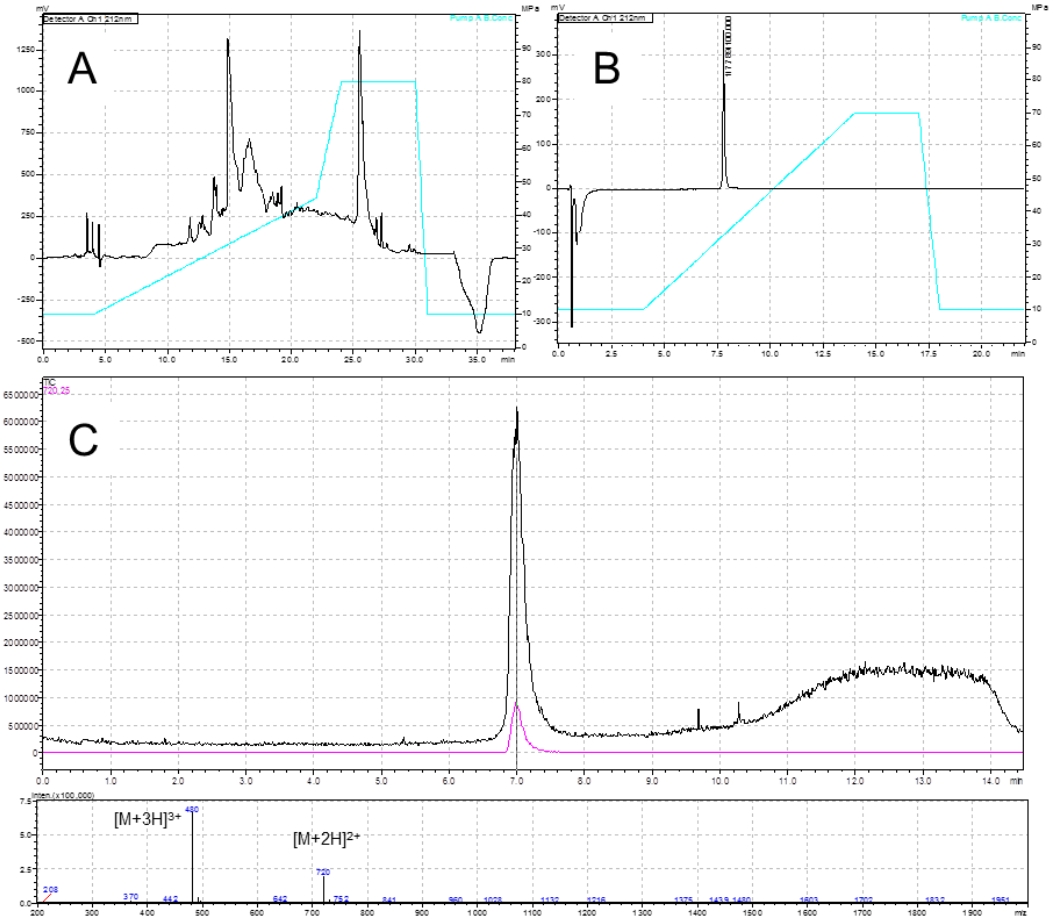

Figure 2.10. Representative purification and analysis of peptides. (A) Crude SRC2-SP2 before semi-preparative HPLC purification. (B) Analytical HPLC chromatogram of purified SRC2-SP2. (C) LC-ESI-MS analysis of purified SRC2-SP2.

TABLE I. ELECTROSPRAY MS DATA FOR PEPTIDES (POSITIVE MODE)

Peptide	Molecular Weight	Found Mass
SRC2-SP1	1438.70	$[M+2H]^{2+}$ =720.25
SRC2-SP2	1438.70	$[M+2H]^{2+}$ = 720.25
SRC2-SP3	1438.70	$[M+2H]^{2+}$ = 720.25
SRC2-SP4	1424.68	$[M+2H]^{2+}$ = 712.95
SRC2-WT	1400.65	$[M+2H]^{2+}$ = 701.35
SRC2-P5	1452.73	$[M+2H]^{2+}$ = 727.25
PFE-SP2	1396.62	$[M+2H]^{2+}$ = 699.10

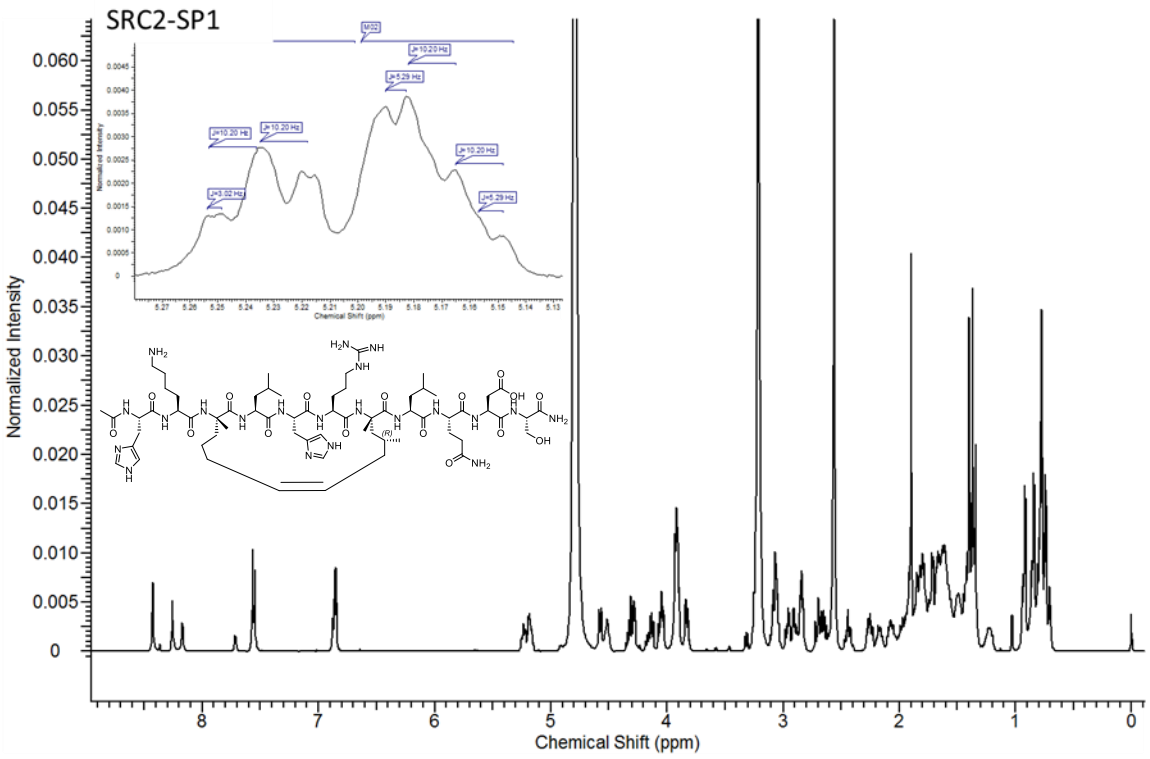

Figure 2.11. ^{1}H NMR spectra for SRC2-SP1 in CD_3OD. The apparent coupling constants for the alkene protons are δ = 5.24 (ddd, *J* = 10.2, 10.2, 3.0 Hz, 1 H), 5.17 (ddd, *J* = 10.2, 10.2, 5.3 Hz, 1 H)

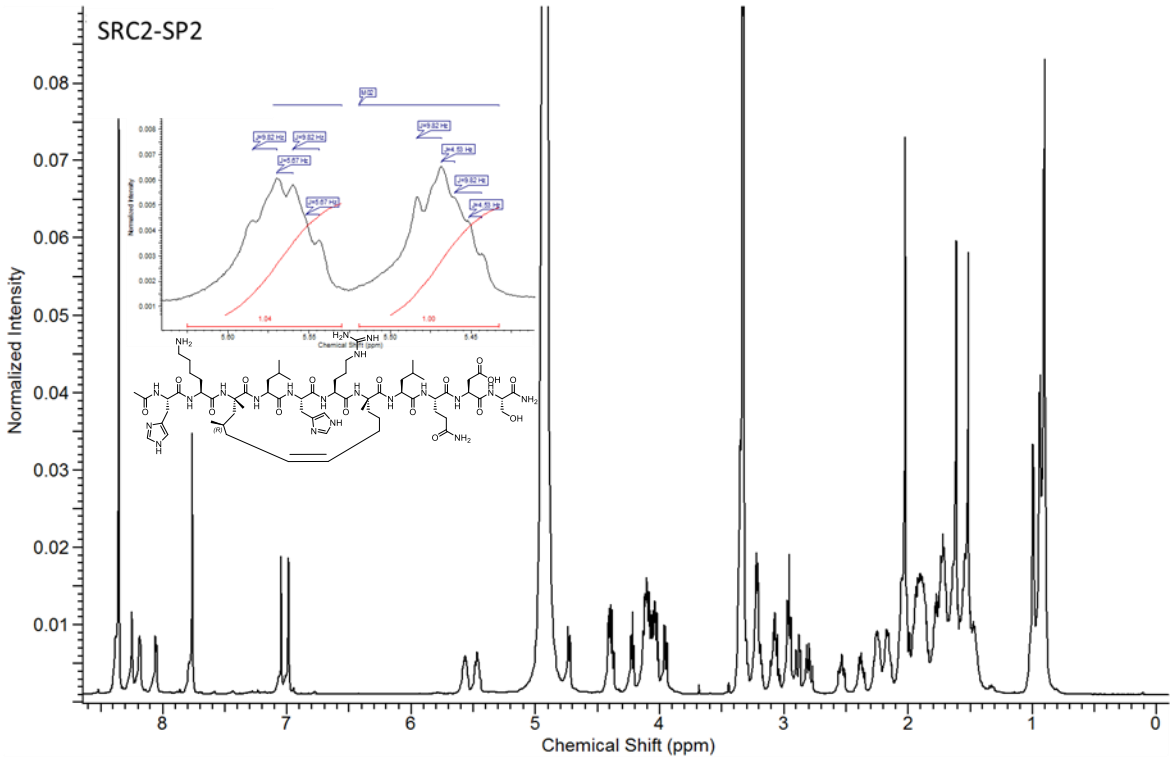

Figure 2.12. ^{1}H NMR spectra for SRC2-SP2 in CD_3OD. The apparent coupling constants for the alkene protons are δ = 5.58 (ddd, *J* = 9.8, 9.8, 5.7 Hz, 1 H), 5.48 (ddd, *J* = 9.8, 9.8, 4.5 Hz, 1 H).

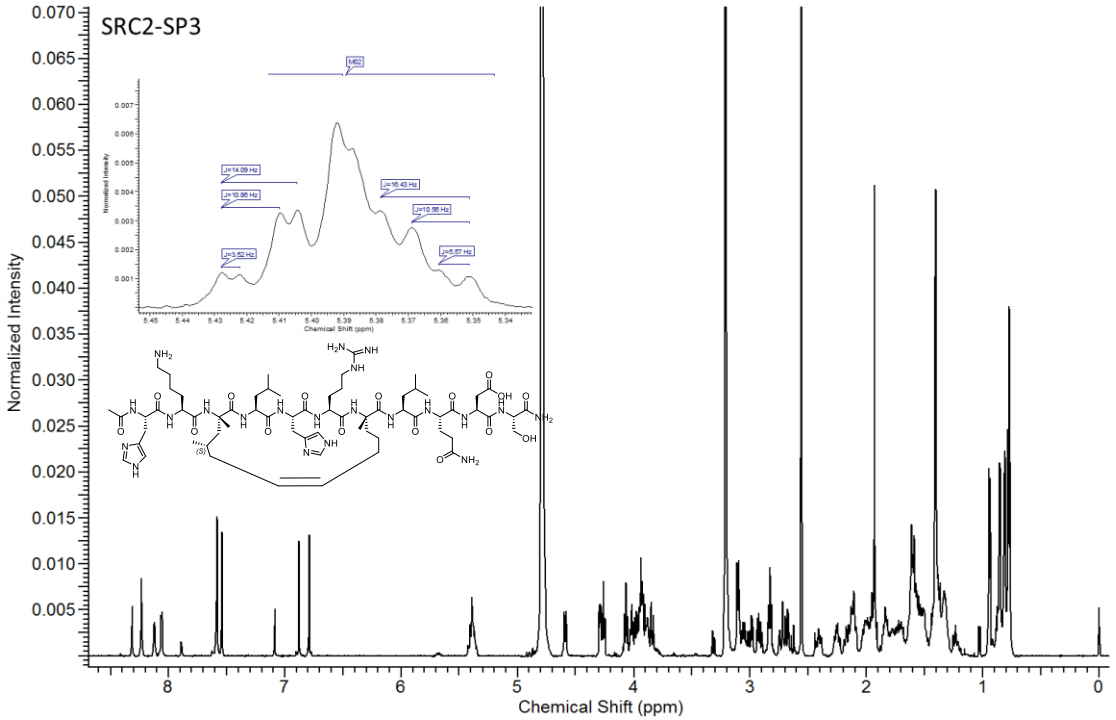

Figure 2.13. ^{1}H NMR spectra for SRC2-SP3 in CD_3OD. The apparent coupling constants for the alkene protons are δ = 5.42 (ddd, *J* = 10.9, 10.9, 3.5 Hz, 1 H), 5.37 (ddd, *J* = 10.6, 10.6, 5.6 Hz, 1 H).

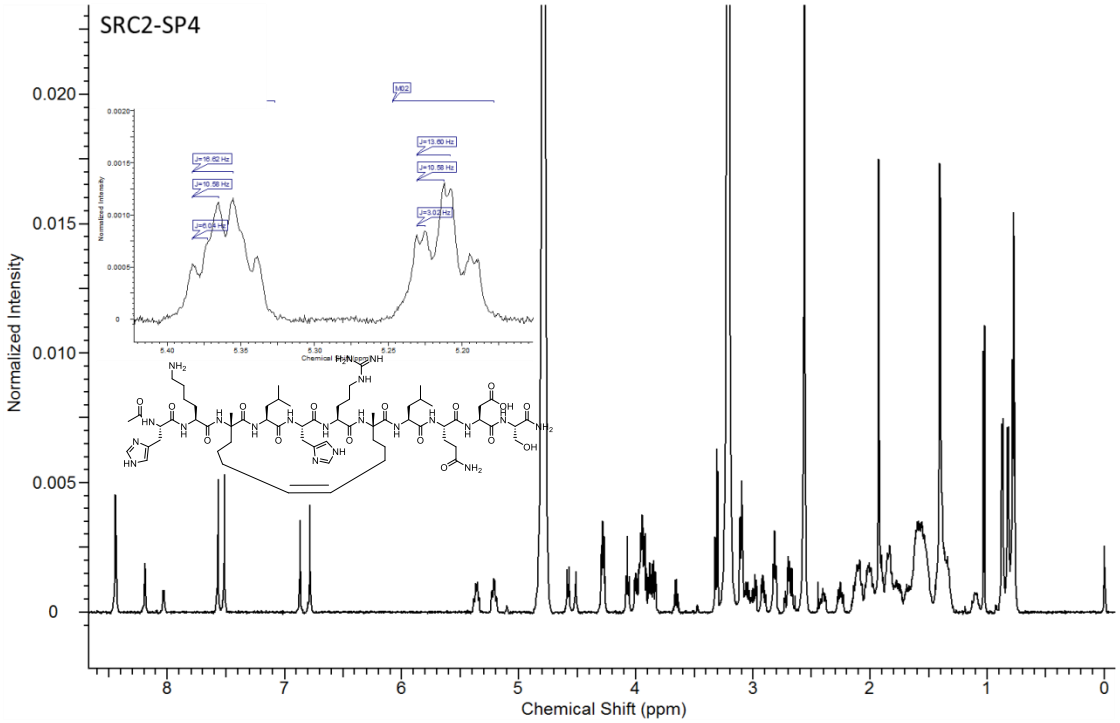

Figure 2.14 ^{1}H NMR spectra for SRC2-SP4 in CD_3OD. The apparent coupling constants for the alkene protons are δ = 5.36 (ddd, *J* = 10.6, 10.6, 6.0 Hz, 1 H), 5.21 (ddd, *J* = 10.6, 10.6, 3.0 Hz, 1 H).

TABLE II. TR-FRET STATISTICAL INFORMATION FOR BEST-FIT VALUES

	SRC2-SP1	SRC2-SP2	SRC2-SP3	SRC2-WT	SRC2-SP4	SRC2-P5	PFizer SP2
Sigmoidal, 4PL,							
X is log(concentration)							
Best-fit values							
Top	0.5248	0.4827	0.4965	0.5044	0.4956	0.4878	0.5114
Bottom	0.002988	0.02142	0.0365	0.02447	0.01778	0.02561	0.05688
LogIC50	-5.744	-7.018	-7.04	-5.965	-6.411	-5.912	-6.121
HillSlope	-0.7228	-1.043	-1.044	-1.032	-0.8722	-1.073	-1.022
IC50	0.000001802	9.587E-08	9.117E-08	0.000001085	3.882E-07	0.000001224	7.575E-07
Span	0.5218	0.4613	0.46	0.4799	0.4779	0.4622	0.4545
Std. Error							
Top	0.01026	0.008562	0.009011	0.007535	0.007867	0.008219	0.008392
Bottom	0.05015	0.01	0.0104	0.021	0.01569	0.02335	0.01989
LogIC50	0.1542	0.04971	0.05205	0.06601	0.06509	0.07427	0.07171
HillSlope	0.1282	0.1116	0.1198	0.1395	0.09551	0.1653	0.1462
95% Confidence Intervals							
Top	0.5039 to 0.5457	0.4652 to 0.5001	0.4781 to 0.5149	0.4890 to 0.5198	0.4796 to 0.5117	0.4710 to 0.5045	0.4943 to 0.5285
Bottom	-0.09921 to 0.1052	0.001039 to 0.04180	0.01528 to 0.05772	-0.01837 to 0.06731	-0.01422 to 0.04979	-0.02197 to 0.07319	0.01635 to 0.09741
LogIC50	-6.059 to -5.430	-7.120 to -6.917	-7.146 to -6.934	-6.099 to -5.830	-6.544 to -6.278	-6.064 to -5.761	-6.267 to -5.974
HillSlope	-0.9841 to -0.4614	-1.271 to -0.8157	-1.289 to -0.8000	-1.316 to -0.7471	-1.067 to -0.6773	-1.410 to -0.7361	-1.320 to -0.7239
IC50	8.73e-7 to 3.71e-6	7.59e-8 to 1.21e-7	7.13e-8 to 1.16e-7	7.95e-7 to 1.47e-6	2.86e-7 to 5.27e-7	8.63e-7 to 1.73e-6	5.41e-7 to 1.06e-6
Span	0.4101 to 0.6335	0.4322 to 0.4904	0.4296 to 0.4904	0.4315 to 0.5284	0.4386 to 0.5171	0.4085 to 0.5158	0.4073 to 0.5016
Goodness of Fit							
Degrees of Freedom	32	32	31	31	31	32	32
R square	0.9601	0.9832	0.9818	0.9757	0.9824	0.9667	0.9698
Absolute Sum of Squares	0.03969	0.02342	0.02478	0.02756	0.02177	0.03539	0.03334

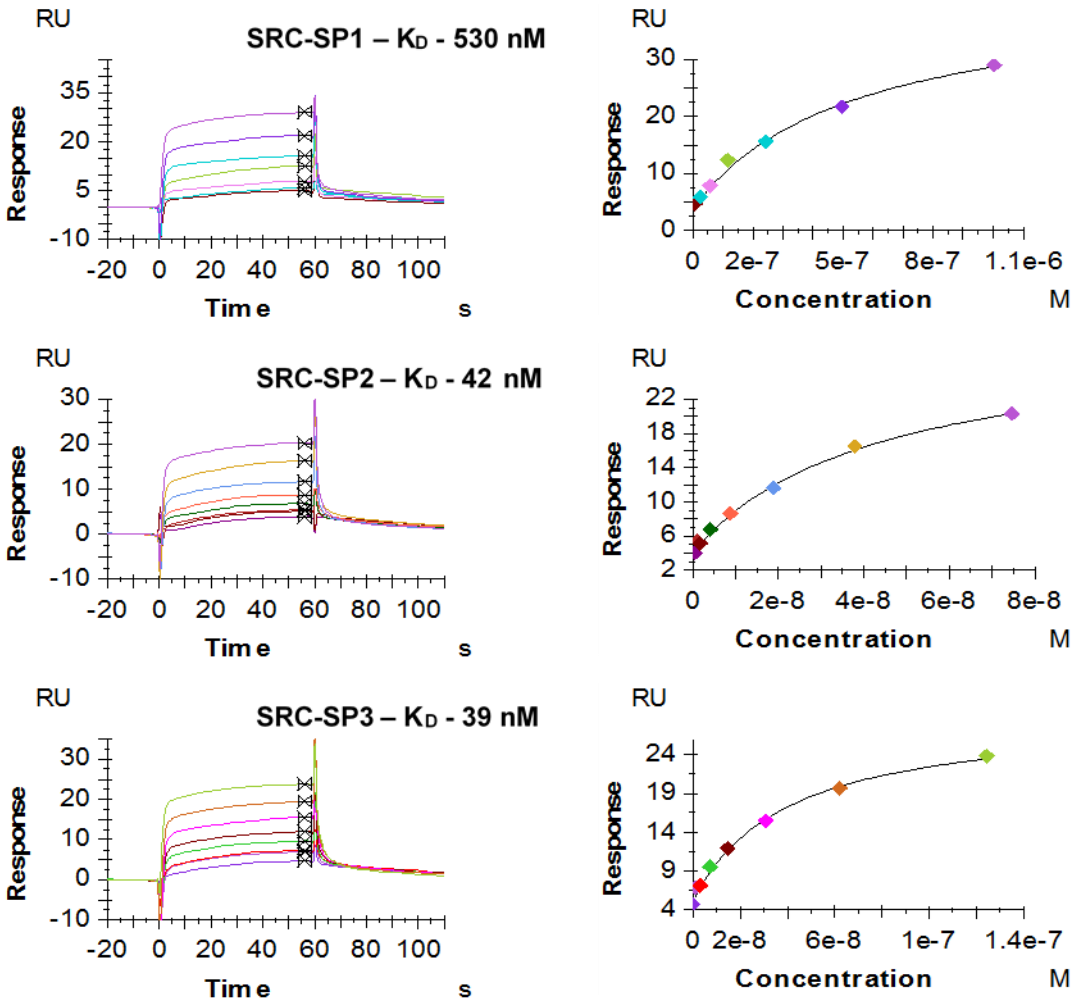

Figure 2.15. SPR sensorgrams and binding curves.

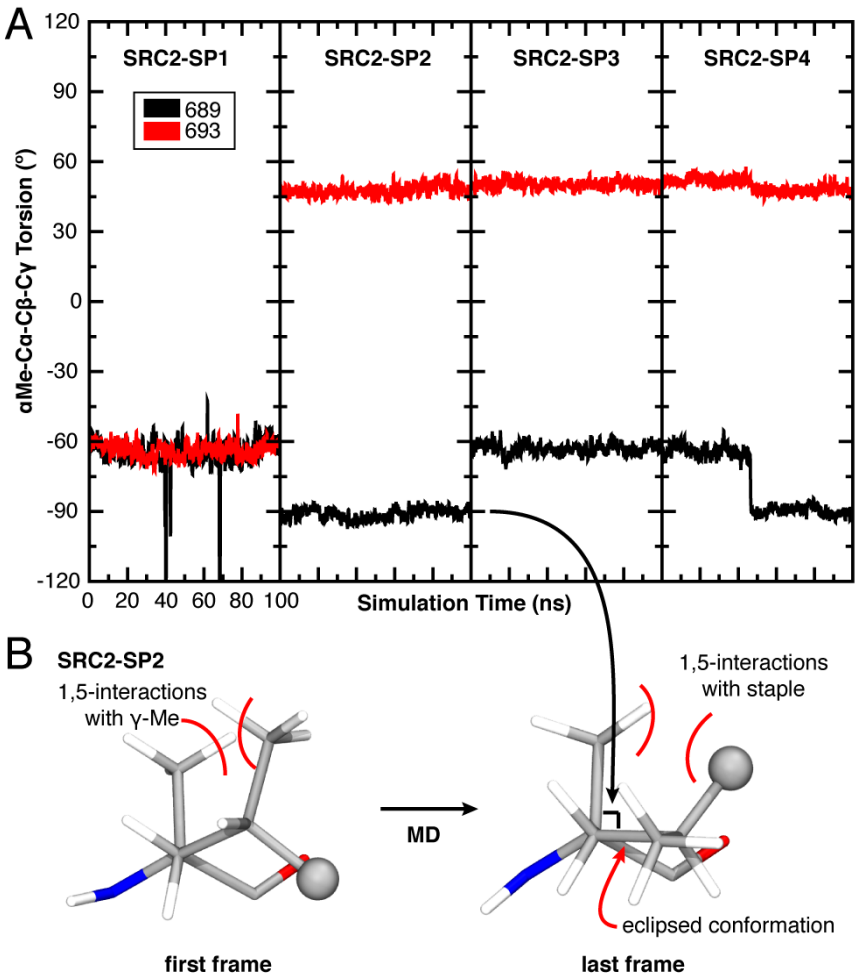

Figure 2.16. Cα-Cβ torsional profile of the staple residues in solution. The αMe-Cα-Cβ-Cγ dihedral angle for residues 689 and 693 is dependent on the position (689 vs. 693) and the stereochemical configuration (*R* vs. *S*) of the γ-Me branch (A). The torsional profile for SRC2-SP1 (A, left) and SRC2-SP3 (A, third panel) match those measured for the receptor-bound peptides (Figure 2.9A), indicating that receptor binding of the peptide does not significantly perturb the internal staple structure. SRC2-SP2 (second panel) and SRC2-SP4 (right) exhibit a unique conformation at residue 689 (B), in which unfavorable 1,5-interactions for both the γ-Me and the staple result in a shift of the dihedral (A, second panel) towards an eclipsed conformation.

Figure 2.17. ^{1}H and ^{13}C NMR spectra for compound **1**

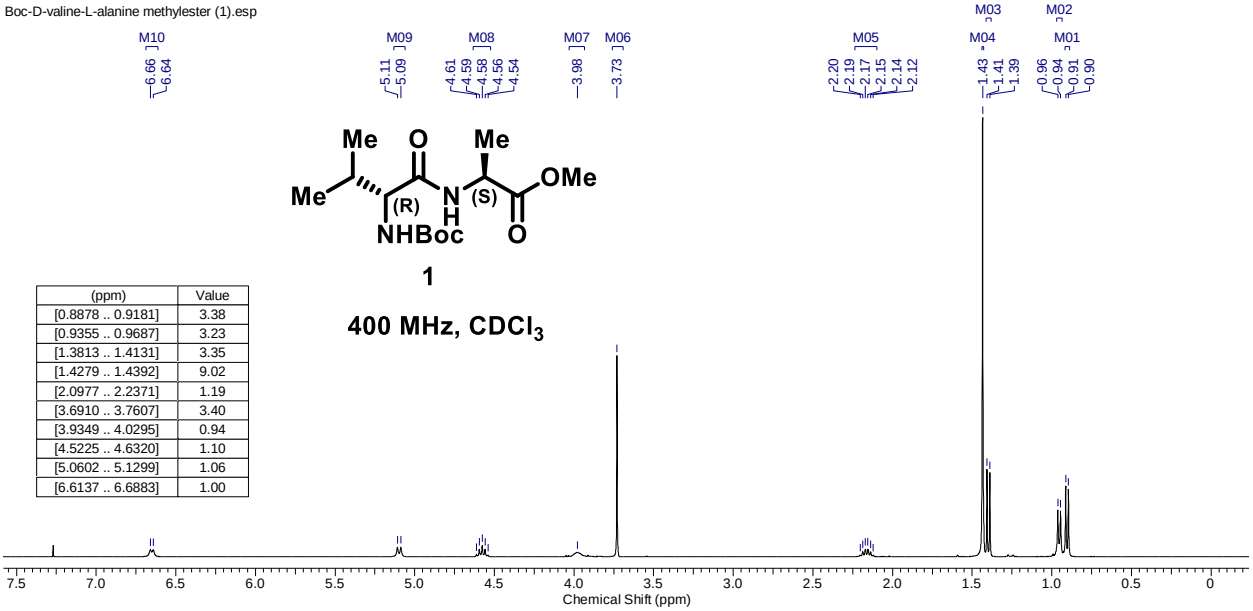

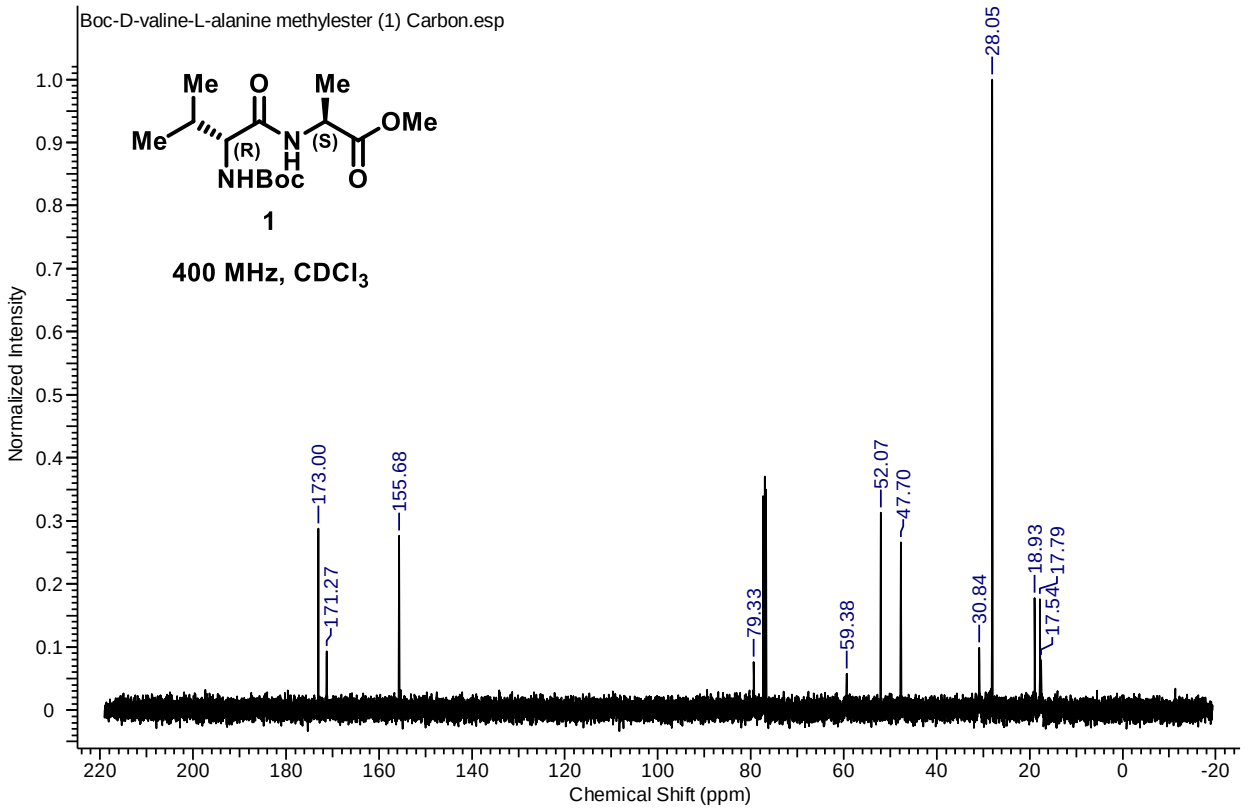

Figure 2.18 ^{1}H and ^{13}C NMR spectra for compound **2**

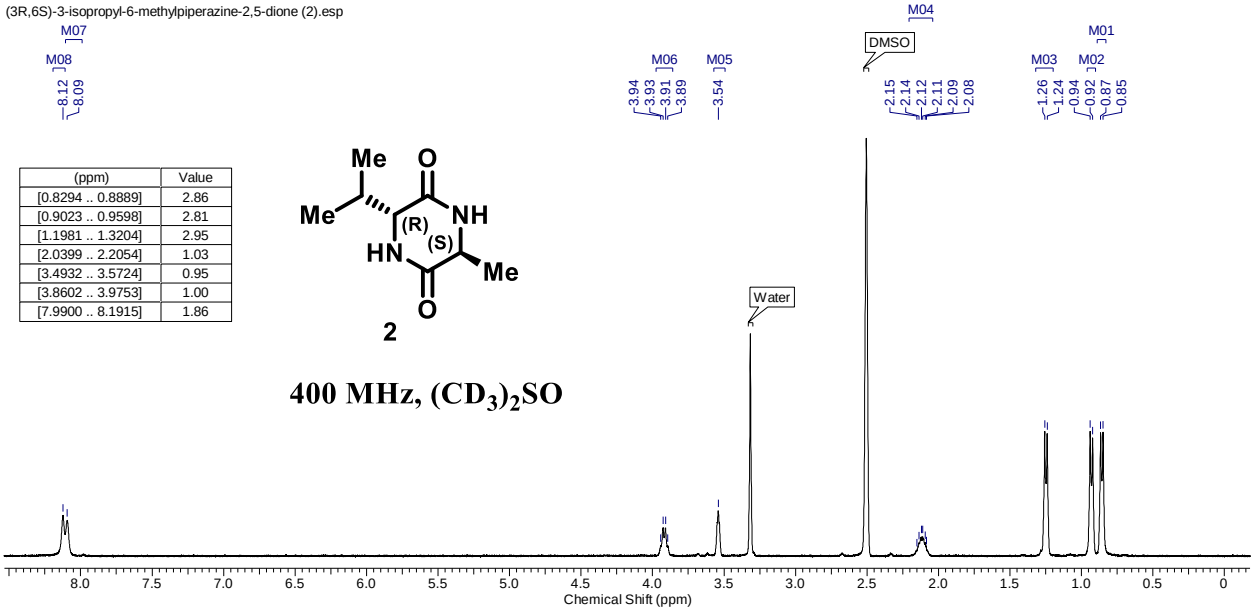

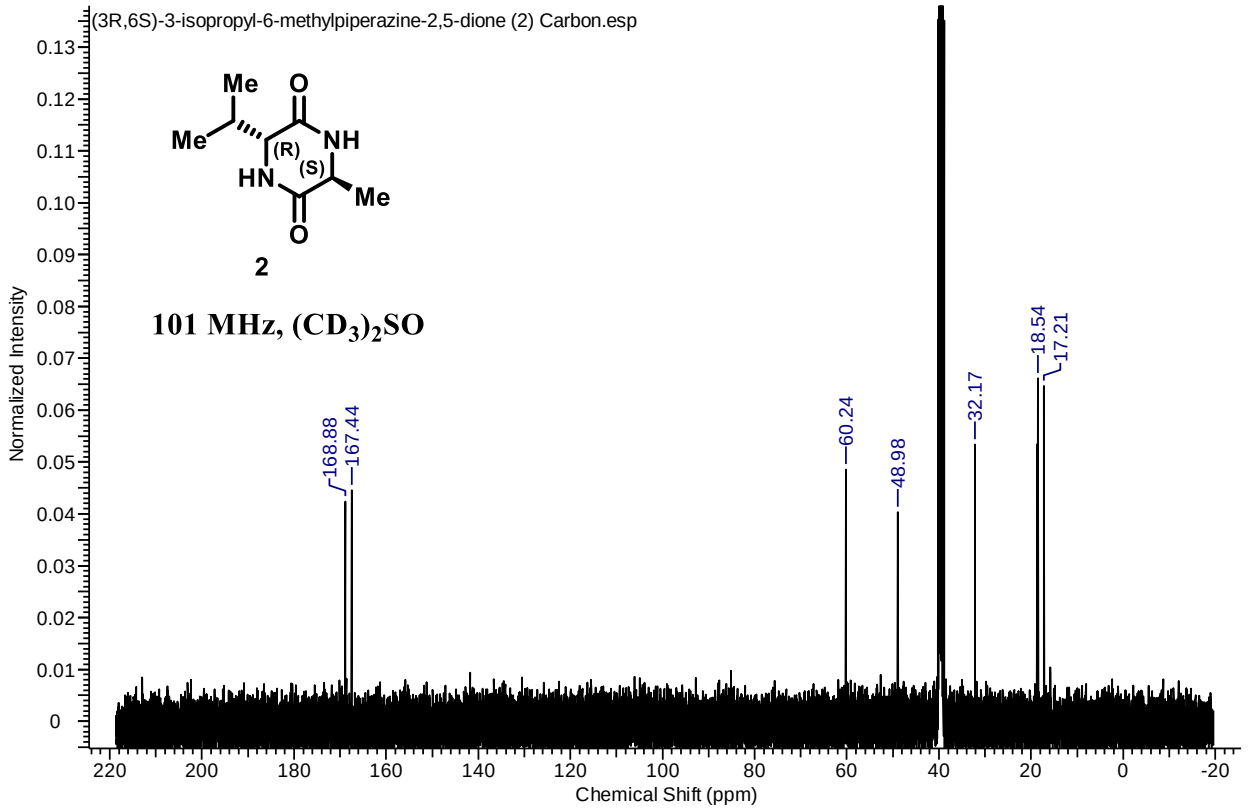

Figure 2.19 ^{1}H and ^{13}C NMR spectra for compound **3**

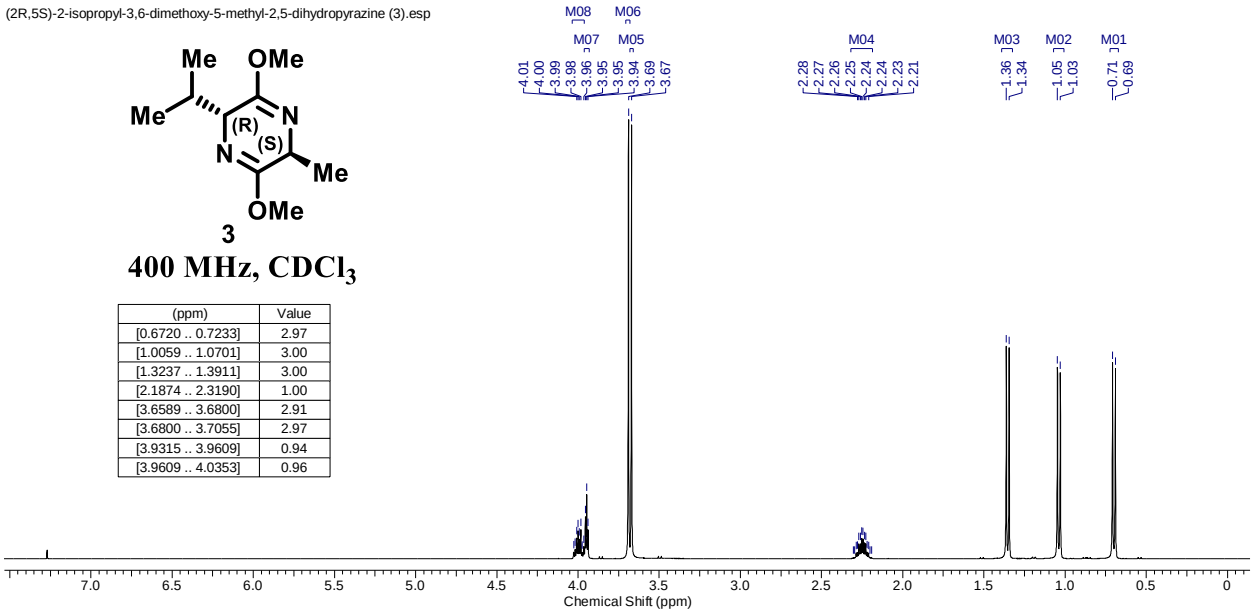

(ppm)	Value
[0.6720 .. 0.7233]	2.97
[1.0059 .. 1.0701]	3.00
[1.3237 .. 1.3911]	3.00
[2.1874 .. 2.3190]	1.00
[3.6589 .. 3.6800]	2.91
[3.6800 .. 3.7055]	2.97
[3.9315 .. 3.9609]	0.94
[3.9609 .. 4.0353]	0.96

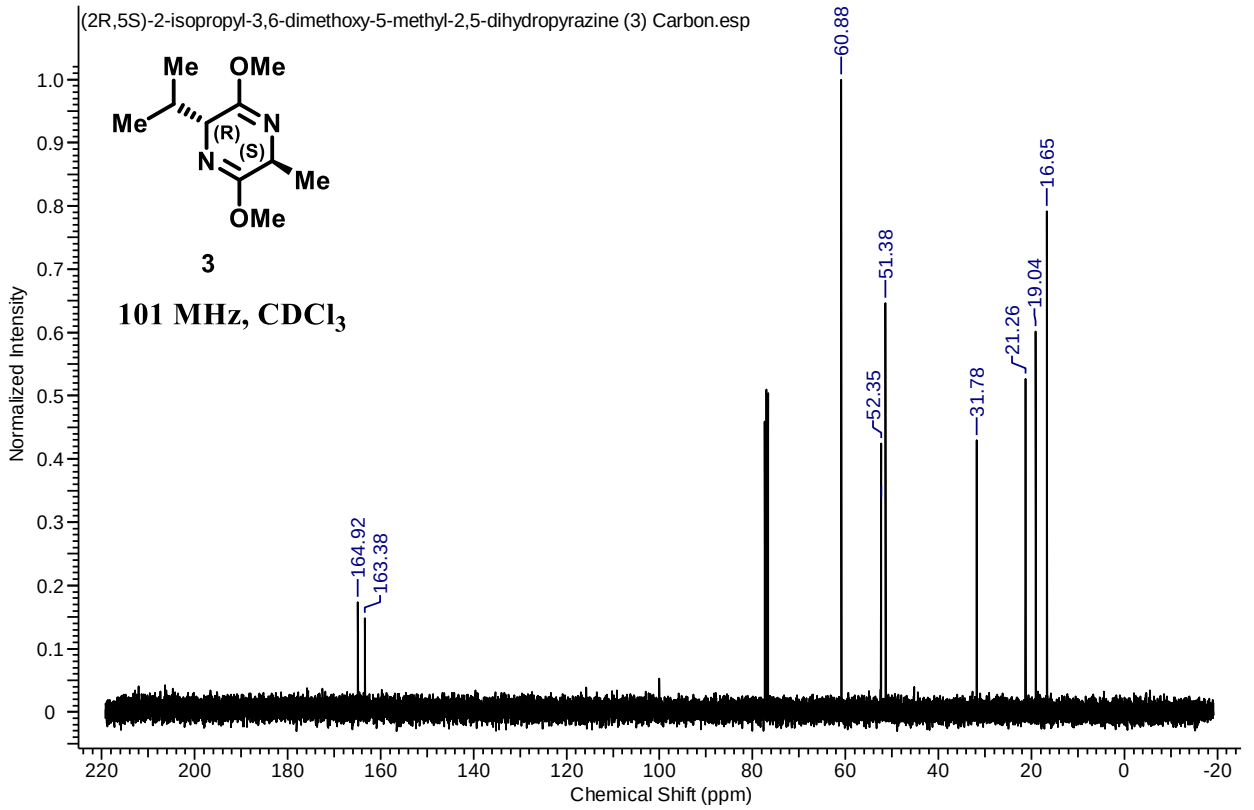

Figure 2.20 ^{1}H and ^{13}C NMR spectra for compound **4a**

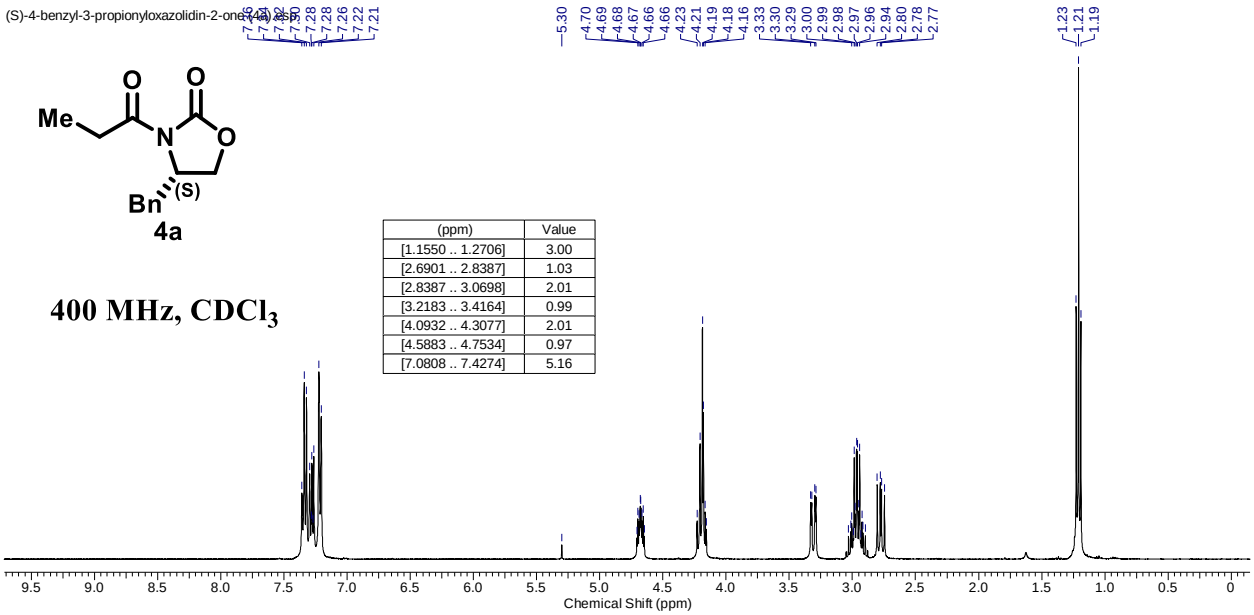

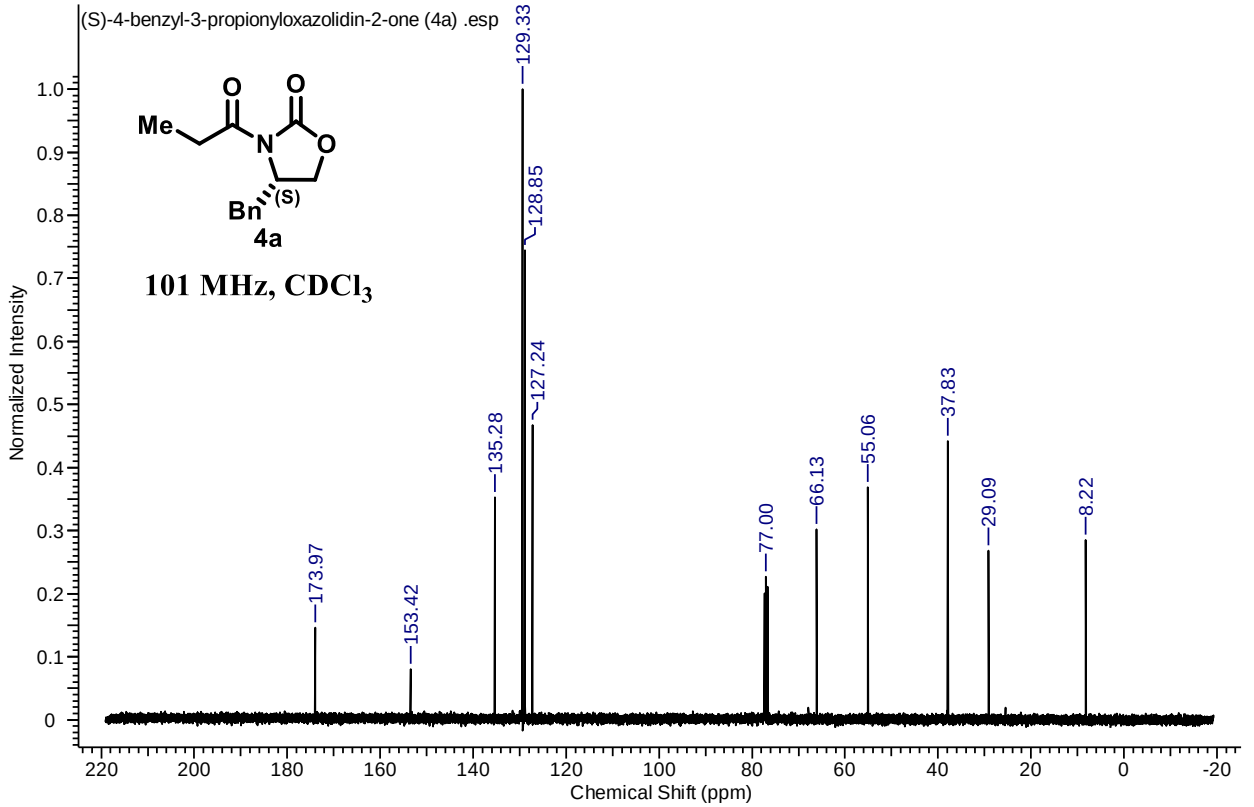

Figure 2.21 ^{1}H and ^{13}C NMR spectra for compound **4b**

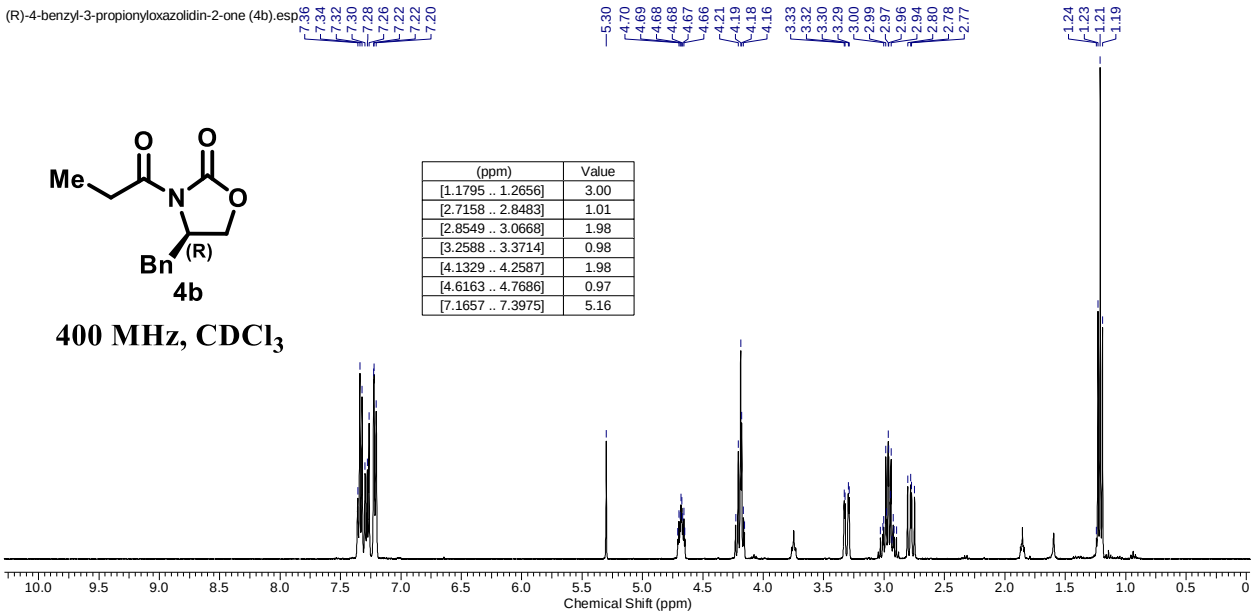

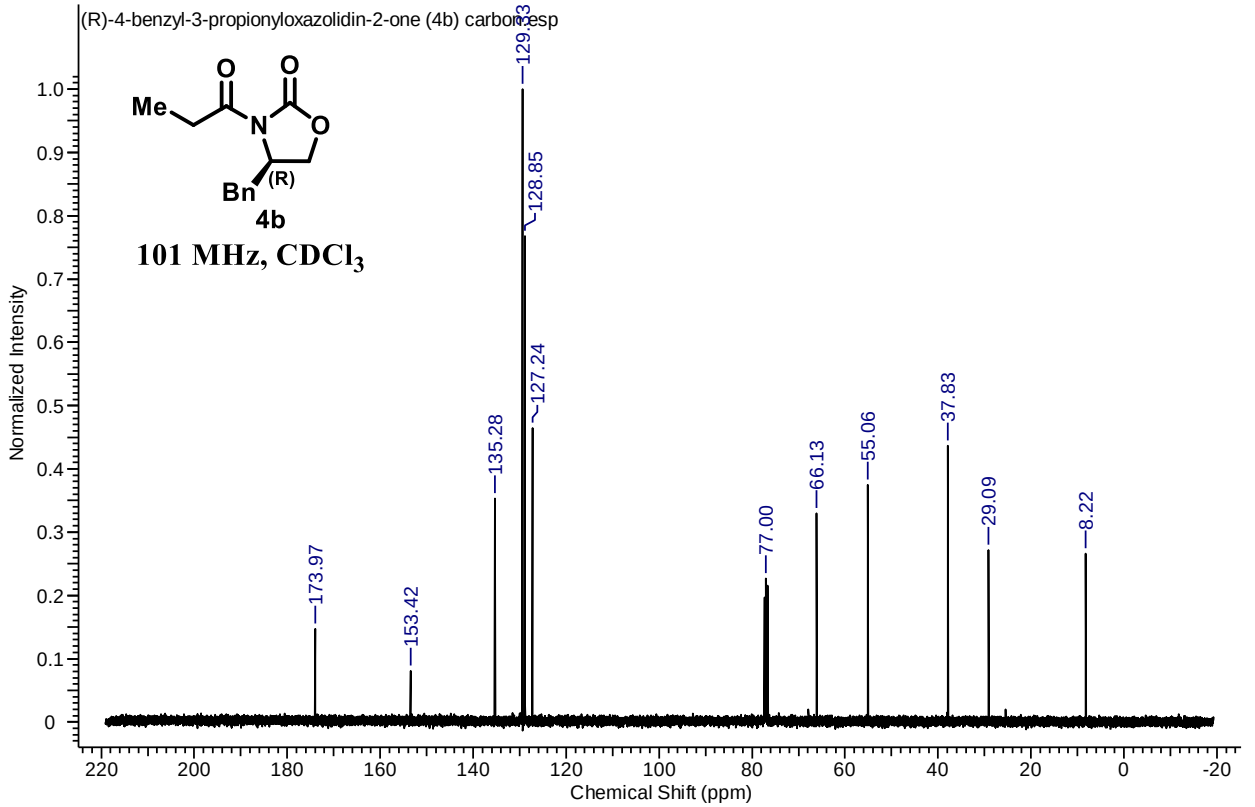

Figure 2.22 ^{1}H and ^{13}C NMR spectra for compound **5a**

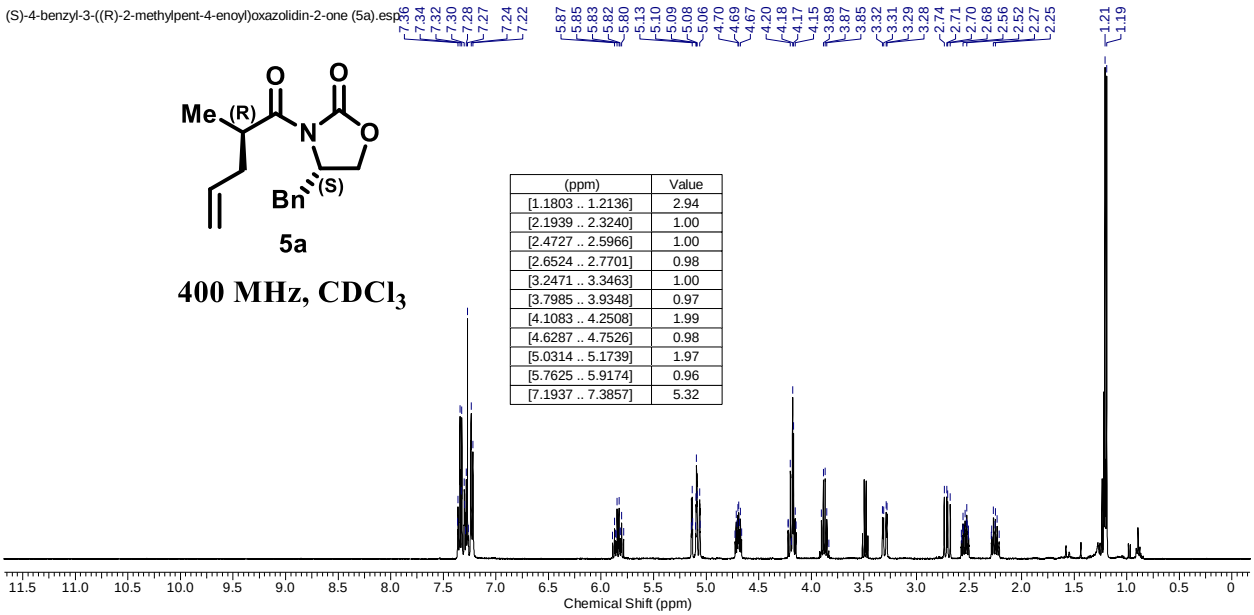

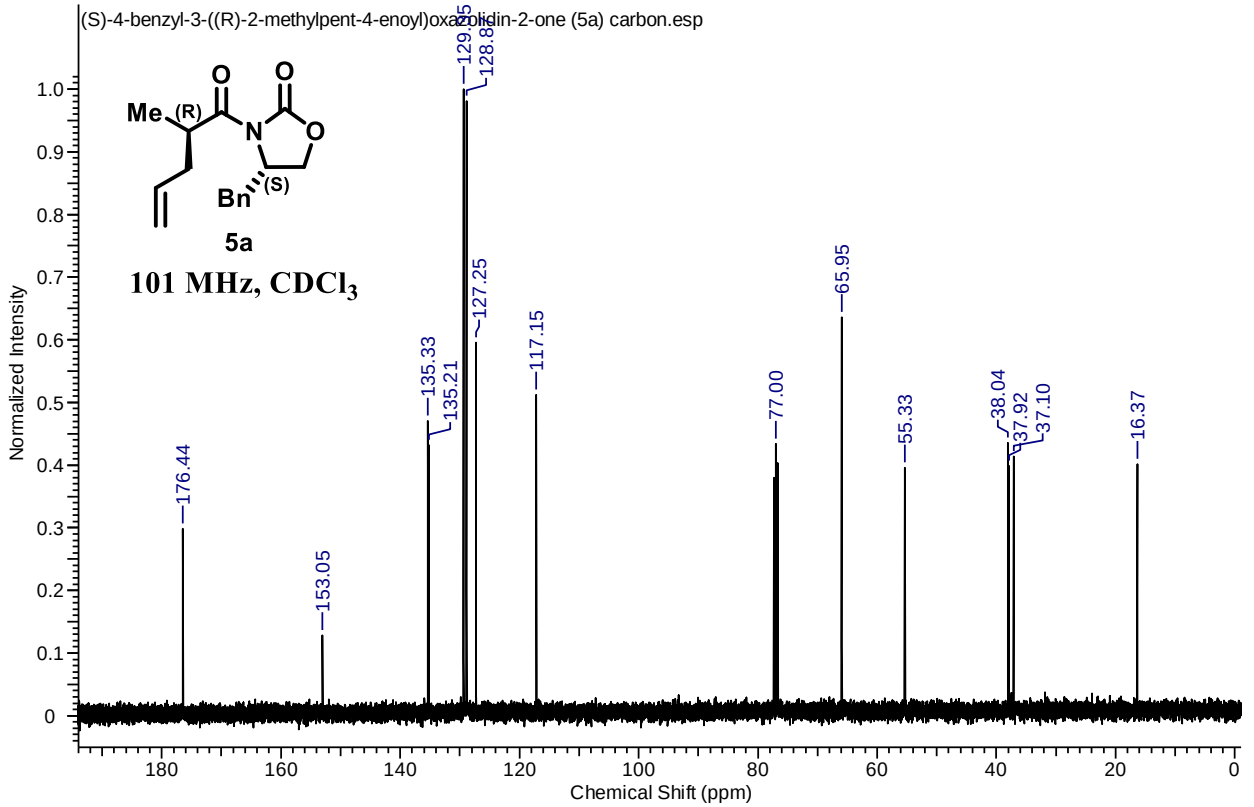

Figure 2.22 ^{1}H and ^{13}C NMR spectra for compound **5b**

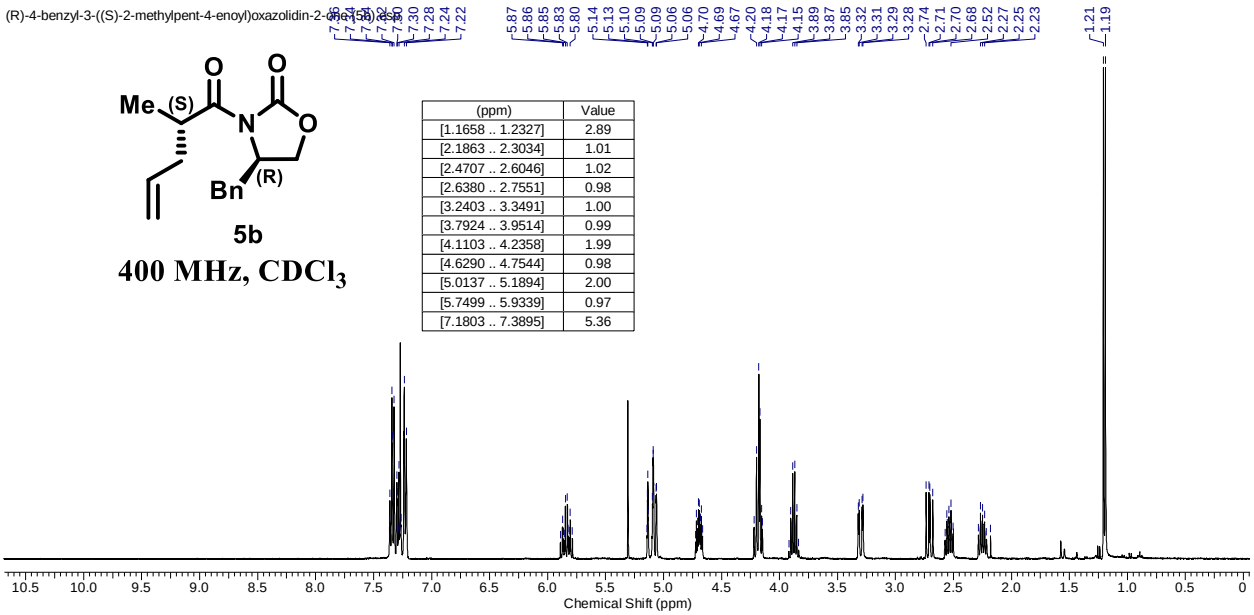

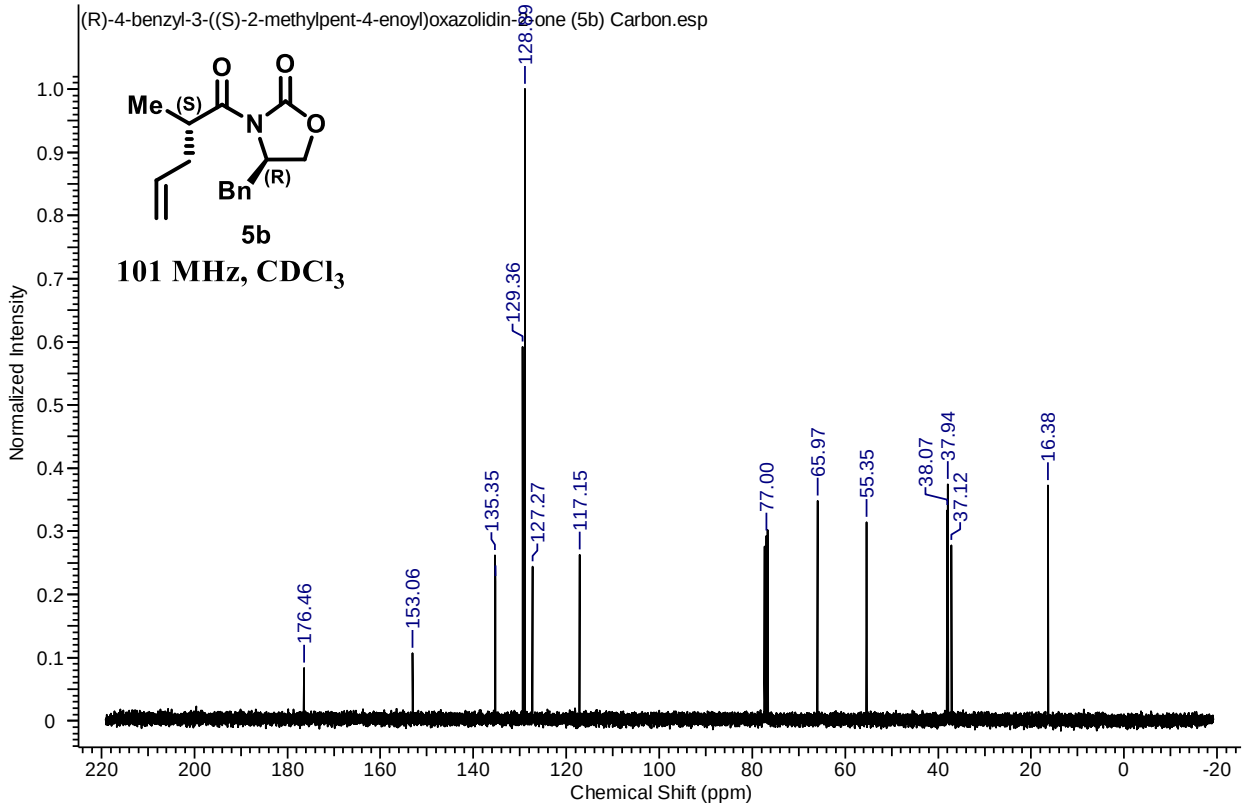

Figure 2.23 ^{1}H and ^{13}C NMR spectra for compound **6a**

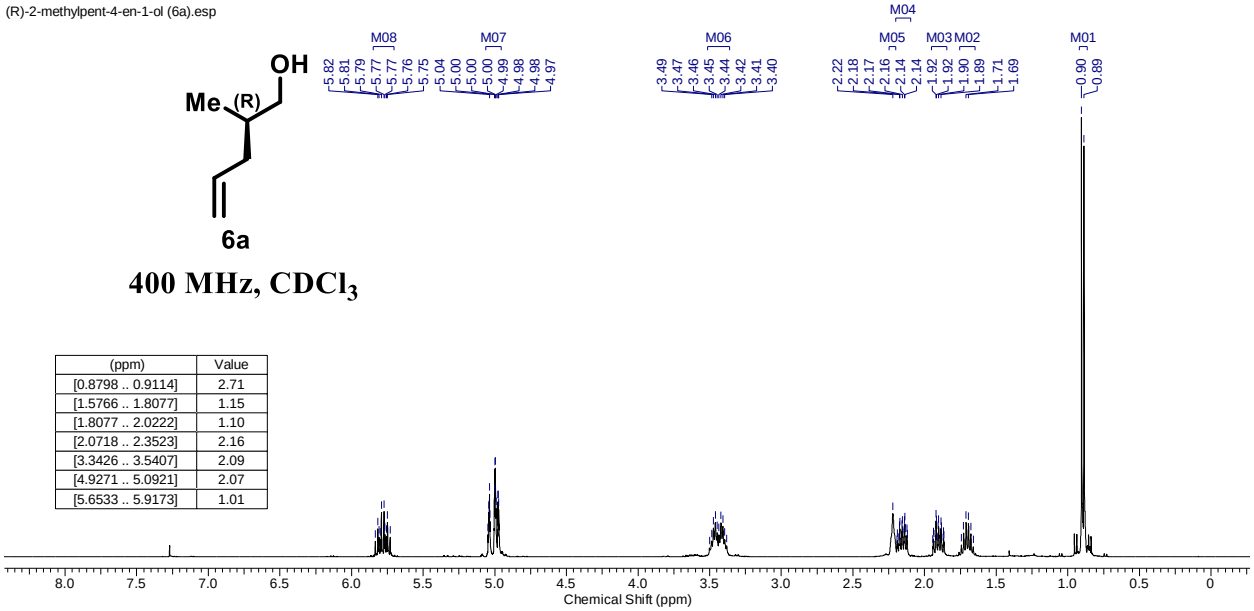

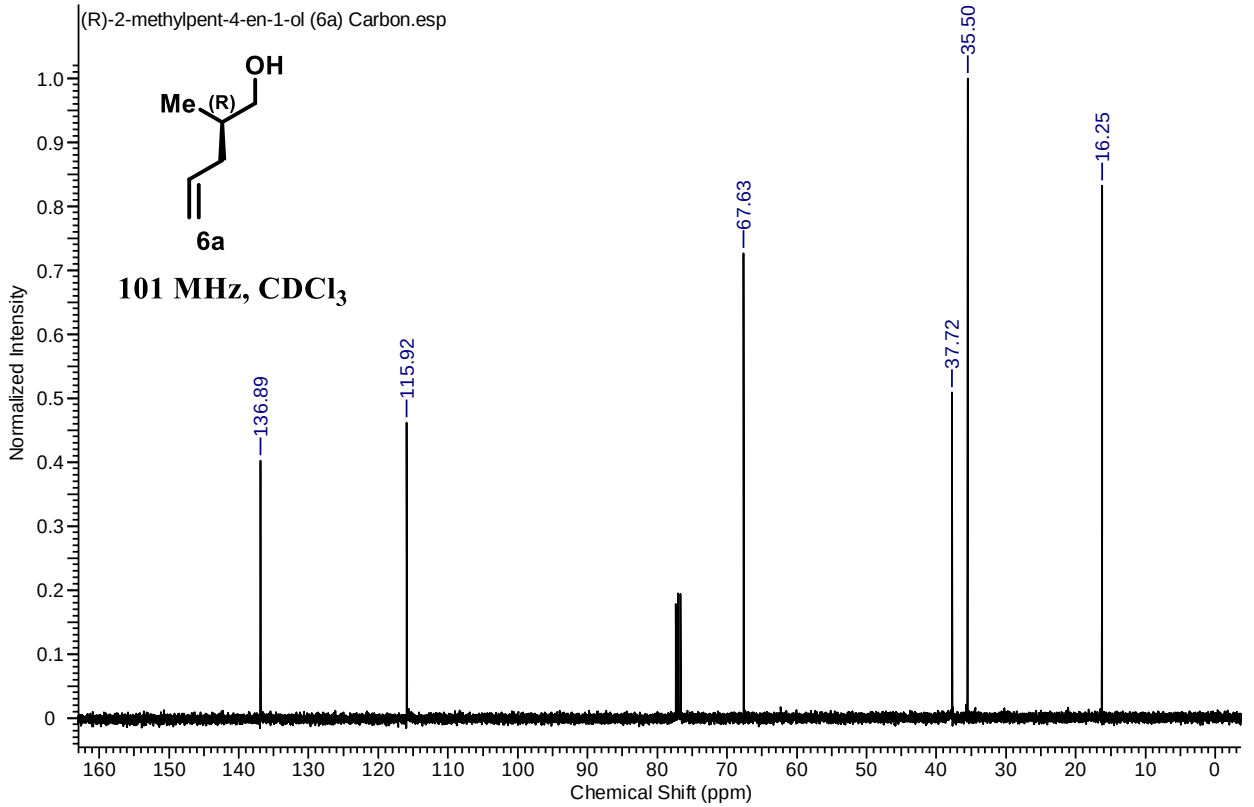

Figure 2.24 ^{1}H and ^{13}C NMR spectra for compound **6b**

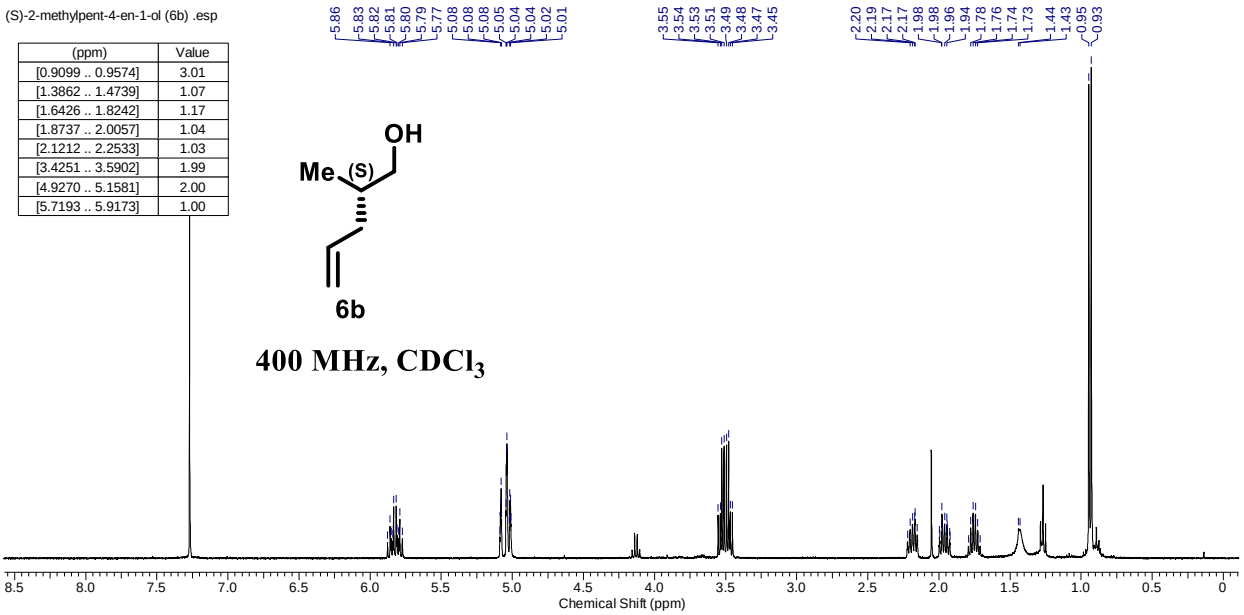

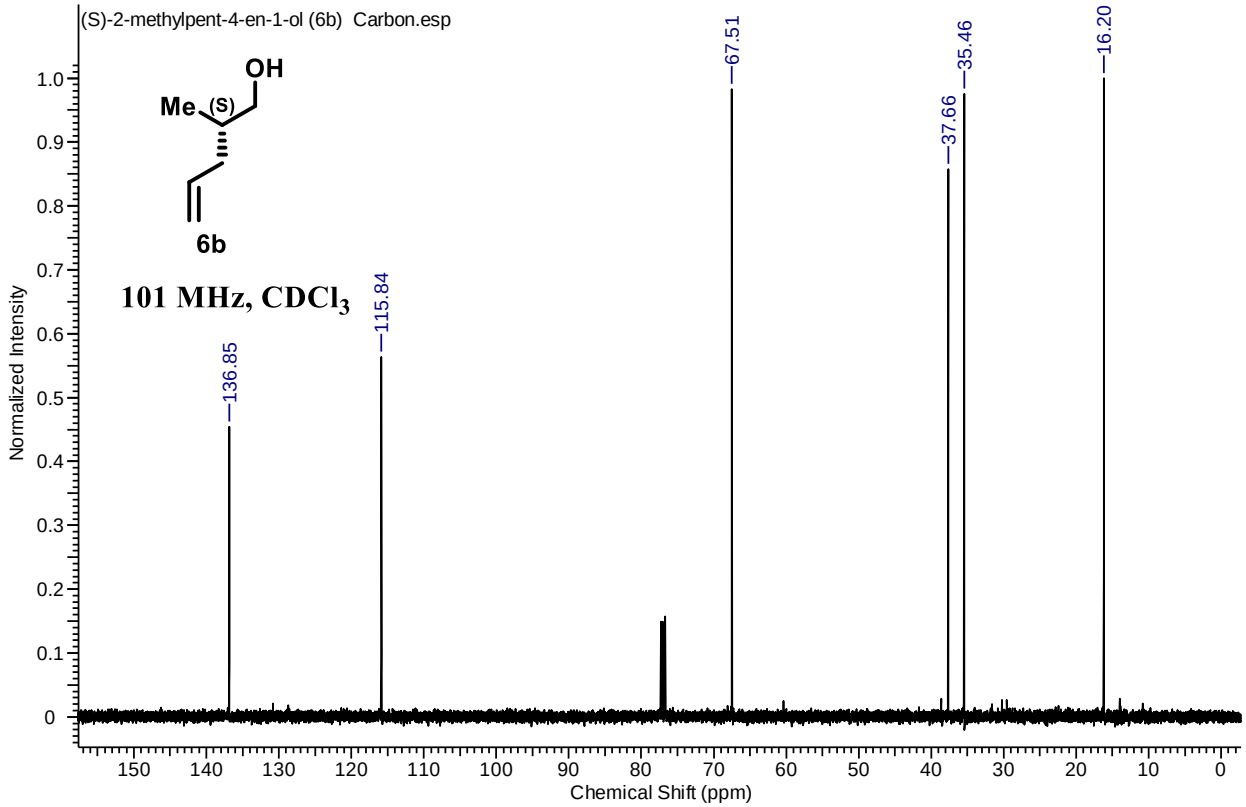

Figure 2.25 ^{1}H and ^{13}C NMR spectra for compound **8a**

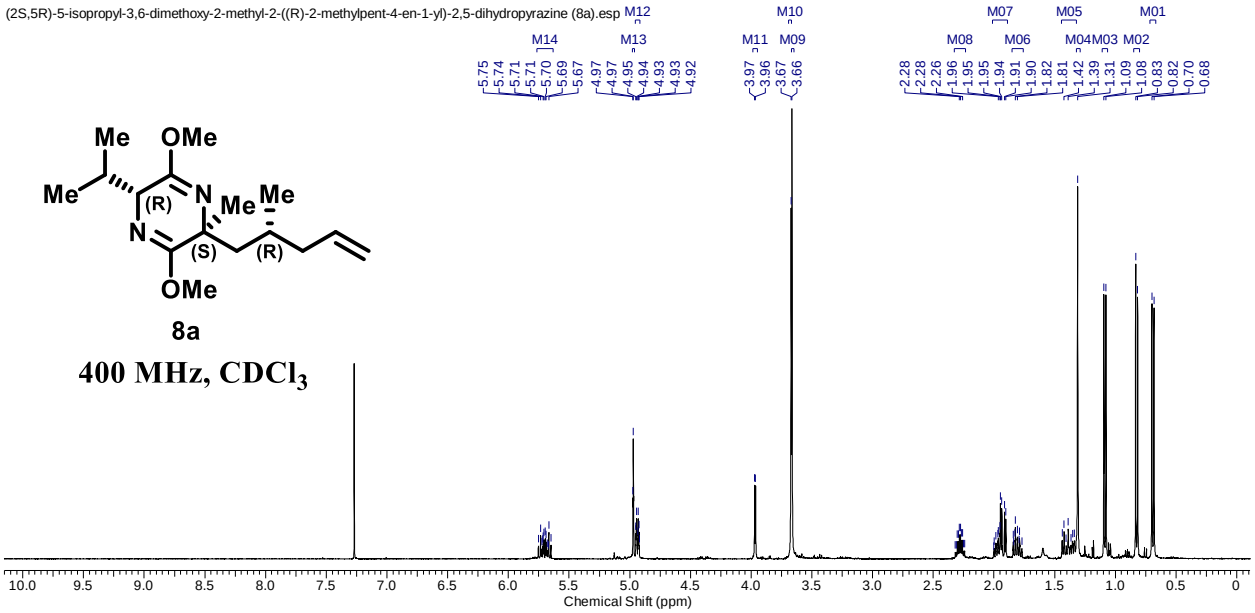

(ppm)	Value
[0.6661 .. 0.7139]	3.13
[0.8022 .. 0.8475]	3.02
[1.0647 .. 1.1101]	3.11

(ppm)	Value
[1.2907 .. 1.3196]	3.05
[1.3196 .. 1.4447]	2.07
[1.7594 .. 1.8525]	1.11

(ppm)	Value
[1.8883 .. 2.0124]	2.11
[2.2344 .. 2.3251]	1.00
[3.6463 .. 3.6665]	3.26

(ppm)	Value
[3.6665 .. 3.6918]	2.90
[3.9488 .. 3.9867]	0.98
[4.9172 .. 4.9544]	0.98

(ppm)	Value
[4.9620 .. 4.9781]	1.00
[5.6331 .. 5.7658]	1.05

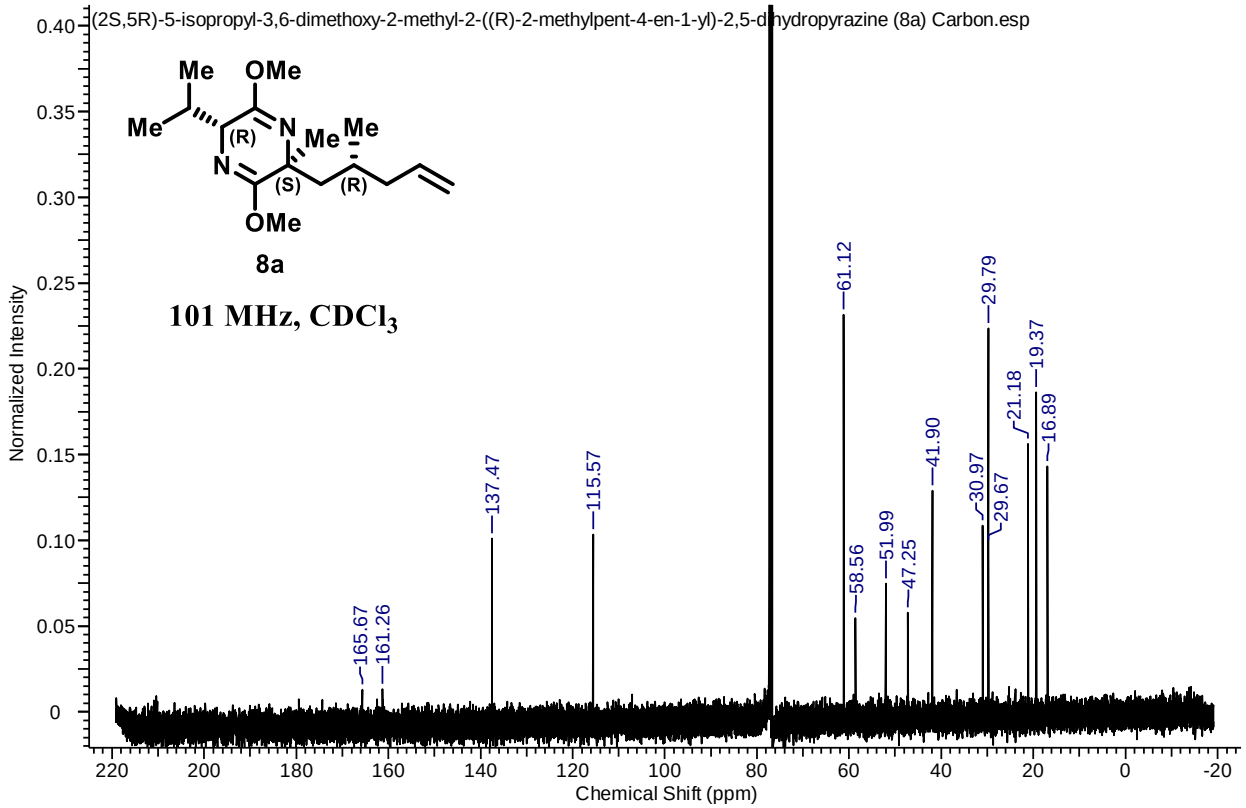

Figure 2.26 ^{1}H and ^{13}C NMR spectra for compound **8b**

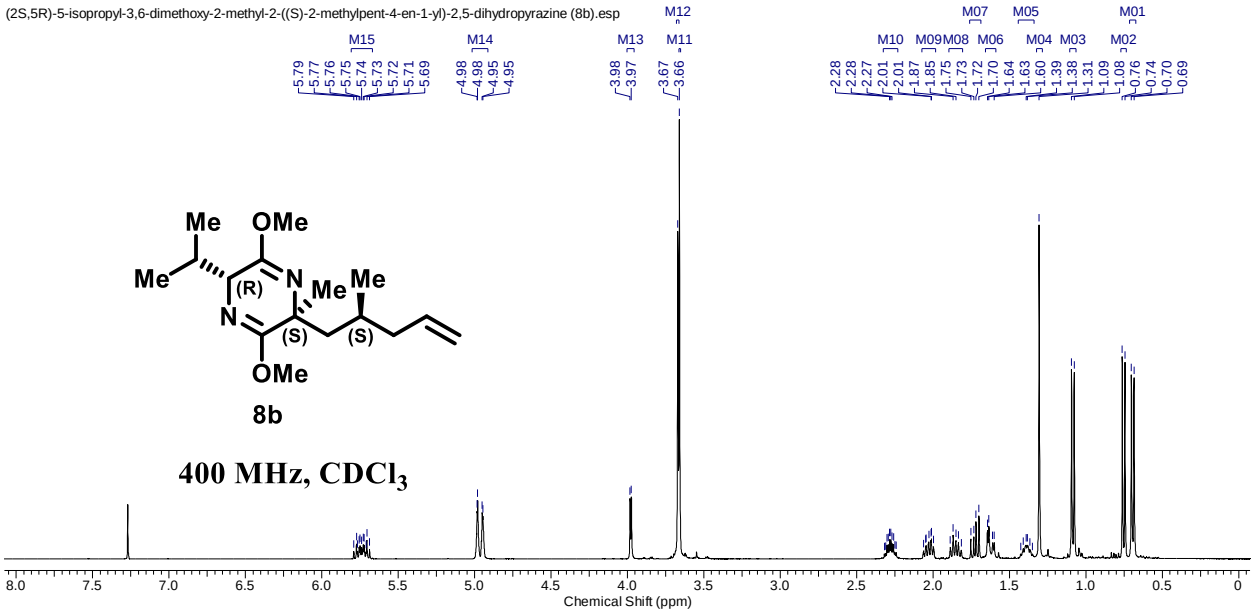

(ppm)	Value	(ppm)	Value	(ppm)	Value	(ppm)	Value	(ppm)	Value
[0.6731 .. 0.7142]	3.17	[1.2855 .. 1.3226]	3.06	[1.6865 .. 1.7609]	1.02	[2.2304 .. 2.3263]	1.01	[3.9557 .. 4.0026]	0.99
[0.7357 .. 0.7709]	2.96	[1.3402 .. 1.4420]	1.07	[1.8059 .. 1.8978]	1.04	[3.6519 .. 3.6643]	3.18	[4.9126 .. 5.0158]	2.07
[1.0644 .. 1.1055]	3.14	[1.5887 .. 1.6572]	1.21	[1.9839 .. 2.0720]	1.00	[3.6643 .. 3.6793]	2.95	[5.6677 .. 5.8085]	1.00

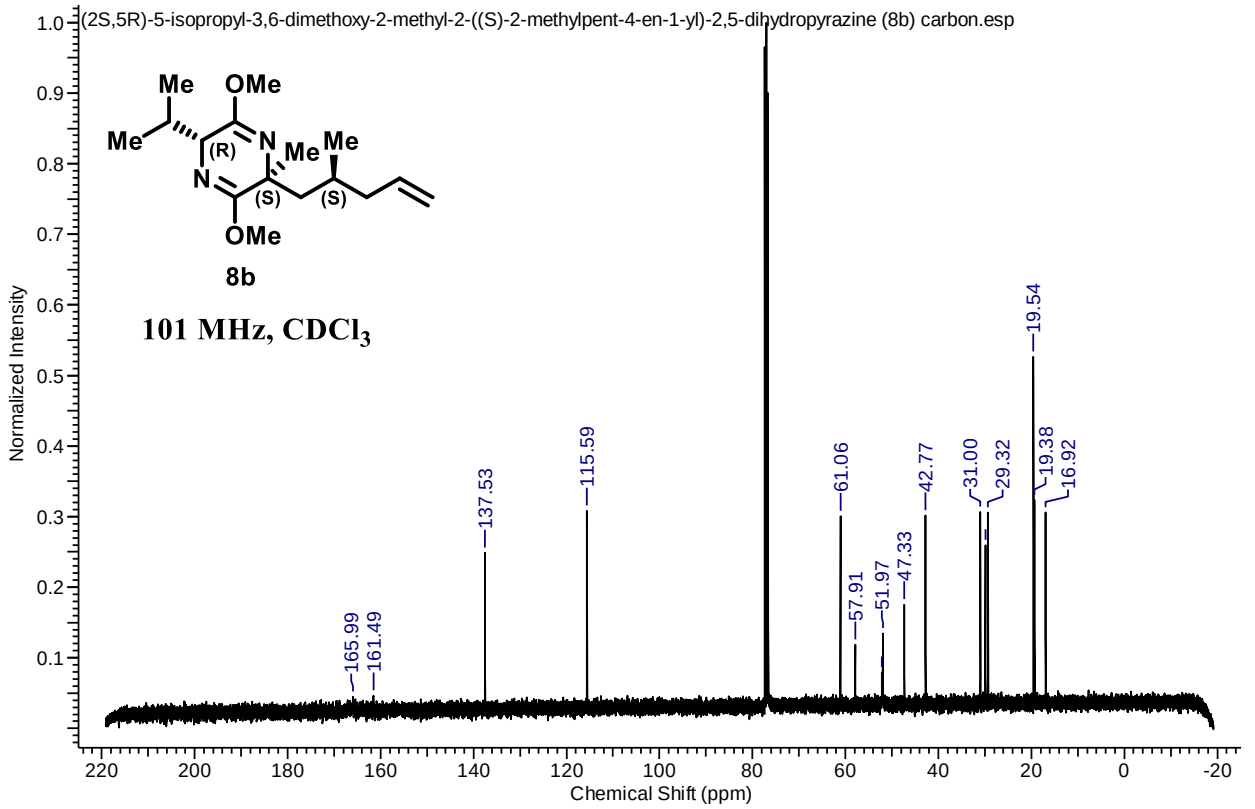

Figure 2.27 ^{1}H and ^{13}C NMR spectra for compound **9a**

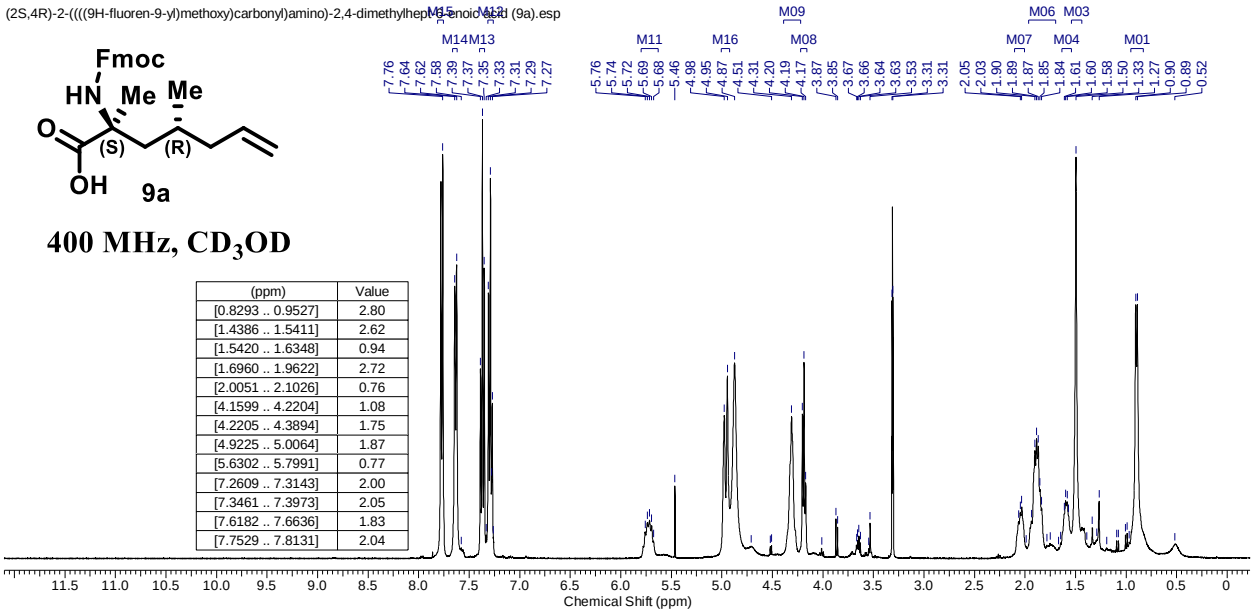

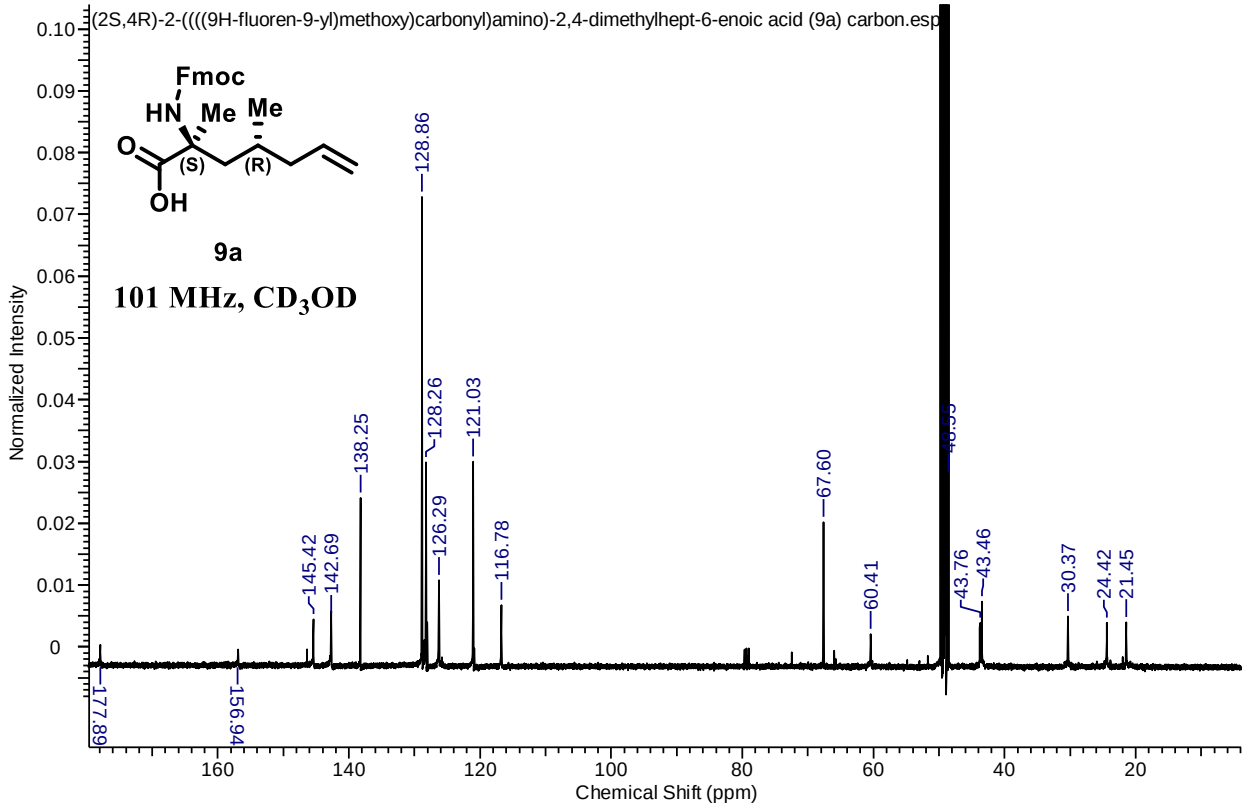

Figure 2.28 ^{1}H and ^{13}C NMR spectra for compound **9b**

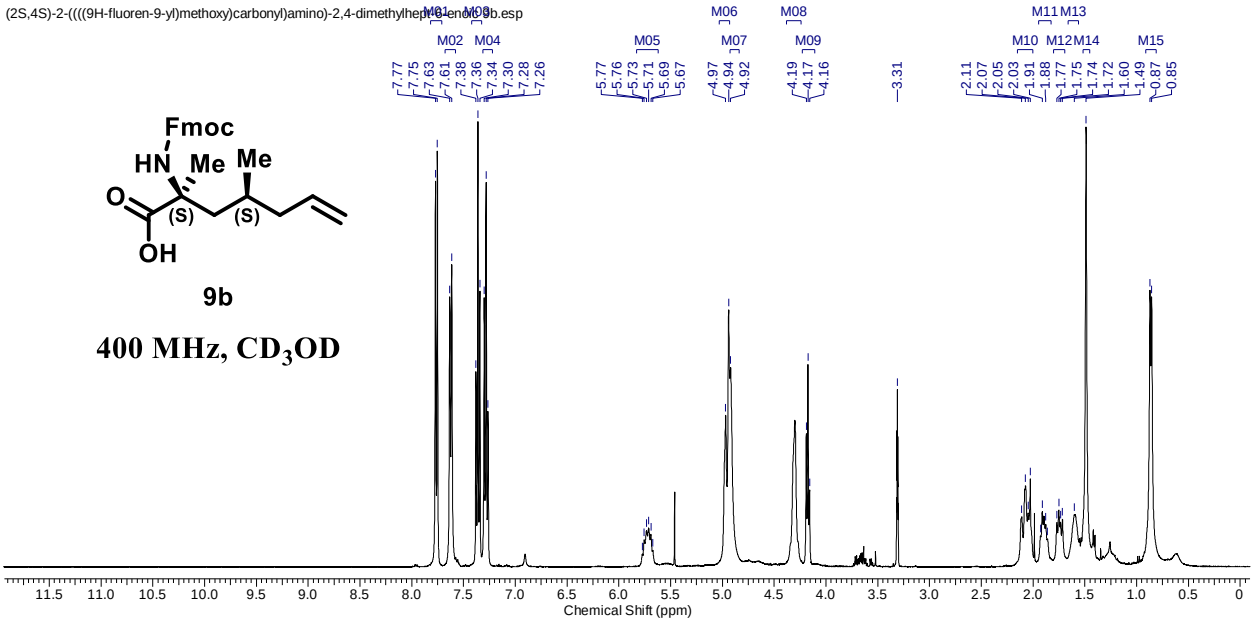

(ppm)	Value	(ppm)	Value	(ppm)	Value	(ppm)	Value	(ppm)	Value
[0.8231 .. 0.8916]	2.86	[1.6857 .. 1.7991]	1.00	[4.1554 .. 4.1981]	1.10	[4.9590 .. 4.9929]	1.04	[7.3389 .. 7.3809]	2.05
[1.4369 .. 1.5345]	2.98	[1.8243 .. 1.9629]	1.07	[4.2524 .. 4.3658]	1.88	[5.6425 .. 5.8021]	0.89	[7.6059 .. 7.6583]	2.06
[1.5551 .. 1.6689]	1.07	[1.9965 .. 2.1519]	1.87	[4.8998 .. 4.9386]	2.01	[7.2586 .. 7.3031]	2.03	[7.7511 .. 7.8095]	1.84

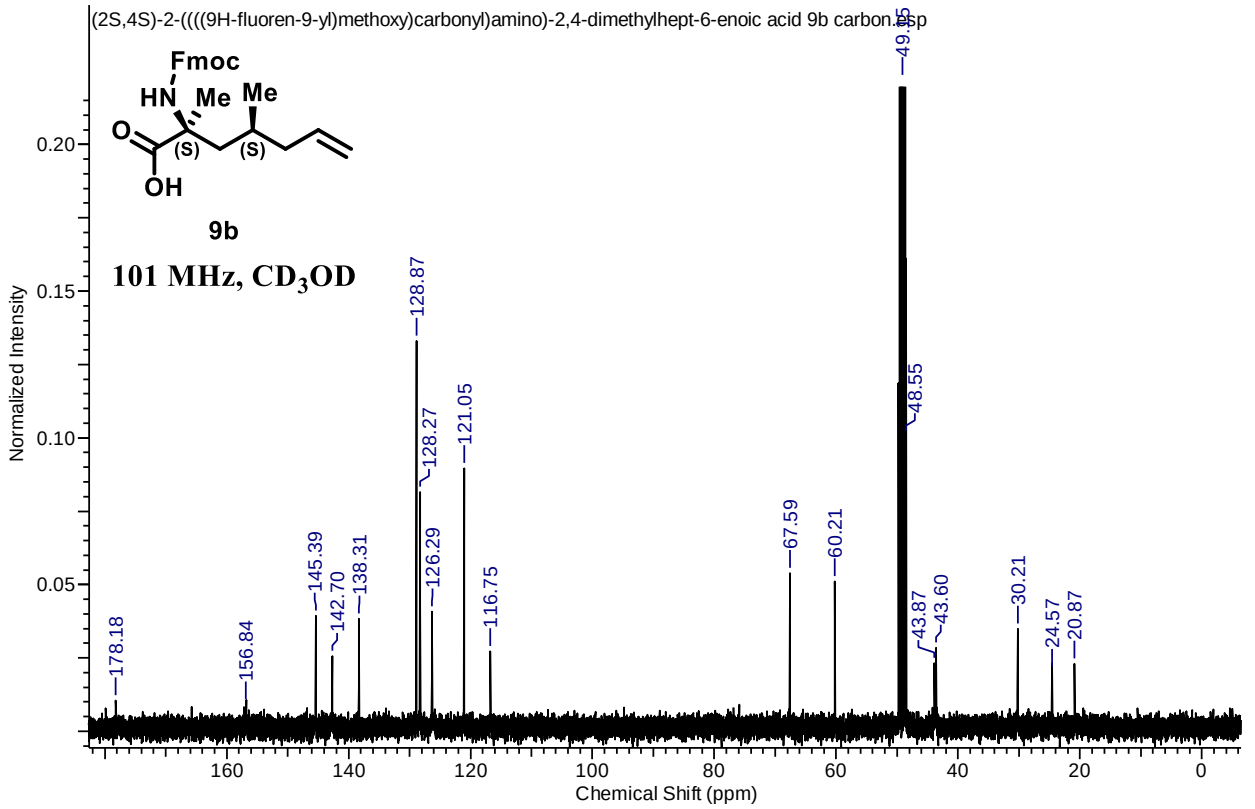

Figure 2.29 ^{1}H spectra for compound **11a**

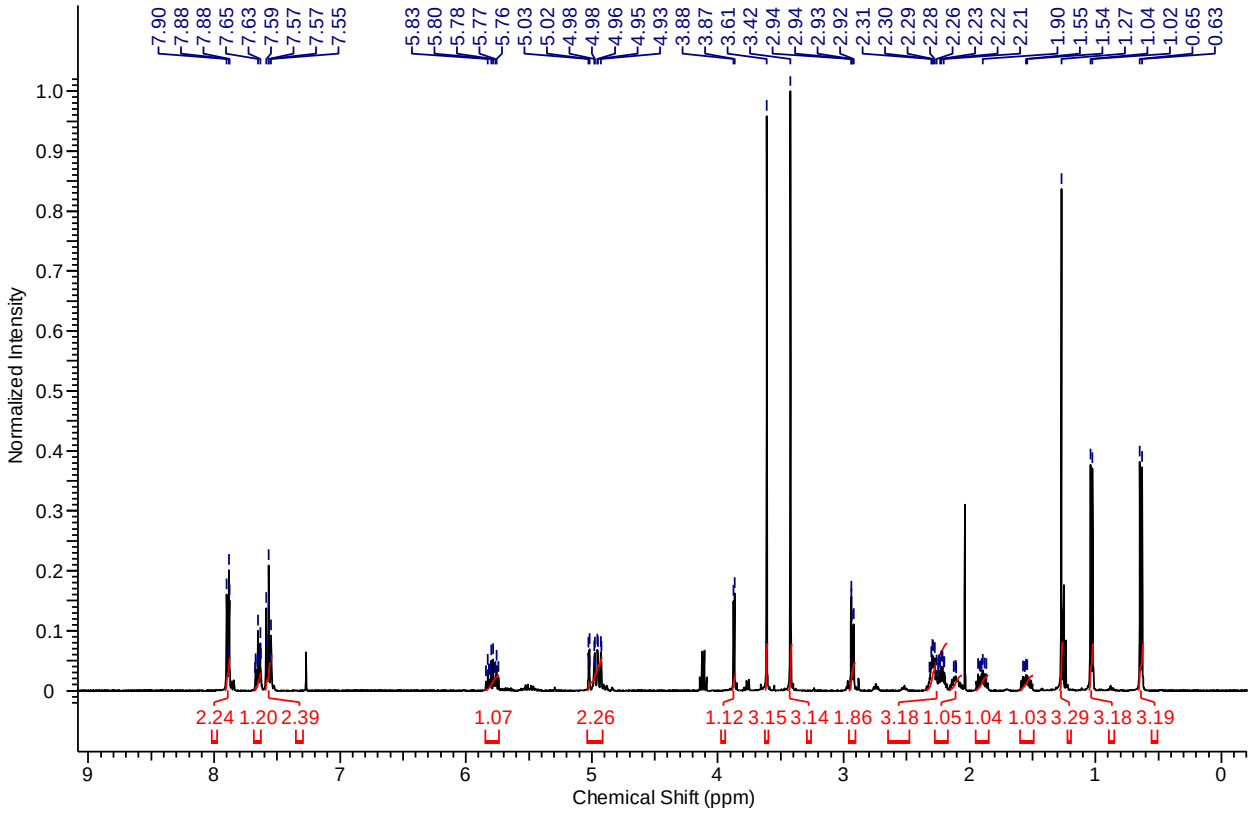

Figure 2.30 ^{1}H NMR spectra for compound **11b**

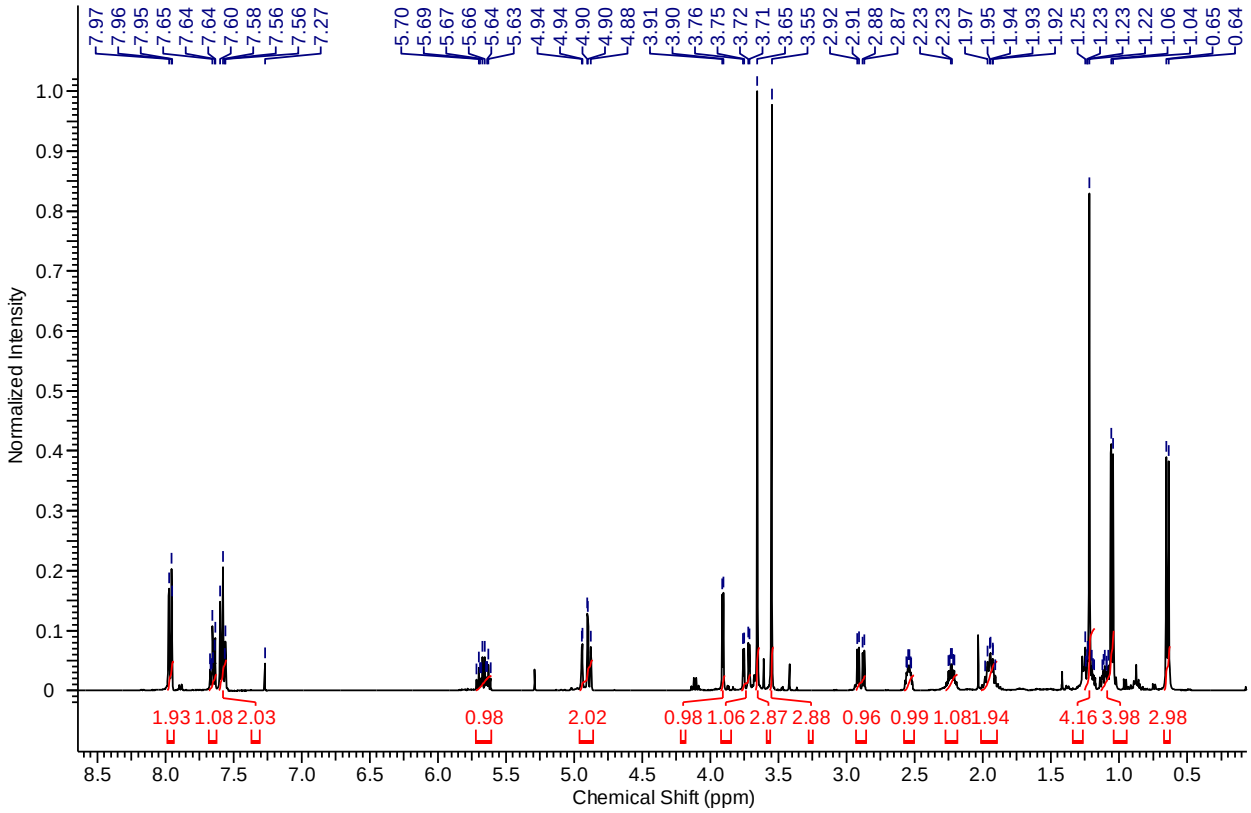

Figure 2.31 ^{13}C NMR spectra for compound **11b**

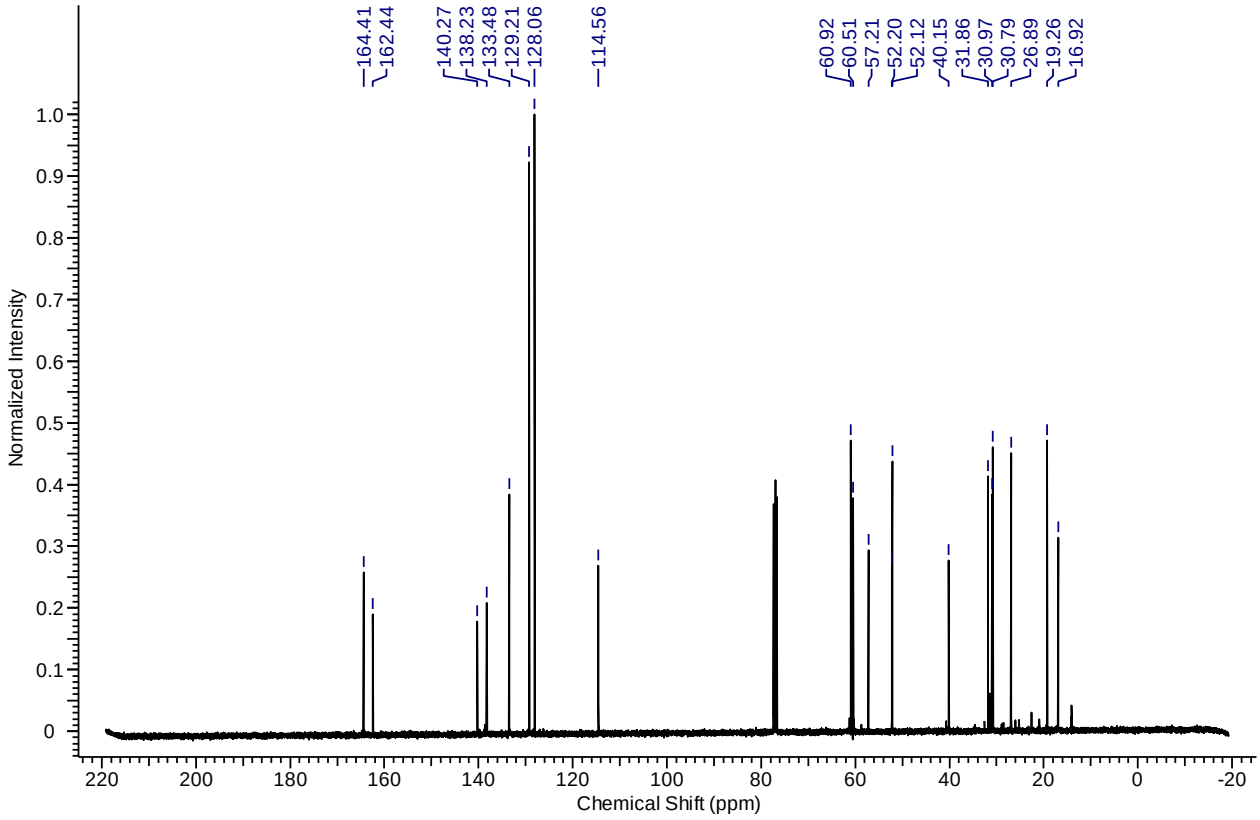

TABLE III. CRYSTALLOGRAPHIC PARAMETERS AND REFINEMENT SUMMARY FOR **11B**

Crystal Data

Formula	C22 H32 N2 O4 S
Formula Weight	420.56
Crystal System	monoclinic
Space group	$P2_1$ (No. 4)
a, b, c [Å]	7.820(1), 32.693(1), 8.890(1)
β [°]	90.032(1)
V [Å^3]	2272.8(4)
Z	4
D(calc) [g cm^{-3}]	1.229
μ(SYNC) [mm^{-1}]	0.168
F(000)	904
Crystal Size [μm]	5 × 20 × 20

Data Collection

Temperature (K)	100
Radiation [A]	0.70846
Theta Min, Max []	2.3, 28.9
Dataset	-10≤h≤10; -44≤k≤44; -12≤l≤12
Total, Unique Data, R(int)	41958, 11835, 0.052
Observed Data [I>2σ_I]	11427

Refinement

Nref, Npar	11835, 534
R, wR2, S	0.0814, 0.2117, 1.13
w = [(F_O^2)+(0.0725P)^2+7.6837P]$^{1/2}$	where P=(F_O^2+2F_C^2)/3
Max. and Av. Shift/Error	0.00, 0.00
Flack x	0.13(2)
Min and Max Residual Density $\Delta\rho$ [e A^{-3}]	-.75, 2.01

TABLE IV. FINAL COORDINATES OF THE NON-HYDROGEN ATOMS **11B**

Atom	x	y	z	U(eq)
S1	0.19086(16)	0.93685(4)	0.33056(16)	0.0151(3)
O1	0.0754(5)	0.91148(14)	0.2430(5)	0.0212(11)
O2	0.2039(6)	0.97954(14)	0.2910(6)	0.0233(12)
C1	0.1379(7)	0.93251(17)	0.5229(6)	0.0143(12)
C2	0.0517(8)	0.8971(2)	0.5704(8)	0.0240(17)
C3	0.0161(9)	0.8924(2)	0.7215(9)	0.0297(19)
C4	0.0664(9)	0.9218(2)	0.8241(8)	0.0277(17)
C5	0.1517(8)	0.9568(2)	0.7755(8)	0.0257(17)
C6	0.1881(8)	0.96226(18)	0.6239(7)	0.0190(16)
C7	0.3977(7)	0.91410(18)	0.3252(7)	0.0167(16)
C8	0.4689(7)	0.90936(16)	0.1637(6)	0.0137(12)
C9	0.6356(7)	0.93385(18)	0.1439(8)	0.0213(16)
C10	0.6071(8)	0.9805(2)	0.1503(9)	0.0273(19)
C11	0.7734(9)	1.0037(2)	0.1465(11)	0.037(2)
C12	0.8056(12)	1.0347(3)	0.0644(18)	0.069(5)
C13	0.4971(6)	0.86289(17)	0.1294(6)	0.0147(14)
C14	0.3269(7)	0.83885(18)	0.1302(7)	0.0183(16)
C15	0.5733(7)	0.85915(17)	-.0264(6)	0.0153(12)
O15	0.4653(6)	0.87525(15)	-.1297(5)	0.0223(12)
C16	0.5221(9)	0.8762(2)	-.2806(7)	0.0270(17)
N15	0.7152(6)	0.84371(15)	-.0645(6)	0.0167(12)
C17	0.8276(7)	0.82825(17)	0.0534(6)	0.0147(14)
C18	0.8816(8)	0.78367(18)	0.0196(6)	0.0183(16)
C19	0.7303(10)	0.75474(19)	0.0251(8)	0.0273(19)
C20	0.9707(9)	0.7815(2)	-.1342(6)	0.0243(16)
C21	0.7510(7)	0.83111(16)	0.2096(7)	0.0143(14)
O21	0.8577(5)	0.81496(13)	0.3124(5)	0.0186(11)
C22	0.7919(8)	0.8139(2)	0.4652(6)	0.0193(16)
N21	0.6064(6)	0.84579(14)	0.2468(5)	0.0153(12)
S2	0.69061(16)	0.58949(4)	0.19643(16)	0.0163(3)
O3	0.5732(6)	0.61422(15)	0.2822(6)	0.0260(14)
O4	0.7061(6)	0.54641(14)	0.2325(6)	0.0257(14)
C31	0.6390(7)	0.59419(17)	0.0035(6)	0.0147(12)
C32	0.5506(8)	0.6291(2)	-.0431(8)	0.0240(17)
C33	0.5129(9)	0.6339(2)	-.1947(9)	0.0277(19)
C34	0.5641(9)	0.6045(2)	-.2980(8)	0.0247(17)
C35	0.6526(9)	0.5698(2)	-.2516(8)	0.0243(17)
C36	0.6890(7)	0.56436(18)	-.0988(7)	0.0183(14)
C37	0.8982(7)	0.61230(17)	0.2018(7)	0.0177(16)
C38	0.9655(7)	0.61780(17)	0.3657(7)	0.0163(14)
C39	1.1308(7)	0.59312(19)	0.3871(8)	0.0243(18)
C40	1.0998(9)	0.5466(2)	0.3936(10)	0.033(2)
C41	1.2657(10)	0.5232(2)	0.4087(16)	0.061(4)
C42	1.3114(12)	0.4921(3)	0.351(2)	0.079(6)
C43	0.9945(7)	0.66439(17)	0.3972(6)	0.0140(12)
C44	0.8246(7)	0.68828(19)	0.3923(7)	0.0190(16)
C45	1.0706(8)	0.66858(18)	0.5536(7)	0.0190(16)
O45	0.9604(6)	0.65260(15)	0.6566(5)	0.0230(12)
C46	1.0170(9)	0.6511(2)	0.8081(7)	0.0260(17)
N45	1.2120(6)	0.68353(15)	0.5909(5)	0.0163(12)
C47	1.3251(6)	0.69868(17)	0.4730(6)	0.0137(12)
C48	1.3827(7)	0.74316(18)	0.5077(6)	0.0177(16)
C49	1.2294(10)	0.7727(2)	0.4992(8)	0.0280(19)
C50	1.4722(9)	0.7453(2)	0.6609(7)	0.0253(17)
C51	1.2500(7)	0.69542(18)	0.3175(6)	0.0137(14)
O51	1.3574(5)	0.71135(13)	0.2123(5)	0.0174(11)
C52	1.2920(8)	0.7125(2)	0.0650(6)	0.0197(17)
N51	1.1065(6)	0.68113(14)	0.2815(5)	0.0150(12)

TABLE V. HYDROGEN ATOM POSITIONS **11B**

Atom	x	y	z	U(iso)
H2	0.01840	0.87680	0.49990	0.0290
H3	-.04340	0.86880	0.75520	0.0350
H4	0.04280	0.91810	0.92800	0.0330
H5	0.18500	0.97710	0.84640	0.0310
H6	0.24650	0.98600	0.59020	0.0230
H7A	0.47770	0.93110	0.38470	0.0200
H7B	0.39210	0.88680	0.37310	0.0200
H8	0.38200	0.92030	0.09150	0.0160
H9A	0.68770	0.92670	0.04590	0.0250
H9B	0.71710	0.92590	0.22400	0.0250
H10A	0.53540	0.98890	0.06390	0.0330
H10B	0.54460	0.98740	0.24370	0.0330
H11	0.86220	0.99450	0.21100	0.0450
H12A	0.72060	1.04500	-.00190	0.0830
H12B	0.91450	1.04750	0.06940	0.0830
H14A	0.34960	0.81000	0.10800	0.0280
H14B	0.25010	0.85010	0.05360	0.0280
H14C	0.27330	0.84120	0.22940	0.0280
H16A	0.62910	0.89170	-.28680	0.0410
H16B	0.43510	0.88940	-.34350	0.0410
H16C	0.54140	0.84820	-.31620	0.0410
H17	0.93360	0.84540	0.05260	0.0180
H18	0.96550	0.77500	0.09820	0.0220
H19A	0.64770	0.76240	-.05300	0.0410
H19B	0.67570	0.75650	0.12400	0.0410
H19C	0.76970	0.72670	0.00770	0.0410
H20A	0.98950	0.75280	-.16150	0.0370
H20B	1.08090	0.79570	-.12880	0.0370
H20C	0.89850	0.79460	-.21040	0.0370
H22A	0.77400	0.84190	0.50130	0.0290
H22B	0.87430	0.79990	0.53070	0.0290
H22C	0.68300	0.79900	0.46680	0.0290
H32	0.51680	0.64930	0.02780	0.0290
H33	0.45180	0.65730	-.22790	0.0330
H34	0.53850	0.60820	-.40160	0.0300
H35	0.68800	0.55000	-.32320	0.0300
H36	0.74720	0.54050	-.06540	0.0220
H37A	0.97920	0.59490	0.14490	0.0210
H37B	0.89360	0.63940	0.15190	0.0210
H38	0.87720	0.60730	0.43730	0.0200
H39A	1.18710	0.60190	0.48150	0.0290
H39B	1.20960	0.59920	0.30290	0.0290
H40A	1.02510	0.54020	0.48040	0.0400
H40B	1.04000	0.53770	0.30100	0.0400
H41	1.34690	0.53530	0.47470	0.0720
H42A	1.23750	0.47810	0.28330	0.0940
H42B	1.42140	0.48130	0.37260	0.0940
H44A	0.84470	0.71670	0.42310	0.0290
H44B	0.74230	0.67560	0.46110	0.0290
H44C	0.77860	0.68780	0.28980	0.0290
H46A	1.11570	0.63280	0.81590	0.0390
H46B	0.92440	0.64100	0.87230	0.0390
H46C	1.05020	0.67860	0.84080	0.0390
H47	1.43010	0.68120	0.47470	0.0160
H48	1.46700	0.75150	0.42900	0.0210
H49A	1.14230	0.76430	0.57220	0.0420
H49B	1.18060	0.77200	0.39770	0.0420

H49C	1.26780	0.80050	0.52240	0.0420
H50A	1.52500	0.77230	0.67330	0.0380
H50B	1.56060	0.72410	0.66620	0.0380
H50C	1.38820	0.74090	0.74100	0.0380
H52A	1.25920	0.68490	0.03380	0.0300
H52B	1.37970	0.72310	-.00340	0.0300
H52C	1.19150	0.73040	0.06200	0.0300

TABLE VI. ANISOTROPIC DISPLACEMENT PARAMETERS **11B**

Atom	U(11)	U(22)	U(33)	U(23)	U(13)	U(12)
S1	0.0086(5)	0.0165(6)	0.0201(6)	0.0017(5)	0.0018(4)	0.0029(5)
O1	0.0105(18)	0.027(2)	0.026(2)	-.0041(17)	-.0033(16)	0.0003(16)
O2	0.017(2)	0.020(2)	0.033(2)	0.0061(18)	0.0021(17)	0.0038(16)
C1	0.011(2)	0.015(2)	0.017(2)	-.001(2)	0.0040(18)	0.0032(19)
C2	0.019(3)	0.020(3)	0.033(3)	0.000(2)	0.006(2)	-.004(2)
C3	0.024(3)	0.021(3)	0.044(4)	0.007(3)	0.014(3)	-.003(2)
C4	0.022(3)	0.033(3)	0.028(3)	0.009(3)	0.004(2)	0.006(3)
C5	0.023(3)	0.024(3)	0.030(3)	-.009(3)	-.003(2)	0.004(2)
C6	0.017(3)	0.013(2)	0.027(3)	0.000(2)	-.002(2)	0.002(2)
C7	0.007(2)	0.021(3)	0.022(3)	0.003(2)	-.0002(19)	0.0043(19)
C8	0.010(2)	0.015(2)	0.016(2)	-.0002(19)	0.0036(18)	0.0040(18)
C9	0.013(2)	0.016(3)	0.035(3)	0.002(2)	0.005(2)	-.001(2)
C10	0.014(3)	0.018(3)	0.050(4)	0.001(3)	0.006(3)	0.000(2)
C11	0.017(3)	0.026(3)	0.068(6)	0.002(3)	0.005(3)	0.001(3)
C12	0.024(4)	0.035(5)	0.149(13)	0.023(6)	0.006(5)	-.005(3)
C13	0.008(2)	0.015(2)	0.021(3)	0.001(2)	0.0049(19)	0.0010(18)
C14	0.011(2)	0.017(3)	0.027(3)	0.003(2)	-.001(2)	-.0008(19)
C15	0.015(2)	0.016(2)	0.015(2)	0.003(2)	0.0026(19)	-.0008(19)
O15	0.018(2)	0.029(2)	0.020(2)	0.0066(18)	0.0015(16)	0.0121(17)
N15	0.013(2)	0.018(2)	0.019(2)	0.0044(18)	-.0003(17)	0.0030(17)
C16	0.030(3)	0.031(3)	0.020(3)	0.006(3)	-.003(2)	0.013(3)
C17	0.011(2)	0.014(2)	0.019(3)	0.004(2)	0.0011(19)	0.0017(18)
C18	0.021(3)	0.021(3)	0.013(2)	0.001(2)	0.002(2)	0.010(2)
C19	0.039(4)	0.015(3)	0.028(3)	0.003(2)	0.000(3)	0.001(2)
C20	0.032(3)	0.032(3)	0.009(2)	0.005(2)	0.009(2)	0.017(3)
C21	0.014(2)	0.010(2)	0.019(3)	0.0010(19)	0.0004(19)	0.0013(19)
O21	0.0139(18)	0.0190(19)	0.023(2)	0.0030(16)	-.0008(15)	0.0070(15)
N21	0.012(2)	0.015(2)	0.019(2)	0.0009(17)	0.0008(17)	0.0001(17)
C22	0.021(3)	0.026(3)	0.011(2)	0.006(2)	0.0003(19)	-.002(2)
S2	0.0093(5)	0.0178(6)	0.0218(6)	0.0027(5)	-.0032(4)	-.0028(5)
O3	0.0119(19)	0.030(2)	0.036(3)	-.003(2)	-.0019(17)	-.0019(17)
O4	0.020(2)	0.021(2)	0.036(3)	0.0080(19)	-.0068(18)	-.0059(17)
C31	0.012(2)	0.015(2)	0.017(2)	0.000(2)	-.0058(18)	-.0022(19)
C32	0.014(3)	0.023(3)	0.035(3)	0.000(2)	-.005(2)	0.002(2)
C33	0.021(3)	0.024(3)	0.038(4)	0.005(3)	-.007(3)	0.005(2)
C34	0.025(3)	0.026(3)	0.023(3)	0.005(2)	-.007(2)	-.006(3)
C35	0.026(3)	0.018(3)	0.029(3)	-.001(2)	0.001(2)	-.004(2)
C36	0.014(2)	0.012(2)	0.029(3)	0.003(2)	-.004(2)	-.0013(19)
C37	0.008(2)	0.015(3)	0.030(3)	-.001(2)	-.002(2)	-.0039(19)
C38	0.007(2)	0.014(2)	0.028(3)	0.002(2)	-.007(2)	-.0006(18)
C39	0.010(2)	0.016(3)	0.047(4)	0.005(3)	-.010(2)	-.001(2)
C40	0.023(3)	0.015(3)	0.061(5)	0.007(3)	-.011(3)	-.001(2)
C41	0.022(4)	0.024(4)	0.136(11)	0.018(5)	-.028(5)	0.000(3)
C42	0.023(4)	0.027(4)	0.186(16)	-.011(6)	-.023(6)	0.005(3)
C43	0.010(2)	0.016(2)	0.016(2)	0.0019(19)	-.0027(18)	-.0037(18)
C44	0.011(2)	0.026(3)	0.020(3)	0.003(2)	-.004(2)	0.002(2)
C45	0.016(2)	0.016(3)	0.025(3)	0.004(2)	0.003(2)	-.002(2)
O45	0.019(2)	0.033(2)	0.017(2)	0.0045(18)	0.0002(16)	-.0115(18)

N45	0.015(2)	0.018(2)	0.016(2)	0.0067(18)	-.0031(17) -.0005(17)
C46	0.030(3)	0.035(3)	0.013(3)	0.005(2)	0.002(2) -.015(3)
C47	0.007(2)	0.020(2)	0.014(2)	0.0003(19)	-.0043(17) -.0029(18)
C48	0.014(2)	0.022(3)	0.017(3)	0.000(2)	-.0027(19) -.008(2)
C49	0.038(4)	0.018(3)	0.028(3)	0.003(2)	0.000(3) 0.002(3)
C50	0.028(3)	0.029(3)	0.019(3)	0.000(2)	0.000(2) -.013(3)
C51	0.011(2)	0.020(3)	0.010(2)	0.0014(19)	0.0015(17) 0.0022(19)
O51	0.0145(18)	0.021(2)	0.0168(19)	0.0039(16)	0.0018(15) 0.0002(16)
N51	0.015(2)	0.014(2)	0.016(2)	0.0028(17)	0.0009(17) -.0001(17)
C52	0.020(3)	0.025(3)	0.014(3)	0.005(2)	0.005(2) -.001(2)

TABLE VII. BOND DISTANCES (Å) **11B**

S1	-O1	1.452(4)	S2 -O3 1.442(5)
S1	-O2	1.443(5)	S2 -O4 1.450(5)
S1	-C1	1.765(6)	S2 -C31 1.769(6)
C1	-C2	1.405(9)	C31 -C32 1.397(9)
C2	-C3	1.381(11)	C32 -C33 1.388(11)
C3	-C4	1.382(10)	C33 -C34 1.389(10)
C4	-C5	1.393(9)	C34 -C35 1.391(10)
C5	-C6	1.389(9)	C35 -C36 1.399(9)
C1	-C6	1.381(8)	C31 -C36 1.390(8)
S1	-C7	1.781(6)	S2 -C37 1.787(6)
C7	-C8	1.548(8)	C37 -C38 1.559(9)
C8	-C9	1.540(8)	C38 -C39 1.536(8)
C9	-C10	1.542(9)	C39 -C40 1.541(9)
C10	-C11	1.506(9)	C40 -C41 1.512(10)
C11	-C12	1.274(14)	C41 -C42 1.194(14)
C8	-C13	1.565(8)	C38 -C43 1.565(8)
C13	-C14	1.546(7)	C43 -C44 1.542(8)
C13	-C15	1.513(7)	C43 -C45 1.518(8)
O15	-C15	1.354(7)	O45 -C45 1.362(8)
O15	-C16	1.414(8)	O45 -C46 1.418(8)
N15	-C15	1.265(7)	N45 -C45 1.253(8)
N15	-C17	1.458(7)	N45 -C47 1.459(7)
C17	-C18	1.547(8)	C47 -C48 1.553(8)
C17	-C21	1.516(8)	C47 -C51 1.505(7)
C18	-C19	1.516(9)	C48 -C49 1.541(9)
C18	-C20	1.537(8)	C48 -C50 1.533(8)
O21	-C21	1.345(7)	O51 -C51 1.361(7)
O21	-C22	1.453(7)	O51 -C52 1.406(7)
N21	-C13	1.460(7)	N51 -C43 1.458(7)
N21	-C21	1.272(7)	N51 -C51 1.257(7)

C2	-H2	0.9500	C32	-H32	0.9500
C3	-H3	0.9500	C33	-H33	0.9500
C4	-H4	0.9500	C34	-H34	0.9500
C5	-H5	0.9500	C35	-H35	0.9500
C6	-H6	0.9500	C36	-H36	0.9500
C7	-H7A	0.9900	C37	-H37A	0.9900
C7	-H7B	0.9900	C37	-H37B	0.9900
C8	-H8	1.0000	C38	-H38	1.0000
C9	-H9A	0.9900	C39	-H39A	0.9900
C9	-H9B	0.9900	C39	-H39B	0.9900
C10	-H10A	0.9900	C40	-H40A	0.9900
C10	-H10B	0.9900	C40	-H40B	0.9900
C11	-H11	0.9500	C41	-H41	0.9500
C12	-H12A	0.9500	C42	-H42A	0.9500
C12	-H12B	0.9500	C42	-H42B	0.9500
C14	-H14A	0.9800	C44	-H44A	0.9800
C14	-H14B	0.9800	C44	-H44B	0.9800
C14	-H14C	0.9800	C44	-H44C	0.9800

C16 -H16A	0.9800	C46 -H46A	0.9800
C16 -H16B	0.9800	C46 -H46B	0.9800
C16 -H16C	0.9800	C46 -H46C	0.9800
C17 -H17	1.0000	C47 -H47	1.0000
C18 -H18	1.0000	C48 -H48	1.0000
C19 -H19A	0.9800	C49 -H49A	0.9800
C19 -H19B	0.9800	C49 -H49B	0.9800
C19 -H19C	0.9800	C49 -H49C	0.9800
C20 -H20A	0.9800	C50 -H50A	0.9800
C20 -H20B	0.9800	C50 -H50B	0.9800
C20 -H20C	0.9800	C50 -H50C	0.9800
C22 -H22A	0.9800	C52 -H52A	0.9800
C22 -H22B	0.9800	C52 -H52B	0.9800
C22 -H22C	0.9800	C52 -H52C	0.9800

TABLE VIII. BOND ANGLES (º) **11B**

O1 -S1 -O2	117.8(3)	O3 -S2 -O4	118.8(3)
O1 -S1 -C1	109.1(3)	O3 -S2 -C31	108.6(3)
O1 -S1 -C7	108.2(3)	O3 -S2 -C37	109.3(3)
O2 -S1 -C1	109.3(3)	O4 -S2 -C31	108.5(3)
O2 -S1 -C7	109.5(3)	O4 -S2 -C37	108.9(3)
C1 -S1 -C7	101.9(3)	C31 -S2 -C37	101.3(3)
S1 -C1 -C2	118.1(4)	S2 -C31 -C32	118.1(5)
S1 -C1 -C6	120.4(4)	S2 -C31 -C36	120.6(4)
C2 -C1 -C6	121.4(5)	C32 -C31 -C36	121.2(5)
C1 -C2 -C3	118.8(6)	C31 -C32 -C33	119.0(6)
C2 -C3 -C4	120.5(6)	C32 -C33 -C34	120.2(6)
C3 -C4 -C5	120.2(7)	C33 -C34 -C35	120.8(7)
C4 -C5 -C6	120.3(6)	C34 -C35 -C36	119.5(6)
C1 -C6 -C5	118.8(6)	C31 -C36 -C35	119.3(5)
S1 -C7 -C8	113.2(4)	S2 -C37 -C38	112.3(4)
C7 -C8 -C9	111.0(5)	C37 -C38 -C39	109.8(5)
C7 -C8 -C13	109.2(4)	C37 -C38 -C43	109.2(5)
C9 -C8 -C13	111.3(4)	C39 -C38 -C43	111.6(5)
C8 -C9 -C10	112.8(5)	C38 -C39 -C40	113.0(5)
C9 -C10 -C11	111.9(5)	C39 -C40 -C41	111.6(5)
C10 -C11 -C12	125.8(8)	C40 -C41 -C42	130.5(10)
N21 -C13 -C14	107.8(4)	N51 -C43 -C44	107.9(4)
N21 -C13 -C8	108.4(4)	N51 -C43 -C38	109.0(4)
C8 -C13 -C15	108.2(4)	C38 -C43 -C45	108.0(5)
N21 -C13 -C15	113.1(4)	N51 -C43 -C45	112.1(5)
C8 -C13 -C14	111.8(4)	C38 -C43 -C44	111.3(4)
C14 -C13 -C15	107.6(4)	C44 -C43 -C45	108.5(5)
N15 -C15 -C13	128.5(5)	N45 -C45 -C43	128.5(5)
O15 -C15 -N15	121.4(5)	O45 -C45 -N45	122.0(6)
O15 -C15 -C13	110.1(4)	O45 -C45 -C43	109.5(5)
C15 -O15 -C16	117.1(5)	C45 -O45 -C46	117.0(5)
N15 -C17 -C21	113.5(5)	N45 -C47 -C51	113.5(4)
C21 -O21 -C22	115.1(4)	C51 -O51 -C52	115.2(4)
C18 -C17 -C21	110.1(4)	C48 -C47 -C51	111.2(5)
C15 -N15 -C17	118.3(5)	C45 -N45 -C47	118.5(5)
N15 -C17 -C18	110.6(4)	N45 -C47 -C48	110.6(4)
C13 -N21 -C21	118.6(5)	C43 -N51 -C51	119.8(5)
C19 -C18 -C20	110.8(5)	C49 -C48 -C50	111.7(5)
C17 -C18 -C19	111.6(5)	C47 -C48 -C49	110.6(5)
C17 -C18 -C20	109.9(5)	C47 -C48 -C50	110.6(5)
O21 -C21 -C17	110.7(5)	O51 -C51 -C47	111.3(4)
O21 -C21 -N21	121.5(5)	O51 -C51 -N51	121.2(5)

N21 -C21 -C17 127.8(5) N51 -C51 -C47 127.4(5)

C1 -C2 -H2 121.00 C31 -C32 -H32 121.00
C3 -C2 -H2 121.00 C33 -C32 -H32 120.00
C2 -C3 -H3 120.00 C32 -C33 -H33 120.00
C4 -C3 -H3 120.00 C34 -C33 -H33 120.00
C3 -C4 -H4 120.00 C33 -C34 -H34 119.00
C5 -C4 -H4 120.00 C35 -C34 -H34 120.00
C4 -C5 -H5 120.00 C34 -C35 -H35 120.00
C6 -C5 -H5 120.00 C36 -C35 -H35 120.00
C1 -C6 -H6 120.00 C31 -C36 -H36 120.00
C5 -C6 -H6 121.00 C35 -C36 -H36 120.00
H7A -C7 -H7B 108.00 H37A -C37 -H37B 108.00
S1 -C7 -H7A 109.00 S2 -C37 -H37A 109.00
S1 -C7 -H7B 109.00 S2 -C37 -H37B 109.00
C8 -C7 -H7A 109.00 C38 -C37 -H37A 109.00
C8 -C7 -H7B 109.00 C38 -C37 -H37B 109.00
C9 -C8 -H8 108.00 C39 -C38 -H38 109.00
C7 -C8 -H8 108.00 C37 -C38 -H38 109.00
C13 -C8 -H8 109.00 C43 -C38 -H38 109.00
C8 -C9 -H9A 109.00 C38 -C39 -H39A 109.00
C8 -C9 -H9B 109.00 C38 -C39 -H39B 109.00
C10 -C9 -H9A 109.00 C40 -C39 -H39A 109.00
C10 -C9 -H9B 109.00 C40 -C39 -H39B 109.00
H9A -C9 -H9B 108.00 H39A -C39 -H39B 108.00
C9 -C10 -H10A 109.00 C39 -C40 -H40A 109.00
C9 -C10 -H10B 109.00 C39 -C40 -H40B 109.00
C11 -C10 -H10A 109.00 C41 -C40 -H40A 109.00
C11 -C10 -H10B 109.00 C41 -C40 -H40B 109.00
H10A -C10 -H10B 108.00 H40A -C40 -H40B 108.00
C10 -C11 -H11 117.00 C40 -C41 -H41 115.00
C12 -C11 -H11 117.00 C42 -C41 -H41 115.00
C11 -C12 -H12A 120.00 C41 -C42 -H42A 120.00
C11 -C12 -H12B 120.00 C41 -C42 -H42B 120.00
H12A -C12 -H12B 120.00 H42A -C42 -H42B 120.00
C13 -C14 -H14A 109.00 C43 -C44 -H44A 110.00
C13 -C14 -H14B 109.00 C43 -C44 -H44B 110.00
C13 -C14 -H14C 109.00 C43 -C44 -H44C 110.00
H14A -C14 -H14B 109.00 H44A -C44 -H44B 109.00
H14A -C14 -H14C 110.00 H44A -C44 -H44C 109.00
H14B -C14 -H14C 110.00 H44B -C44 -H44C 109.00
O15 -C16 -H16A 109.00 O45 -C46 -H46A 110.00
O15 -C16 -H16B 109.00 O45 -C46 -H46B 110.00
O15 -C16 -H16C 110.00 O45 -C46 -H46C 109.00
H16A -C16 -H16B 109.00 H46A -C46 -H46B 110.00
H16A -C16 -H16C 109.00 H46A -C46 -H46C 109.00
H16B -C16 -H16C 109.00 H46B -C46 -H46C 109.00
C18 -C17 -H17 107.00 C48 -C47 -H47 107.00
C21 -C17 -H17 107.00 C51 -C47 -H47 107.00
N15 -C17 -H17 107.00 N45 -C47 -H47 107.00
C19 -C18 -H18 108.00 C49 -C48 -H48 108.00
C20 -C18 -H18 108.00 C50 -C48 -H48 108.00
C17 -C18 -H18 108.00 C47 -C48 -H48 108.00
C18 -C19 -H19A 109.00 C48 -C49 -H49A 109.00
C18 -C19 -H19B 109.00 C48 -C49 -H49B 109.00
C18 -C19 -H19C 109.00 C48 -C49 -H49C 109.00
H19A -C19 -H19B 109.00 H49A -C49 -H49B 109.00
H19A -C19 -H19C 110.00 H49A -C49 -H49C 109.00
H19B -C19 -H19C 110.00 H49B -C49 -H49C 110.00
C18 -C20 -H20A 109.00 C48 -C50 -H50A 109.00
C18 -C20 -H20B 109.00 C48 -C50 -H50B 109.00
C18 -C20 -H20C 109.00 C48 -C50 -H50C 109.00

H20A	-C20	-H20B	109.00	H50A	-C50	-H50B	110.00
H20A	-C20	-H20C	109.00	H50A	-C50	-H50C	109.00
H20B	-C20	-H20C	109.00	H50B	-C50	-H50C	110.00
O21	-C22	-H22A	110.00	O51	-C52	-H52A	110.00
O21	-C22	-H22B	109.00	O51	-C52	-H52B	109.00
O21	-C22	-H22C	109.00	O51	-C52	-H52C	109.00
H22A	-C22	-H22B	110.00	H52A	-C52	-H52B	109.00
H22A	-C22	-H22C	110.00	H52A	-C52	-H52C	109.00
H22B	-C22	-H22C	109.00	H52B	-C52	-H52C	109.00

TABLE IX. TORSION ANGLES (º) **11B**

O1	-S1	-C1	-C2	24.0(5)	O3	-S2	-C31 -C32 23.5(5)
O1	-S1	-C1	-C6	-159.3(5)	O3	-S2	-C31 -C36 -158.1(5)
O2	-S1	-C1	-C2	154.1(5)	O4	-S2	-C31 -C32 153.9(5)
O2	-S1	-C1	-C6	-29.2(6)	O4	-S2	-C31 -C36 -27.7(5)
C7	-S1	-C1	-C2	-90.2(5)	C37	-S2	-C31 -C32 -91.6(5)
C7	-S1	-C1	-C6	86.6(5)	C37	-S2	-C31 -C36 86.9(5)
O1	-S1	-C7	-C8	58.7(5)	O3	-S2	-C37 -C38 57.5(5)
O2	-S1	-C7	-C8	-70.7(5)	O4	-S2	-C37 -C38 -73.7(5)
C1	-S1	-C7	-C8	173.6(4)	C31	-S2	-C37 -C38 172.0(4)
C2	-C1	-C6	-C5	-.1(9)	C32	-C31	-C36 -C35 1.1(9)
S1	-C1	-C2	-C3	177.2(5)	S2	-C31	-C32 -C33 178.3(5)
C6	-C1	-C2	-C3	0.4(9)	C36	-C31	-C32 -C33 -.2(9)
S1	-C1	-C6	-C5	-176.8(5)	S2	-C31	-C36 -C35 -177.3(5)
C1	-C2	-C3	-C4	-.8(10)	C31	-C32	-C33 -C34 -.6(10)
C2	-C3	-C4	-C5	0.9(10)	C32	-C33	-C34 -C35 0.4(10)
C3	-C4	-C5	-C6	-.5(10)	C33	-C34	-C35 -C36 0.6(10)
C4	-C5	-C6	-C1	0.2(9)	C34	-C35	-C36 -C31 -1.3(9)
S1	-C7	-C8	-C9	118.8(4)	S2	-C37	-C38 -C39 118.9(4)
S1	-C7	-C8	-C13	-118.1(4)	S2	-C37	-C38 -C43 -118.6(4)
C7	-C8	-C9	-C10	-67.9(7)	C37	-C38	-C39 -C40 -72.2(7)
C13	-C8	-C9	-C10	170.3(5)	C43	-C38	-C39 -C40 166.6(6)
C9	-C8	-C13	-N21	68.2(6)	C39	-C38	-C43 -N51 67.2(6)
C7	-C8	-C13	-N21	-54.7(5)	C37	-C38	-C43 -N51 -54.4(6)
C9	-C8	-C13	-C14	-173.2(5)	C39	-C38	-C43 -C44 -173.9(5)
C9	-C8	-C13	-C15	-54.8(6)	C39	-C38	-C43 -C45 -54.9(6)
C7	-C8	-C13	-C14	63.9(6)	C37	-C38	-C43 -C44 64.6(6)
C7	-C8	-C13	-C15	-177.8(4)	C37	-C38	-C43 -C45 -176.4(4)
C8	-C9	-C10	-C11	174.2(6)	C38	-C39	-C40 -C41 177.8(8)
C9	-C10	-C11	-C12	133.6(10)	C39	-C40	-C41 -C42 -139.6(14)
C8	-C13	-C15	-N15	119.7(6)	C38	-C43	-C45 -N45 119.2(7)
C14	-C13	-C15	-N15	-119.3(6)	C44	-C43	-C45 -N45 -120.1(7)
C14	-C13	-C15	-O15	60.6(6)	C44	-C43	-C45 -O45 60.7(6)
C8	-C13	-C15	-O15	-60.4(6)	C38	-C43	-C45 -O45 -60.1(6)
N21	-C13	-C15	-O15	179.5(4)	N51	-C43	-C45 -O45 179.8(5)
N21	-C13	-C15	-N15	-.3(8)	N51	-C43	-C45 -N45 -1.0(9)
C16	-O15	-C15	-C13	176.6(5)	C46	-O45	-C45 -C43 175.3(5)
C16	-O15	-C15	-N15	-3.6(8)	C46	-O45	-C45 -N45 -4.0(9)
C15	-N15	-C17	-C18	127.4(5)	C45	-N45	-C47 -C48 127.9(5)
C15	-N15	-C17	-C21	3.1(7)	C45	-N45	-C47 -C51 2.2(7)
C17	-N15	-C15	-O15	177.9(5)	C47	-N45	-C45 -O45 177.8(5)

C17 -N15 -C15 -C13 -2.3(9)	C47 -N45 -C45 -C43 -1.3(9)
C18 -C17 -C21 -O21 53.0(6)	C48 -C47 -C51 -O51 52.2(6)
C18 -C17 -C21 -N21 -126.2(6)	C48 -C47 -C51 -N51 -126.2(6)
N15 -C17 -C18 -C19 -65.5(6)	N45 -C47 -C48 -C49 -66.7(6)
N15 -C17 -C18 -C20 57.7(6)	N45 -C47 -C48 -C50 57.6(6)
C21 -C17 -C18 -C19 60.7(6)	C51 -C47 -C48 -C49 60.4(6)
C21 -C17 -C18 -C20 -176.0(5)	C51 -C47 -C48 -C50 -175.3(5)
N15 -C17 -C21 -O21 177.6(4)	N45 -C47 -C51 -O51 177.7(4)
N15 -C17 -C21 -N21 -1.6(8)	N45 -C47 -C51 -N51 -.8(8)
C22 -O21 -C21 -C17 -176.4(5)	C52 -O51 -C51 -C47 -175.3(5)
C22 -O21 -C21 -N21 2.8(7)	C52 -O51 -C51 -N51 3.3(8)
C21 -N21 -C13 -C15 2.0(7)	C51 -N51 -C43 -C45 2.3(7)
C21 -N21 -C13 -C8 -118.0(5)	C51 -N51 -C43 -C38 -117.2(6)
C21 -N21 -C13 -C14 120.8(5)	C51 -N51 -C43 -C44 121.8(6)
C13 -N21 -C21 -O21 179.9(5)	C43 -N51 -C51 -O51 -179.9(5)
C13 -N21 -C21 -C17 -1.0(8)	C43 -N51 -C51 -C47 -1.5(9)

TABLE X. HYDROGEN BONS (Å, º) **11B**

D - H	**... A**	**D-H**	**H...A**	**D...A**	**DHA**
C2 - H2	... O1	0.9500	2.5900	2.954(8)	103.00
C32 - H32	... O3	0.9500	2.5700	2.938(9)	103.00
C3 - H3	... N15	0.9500	2.6100	3.420(9)	144.00
C33 - H33	... N45	0.9500	2.6200	3.435(9)	145.00
C5 - H5	... O4	0.9500	2.5200	3.134(8)	122.00*
C35 - H35	... O2	0.9500	2.4700	3.177(8)	131.00
C6 - H6	... O4	0.9500	2.5500	3.144(8)	120.00*
C7 - H7B	... N21	0.9900	2.4200	2.853(7)	106.00
C37 - H37B	... N51	0.9900	2.4400	2.867(7)	105.00
C14 - H14B	... O15	0.9800	2.4800	2.816(8)	100.00
C18 - H18	... O21	1.0000	2.4600	2.803(7)	100.00
C48 - H48	... O51	1.0000	2.4800	2.831(7)	100.00
C20 - H20C	... N15	0.9800	2.5100	2.918(8)	105.00

*Symmetry operation for atom A: 1+x, y, 1+z

No “classical” hydrogen bonds.

3. AN ORTHOGONALLY DOUBLE-STAPLED PEPTIDE WITH IMPROVED HELICITY AND PROTEOLYTIC STABILITY

3.1. Introduction

Many protein-protein interactions occur when a helix binds to a groove, and these helix-groove interactions may be inhibited using constrained peptides that adopt a helical conformation. An example of these are “stapled” peptides, which are constrained by virtue of two appropriately placed side chains joined together by an olefin or other linkages. Extending this approach to bicyclic peptides has emerged as a strategy to further enhance helicity and proteolytic stability of constrained α-helical peptides. Verdine and coworkers[61] have described “stitched” peptides that contain two tandem hydrocarbon staples to enhance helicity, and multiple groups have reported peptides with enhanced proteolytic stability by spacing two hydrocarbon staples near each end of the peptide backbone.[95-97] While it is has been shown that different cyclizing constraints can imbue distinct properties,[98] combining orthogonal stapling strategies remains relatively unexplored, and we are not aware of any bicyclic alpha helical peptides that are stabilized by two orthogonal constraints.

In our work to inhibit estrogen receptor/coactivator interactions, we saw an opportunity to prepare orthogonally stapled peptides and to study their potential benefits on helicity, stability, and affinity. The estrogen receptor is a clinically validated target in estrogen receptor-positive breast cancer, but, because of issues of resistance to current endocrine therapies, new mechanisms of antagonizing the estrogen receptor are needed. A proposed alternative mechanism for blocking the action of estrogen receptor involves

using small molecules and constrained helical peptides to directly inhibit binding of the coactivator LXXLL motif to estrogen receptor.[30, 32, 35, 37, 42, 81, 99, 100]

In Chapter 2,[71] a stapled peptide, SRC2-SP4, was shown to inhibit the estrogen receptor/coactivator interaction. In addition to the olefin staple, SRC2-SP4 contains an *i - i+4* salt bridge (Arg692-Asp696). We noticed an increase in helicity, binding affinity, and proteolytic stability for SRC2-SP4 vs. a homologous stapled peptide, PFE-SP2,[30] that lacked a salt bridge because of a single amino acid change (Arg692→Asn). MD simulations of these peptides in solution suggested that the formation of a salt bridge enhanced helical stability. To verify this observation, we ran prolonged simulations of SRC2-SP4 in solution and observed that breakage and formation of hydrogen bonds between the arginine and aspartate side chains were closely associated with changes in peptide helicity (**Figure 3.1A**). PFE-SP2, which was unable to form this stabilizing salt bridge, unfolded during the course of the simulation (**Figure 3.5**), in agreement with our experimental observations. There is a rich literature on helical stabilization mediated by salt bridges,[101-102] which well supports our observations. In this work, we describe a strategy to introduce two orthogonal staples (lactam and olefin) with differing electrostatic properties. Our design principles were guided by molecular dynamics (MD) simulations and x-ray crystallography, and, gratifyingly, they have yielded novel peptides demonstrating high helicity and stability.

3.2 Molecular dynamics-guided design of bicyclic stapled peptide

To obtain a quantitative analysis of helical stability, we applied a new computational approach that profiles the potential of mean force for peptide unfolding by describing α-

helicity as a summation of distance and dihedral measurements applied to Bias Exchange Umbrella Sampling (BEUS).[103] This method yielded free energy profiles to quantitatively describe helical folding states for wild-type or macrocyclic peptides (**Figure 3.1C-D**). The relative free energy profile for SRC2-WT (yellow) showed a distinct minimum at <0.30 helicity, whereas incorporating an olefin-based staple, SRC2-SP4 (red), introduced a more helical character with an additional minimum at ~0.75 helicity. The increase in helicity of SRC2-SP4 relative to PFE-SP2 was associated with a ca. 2 kcal/mol reduction in free energy at high helicity (**Figure 3.1C**, red vs. orange), a finding which can be attributed to the "pseudo-stapled" nature of the Arg692-Asp696 salt bridge. This was further supported by the ca. 2 kcal/mol reduction in free energy at high helicity seen between the comparable unstapled peptides SRC2-WT (yellow) and SRC2-R692Q (brown). Based on these data, we envisioned preparing a bicyclic peptide which would maintain the hydrocarbon staple and covalently replicate the Arg692-Asp696 salt-bridge. Computational analysis of such peptides predicted that converting the salt bridge to a covalent lactam linkage alone would not produce significant stabilization (**Figure 3.1D**, yellow vs. green); however, coupling the previously described SRC-SP4 olefin staple with an additional lactam staple to enforce the 692-696 interaction in a covalent manner should substantially increase the α-helical content of the peptide (**Figure 3.1D**, red vs. blue).

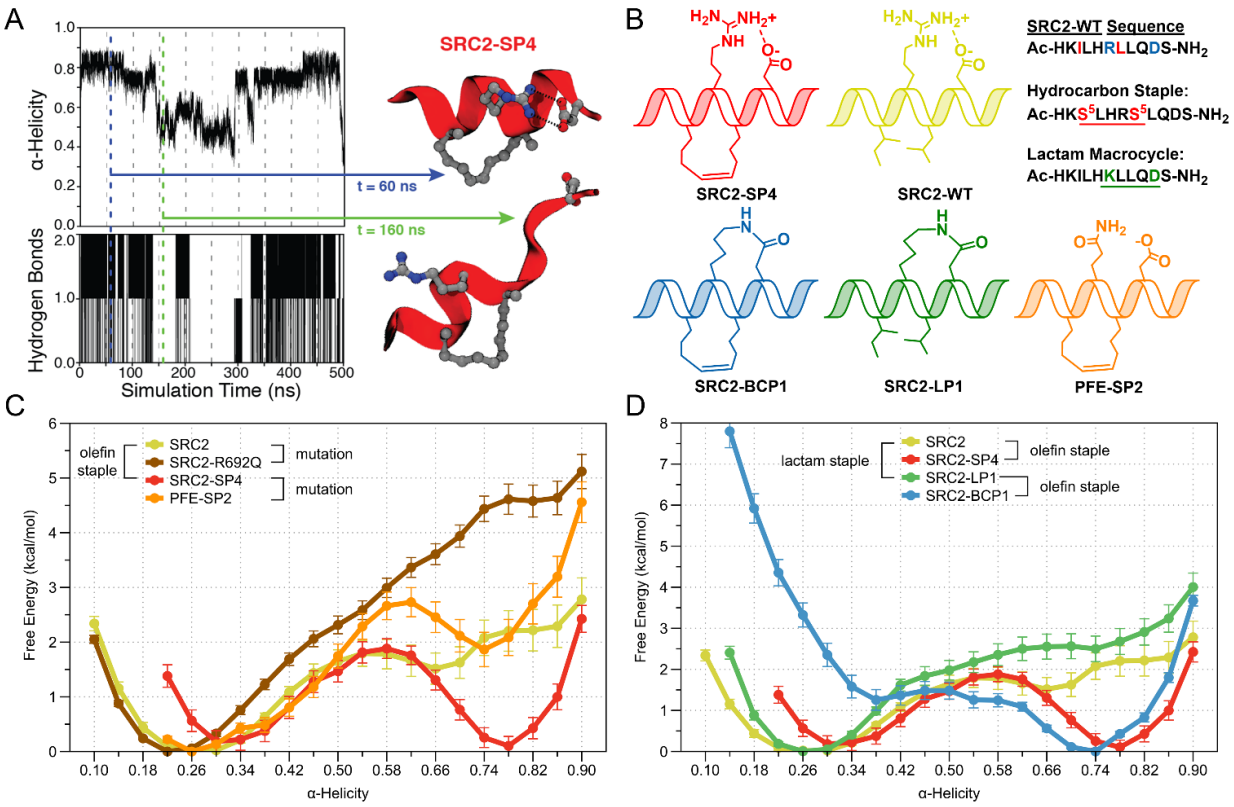

Figure 3.1. Computationally derived free energy profiles for peptide folding. A) Long-timescale simulations of a hydrocarbon-stapled peptide representing coactivator protein demonstrated that α-helicity correlated with presence or absence of a salt bridge between Arg692 and Asp696. B) Several additional peptides were designed to reinforce the salt bridge interaction with a covalent linkage, both in the presence and absence of the hydrocarbon staple. C) Computationally derived potential of mean force describing the relative free energy across a range of helical states indicated that the Arg692-Asp696 salt bridge provided ~2 kcal/mol of stabilizing energy. D) In silico models that install a covalent replacement for the salt bridge via an amide linkage alone were not predicted to increase helicity; however, combining the hydrocarbon and amide linkages yielded a "stitched" peptide with predicted highly stable, highly helical conformations.

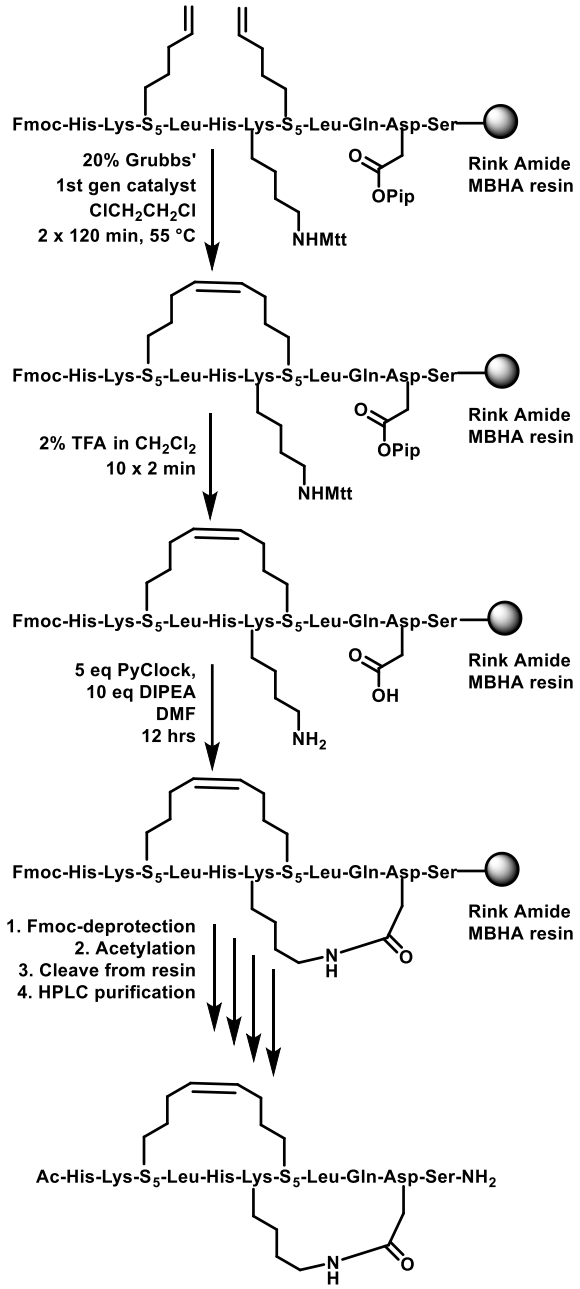

Figure 3.2. Synthesis of hydrocarbon/lactam bicyclic peptide BCP-1

3.3 Synthetic strategy for bicyclic peptides

Guided by the computational results, we synthetically replaced the salt bridge with an amide-based covalent linkage. Critically, the conditions of lactam formation were orthogonal to olefin staple formation, which allowed us to avoid issues of selectivity. This approach also allowed us to replace the hydrophobic residues Ile689 and Leu693 with a hydrocarbon staple while replacing the solvent-exposed salt bridge with a relatively polar amide linkage. Moreover, Fairlie and coworkers recently showed that lactams are uniquely suited to ensuring high levels of helicity in short peptide sequences.[104] Using this orthogonal stapling approach, bicycle SRC2-BCP1 was prepared using solid phase peptide synthesis (**Figure 3.2**). The orthogonal installation of the constraints proceeded sequentially, to near completion, and with no observed cross-reactivity.

3.4 Biophysical characterization of bicyclic peptides

To experimentally determine the secondary structure of the bicyclic peptides, we measured molar ellipticity by circular dichroism at several temperatures and converted [θ]222 readings to percent helicity (**Figures 3.3** and **3.7-3.12**) using an equation previously described by Luo and Baldwin.[105] Gratifyingly, experimental measurements closely matched our computational analysis, with bicyclic peptide SRC2-BCP1 showing the highest helicity (53%), followed by hydrocarbon-stapled peptides PFE-SP2 and SRC2-SP4 (29% and 33%) and lactam-cyclized peptide SRC2-LP1 (23%). The unconstrained SRC2-WT peptide displayed an ellipticity curve indicative of a disordered structure, and this was the only point of departure from the BEUS calculations, which predicted that the helicity of the wild-type peptide should be similar to lactam SRC2-LP1. One possible explanation for this could be that the relative contributions in the α-helicity

reaction coordinate, a collective variable comprising hydrogen bonding and dihedral angle terms, may be suboptimal for reproducing the spectroscopically measured helicity values at the low end of the range. Given that this discrepancy occurred in the low-helicity case, rather than in the desired high helicity cases, the MD simulations successfully informed our staple design to prospectively yield highly stable constrained peptides.

3.5 Proteolytic stability of bicyclic peptides

To measure the stability of this peptide series, we used proteinase K, a serine protease with a broad spectrum of endopeptidase activity.[106] Mass spectrometric analysis of SRC-WT subjected to proteinase K showed cleavage sites at the C-terminal amide bonds of leucine, arginine, and glutamine (**Figure 3.6** and **Table XI**). The unconstrained peptide was rapidly degraded under experimental conditions ($t_{1/2}$ = 0.27 min), whereas SRC2-BCP1 displayed a half-life of ~2,000 minutes, improved by nearly four orders of magnitude. For singly constrained peptides, the hydrocarbon staple provided a higher level of proteolytic stability relative to the lactam bridge. The proteolytic stability of this peptide series was correlated with both %-helicity and the computational energy barrier for peptide unfolding at low helicity scores, suggesting that reinforcing a helical conformation precluded access to peptide bonds from the active site of proteinase K. Because %-helicity tracked with proteolytic stability, our above-mentioned BEUS method may be able to predict both helicity and relative proteolytic stability within a series.

3.6 Peptides inhibit ER/Coactivator binding interaction

We used a TR-FRET assay to measure the peptides' ability to inhibit coactivator recruitment to estrogen receptor (**Figure 3.3C-D** and **Table XII**).[88] All constrained

peptides had higher affinity than SRC2-WT (1.1 μM) with the most active peptide being lactam SRC2-LP1 (78 nM, 14-fold vs. WT). Combining the hydrocarbon staple with the lactam to create bicycle SRC2-BCP1 gave a peptide that was intermediate in affinity between lactam SRC2-LP1 and hydrocarbon stapled peptide SRC2-SP4, even though SRC2-BCP1 showed higher helicity. The ordering of affinities (SRC2-LP1 < SRC2-BCP1 < SRC2-SP4 < SRC2-WT) suggested that stabilizing the helical peptide with a constraint had a positive impact on binding affinity, but that replacing Ile689 and Leu693 with a hydrocarbon staple was slightly deleterious for binding affinity. Phillips et al.[30] previously reported a stapled peptide that had a hydrocarbon staple in place of the lactam of SRC2-LP1. Its binding affinity was poor (>15 μM), suggesting that our approach of installing a more polar staple may be advantageous at this solvent-exposed site.

3.7 Crystal structure analysis of ER/peptide interaction

To further elucidate the molecular factors at play upon binding, we solved crystal structures of bicycle SRC2-BCP1 and lactam SRC2-LP1 bound to the ligand-binding domain of estrogen receptor α (**Figures 3.4** and **3.13** and **Table XIII**). In good agreement with our computational predictions, each peptide bound in a helical conformation between charge clamp residues Lys362 and Glu542, similar to our previously reported structure of SRC2-SP4. The hydrocarbon staple of SRC2-BCP1 supplanted Ile689 and Leu693 of the ILXXLL motif, whereas the lactam staple supplanted non-interacting solvent-exposed residues Arg692 and Asp696. The differences in IC_{50} were only 4-fold, so it might be difficult to ascertain from the structure why SRC2-LP1 was more potent than SRC2-BCP1. Indeed, it was not obvious why replacement of Ile689 and Leu693 with a hydrocarbon staple showed slightly lower affinity, but it may have been due to sub-optimal

hydrophobic interactions formed between the staple and the surface of the estrogen receptor (**Figure 3.4**).

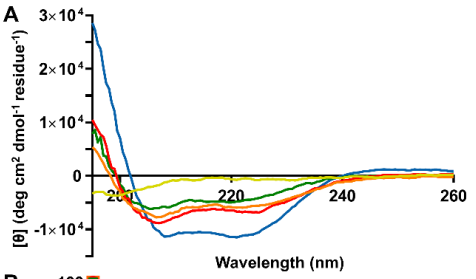

D

Peptide	% α-Helicity (37 ˚C)	$t_{1/2}$ (min)	IC_{50} (μM)
SRC2-BCP1	53	2100	0.33
SRC2-SP4	33	120	0.39
PFE-SP2	29	69	0.76
SRC2-LP1	23	2.1	0.078
SRC2-WT	4	0.27	1.1

Figure 3.3. Biophysical characterization of bicyclic peptides. A) Circular diochroism analysis of 50 μM peptide at 37 °C. B) Proteolytic stability of peptides treated with proteinase K. C) Inhibition of estrogen receptor/steroid receptor coactivator interaction measured by TR-FRET. D) The % α-helicity was calculated using $[\theta]_{222}$ values, the proteolytic $t_{1/2}$ for peptides were found using a non-linear one phase decay fit, and the IC_{50} values were found using a TR-FRET assay

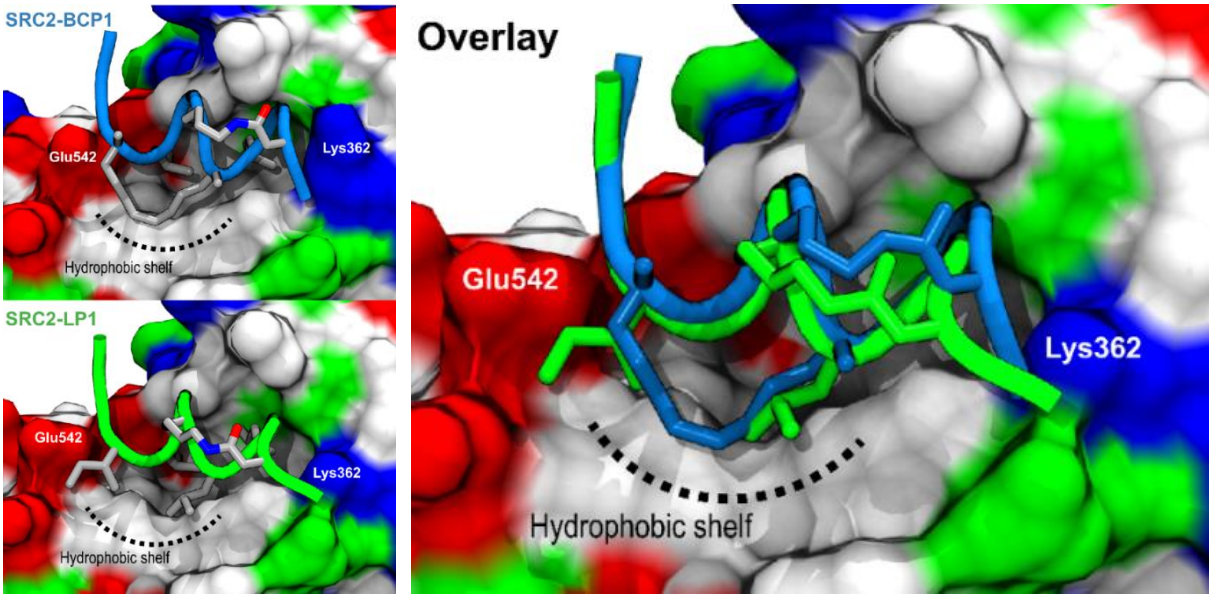

Figure 3.4. X-ray co-crystal structures of bicyclic peptide SRC-BCP1 (top, PDB 5WGQ) and stapled cyclic peptide SRC2-LP1 (middle, PDB 5GWD) bound to the coactivator binding cleft of estrogen receptor α (surface: red = acidic, blue = basic, white = nonpolar, green = polar). The peptide backbone forms a helical conformation oriented between Lys 362 and Glu542. Overlaying the two structures (bottom) highlights the expanded hydrophobic contacts between Ile689 and Leu693 with the hydrophobic shelf, relative to the unbranched hydrocarbon staple, and a different conformation of the lactam linking Arg692 and Asp696.

3.8 Conclusion

In conclusion, we have developed a novel orthogonal stapling strategy to create estrogen receptor-binding bicyclic peptides that showed high helicity and proteolytic stability while retaining nanomolar binding affinities. Our work was informed by both computation and structural biology: a powerful biased exchange umbrella sampling

approach can be used in a prospective manner to predict helicity of short peptide sequences, and x-ray crystal structures of peptides bound to estrogen receptor confirmed our predictions of binding poses. Given the straightforward methods using commercially available amino acids to prepare these peptides, this methodology could be readily applied to other protein-protein interactions.

3.9 Experimental

3.9.1 Computational studies

System Preparation. Molecular systems for PFE-SP2, SRC2-WT, and SRC2-SP4, were constructed as previously described.[71] The WT-R692Q peptide variant was constructed following the same protocol as described for SRC2-WT; however, a PSFGen “mutate” statement was added to the segment-creating part to perform the point mutation in silico.

Equilibrium Simulations. All simulations were performed using the NAMD 2.11 & 2.12 software packages.[90] The peptides were described using the CHARMM36 force field,[107] including CMAP terms and updated NBFIX potentials,[108] and TIP3P was used for explicit solvent.[109] Periodic boundary conditions were configured with full electrostatics calculated out to 10 Å and a switching function to taper contributions to a full cutoff at 12 Å; the Particle Mesh Ewald (PME) method[110] with a grid density >1/Å^3 was used to approximate long-range electrostatics. All simulations were performed under an NPT ensemble maintained by a Nosé-Hoover thermostat (1 atm, 310 K) and Langevin piston (period: 100 fs, decay: 50 fs, damping coefficient 0.5 ps-1).[111] The simulation timestep was set to 2 fs with atomic coordinates recorded every 500 steps (1 ps/frame). Non-bonded forces

were updated at every timestep, while PME calculations were performed at every other step.

Simulations of PFE-SP2 and SRC2-SP4 were each performed under equilibrium conditions in free solution for 0.5 μs. Simulation trajectories were analyzed by computing the α-helicity for the full peptide using the COLVARs module[112] in VMD.[91] Additionally, explicit interactions between residues Arg/Gln692 and Asp696 were quantified by measuring the number of hydrogen bonds observed between the side chains using the HBonds plugin of VMD.

Bias Exchange Umbrella Sampling (BEUS).[103] An initial simulation was performed for each peptide whereby a COLVAR (collective variable) representing the α-helicity was driven by a harmonic potential (k = 1000) from 1.0 to 0.0 over 8 ns. Plots of the measured α-helicity and the force applied throughout the simulation were inspected to assess appropriate bounds on α-helicity as a reaction coordinate. From these data, windows were designed with a width of 0.04 ranging from 0.9 to 0.1 (21 windows) for WT and WT-R692Q, 0.9 to 0.22 (18 windows) for SRC2-SP4 and PFE-SP2, and 0.9 to 0.14 (20 windows) for SRC2-LP1 and SRC2-BCP1. Frames from the driven simulation trajectories were binned according to α-helicity. A random coordinate set was selected from each bin to seed the window, minimized for 500 steps, and simulated for 1 ns while applying a harmonic biasing potential defined by the window center (k = 660). BEUS simulations were then performed using the replica-exchange module of NAMD with exchanges allowed between adjacent windows every 500 steps. To ensure efficient exchange between windows, the force constant for each harmonic restraining potential was tuned using short simulations until achieving an exchange rate of approximately 20-40% over

500 exchange attempts (500 ps). After completing the tuning process, production BEUS simulations were run for 100 ns. The entire BEUS method required over 11.8 μs of aggregate simulation time.

The resulting BEUS simulation data were preprocessed by sorting the replicas using the ”sortreplicas” binary provided with NAMD and dividing the trajectory data into 10-ns blocks; the initial 20 ns of production simulation data were discarded. The potential of mean force (PMF) profile for unfolding was then computed using the generalized weighted histogram analysis method (WHAM) with bootstrapping error analysis.[103, 113]

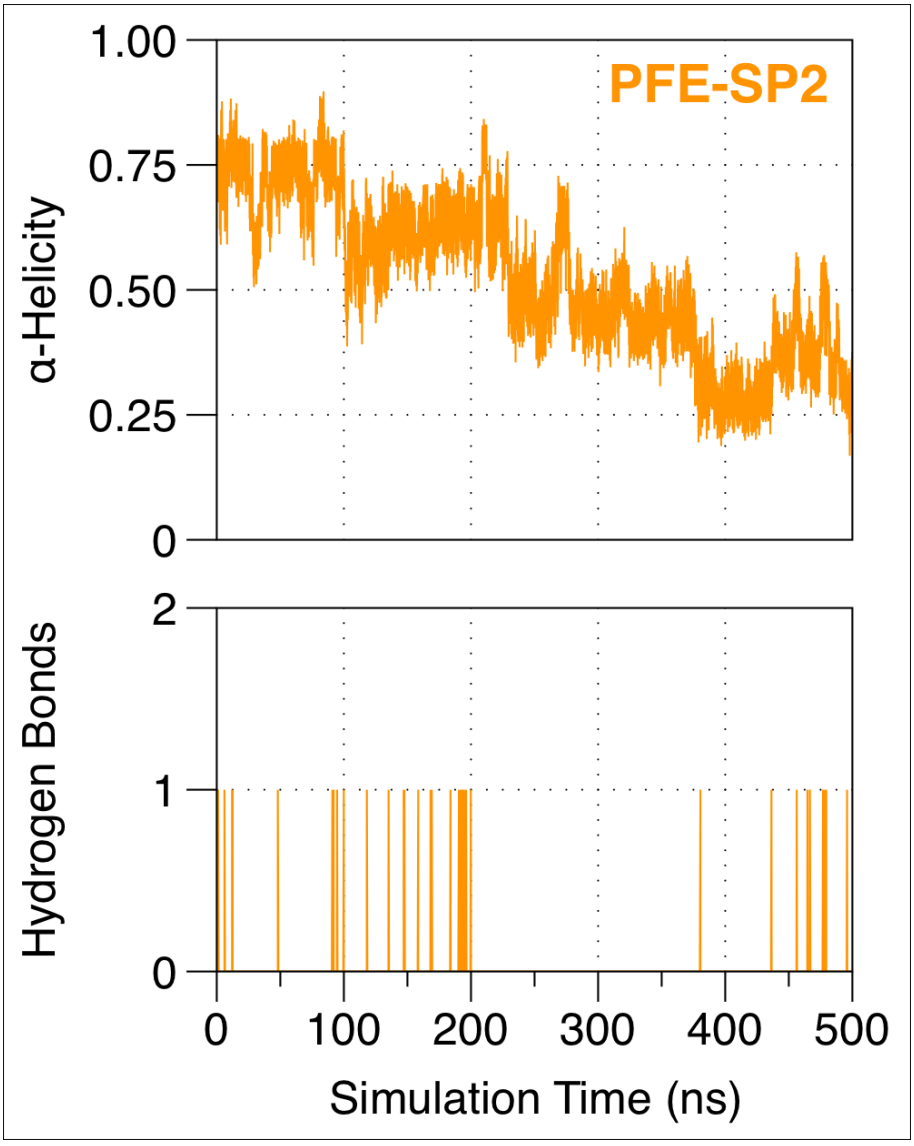

Figure 3.5. Long time-scale simulation of hydrocarbon stapled peptide PFE-SP2 in solution. The frequency of hydrogen bond formation between Gln692 and Asp696 side-chains is depicted.

3.9.2 Peptide synthesis

Peptide synthesis was accomplished by adapting previously described procedures.[57, 92, 104] All peptides were manually synthesized on 30 μmol scale using standard Fmoc solid phase peptide synthesis. Fmoc deprotection was carried out for 2 × 10 minutes using 25% piperidine in DMF with 0.1 M HOBt. Amino acids were coupled using 5 eq of amino acid, 5 eq of PyClock, and 10 eq of DIPEA in 0.75 mL of DMF. Stapling amino acid S5 was coupled for 2 hrs, amino acids following S5 were coupled for 2 × 90 min, and all other amino acids were coupled for 2 × 20 min. Ring closing metathesis was performed 2 × 120 min at 55 °C using 1 mL of 20% mol Grubb's 1st generation catalyst in DCE. Lactam cyclization was performed on resin by selectively deprotecting Lysine (Mtt) and aspartate (Opip) with 10 × 2 min treatments of 2% TFA in DCM followed by extensive washing (DCM) and a 12 hr coupling reaction using 5 eq of PyClock and 10 eq of DIPEA in DMF. Acetylation and cleavage were carried out as previously described.[92] The crude peptides were purified by semi-preparative HPLC (Solvent System MeCN:H_2O with 0.1% formic acid; 0-4 min, 10% MeCN; 4-24 min 10-50% MeCN; 24-25 min, 50-80% MeCN; 25-30 min, 80% MeCN; 30-31 min 80-10% MeCN. Column: Phenomenex Luna 5 μm C18(2), 100 Å, 250 x 10 mm). Peptide mass was measured using a Bruker Autoflex MALDI-TOF mass spectrometer. Peptide purity was determined using analytical HPLC (Solvent System MeCN:H_2O with 0.1% trifluoroacetic acid; 0-2 min, 4% MeCN; 2-12 min 4-70% MeCN; 12-13 min, 70% MeCN; 13-14 min, 70-4% MeCN; 14-17 min 4% MeCN. Column: Phenomenex Kinetex 5 μm C18, 100 Å, 50 x 4.6 mm). See **Table XIV**.

3.9.3 Proteolytic assay

Peptide (1 µL of 50 mM DMSO stock) was added to 999 µL of phosphate buffer (20 mM, pH 7.4) in a 1.5 mL centrifuge tube and incubated at 37 °C for the reaction. A 50 µL aliquot of the solution was removed from the reaction tube and added to the quenching liquid (100 µL of 1:1 water/acetonitrile with 1% TFA) to record the initial peptide concentration. The reaction was then started by adding proteinase K (5 µL of 2 mg/mL stock) to the peptide solution. A 50 µL aliquot of the solution was removed from the reaction tube at each time point and transferred to another tube containing the quenching liquid. The quenched samples were centrifuged at 10,000 RCF for 5 min and subjected to HPLC analysis. The amount of peptide remaining in each sample relative to the initial peptide in the reaction was found by taking the ratio of the peak integration (220 nm) at each timepoint over the peak area of the initial sample. The percent of peptide remaining as a function of time was analyzed using a non-linear one phase decay fit embedded within GraphPad Prism.

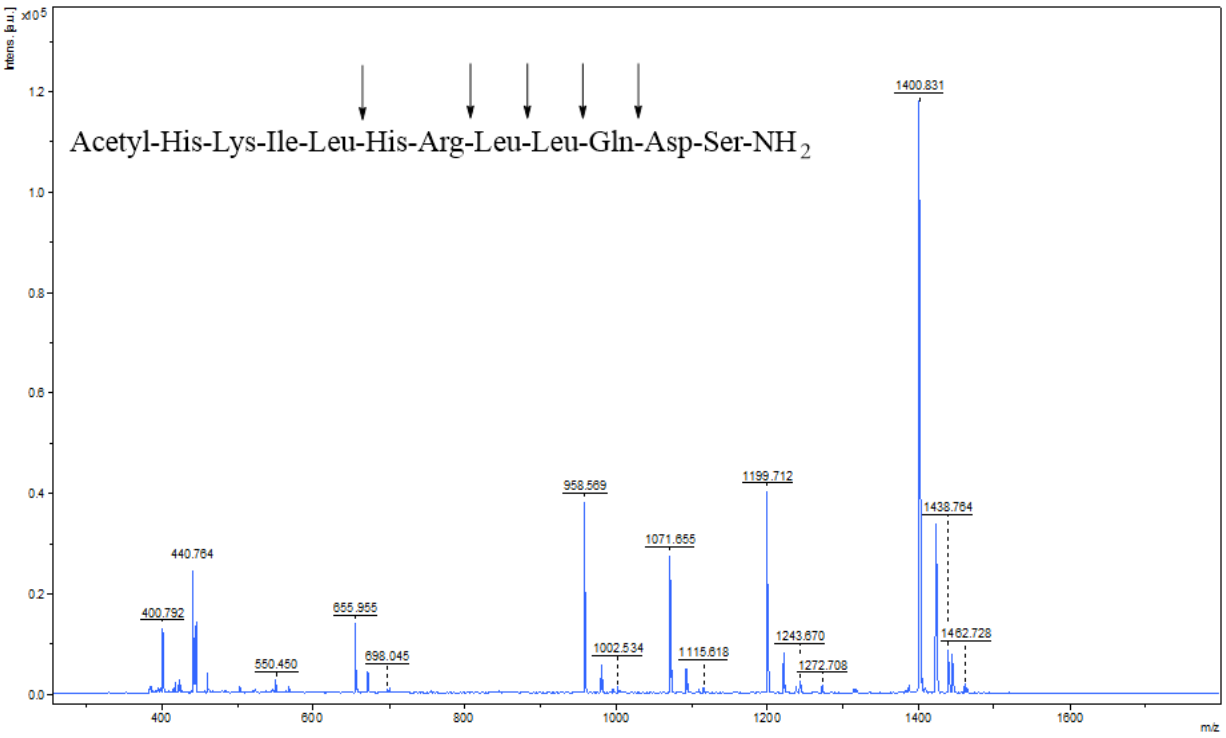

Figure 3.6. MALDI-MS analysis of SRC2-WT after treatment with Proteinase K for 10 seconds.

TABLE XI. SUMMARY OF OBSERVED CLEAVAGE PRODUCTS AND INDICATED CLEAVAGE SITES

Sequence	Exact Mass [M+H$^+$]	Observed Mass [M+H$^+$]
Ac-HKILHRLLQDS-NH2	1400.812	1400.831
Ac-HKILHRLLQ-OH	1199.737	1199.712
Ac-HKILHRLL-OH	1071.679	1071.655
Ac-HKILHRL-OH	958.594	958.569
Ac-HKILHR-OH*	845.51	845.644
Ac-HKIL-OH**	552.35	552.199

*This fragment mass was observed at 3 hr timepoint

**This fragment mass was observed at 24 hr timepoint

3.9.4 Circular dichroism

Circular dichroism (CD) data were collected using a Jasco J810 CD spectrometer with a PTC 4235 temp control. Peptides were diluted to 50 μM in 50 mM phosphate buffer pH 7.4. Spectra were acquired at 5, 15, 25, 37, 45, 55, 65, 75, 85 and 95°C, over the range

of 260–190 nm using the following instrument settings: 0.5 nm pitch, 1 nm band width, 1 second response, 20 nm/min scan speed, 0.1 cm cell length, and 3 accumulations. The baseline from a blank sample of 50 mM phosphate buffer pH 7.4 was subtracted from each data set, and the data were minimally smoothed using the same level of adaptive smoothing. mdeg values recorded on the spectrometer were converted to mean residue ellipticity [θ] (deg cm^2 $dmol^{-1}$ $residue^{-1}$ using equation 1:

$$[\theta] = \text{mdeg} / (10 * C * l * r) \qquad (1)$$

where *C* is the peptide concentration (M), *l* is the pathlength of the sample cuvette (cm) and *r* is the number of residues in the peptide.

Percent helicity was calculated using the methods previously described by Sholtz[114] and Luo[115] and applied by Fairlie[104] (equation 2):

$$\% \ \alpha\text{-helicity} = (\theta_{obs} - \theta_C) / (\theta_H - \theta_C) \qquad (2)$$

θ_{obs} is the molar ellipticity measured at 222 nm, θ_C is the molar ellipticity of a complete coil at 222 nm (equation 3), and θ_H is the calculated molar ellipticity of the complete helix (equation 4):

$$\theta_C = 2200 - 53T \qquad (3)$$

$$\theta_H = (-44{,}000 + 250T) * (1 - k/n) \qquad (4)$$

where *k* is the peptide length correction factor, *n* is the total number of residues, and *T* is temperature in Celsius. We set *k* equal to 4 and *n* to 11.

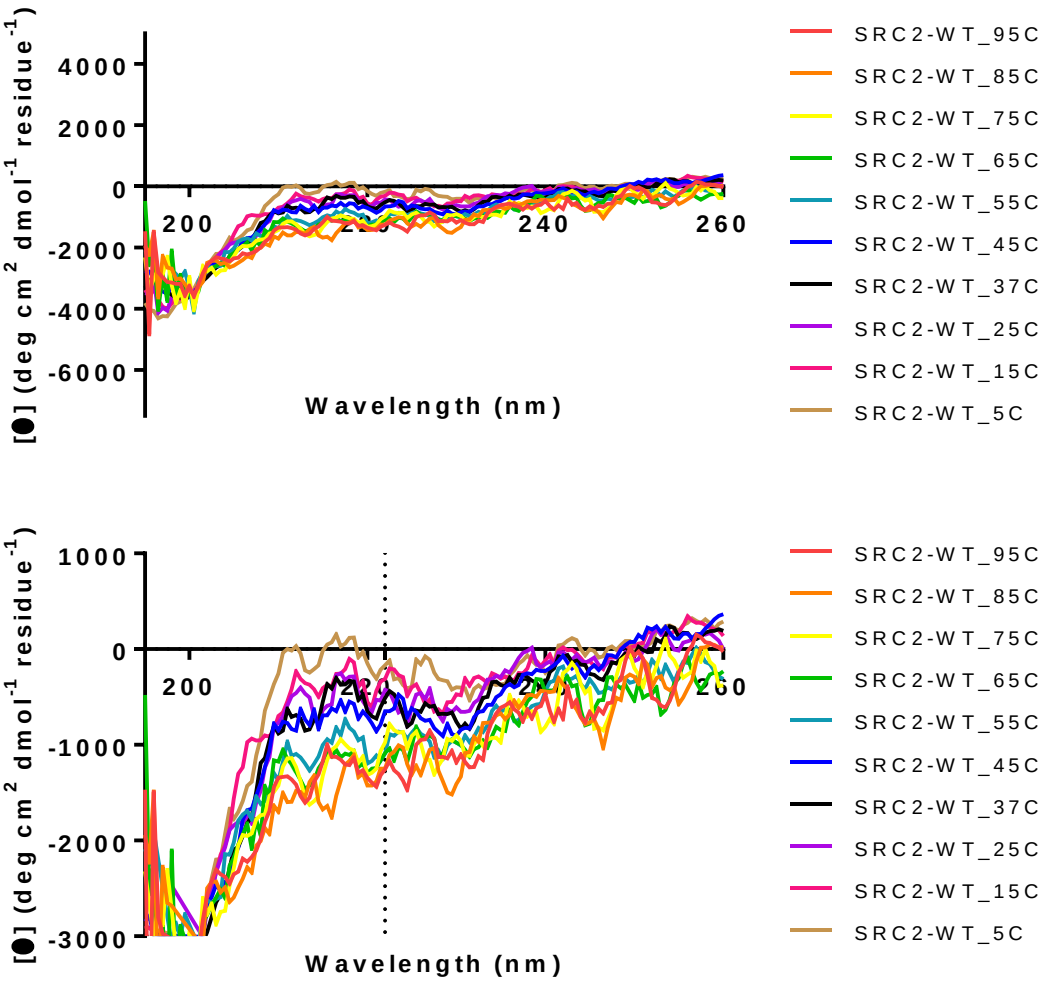

Figure 3.7. Circular dichroism analysis of SRC2-WT from 5-95 °C.

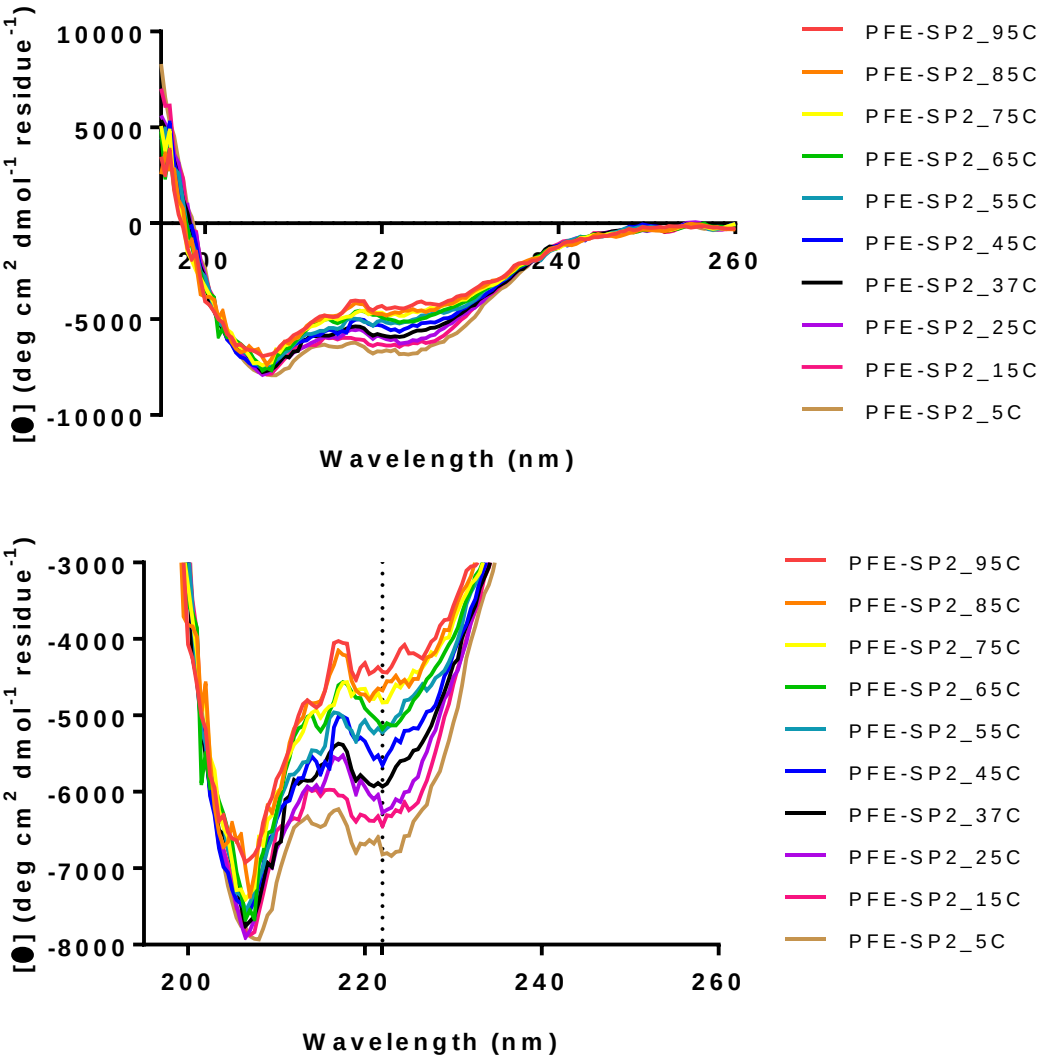

Figure 3.8. Circular dichroism analysis of PFE-SP2 from 5-95 °C.

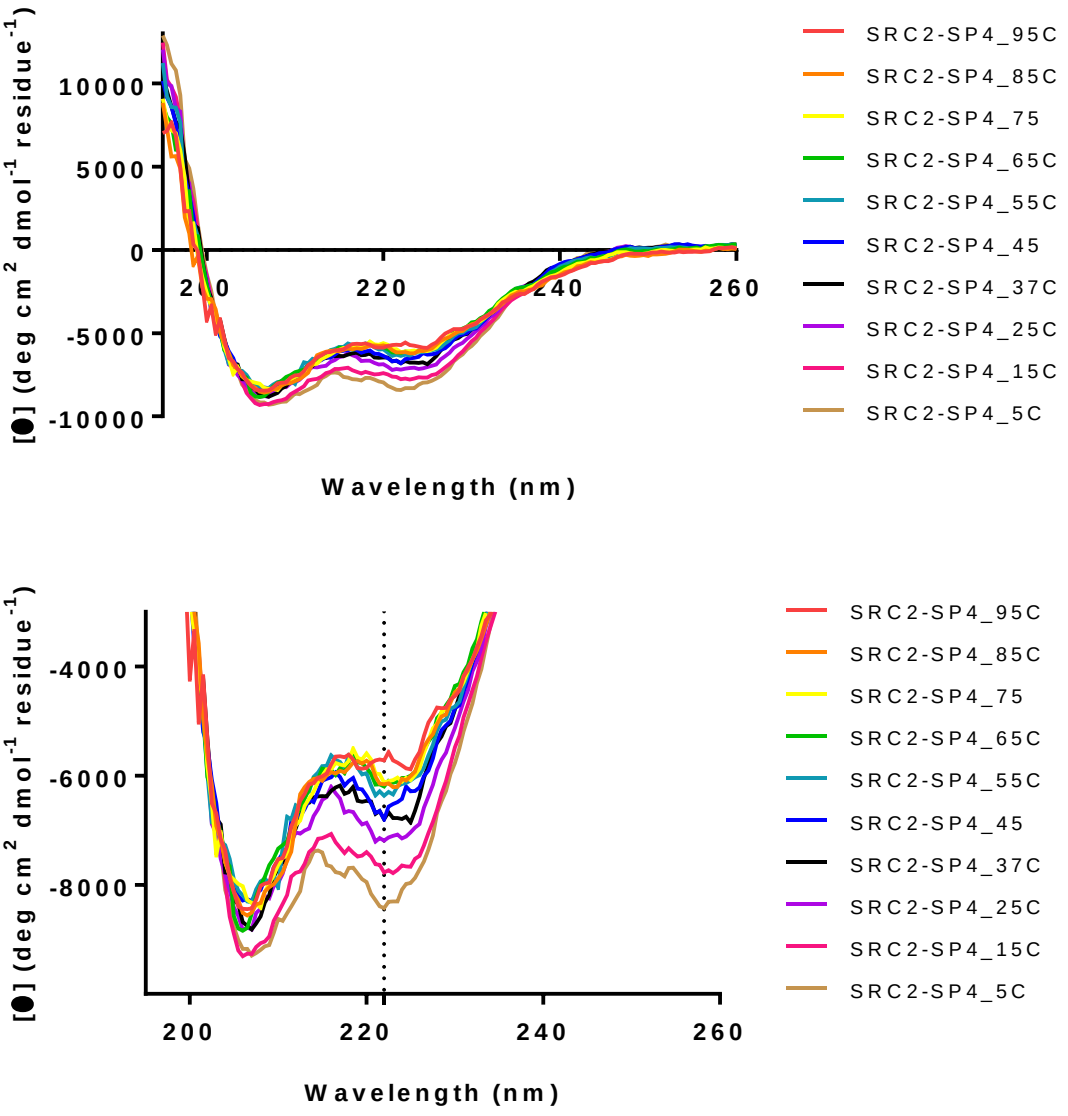

Figure 3.9. Circular dichroism analysis of SRC2-SP4 from 5-95 °C.

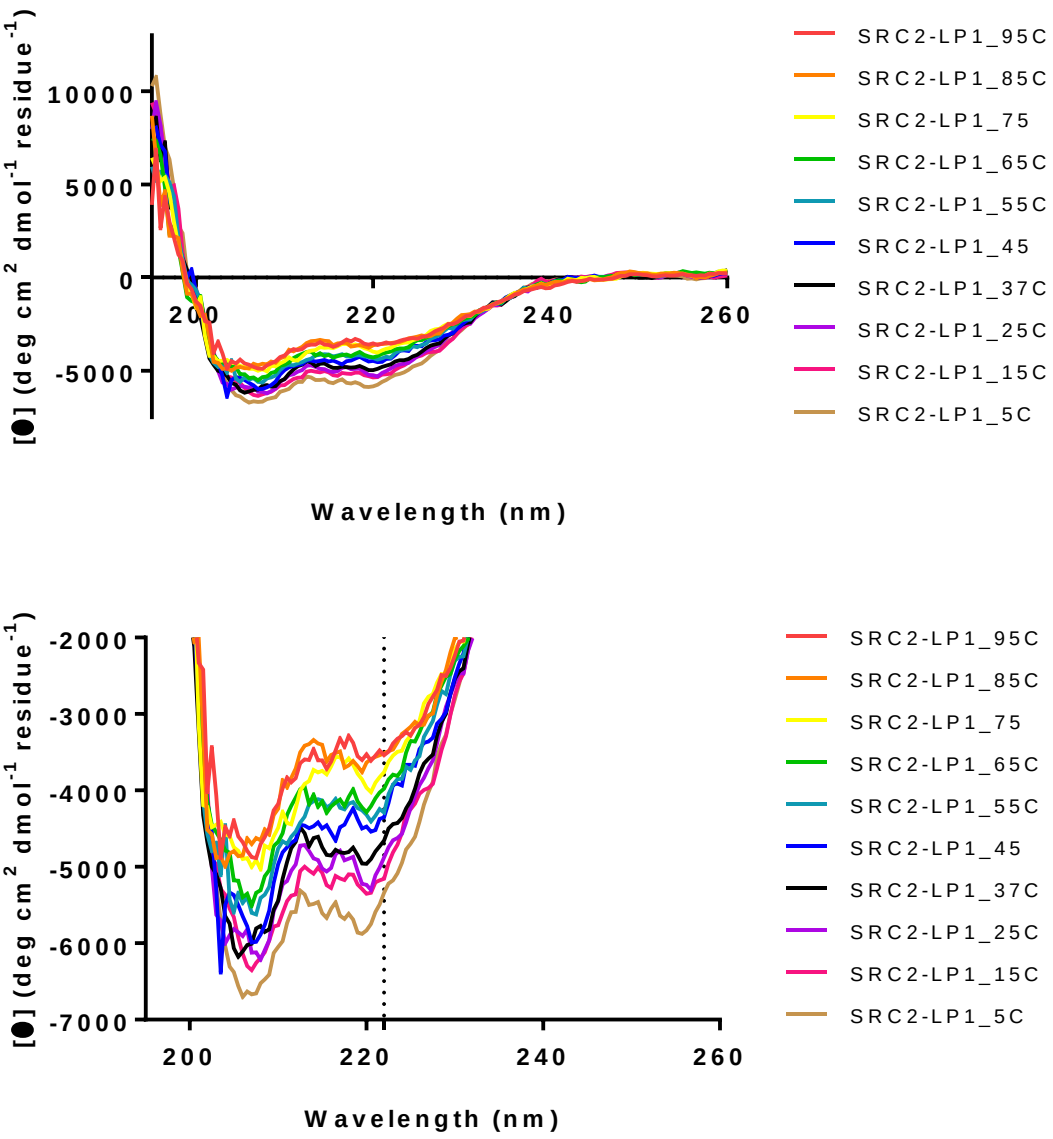

Figure 3.10. Circular dichroism analysis of SRC2-LP1 from 5-95 °C.

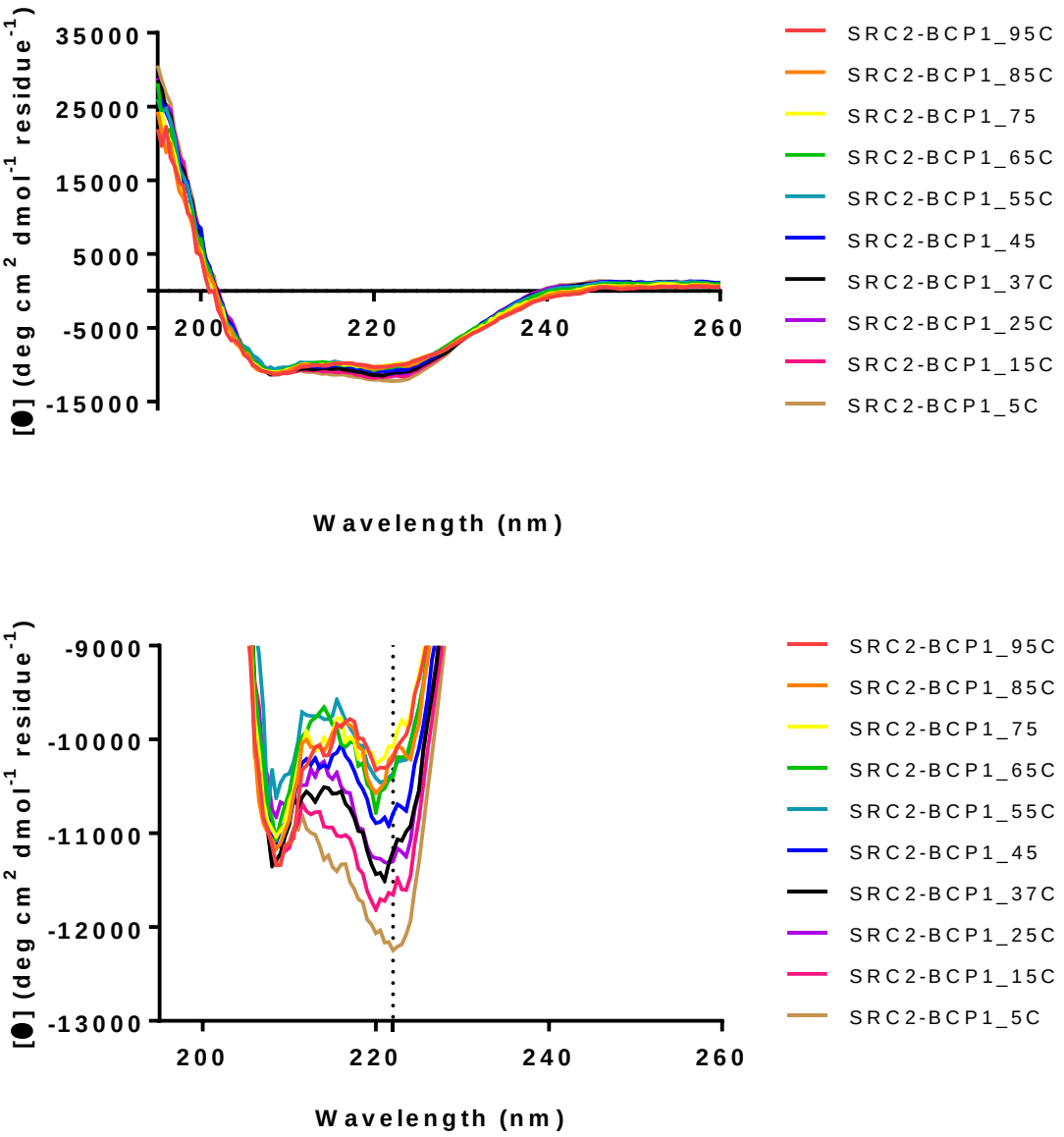

Figure 3.11. Circular dichroism analysis of SRC2-BCP1 from 5-95 °C.

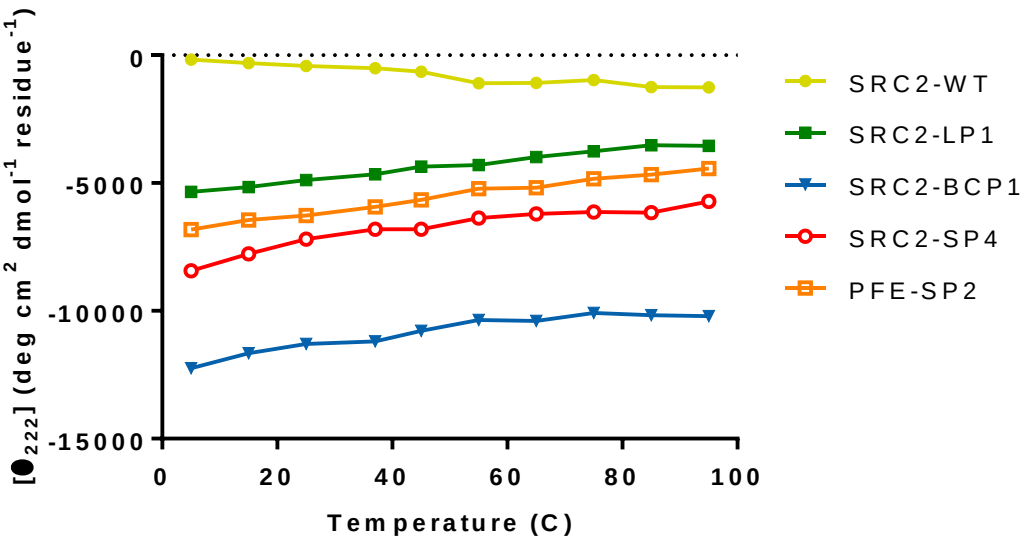

Figure 3.12. Thermal stability of peptides.

3.9.5 TR-FRET assay

The TR-FRET assay was carried out as previously described. [71]

TABLE XII. TR-FRET STATISTICAL INFORMATION FOR BEST-FIT VALUES

	SRC2-LP1	SRC2-BCP1	SRC2-SP4	SRC2-WT	PFE-SP2
Top	0.4134	0.4216	0.4956	0.5044	0.5114
Bottom	0.007734	0.03678	0.01778	0.02447	0.05688
LogIC50	-7.111	-6.481	-6.411	-5.965	-6.121
HillSlope	-1.001	-0.8856	-0.8722	-1.032	-1.022
IC50	7.752E-08	3.304E-07	3.882E-07	0.000001085	7.575E-07
Span	0.4057	0.3848	0.4779	0.4799	0.4545
Std. Error					
Top	0.01024	0.01325	0.007867	0.007535	0.008392
Bottom	0.0113	0.0246	0.01569	0.021	0.01989
LogIC50	0.06676	0.1236	0.06509	0.06601	0.07171
HillSlope	0.1378	0.199	0.09551	0.1395	0.1462
Span	0.01663	0.03073	0.01923	0.02376	0.02315
95% CI (asymptotic)					
Top	0.3925 to 0.4343	0.3946 to 0.4486	0.4796 to 0.5117	0.489 to 0.5198	0.4943 to 0.5284
Bottom	-0.01528 to 0.03075	-0.01333 to 0.0869	-0.01421 to 0.04978	-0.01836 to 0.0673	0.01637 to 0.09739
LogIC50	-7.247 to -6.975	-6.733 to -6.229	-6.544 to -6.278	-6.099 to -5.83	-6.267 to -5.975
HillSlope	-1.281 to -0.7199	-1.291 to -0.4803	-1.067 to -0.6774	-1.316 to -0.7472	-1.32 to -0.724
IC50	5.668e-008 to 1.06e-007	1.85e-007 to 5.9e-007	2.86e-007 to 5.27e-007	7.955e-007 to 1.479e-006	5.411e-007 to 1.06e-006
Span	0.3718 to 0.4395	0.3222 to 0.4474	0.4386 to 0.5171	0.4315 to 0.5284	0.4073 to 0.5016
Goodness of Fit					
Degrees of Freedom	32	32	31	31	32
R square	0.9718	0.928	0.9824	0.9757	0.9698
Absolute Sum of Squares	0.03046	0.063	0.02177	0.02756	0.03334
Sy.x	0.03085	0.04437	0.0265	0.02982	0.03228
Number of points					
# of X values	36	36	36	36	36
# Y values analyzed	36	36	35	36	36
Outliers (excluded, Q=1%)	0	0	0	1	0

3.9.6 X-Ray structure solution

ERα ligand binding domain Y537S mutant was expressed and purified as previously described.[71] For each stapled peptide complex, 5 mg/mL protein was incubated with 1 mM estradiol (E2) and 1.5 mM peptide overnight at 4 °C. The next morning, the protein complexes were centrifuged at 16.1 × g for 15 minutes at 4 °C to remove any precipitate. The complexes were crystallized using hanging drop vapor diffusion using pre-greased Hampton VDX plates (Hampton Research) at room temperature with a 1:1 µL protein:precipitant ratio. For the SRC2-LP1 complex, clear rectangular crystals were observed after 48 hours in 15% PEG 3,350, 200 mM $MgCl_2$, Tris pH 8.5. For the SRC2-BCP1 complex, clear rectangular crystals were observed after 48 hours in 15% PEG 3,350, 200 mM $MgCl_2$, Tris pH 8.5. All x-ray data sets were collected at the Structural Biology Consortium 19-BM beamline at the Advanced Photon Source, Argonne National Laboratories, Argonne, Illinois.

Data were indexed, scaled, and merged using HKL-3000.[116] Phenix was used for all molecular replacement and refinements[117] with PDB: 5DXE was used as the starting model for each of the data sets after removing ligands, peptides, and waters.[71] All structures show one dimer in the asymmetric unit. Phenix was used for all refinements using iterative rounds of Phenix Refine and manual inspection with Coot.[117-118] ELBOW was used to generate the atomic constraints of stapled peptides.[117] Clear electron densities were observed for the E2 and stapled peptides after one round of refinement (**Figure 3.13**). Unresolved atoms were not included in the final model. All structures were deposited in the Protein Data Bank with accession codes 5WGD (SRC2-LP1) and 5WGQ (SRC2-BCP1).

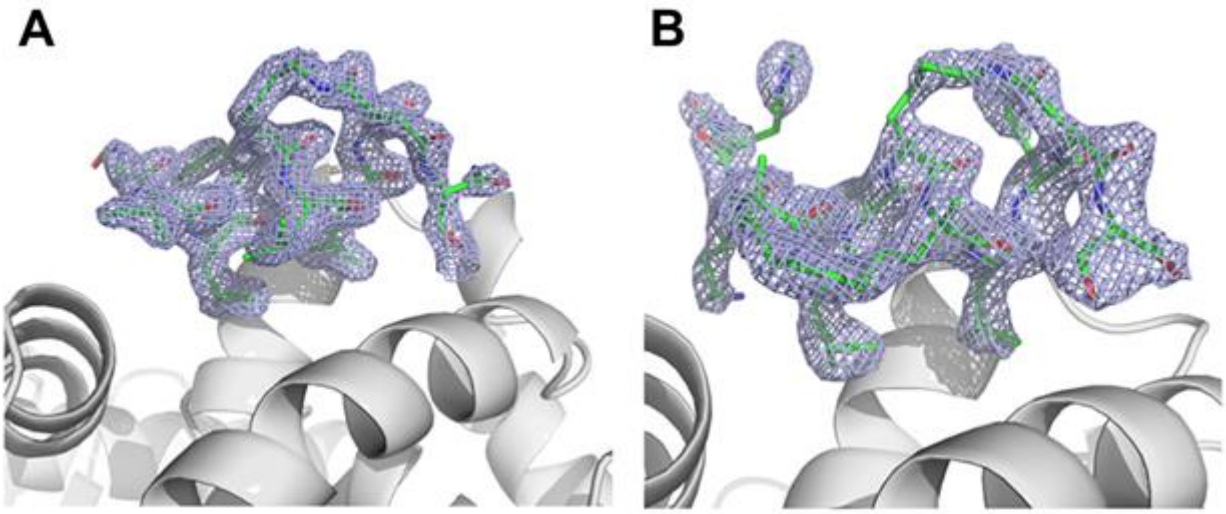

Figure 3.13. Simulated annealing composite omit map for (A) SRC2-LP1 and (B) SRC2-BCP1 contoured to 1.5σ.

TABLE XIII. DATA COLLECTION AND REFINEMENT STATISTICS FOR X-RAY CRYSTAL STRUCTURES

	Y537S-E2-SRC2-LP1	**Y537S-E2-SRC2-BCP1**
PDB	5GWD	5WGQ
Data collection		
Space group	P1211	P1211
Cell dimensions		
a, b, c (Å)	56.03, 83.83, 58.38	54.04, 84.04, 58.21
α, β, γ	90.00, 108.32, 90.00	90.00, 111.25, 90.00
Resolution (Å)	50.00 – 1.80	50 – 2.29
$cc^{1/2}$	0.076 (0.633)	0.264 (0.534)
Completeness (%)	96.4 (94.2)	98.3 (97.6)
Redundancy	3.5 (3.3)	3.7 (3.5)
Refinement		
Resolution (Å)	26.60 – 1.80	31.08 – 2.29
No. Reflections	42687	23707
R_{work}/R_{free}	17.7/20.84	20.56/24.0
No. Atoms		
Protein	4184	3763
Ligand/ion	40	40
Water	450	106
B-factors		
Protein	25.1	37.9
Ligand/ion	19	30.9
Water	36	49.7
R.m.s. deviations		
Bond lengths (Å)	0.009	0.009
Bond angles (°)	1.16	1.17

*Highest-resolution shells are shown in parentheses. computing Center.

TABLE XIV. PEPTIDE CHARACTERIZATION

Peptide	Sequence	Exact Mass ($M+H^+$)	Observed Mass ($M+H^+$)	RT (min)
SRC2-LP1	Ac-HKILHKLLQDS-NH_2	1354.795	1354.927	7.9
SRC2-BCP1	Ac-HKIXHKXLQDS-NH_2	1378.795	1378.903	7.9
SRC2-SP4	Ac-HKIXHRXLQDS-NH_2	1425.819	1424.85	7.62
PFE-SP2	Ac-HKIXHQXLQDS-NH_2	1396.77	1396.883	7.77
SRC2-wt	Ac-HKILHRLLQDS-NH_2	1400.812	1400.87	6.87

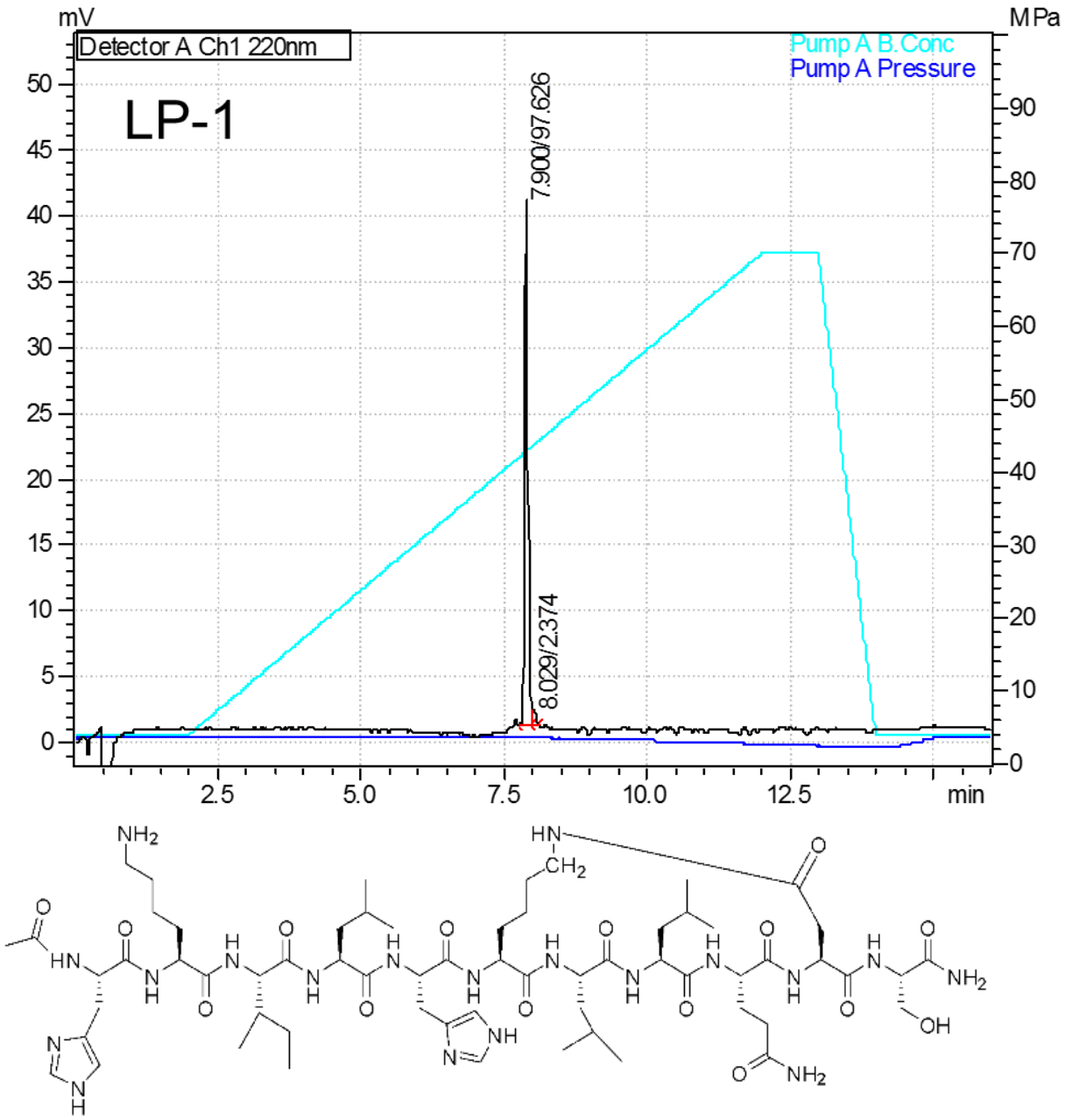

Figure 3.14. Structure and HPLC chromatogram for SRC2-LP1

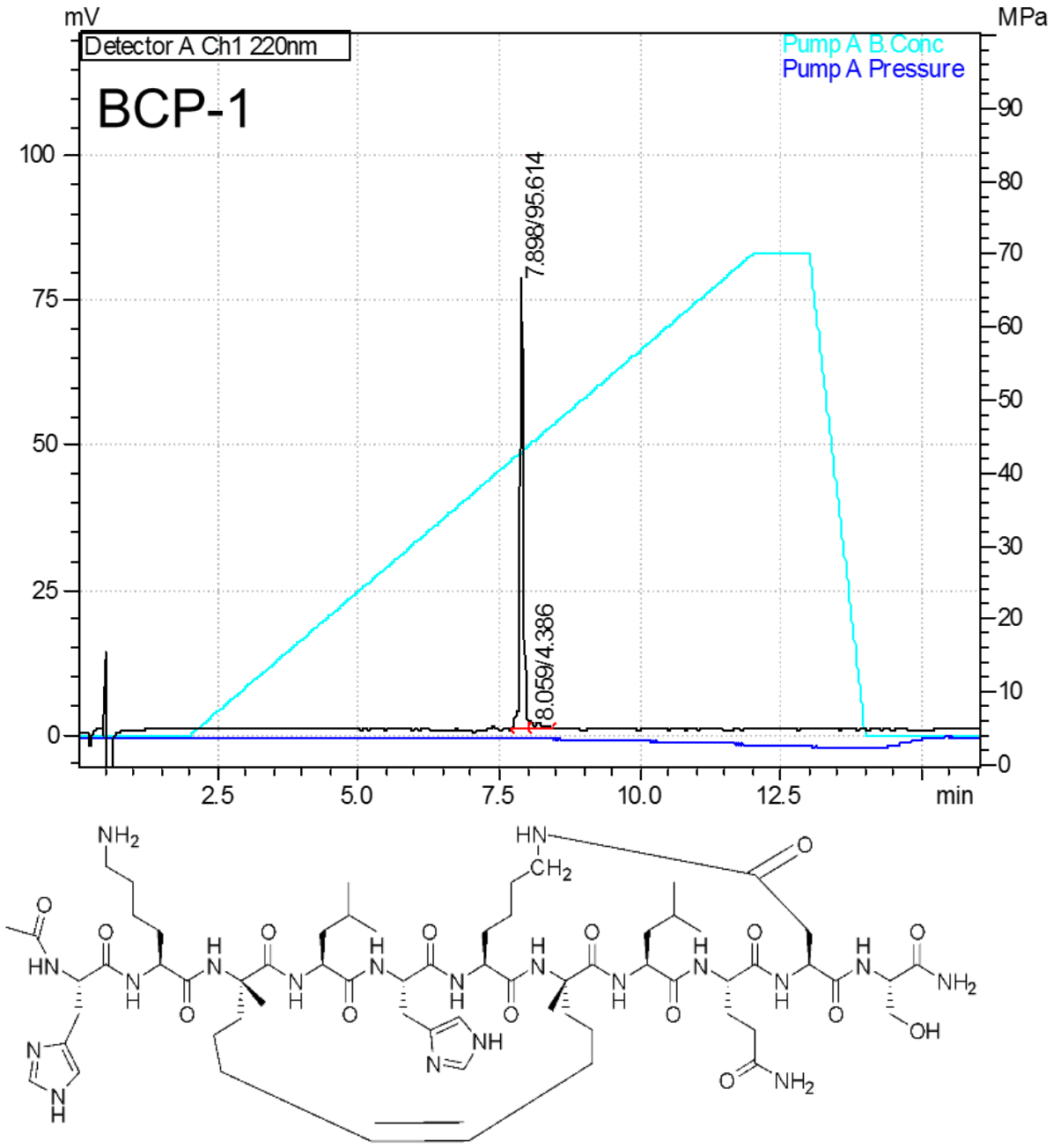

Figure 3.15. Structure and HPLC chromatogram for SRC2-BCP-1

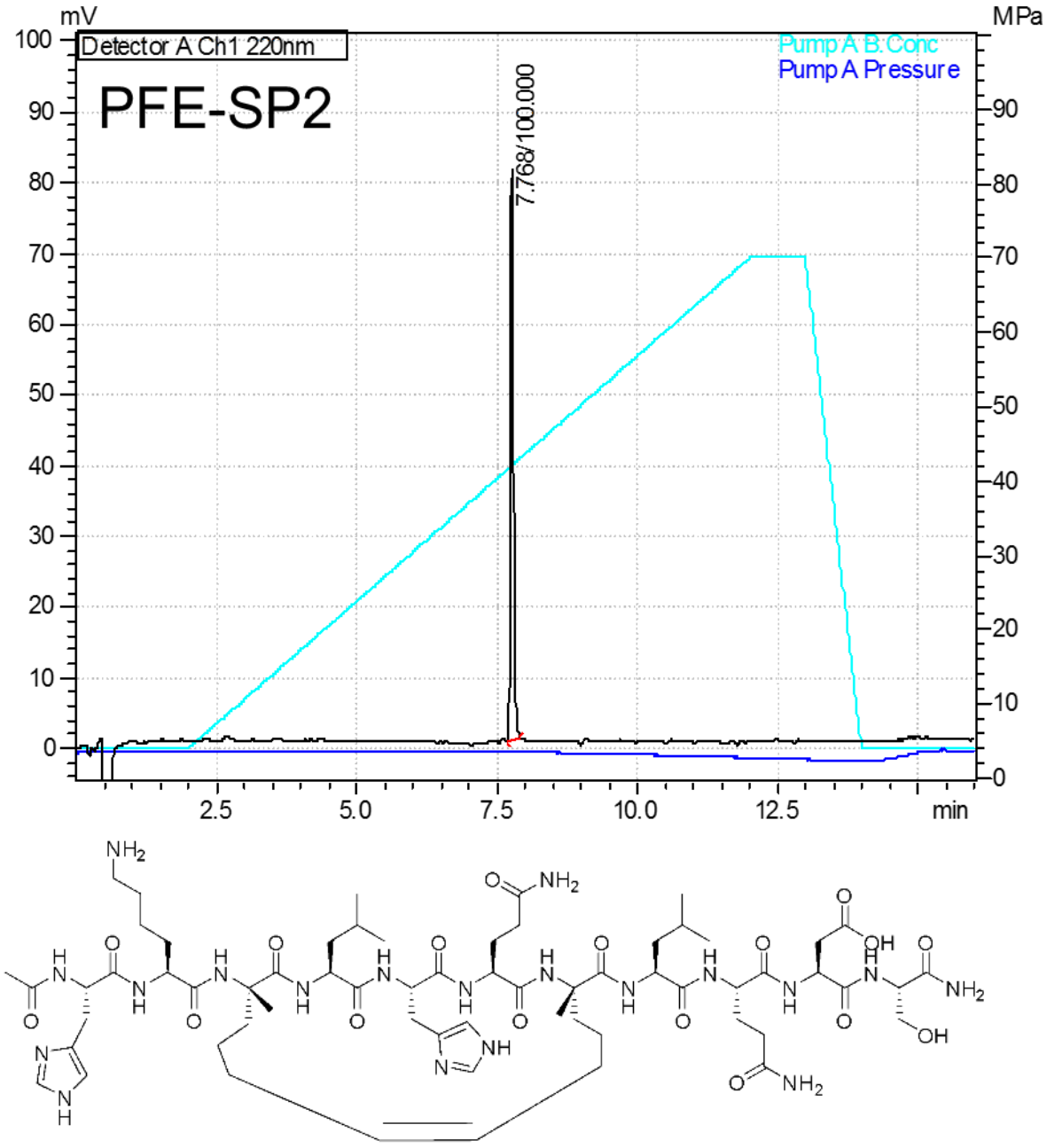

Figure 3.16. Structure and HPLC chromatogram for PFE-SP2

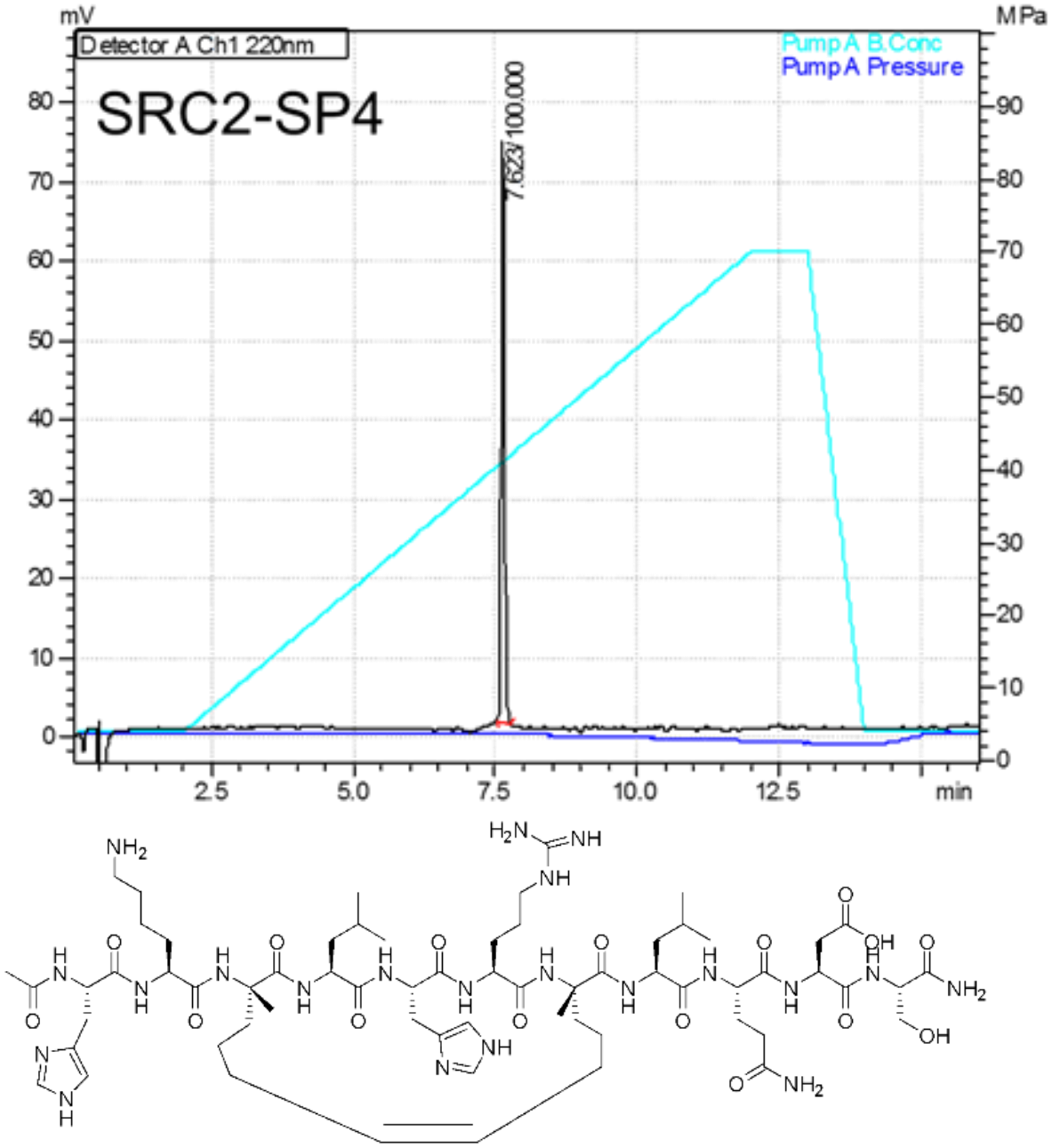

Figure 3.17. Structure and HPLC chromatogram for SRC2-SP4.

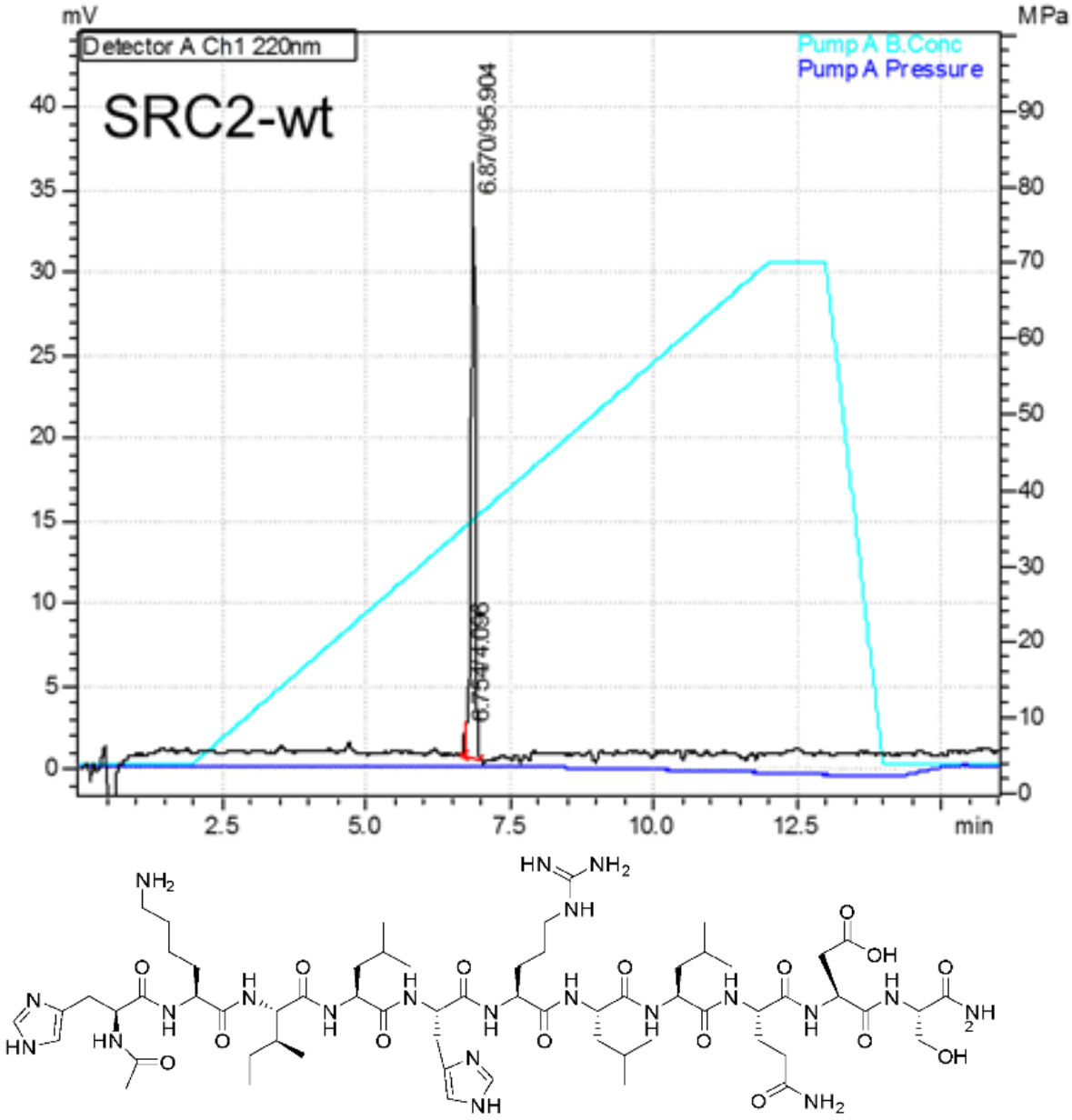

Figure 3.18. Structure and HPLC chromatogram for SRC2-WT

4. A CELL-PERMEABLE STAPLED PEPTIDE INHIBITOR OF THE ESTROGEN RECEPTOR/COACTIVATOR INTERACTION.†

4.1 Introduction

The most well-characterized coactivators are the steroid receptor coactivators (SRCs). These coactivators bind to ERα over two turns of an α-helix though an LXXLL motif, also known as a nuclear receptor box (NR-box).[39, 119] In addition to their effects at ERα, coactivators also regulate the activity of other transcription factors, including other members of the nuclear receptor superfamily. In particular, SRC3, also known as AIB1 (amplified in breast cancer 1), is upregulated in up to 60% of breast cancer cases[16] and is correlated with poor survival rates.

A mechanistic hypothesis in the breast cancer literature has been that directly blocking the ER/coactivator interaction may provide an alternative to antagonizing ER, and that this approach may be useful in treating ER+ breast cancers that have become refractory to current endocrine therapy.[99] A major limitation to testing this hypothesis has been in developing peptides and small molecules that are active in cellular models of ER+ breast cancer.[26, 31-32, 120-121] With a notable exception,[37] many of the reported small molecule and peptide coactivator binding inhibitors show activity in *in vitro* assays of ER binding and activity but not in more advanced assays of native gene regulation or of ER+ breast cancer phenotypes.

---

†Reprinted (adapted) with permission from Speltz, T. E.; Danes, J. M.; Stender, J. D.; Frasor, J.; and Moore, T. W. A Cell-Permeable Stapled Peptide Inhibitor of the Estrogen Receptor/Coactivator Interaction. *ACS Chemical Biology*. **2018**, 13 (3), 676-684. Copyright 2018 American Chemical Society.

In this work, we used molecular dynamics simulations to design a cell-permeable stapled peptide, R4K1, that inhibits the ER/coactivator interaction *in vitro* with low nanomolar potency. R4K1 is taken up by breast cancer cells, blocks ERα-mediated gene transcription, and inhibits the proliferation of breast cancer cells. We also examine the effects of R4K1 on global gene transcription using RNA-Seq. R4K1 provides a significant proof-of-concept for preparing cell-permeable stapled peptide inhibitors of the ER/coactivator interaction.

4.2 Molecular dynamics-guided design

Because the LXXLL motif of coactivators occurs over two turns of an α-helix, stapled peptides provide a good starting point for developing ERα/coactivator binding inhibitors. Indeed, a group at Pfizer used the LXXLL motif to design stapled peptides with nanomolar affinity for ERα.[30] Unfortunately, there are no reports of cellular activity associated with the Pfizer peptides, and we found that several stapled peptides reported by us [71] and Phillips, et al.[30] were unable to decrease expression of native genes that are under the control of ERα (**Figures 4.17** and **4.18**). This finding may be explained by poor cell penetration (see microscopy studies below). Guided by this hypothesis, we set out to design a high-affinity stapled peptide that would also show cell-permeability.

Chu et al. recently published a comprehensive study aimed at understanding cell penetration by stapled peptides. They found that stapled peptides with a formal charge of +5 at pH 7.5 can display high levels of cellular uptake.[63] To replicate this approach, we examined our previously reported crystal structure of ERα bound to stapled peptide SRC2-SP4 (PDB: 5DXE) to decide where to place additional charged residues. ERα contains four surface-exposed aspartate/glutamate residues near the *N*-terminal region

of the SRC2-SP4 binding site (**Figure 4.1A**). We reasoned that this region of ERα may provide electrostatic complementarity for positively charged residues of SRC2 because three of six residues preceding the SRC2-Box2 LXXLL motif are lysine (-KEKHKI**L**HR**LL**-). Replacement of -KEKHK- with -RRRRK- would generate an SRC stapled peptide with a +5 formal charge that mimics the structural motif of primary amphipathic cell penetrating peptides[122] and contains a variation of the putative nuclear localization signal sequence.[123]

To provide evidence of electrostatic complementarity, we carried out a total of 1.5 μs of molecular dynamics simulations of ERα bound to either SRC2-SP4 (magenta in **Figure 4.1A-1B**) or a version of SRC2-SP4 that contains four Arg residues (R4K1, beige in **Figure 4.1A-1B**). The percentage of time in each simulation that SRC2-SP4 (magenta) or R4K1 (beige) formed at least one H-bond with negatively charged residues Glu380, Asp538, Glu542, or Asp545 is shown (Figure 4.1D). In the simulations, R4K1 showed a statistically significant increase in the number of H-bonds formed at three of four residues, although the effect seemed to be most pronounced at residue Glu542, part of the so-called “charge clamp.”[11] While arginine residues were incorporated to increase cell permeability, these data suggested that they may also contribute to higher binding affinity.

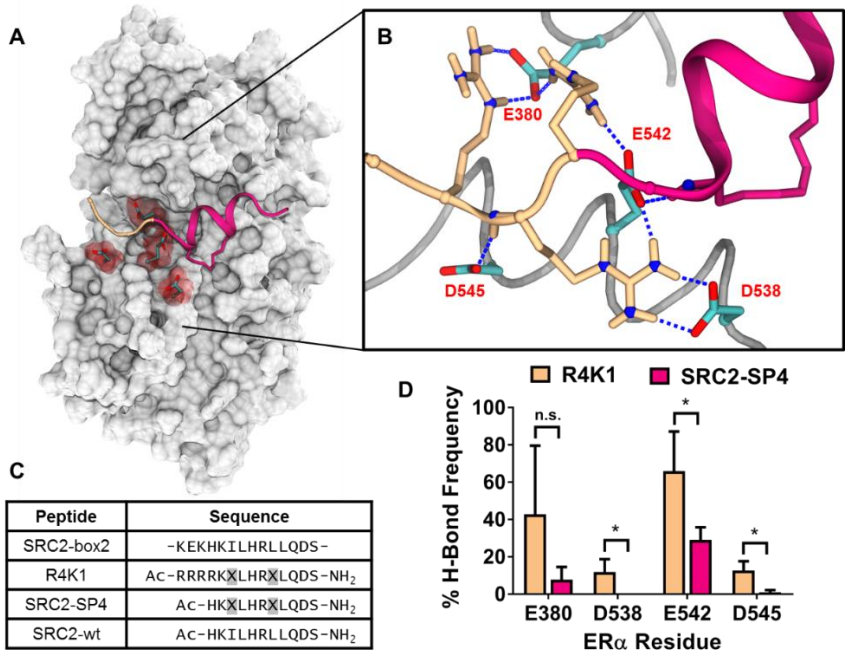

Peptide	Sequence
SRC2-box2	-KEKHKILHRLLQDS-
R4K1	Ac-RRRRKXLHRXLQDS-NH_2
SRC2-SP4	Ac-HKXLHRXLQDS-NH_2
SRC2-wt	Ac-HKILHRLLQDS-NH_2

Figure 4.1. Molecular dynamics-guided design of R4K1 A) The ligand-binding domain of estrogen receptor α (gray) contains four negatively charged residues (red) at the N-terminal region of our previously reported stapled peptide SRC2-SP4 (magenta, PDB: 5DXE). B) Snapshot of an MD simulation showing hydrogen bond interactions between arginine residues of R4K1 (beige/magenta) and nearby acidic residues E380, D538, E542, and D545 (cyan) of estrogen receptor. C) Sequences of the nuclear receptor interacting box 2 of steroid receptor coactivator 2 (SRC2-box2) and peptides R4K1, SRC2-SP4, SRC2-wt used in this study. X indicates the position of stapling amino acid S^5. D) MD simulations were carried out for 3 × 250 ns using estrogen receptor ligand-binding domain and either R4K1 (beige) or SRC2-SP4 (magenta). The mean percentage of simulations in which Glu380, Asp538, Glu542, or Asp545 formed a hydrogen bond with a residue from R4K1 or SRC2-SP4 is shown. Each simulation was carried out starting from distinct peptide conformations. Error bars represent the standard deviation; *, $p < 0.05$.

4.3 Cell permeability of R4K1

We hypothesized that inclusion of the Arg_4 sequence should increase cell permeability. To examine this, we carried out confocal microscopy studies of fluorescein isothiocyanate (FITC)-labeled peptides. MCF-7 cells were treated with 10 nM estradiol and 15 μM FITC-SRC-WT, FITC-SRC-SP, or FITC-R4K1 for 4, 8, and 24 hours, and confocal images were obtained. FITC-R4K1 was taken up more substantially by MCF-7 cells than either FITC-SRC-WT or FITC-SRC-SP (Figure 4.2, 4.13 and 4.14).

At 24 hours FITC-R4K1 was fully distributed throughout the cell, with enhanced accumulation in nucleoli, similar to previously reported results (**Figure 4.15**).[31] By comparing overlap of Hoechst stain and FITC-R4K1, we quantitated the percentage of nuclear volume containing FITC-R4K1 as 78 ± 2%. We also quantitated the cytoplasmic volume that contained FITC-R4K1 by comparing brightfield images to FITC images. According to this analysis, 89 ± 5.6% of the cytoplasmic area also contained R4K1. These data indicated that R4K1 was present in both nucleus and cytoplasm, so that it was available to bind either cytosolic- or nuclear-localized ER.

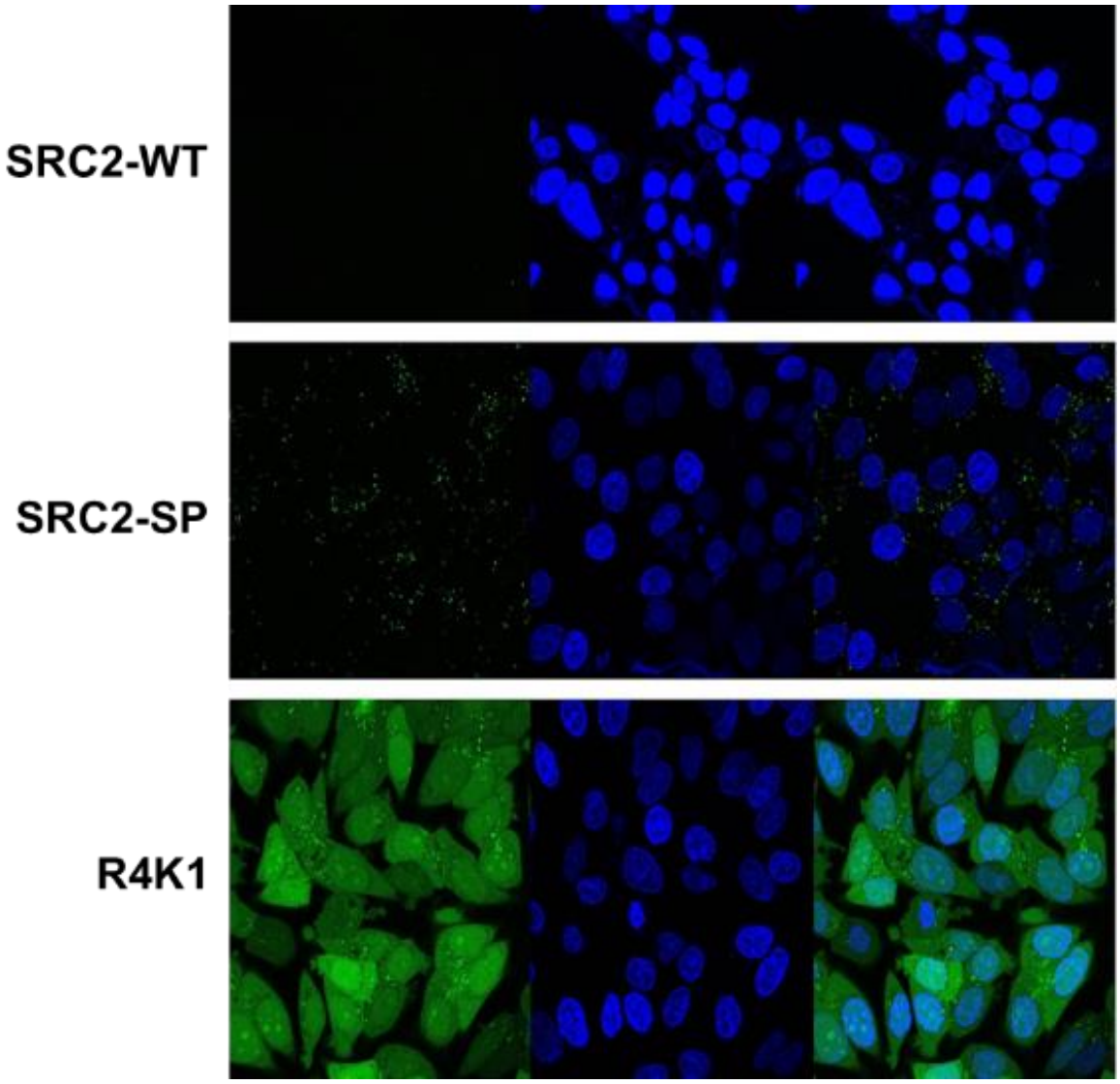

Figure 4.2. MCF-7 cells show enhanced uptake of R4K1. MCF-7 cells were treated for 24 hours with 15 μM fluorescein isothiocyanate (FITC)-labeled SRC2-WT (top), SRC2-SP (center), or R4K1 (bottom). Images from left to right include FITC channel, Hoechst stained nucleus and FITC/Hoechst overlay at 63× magnification.

4.4 Inhibition of ER/SRC interaction

In order to measure dissociation constants of SRC2-WT, SRC2-SP4 or R4K1 for ERα, we used a surface plasmon resonance (SPR) assay in which the ligand-binding domain of ERα was immobilized onto a CM5 chip. The K_d of R4K1 (19 nM) for ERα was

22-fold higher than that of SRC2-SP4 (420 nM) and 137-fold higher than the K_d of SRC2-WT (2600 nM) (**Figure 4.3**). The only difference between the sequences of SRC2-SP4 and R4K1 were four additional arginines, implying that the enhanced binding affinity of R4K1 was mediated through the appended arginines, in agreement with the molecular dynamics simulations. To provide evidence that the peptides would block the ER/coactivator interaction, we measured the ability of the peptides to block recruitment of a fluorescein-labeled SRC fragment to a terbium-labeled ERα ligand binding domain using time-resolved Förster resonance energy transfer (TR-FRET).[88] The IC_{50} value decreased from 1100 nM to 380 nM as the ILXXLL motif of SRC2-WT (blue) was replaced by the S^5LXXS^5L motif of SRC2-SP4 (magenta, **Figure 4.3D**). The IC_{50} further decreased to 5.1 nM as the Arg sequence of R4K1 (beige) was appended. These data were in good agreement with the SPR assay and implied that the stapled peptides bind at the coactivator binding region and inhibit interaction of ER with coactivator.

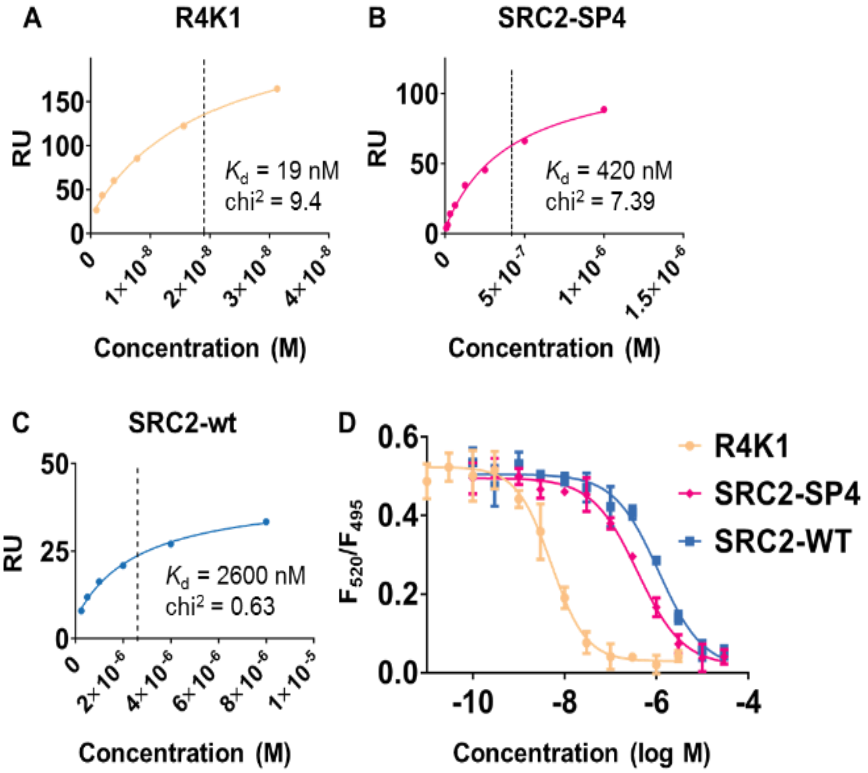

Figure 4.3. Stapled peptides bind to estrogen receptor and R4K1 inhibits the ER/coactivator interaction with high potency. A surface plasmon resonance (SPR) assay using immobilized estrogen receptor α ligand binding domain was used to determine K_d for R4K1 (beige, A), SRC2-SP2 (magenta, B), and SRC2-WT (blue, C). Data were analyzed using a steady-state fit. D) Interaction of estrogen receptor α ligand-binding domain, labeled with a long lifetime time-resolved fluorescence resonance energy transfer (TR-FRET) donor (terbium), and a steroid receptor coactivator fragment, labeled with TR-FRET acceptor fluorescein, was inhibited with increasing concentrations of R4K1, SRC2-SP4, or SCR2-WT. The ratio of fluorescent emissions of fluorescein acceptor and terbium donor is plotted along the *y*-axis (F_{520}/F_{495}), and the log of molar concentration of inhibitor is plotted along the *x*-axis. Error bars represent the standard deviation.

4.5 Quantitation of membrane integrity

Appending positively charged residues onto a peptide is a commonly used procedure for enhancing uptake of peptides by cells;[81, 124] however, some groups have shown that incorporating many positively charged residues may lead to loss of membrane integrity.[125-127] To guard against this possibility, we carried out lactate dehydrogenase release assays to determine safe concentrations to use in our cell-based experiments. In this assay, increased release of the cytoplasmic protein lactate dehydrogenase is indicative of membrane disruption and can be quantified relative to maximum lysis with detergent.

We carried out LDH release assays at one concentration (30 μM) after one-hour treatment of two ER+ breast cancer cell lines, MCF-7 and T47D, with peptides. None of the peptides showed release of LDH that was significantly different from vehicle (**Figure 4.16**).

To guard against the potential for bias introduced by examining the conditions above, we measured lactate dehydrogenase release in a time vs. concentration vs. response mode. Specifically, we measured release of lactate dehydrogenase at four timepoints and at five concentrations (**Figure 4.4**). There was no significant lactate dehydrogenase release at 5, 10, and 15 μM, even at 24 hours. These data suggested that 15 μM R4K1, even at long time points, would not damage the membrane and would be a safe concentration to use to examine cellular effects of R4K1.

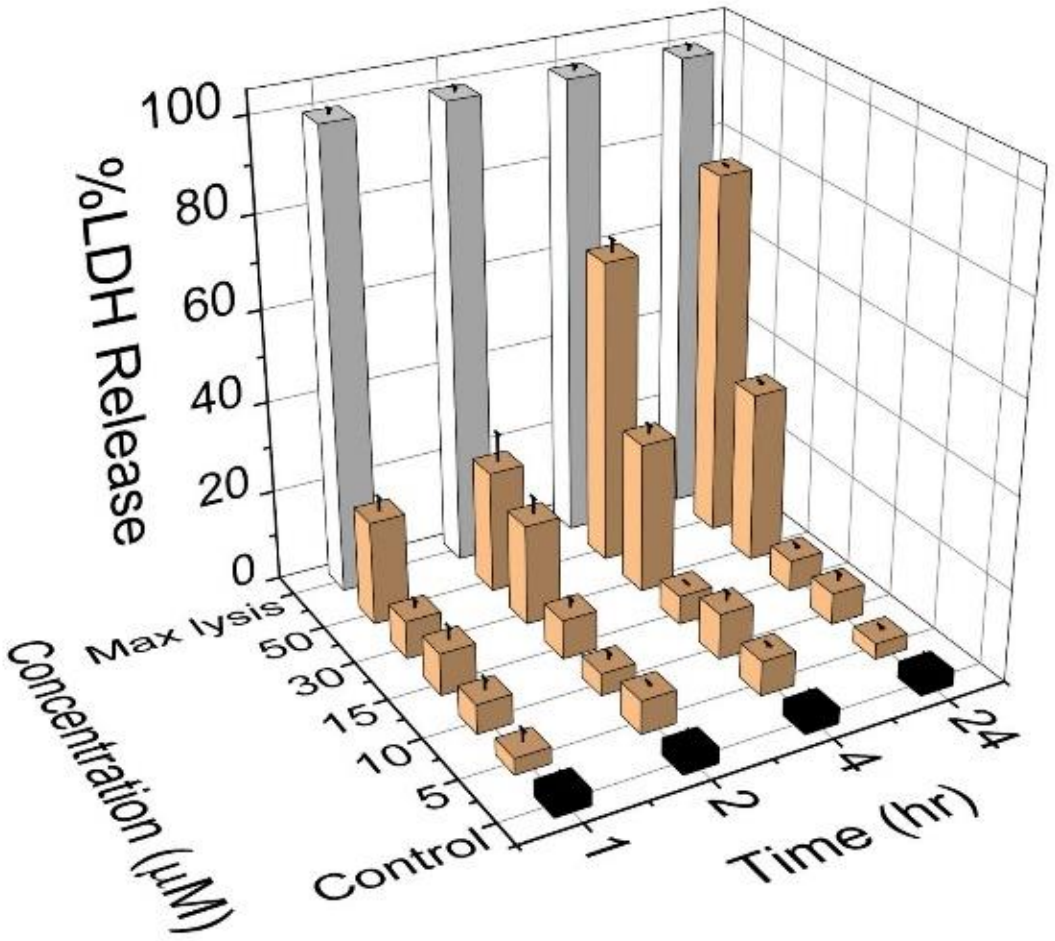

Figure 4.4. R4K1 does not cause loss of membrane integrity at efficacious concentrations. MCF-7 cells were treated with 5, 10, 15, 30 or 50 μM stapled peptide R4K1. Release of lactate dehydrogenase (LDH) was measured at 1, 2, 4, or 24 hours after treatment. %LDH release is plotted vs. time and concentration, relative to maximum lysis.

4.6 Transcriptional regulation of native genes

Our central hypothesis was that blockade of coactivator recruitment with R4K1 should show repression of estradiol-mediated gene expression, similar to that of selective estrogen receptor modulators, like 4-hydroxytamoxifen. We further hypothesized that R4K1 would not show estrogenic activity.

We first carried out a screening assay to determine what anti-estrogenic benefit R4K1 might have over SRC2-WT or SRC2-SP4. We treated MCF-7 cells with 10 nM estradiol and 15 μM SRC2-WT, SRC2-SP4, or R4K1 (**Figure 4.19**). For each of these treatment conditions, we measured transcript levels of five genes known to be stimulated by estradiol: PTGES, PR, PS2, EGR3, and IGFBP4. Treatment with estradiol showed upregulation of all genes. When cells were also treated with R4K1, all five genes showed a decrease in gene expression that was not seen with SRC2-SP4 or SRC2-WT, although only four reached statistical significance.

Based on the results of the screening assay, we compared estrogenic and anti-estrogenic activities of R4K1 to 4-hydroxytamoxifen in two different breast cancer cell lines. MCF-7 and T47D cells were treated with vehicle, 4-hydroxytamoxifen (4OHT) or R4K1 in the presence or absence of estradiol (E2, **Figure 4.5**). Estradiol induced expression of each of the five genes from above. This effect was reversed by co-treatment with estradiol plus 4OHT or estradiol plus R4K1, although the magnitude of the effect of R4K1 was smaller than that of 4OHT. There was no statistically significant difference in gene expression between cells treated with vehicle alone (i.e., no estradiol) and those that were treated with 4OHT or R4K1 alone. These effects were similar in a second ER+ breast cancer cell line (**Figure 4.20**), suggesting that R4K1 can broadly inhibit ER activity

and is not acting in a cell-specific manner. Taken together, these data supported our hypothesis that blocking the ER/coactivator interaction represses estrogen-stimulated gene expression.

We also tested whether R4K1 had effects on genes regulated by a different transcription factor, NFκB, which is also coactivated by SRC3.[128] We measured expression of NFκB-regulated genes RelB, ICAM1, and TNFα in the presence or absence of NFκB-stimulating cytokine, TNFα. There was little, if any, difference in expression between those genes that were treated with vehicle versus those treated with R4K1 (**Figure 4.5F-H**). These data implied that R4K1 did not non-specifically repress the activity of all transcription factors.

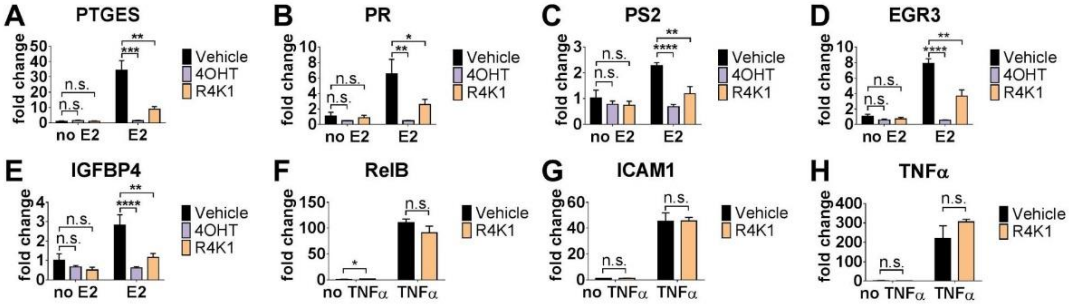

Figure 4.5. R4K1 inhibits transcription of ER-regulated native genes, but not NFκB-regulated genes. mRNA levels for ER-regulated genes PTGES (A), PR (B), PS2 (C), EGR3 (D), and IGFBP4 (E) and NFκB-regulated genes RelB (F), ICAM1 (G) and TNFα (H) were examined in MCF-7 cells by RT-QPCR. Cells were pretreated with R4K1 (15 μM, 24 hrs), 4OHT (1 μM, 2 hrs) or DMSO control, followed by 10 nM 17β-estradiol (E2) treatment for 2 hrs. Data were normalized to 36B4 (A-E) or GAPDH (F-H) internal controls and presented as fold change relative to DMSO vehicle. Error bars represent the standard deviation. n.s., not statistically significant; *, $p<0.05$; **, $p<0.01$; ***, $p<0.001$; ****, $p<0.0001$.

4.7 Proliferation of MCF-7 cells

Proliferation of ER+ breast cancer cell lines is enhanced by treatment with estradiol. We treated the ER+ breast cancer cell line MCF-7 with 15 μM R4K1 in the presence or absence of 10 nM estradiol and measured proliferation of these cells (**Figure 4.6**). Estradiol stimulated proliferation of MCF-7 cells, but R4K1 alone had no effect on proliferation of MCF-7 cells. Administering R4K1 with estradiol decreased proliferation to vehicle-treated levels. These data implied that blocking the ER/coactivator complex can repress proliferation that is stimulated by estradiol.

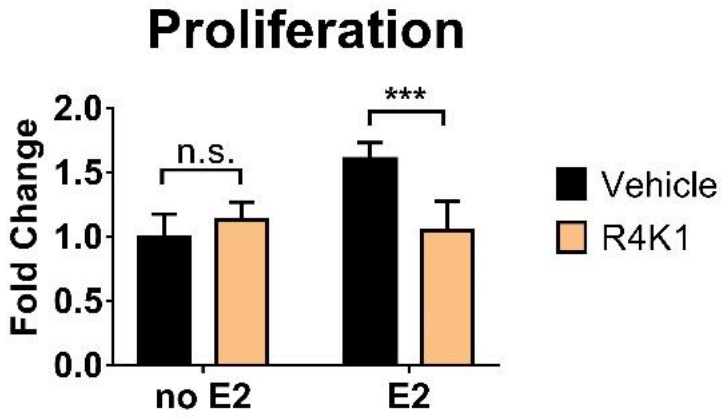

Figure 4.6. R4K1 reverses estradiol-stimulated proliferation. MCF-7 cells were treated with vehicle or 15 μM stapled peptide R4K1 in the presence or absence of 10 nM estradiol (E2). Treatment was initiated on day 3, and cell numbers were measured 24 hours later. Fold change was determined relative to vehicle control for three independent experiments. Error bars represent the standard deviation. n.s., not statistically significant; ***, $p<0.001$.

4.8 R4K1 modulation of estrogen receptor expression

Tamoxifen is a selective estrogen receptor modulator (SERM). It induces a conformation of ER that recruits a distinct set of coactivators and corepressors, so that it has both agonist and antagonist properties, depending on context and tissue type. Another class of ER ligands are referred to as selective estrogen receptor degraders (SERDs), which include the breast cancer drug fulvestrant. SERDs cause degradation of ER, but SERMs do not.

We were curious whether the mechanism-of-action of R4K1 would more closely resemble that of SERMs or SERDs. We measured protein levels of ER in the presence or absence of R4K1 and with or without estradiol in both MCF-7 and T47D cells (**Figure 4.7**). R4K1 showed no significant difference from vehicle-treated cells in the presence or absence of estradiol. There was a statistically significant decrease in ER levels in vehicle-treated T47D cells in the absence of estradiol, but this effect disappeared in the presence of estradiol. These data implied that, if R4K1 has SERD activity, it is only modest at best.

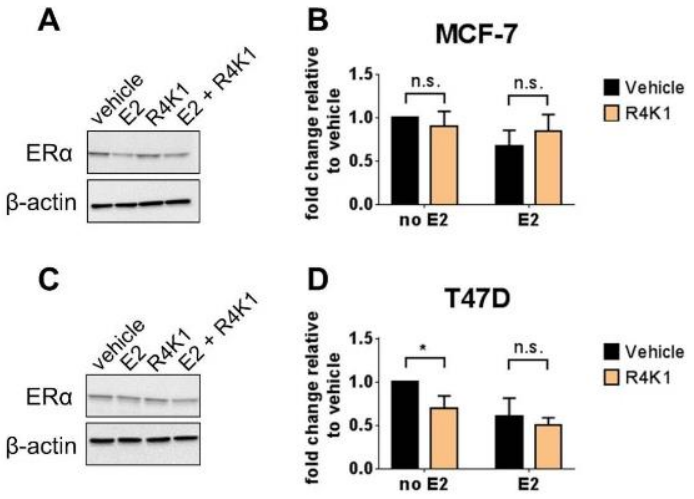

Figure 4.7. R4K1 has little, if any, estrogen receptor-degrading activity. MCF-7 (top) or T47D (bottom) cells were pretreated with R4K1 (15 μM, 24 hrs), 4OHT (1 μM, 2 hrs) or DMSO control, followed by 10 nM 17β-estradiol (E2) treatment for 2 hrs. Western blot was performed for ERα. β-actin was used as loading control. Vehicle-treated sample value was used as one arbitrary unit. Error bars represent the standard deviation from three independent experiments. n.s., not statistically significant; *, p <0.05.

4.9 Analysis global gene expression

To more fully understand a ligand's effects on transcription mediated by ER, it is necessary to look at global gene expression, rather than individual genes. We used RNA-Seq to analyze the transcriptome of MCF-7 cells to compare the global effects of R4K1 with those of 4-hydroxytamoxifen.

MCF-7 cells were treated under six different conditions, shown as columns in the heatmap of **Figure 4.8**: 1) 10 nM 17β-estradiol (E2), 2) 1 μM 4-hydroxytamoxifen (4OHT), 3) 10 nM E2 + 1 μM 4OHT, 4) 15 μM R4K1, 5) 10 nM E2 + 15 μM R4K1 and vehicle alone. Across the five experimental conditions, 1,041 transcripts were expressed at levels that were at least 2-fold different from vehicle control (FDR<0.05, **Figure 4.8A**). These

genes clustered into nine sets, depicted by rows in the heatmap of **Figure 4.8A**: 1) genes up-regulated similarly by E2, 4OHT, and to a lesser extent by R4K1; 2 and 3) genes down- or up-regulated by E2 that were fully reversed by 4OHT and partially by R4K1; 4) genes down-regulated similarly by E2 and 4OHT, and, to a lesser extent, by R4K1; 5) genes up-regulated by E2 that were reversed by 4OHT and not R4K1; 6) genes up-regulated by 4OHT that were not affected by E2 or R4K1; 7) genes repressed by R4K1 that were reversed by E2; 8) genes repressed by 4OHT that were reversed by E2; and 9) genes up-regulated by R4K1 that were reversed by E2.

Of particular relevance were clusters 2 and 3, which contained E2-regulated genes that were reversed by R4K1 (**Figure 4.8B/C**). Cluster 2 contained 226 E2-stimulated genes that were reversed fully by 4OHT and partially by R4K1. Cluster 3 contained 87 E2-repressed genes that were reversed fully by 4OHT and partially by R4K1. These data indicated that R4K1 reversed E2-regulated genes, but not to the same extent as 4OHT. R4K1 also showed gene regulation that was distinctly different from 4OHT but was reversed by E2, as seen in clusters 7 and 9 (**Figure 4.8D/E**), suggesting that these genes may be related to ER activity.

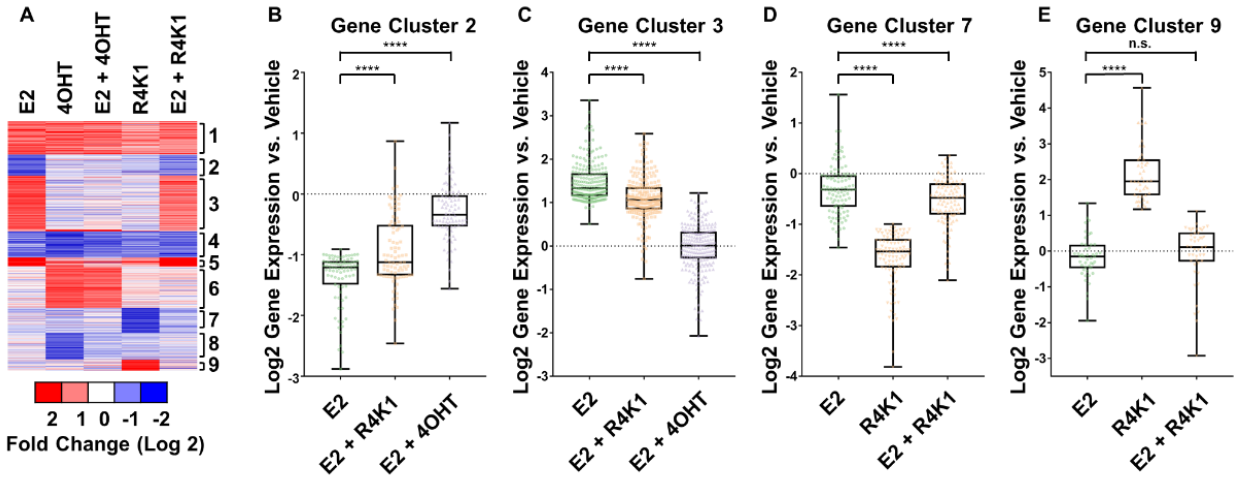

Figure 4.8. **RNA-Seq analysis of differentially expressed genes in MCF7 cells**. (A) RNA-Seq heatmap for 1,041 mRNA transcripts differentially expressed in MCF7 cells treated with 10 nM estradiol (E2), 1 μM 4-hydroxytamoxifen (4OHT), 10 nM E2 + 1 μM 4OHT, 15 μM R4K1, and 10 nM E2 + 15 μM R4K1. Data are normalized to vehicle treatment. Blue bars represent transcripts that are repressed relative to vehicle, and red bars represent transcripts that are stimulated relative to vehicle. Genes were grouped into 9 clusters using the k-means algorithm embedded within Gene Cluster 3.0 (B) Box-and-whiskers plot for cluster 2, mRNA transcripts repressed by E2 (green) that are reversed by co-treatment with either 4OHT (purple) or R4K1 (beige). (C) Box-and-whiskers plot for cluster 3, mRNA transcripts stimulated by E2 that are repressed by co-treatment with either 4OHT or R4K1. (D) Box-and-whiskers plot for cluster 7, mRNA transcripts repressed by R4K1 that are reversed by co-treatment with E2. (E) Box-and-whiskers plot for cluster 9, mRNA transcripts stimulated by R4K1 that are repressed by co-treatment with E2. In panels B, C, D, and E, the box represents the first through third quartiles, and the vertical "whiskers" represent the range. n.s., not statistically significant; ****, $p<0.0001$.

4.10 Discussion of R4K1 biological activity

R4K1 is among the first stapled peptides that block the action of ER in cellular models of breast cancer. There have been several other peptides and small molecules that block the ER/coactivator interaction *in vitro*, but, generally, the extant studies are limited in nature. Much of the characterization for these molecules has been restricted to *in vitro* studies (see[26, 82] for reviews of the literature), and, of those molecules that have cellular characterization, there are several common features: many are active in reporter gene and mammalian two-hybrid assays, but whether they can repress the activity of native genes or breast cancer phenotypes regulated by ER is unknown.[129-130] There are a few exceptions, including peptides synthesized by Brunsveld and coworkers,[31] as well as Li and coworkers,[100] although even these most advanced examples have been characterized using only one native gene.

The most well-characterized molecule for inhibiting the ER/coregulator interaction comes from Raj et al. who recently described ERX-11, a small molecule that is active in several different models of ER+ breast cancer, including a tumor xenograft model.[37] ERX-11 is an oligoamide that was designed to bind to ER at the coregulator-binding region, but even after careful experimentation and design, the precise binding site and mode of action is not fully understood for ERX-11, demonstrating the difficult nature of designing inhibitors of this protein-protein interaction.

To address the lack of cell-permeable, well-characterized ER/coactivator binding inhibitors, we redesigned a cell-impenetrant stapled peptide so that it would show cell permeability and activity in cell-based models of ER function. The computationally informed placement of arginine residues led to an increase in binding affinity as a result

of enhanced hydrogen bonding to negatively charged residues. This finding is in agreement with strategies that have been previously used to prepare high affinity peptides for ER via proline-primed helices,[81] isoaspartic-acid cyclized peptides,[100] and lysine-to-arginine substituted peptides.[32] In this work, we have been guided by the principle of linking a thorough understanding of the molecular basis of ER/stapled peptide binding with *in vitro* and cellular studies. The product of this work, R4K1, represents a significant proof-of-principle molecule for the future design of cell-permeable stapled peptides to inhibit the ER/coactivator interaction.

Our studies suggest that R4K1 is taken up by cells, and that relatively long incubation times may be required for R4K1 to distribute throughout the cell so that it can have its effects at the nucleus. These studies also indicate that, for this molecule, the arginine sequence that we have used is necessary for cell penetration, as poor cell penetration was seen with both SRC2-WT and SRC2-SP. Mechanistically, R4K1 acts more similarly to selective estrogen receptor modulators (SERMs) rather than selective estrogen receptor degraders (SERDs) in that it does not cause ER degradation. Based on our understanding of R4K1 binding, R4K1 does not expose hydrophobic residues, nor does it cause exposure of hydrophobic ER residues. Exposure of hydrophobic residues could lead to degradation, so that this finding is in keeping with our understanding of the mechanism of action of blocking coactivator binding.

Most importantly, our studies suggest that essentially all gene regulatory actions of R4K1 are ER-associated. First, RNA-seq data suggest that R4K1 acts similarly to 4OHT on both up- and down-regulated genes (Clusters 1-5), albeit with lower magnitude. Given our mechanism of blocking coactivator recruitment, understanding how R4K1

reverses E2-stimulated genes is straightforward, but the mechanism by which R4K1 reverses E2-repressed genes is unclear. One explanation is that coregulators may directly have dual activating and repressive functions. Some coregulators (e.g., PELP-1,[131] RIP140[132]) are known to have different activities at different transcription factors, but the extent to which they repress or stimulate gene expression at a single transcription factor is not completely understood, so that an improved version of R4K1 could be used to shed light on this problem. Second, there are essentially no R4K1-specific effects that are not reversed by E2 (Clusters 7 and 9). If R4K1 were non-selective for ER and able to affect other transcription factors, we might expect to see up- or down-regulation of gene expression that is not reversed by E2. This is further supported by the lack of R4K1 effect on NFκB target genes. The mechanism by which R4K1 regulates genes in the presence of unliganded ER is unclear. One possible explanation for these activities could be that R4K1 shows a preference for binding to folded, liganded ER, but that, in the absence of folded, liganded ER, R4K1 may bind to a subset of transcription factors and block coactivator recruitment, which could also help to explain how R4K1 reverses E2-repressed genes. This explanation is similar to the “squelching” hypothesis in the coactivator literature, wherein binding of a limited pool of coactivators at one transcription factor may lead to repression of genes regulated by other transcription factors.[133-134] Overall, the work here could lay the groundwork for providing tools to probe incompletely understood mechanisms of coregulators, including the dual-function and squelching mechanisms.

4.11 Conclusion

In conclusion, we have described a cell-permeable stapled peptide, R4K1, that modulates the activity of estrogen receptor in breast cancer cell lines. These studies are informed by a detailed molecular understanding of inhibiting the estrogen receptor/coactivator interaction. R4K1 provides a proof-of-concept that cell-permeable stapled peptides may be used to inhibit the estrogen receptor/coactivator interaction and that this disruption may prove advantageous in models of ER+ breast cancer. While R4K1 is a promising proof-of-principle probe, these studies also suggest that future cell-permeable stapled peptides need to show higher efficacy, which could come from increased uptake and/or higher affinity for estrogen receptor.

4.12 Experimental methods

4.12.1 General considerations

Peptide synthesis was accomplished using a literature procedure.[92] The TR-FRET assay protocol was carried out as previously described.[71, 88] Molecular dynamics simulations were performed using XSEDE resources[135] as previously described [71] with some exceptions that are fully explained in sections 4.11.2. Unless otherwise noted, cell culture experiments were carried out in the presence of charcoal-dextran-stripped 5% fetal bovine serum (FBS). Lower concentrations of FBS resulted in low estrogen-responsiveness (data not shown). 17β-estradiol (E2) and 4-hydroxytamoxifen (4OHT) were purchased from Sigma, item #E8875 and item #H7904, respectively. Fmoc-S5-OH and Grubb's 1st generation catalyst were purchased from Sigma-Aldrich. Fmoc-protected amino acids and all other reagents are commercially available and were purchased from Chem-Impex, Oakwood, Novabiochem, or Sigma-Aldrich and used as supplied. All

primers were purchased from Integrated DNA Technologies (IDT). Cell culture reagents were purchased from Gibco/Life Technologies and cell culture ware from BD Falcon, unless otherwise stated. Human MCF-7 and T47D cells were obtained from Dr. Debra Tonetti (University of Illinois at Chicago) and were maintained in Roswell Park Memorial Institute (RPMI) media supplemented with 10% fetal bovine serum (FBS), 1% non-essential amino acids, 2 mM L-glutamine, 1% antibiotics penicillin-streptomycin, and 6 ng/mL human recombinant insulin at 37 °C in 5% CO_2. Before treatment with ligands, inhibitors, or stapled peptides, cells were cultured in phenol red-free RPMI 1640 media supplemented with 5% charcoal/dextran–stripped fetal bovine serum (i.e. treatment media) for at least 48 hrs. Cell line authentication was previously performed for both MCF-7 and T47D cell lines using short tandem repeats (STR) by the facility (DNAS), Research Resources Center (RRC), UIC.

4.12.2 Computational modeling of stapled peptides

The molecular system of SRC2-SP4 was constructed as previously described, starting from the x-ray crystal of estrogen receptor α complexed with diethylstilbestrol (DES) in the ligand binding pocket and GRIP-1 NR box II peptide bound to the coactivator binding groove.[71] The phi and psi angles for H687 or R684-R687 and K688 were manually adjusted to prepare three different starting conformations. For SRC2-SP4, conformation 1 aligns with the SRC2 peptide of PDB Code 3ERD and the stapled peptide reported in PDB Code 2YJA, conformation 2 aligns with the structure of SRC2-SP4 bound to estrogen receptor alpha Y537S (PDB 5DXE), and the phi and psi angles for conformation 3 were randomly assigned. The MOE protein builder module was then used to build R4K1 by deleting residue H687 and appending four arginine residues to the N-terminus of the

SRC2-SP4 peptide. The phi and psi angles for residues 684 to 688 of R4K1 were randomly adjusted to generate three conformations of R4K1. The six resulting structures were exported from MOE in PDB format.

The PSFGEN plugin within VMD[91] was used to construct molecular systems in CHARMM format (PSF+PDB). A patching protocol was used to perform ring-closing metathesis *in silico* and cap the ends of coactivator peptide with an N-terminal acetyl and C-terminal amide. The N- and C- terminal ends of estrogen receptor were capped using acetyl and N-methylamido patches. The SOLVATE plugin was used to add TIP3P[109] water to 20 Å on each side of the receptor. The AutoIonize plugin was used to neutralize the system and place Na^+ and Cl^- ions > 5 Å from the receptor to yield a final salt concentration of 0.1 M NaCl. The fully solvated systems SRC2-SP4 and R4K1 totaled ~64.4k or ~65k atoms respectively.

All MD simulations were performed using NAMD 2.12 software package.[90] The protein and ions were described using the refined CHARMM36m force field.[136, 107] Parameters required to describe the staple were manually assigned by analogy from the CHARMM36m and CGenFF[137] parameter sets. The parameters required for diethylstilbestrol were assigned using the CGenFF Program webserver.[137] MD simulations were performed for NPT ensembles with a target pressure of 1 atm and temperature of 310 K using a Nosé-Hoover thermostat and a Langevin piston with a period of 100 fs, decay of 50 fs, and damping coefficient of 0.5/ps.[111, 138] Periodic boundary conditions were applied, and non-bonded interactions were treated using an exponential switching function starting from 10 Å with a cutoff at 12 Å. Full system periodic electrostatics were computed using the particle mesh Ewald (PME) method[110] with a grid

density >1.0/Å^3. Nonbonded forces were computed at every timestep (2 fs/step), PME calculations were performed at every other step, and atomic coordinates were recorded every ps.

The solvated and ionized SRC2-SP4 and R4K1 molecular systems were energy minimized for 10,000 steps and equilibrated for 0.1 ns using a harmonic positional restraint (k = 1 kcal/mol·Å^2) applied to all protein, coactivator, and ligand heavy atoms except protein residues 460–471 and coactivator residues 684 to 694—residues that were either missing from the x-ray crystal structure or modified to apply the staple or arginine residues. Water and ion atoms were allowed to equilibrate without any external restraints during this simulation. Production simulations were performed under equilibrium conditions for 250 ns per system. In total, the current study comprises 1.5 μs of production simulation time.

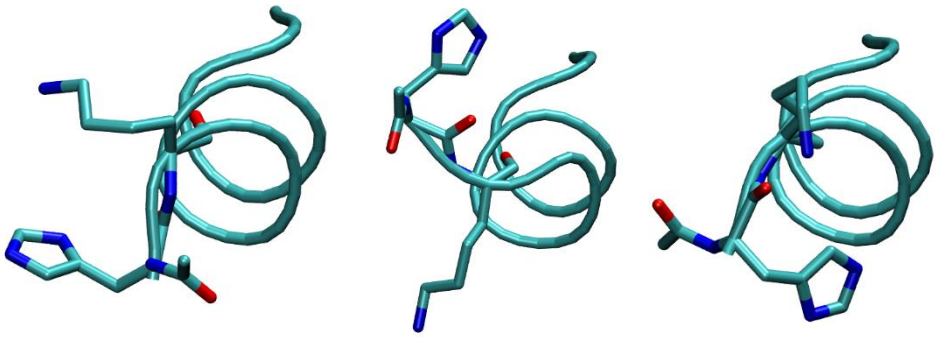

Figure 4.9. Three different conformations of His687 and Lys688 from SRC2-SP4 at the start of the production simulation.

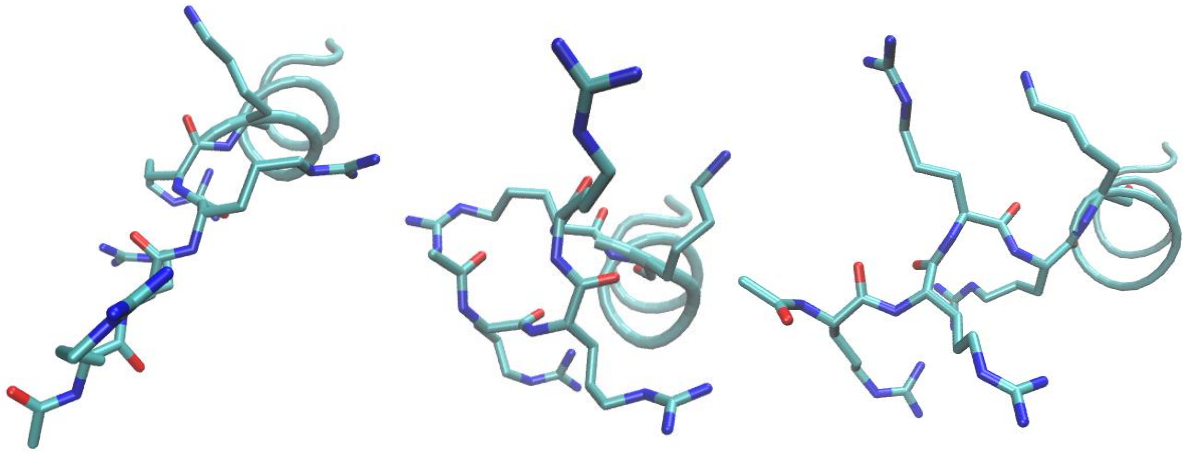

Figure 4.10. Three different conformations of Arg684, Arg685, Arg686, Arg687 and Lys688 from R4K1 at the start of the production simulation.

4.12.3 Peptide synthesis

All peptides were manually prepared on 30 μmol scale using standard Fmoc solid phase peptide synthesis and rink amide MBHA resin. Fmoc deprotection was carried out for 2 × 10 minutes using 25% piperidine in DMF with 0.1 M HOBt. Amino acids were coupled using 5 eq of amino acid, 5 eq of PyClock, and 10 eq of DIPEA in 0.75 mL of DMF. Stapling amino acid S5 was coupled for 2 hrs, amino acids following S5 were coupled for 2 × 1.5 hrs, and all other amino acids were coupled for 2 × 20 min. Ring closing metathesis was performed 2 x 120 min at 55 °C using 1 mL of 4.94 mg/mL Grubb's 1st generation catalyst in DCE. Acetylation or FITC labeling, and peptide cleavage/deprotection were carried out as previously described.[92] The crude peptides were purified to >95% homogeneity by semi-preparative HPLC (Solvent System MeCN:H_2O with 0.1% formic acid; 0-4 min, 10% MeCN; 4-24 min 10-50% MeCN; 24-25 min, 50-80% MeCN; 25-30 min, 80% MeCN; 30-31 min 80-10% MeCN. Column:

Phenomenex Luna 5 µm C18(2), 100 Å, 250 × 10 mm). Peptide purity was confirmed using analytical HPLC (Solvent System MeCN:H_2O with 0.1% trifluoroacetic acid; 0-2 min, 4% MeCN; 2-12 min 4-70% MeCN; 12-13 min, 70% MeCN; 13-14 min, 70-4% MeCN; 14-17 min 4% MeCN. Column: Phenomenex Kinetex 5 µm C18, 100 Å, 50 × 4.6 mm). Peptide mass was measured using a Bruker Autoflex MALDI-TOF mass spectrometer (Table XV). The matrix used to prepare dried droplet samples was composed of a saturated solution of α-cyano-4-hydroxycinnamic acid in 50:50 water/acetonitrile with 0.1% TFA.

TABLE XV. MALDI-TOF ANALYSIS OF PEPTIDES

Peptide	Sequence	Chemical Formula [M+H$^+$]	Exact Mass	Observed Mass
SRC2-WT	Ac-HKILHRLLQDS-NH_2	$C_{62}H_{106}N_{21}O_{16}$+	1400.813	1400.870
SRC2-SP4	Ac-HKS^5LHRS^5LQDS-NH_2	$C_{64}H_{106}N_{21}O_{16}$+	1424.813	1424.850
R4K1	Ac-RRRRKS^5LHRS^5LQDS-NH_2	$C_{82}H_{147}N_{34}O_{19}$+	1912.158	1912.164
SRC2-SP-FITC	FITC-β_{ala}-HKλ^{s5}LHRS^5LQDS-NH2	$C_{87}H_{122}N_{23}O_{21}S$+	1856.891	1856.896
R4K1-FITC	FITC-β_{ala}-RRRRKS^5LHRS^5LQDS-NH_2	$C_{104}H_{161}N_{36}O_{24}S$+	2330.221	2330.216
SRC2-WT-FITC	FITC-β_{ala}-HKILHRLLQDS-NH_2	$C_{84}H_{120}N_{23}O_{21}S$+	1818.874	1818.954

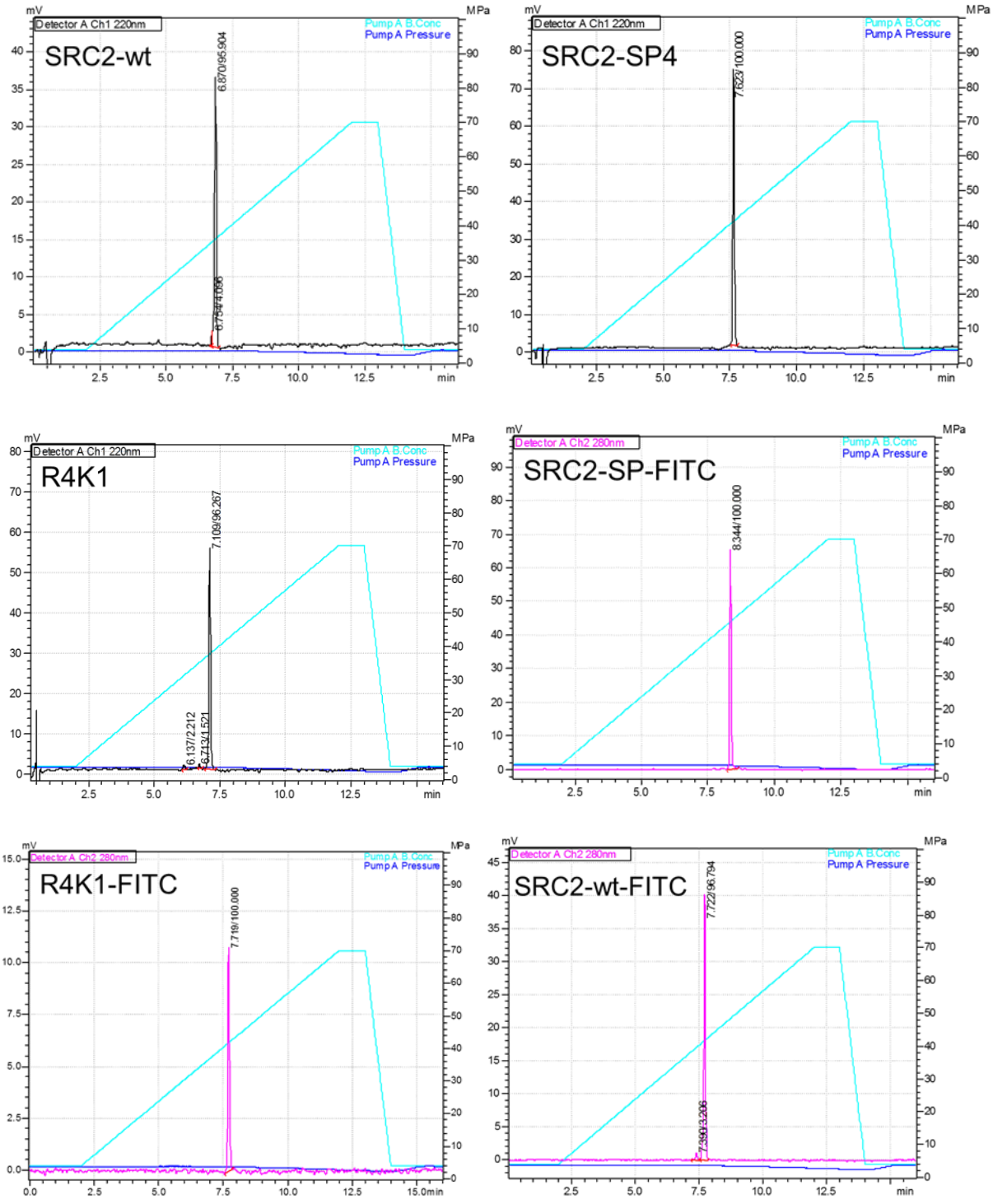

Figure 4.11. HPLC analysis of purified peptides.

4.12.4 Surface plasmon resonance (SPR)

The SPR assay protocol was based on previously reported conditions,[30] with the following changes: SPR analysis was performed on a BiacoreT200; ERα ligand binding domain construct contained amino acids 299–554, including N-terminal 6His-tag; final ERα surface density was ~9500 RU; stapled peptide solutions at a series of increasing concentrations were applied to flow cells at a 30 µL/min flow rate using a contact time of 60 s and a dissociation time of 120 s; K_D values were determined by fitting reference subtracted data to a steady-state affinity equation embedded in the Biacore T200 evaluation software 3.0; and kinetic fittings were done using the two state reaction binding equation embedded in the Biacore T200 evaluation software 3.0 (Figure 4.12).

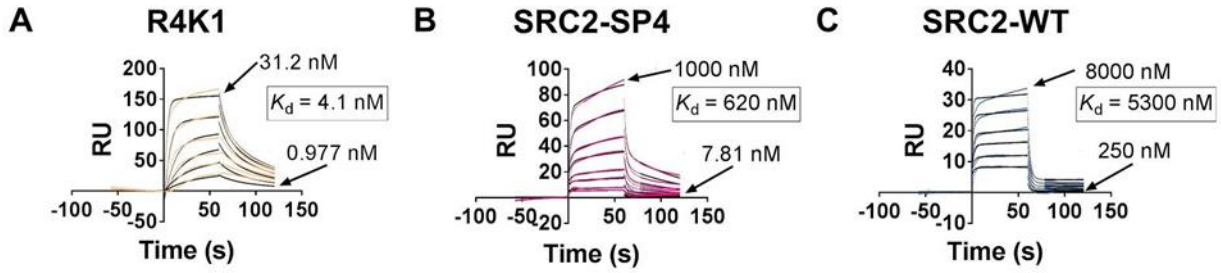

Figure 4.12. SPR fit kinetic analysis. A surface plasmon resonance (SPR) assay using immobilized estrogen receptor α ligand binding domain was used to determine dissociation constants for R4K1 (beige, A), SRC2-SP2 (magenta, B), and SRC2-WT (blue, C). Data were analyzed using a kinetic fit.

TABLE XVI. TR-FRET DATA ANALYSIS

	R4K1	SRC2-SP4	SRC2-WT
Sigmoidal, 4PL, X is log(concentration)			
Best-fit values			
Top	0.524	0.4956	0.5053
Bottom	0.02911	0.01778	0.01084
LogIC50	-8.289	-6.411	-5.953
HillSlope	-1.14	-0.8722	-0.8931
IC50	5.14E-09	3.88E-07	1.11E-06
Span	0.4949	0.4779	0.4945
Std. Error			
Top	0.009898	0.007867	0.009079
Bottom	0.01243	0.01569	0.02845
LogIC50	0.05964	0.06509	0.09057
HillSlope	0.1533	0.09551	0.1349
Span	0.01677	0.01923	0.03212
95% CI (profile likelihood)			
Top	0.5041 to 0.5448	0.4797 to 0.513	0.4864 to 0.5263
Bottom	0.003243 to 0.05325	-0.01813 to 0.0463	-0.06737 to 0.05821
LogIC50	-8.41 to -8.168	-6.538 to -6.277	-6.112 to -5.736
HillSlope	-1.518 to -0.8717	-1.1 to -0.6902	-1.269 to -0.6306
IC50	3.89e-009 to 6.786e-009	2.9e-007 to 5.283e-007	7.727e-007 to 1.838e-006
Goodness of Fit			
Degrees of Freedom	38	31	32
R square	0.9719	0.9824	0.9675
Absolute Sum of Squares	0.05685	0.02177	0.0369
Sy.x	0.03868	0.0265	0.03396
Number of points			
# of X values	48	36	36
# Y values analyzed	42	35	36

4.12.5 Confocal microscopy

Breast cancer cells were cultured as previously described.[139] For microscopy studies, cells were incubated with 15 μM FITC-conjugated stapled peptides for 4, 8, or 24 hr. Hoechst dye was used for nuclear staining, at a concentration of 4 mg/mL for 30 minutes (Life Technologies). Images were taken with a Zeiss confocal LSM 710 microscope. The percentage of stapled peptide in the nucleus was determined by FITC and Hoechst co-localization, and the percentage cytoplasmic stapled peptide relied on FITC and brightfield overlap. Corrected total cell fluorescence was evaluated using Image J software with the SEM for each treatment group.

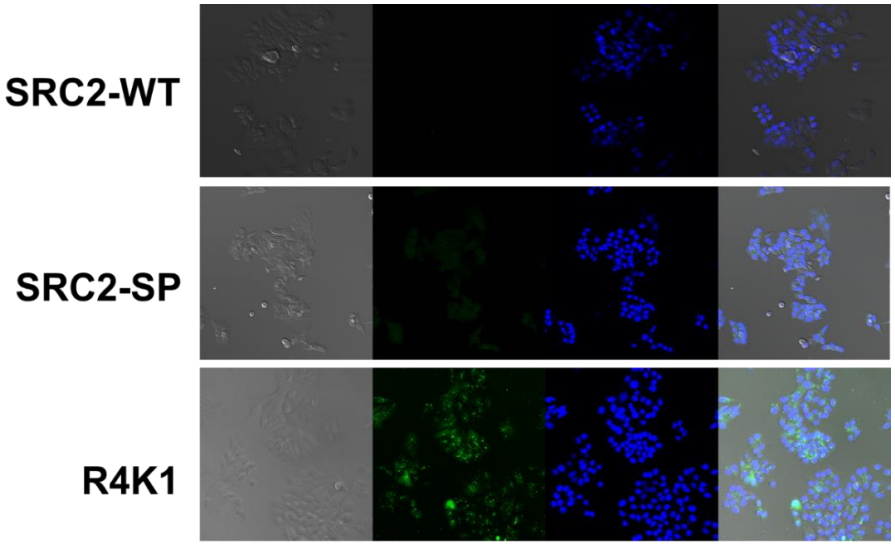

Figure 4.13. Uptake of FITC conjugated peptides (4 Hrs.). MCF-7 cells were treated for 4 hours with 15 μM fluorescein isothiocyanate (FITC)-labeled SRC2-WT (top), SRC2-SP (center), or R4K1 (bottom). Images from left to right include brightfield, FITC channel, Hoechst stained nucleus and FITC/Hoechst overlay at 20× magnification.

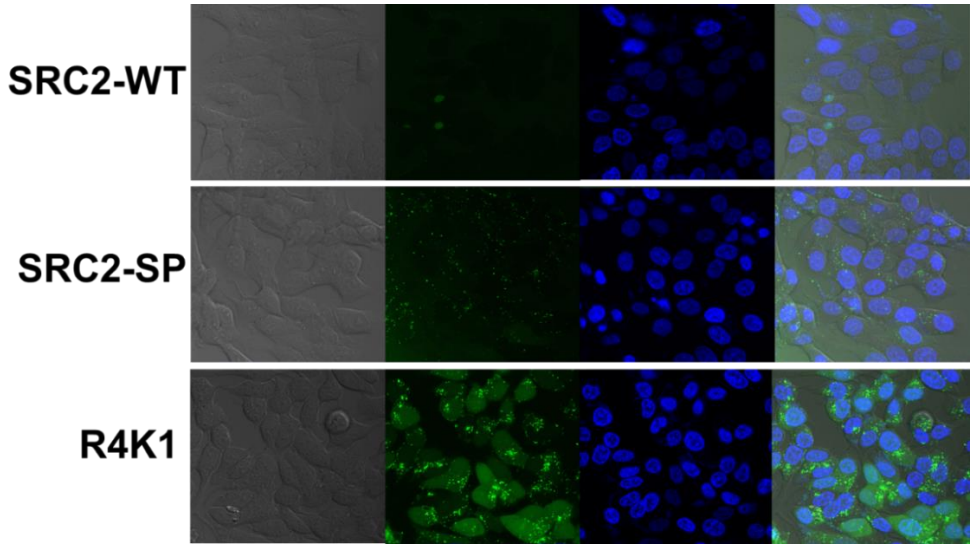

Figure 4.14. Uptake of FITC conjugated peptides (8 Hrs.). MCF-7 cells were treated for 8 hours with 15 μM fluorescein isothiocyanate (FITC)-labeled SRC2-WT (top), SRC2-SP (center), or R4K1 (bottom). Images from left to right include brightfield, FITC channel, Hoechst stained nucleus and FITC/Hoechst overlay at 63× magnification.

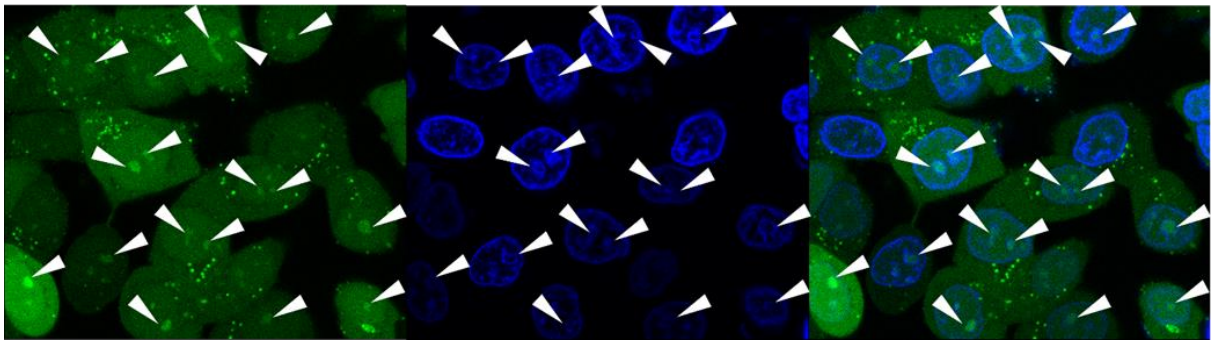

Figure 4.15. R4K1 localization to nucleoli. MCF-7 cells were treated for 24 hours with 15 μM fluorescein isothiocyanate (FITC)-labeled R4K1. Images from left to right include FITC channel, Hoechst stained nucleus, and FITC/Hoechst overlay at 63× magnification. White arrows indicate peptide localization to nucleoli.

4.12.6 Lactate dehydrogenase assay

Cytotoxicity was measured according to the manufacturer's instructions (CytoTox 96, Promega). Absorbance was read at 490 nm on a BioTek Synergy HT plate reader. A maximum release LDH reagent (provided with the kit) was used as a positive control. All samples were evaluated as a percentage of LDH released relative to maximum.

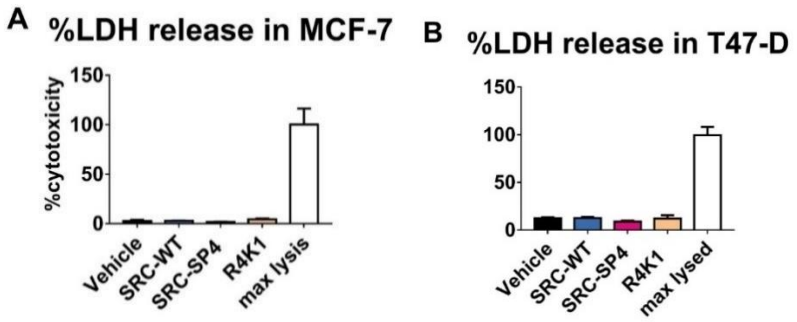

Figure 4.16. LDH assay. (A) MCF-7 or (B) T47D cells were treated for one hour with DMSO vehicle, 30 μM SRC2-WT, 30 μM SRC2-SP4, or 30 μM R4K1. Percent release of lactate dehydrogenase (LDH) was measured relative to maximum lysis with sodium dodecyl sulfate.

4.12.7 RNA and RT-qPCR

Total RNA was isolated and RT-qPCR was performed as previously described.[8] 36B4 or GAPDH were used as internal controls, and fold change was calculated using the ΔΔCt method. qPCR primers are listed in **Table XVII**.

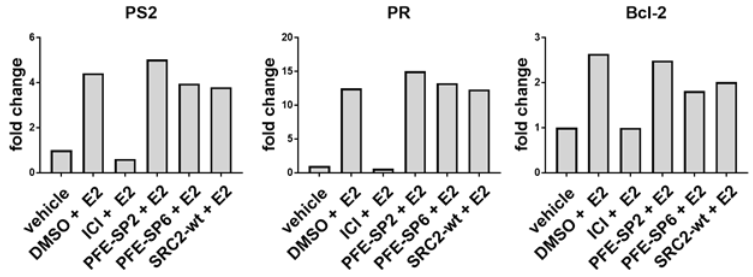

Figure 4.17. PFE-SP2 and PFE-SP6 do not inhibit transcription of ER-regulated native genes. mRNA levels for ER-regulated genes PS2, PR, and Bcl-2 were examined in MCF-7 cells treated for 24 hours with vehicle, 10 nM estradiol (E2) alone, 10 nM E2 + 1 μM ICI, 10 nM E2 + 50 μM PFE-SP2, 10 nM E2 + 50 μM PFE-SP6, and 10 nM E2 + 50 μM SRC2-wt. Data are normalized to beta-actin internal control and presented as fold change relative to DMSO vehicle.

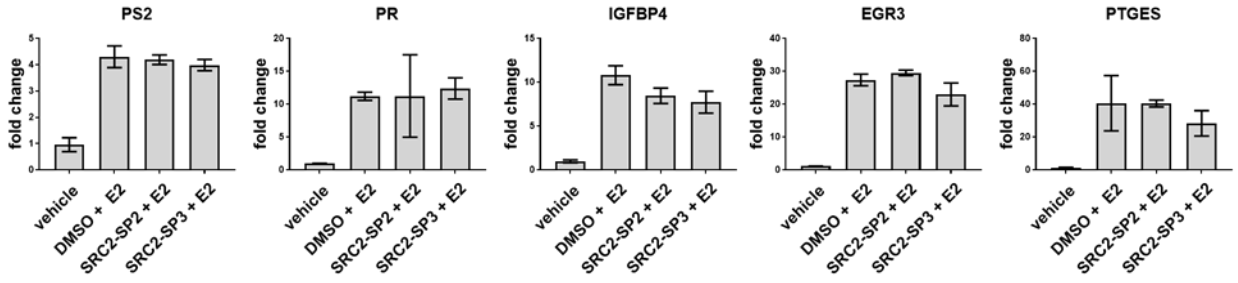

Figure 4.18. SRC2-SP2 and SRC-SP3 do not inhibit transcription of ER-regulated native genes. mRNA levels for ER-regulated genes PTGES, PR, PS2, EGR3, and IGFBP4 were examined in MCF-7 cells treated for 24 hours with vehicle, 10 nM estradiol (E2) alone, 10 nM E2 + 15 μM SRC2-SP2, and 10 nM E2 + 15 μM SRC2-SP3. Data are normalized to beta-actin internal control and presented as fold change relative to DMSO vehicle. Error bars represent the standard deviation from the mean. No stapled peptide treatments were significantly different from E2 treatment.

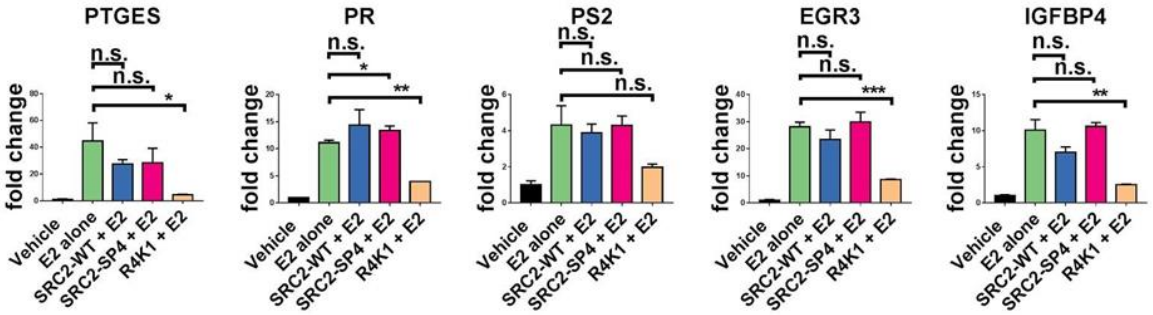

Figure 4.19. R4K1, but not SRC2-SP4 or SRC2-WT, inhibits transcription of ER-regulated native genes. mRNA levels for ER-regulated genes PTGES, PR, PS2, EGR3, and IGFBP4 were examined in MCF-7 cells treated for 24 hours with vehicle, 10 nM estradiol (E2) alone, 10 nM E2 + 15 μM SRC2-WT, 10 nM E2 + 15 μM SRC2-SP4, or 10 nM E2 + 15 μM R4K1. Data are normalized to beta-actin internal control and presented as fold change relative to DMSO vehicle. Error bars represent the standard deviation from the mean. n.s., not statistically significant; *, $p<0.05$; **, $p<0.01$; ***, $p<0.001$.

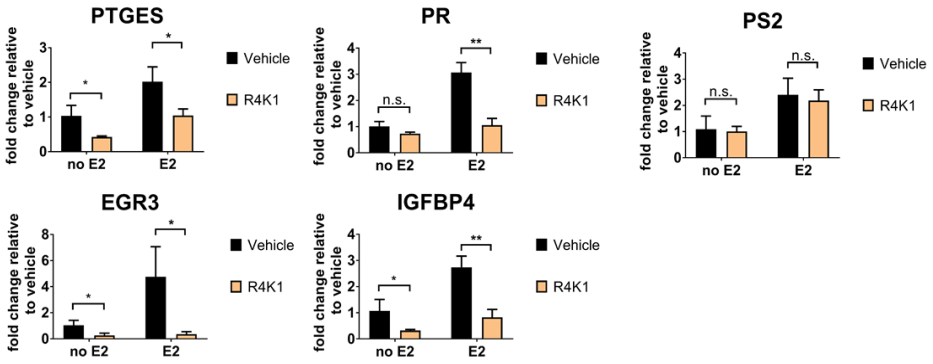

Figure 4.20. R4K1 inhibits transcription of ER-regulated native genes. mRNA levels for ER-regulated genes PTGES, PR, EGR3, PS2, and IGFBP4 were examined in T47D cells treated for 24 hours with vehicle, 10 nM estradiol (E2) alone, 15 μM R4K1 alone, or 10 nM E2 + 15 μM R4K1. Data are normalized to beta-actin internal control and presented as fold change relative to DMSO vehicle. Error bars represent the standard deviation from the mean. n.s., not statistically significant; *, $p<0.05$; **, $p<0.01$.

4.12.8 Western blot

Whole cell extracts were prepared using radioimmunoprecipitation assay buffer (RIPA) buffer; proteins were denatured and separated by SDS-PAGE using a 5-12% gradient gel (Invitrogen) and then transferred to nitrocellulose membranes. The membranes were blocked for 1 hr in 5% non-fat dry milk. Membranes were incubated overnight at 4 °C with appropriate primary antibody (ERα [Cell Signaling #8644] or β-actin [Sigma #A5441]. The next day, membranes were washed and incubated in horseradish peroxidase conjugated secondary antibodies. The signal was visualized using Chemi-doc XRS (Bio-Rad laboratories) following incubation with the Pierce Supersignal West Pico Chemiluminescent Substrate.

4.12.9 Proliferation assay

Cell counts were determined using an imaging cytometer (Celigo) on the brightfield channel following 24 hr of treatment. Fold change was calculated relative to vehicle control.

4.12.10 RNA-seq experimental design and data analysis

RNA isolated for qPCR was provided to the Genomics Core Facility, RRC at UIC, for RNA-Seq analysis. Libraries were prepared from two biological replicates per condition using the QuantSeq 3' mRNA-Seq Library Prep kit (Lexogen). Library yields were assessed with the Qubit dsDNA HS reagent (Invitrogen) and TapeStation D1000 tape (Invitrogen). Libraries were pooled and sequenced on NextSeq 500 (Illumina), 1x75 nt reads, High Output kit (~450 million clusters). RNA-Seq results were trimmed and aligned to the hg38 assembly using ELAND allowing up to 2 mismatches. Differential gene expression was determined using edgeR as a component of the HOMER software suite.[53] Detailed instructions for analysis can be found at http://homer.ucsd.edu/homer/. Genes were considered differentially regulated if fold change >2 and p-value <0.05 compared to vehicle treatments. Heatmaps were generated using CLUSTER and visualized using JavaTreeView software[140] Box-and-whiskers plots were prepared using Graphpad Prism 7.03. A paired t-test was used to calculate statistical significance. All data are publicly available through GEO (accession # GSE108308).

TABLE XVII. RNA PRIMERS

EGR3 forward: TTCTCGTACAGGGTGGCTCC

EGR3 reverse: GGCAGAGAGCAACCTTCCC

PTGES forward: CTTCCTTTTCCTGGGCTTCG

PTGES reverse: GAAGACCAGGAAGTGCATCCA

PS2 forward: GTGTGCAAATAAGGGCTGCTG

PS2 reverse: TGGAGGGACGTCGATGGTA

PR forward: GTCGCCTTAGAAAGTGCTGTCAG

PR reverse: GCTTGGCTTTCATTTGGAACGCC

ER forward: TGCCCTACTACCTGGAGAAC

ER reverse: CCATAGCCATACTTCCCTTGTC

ICAM1 forward: TGACGAAGCCAGAGGTCTCAG

ICAM1 reverse: AGCGTCACCTTGGCTCTAGG

36B4 forward: GTGTTCGACAATGGCAGCAT

36B4 reverse: GACACCCTCCAGGAAGCGA

GAPDH forward: GTCTCCTCTGACTTCAACAGCG

GAPDH reverse:ACCACCCTGTTGCTGTAGCCAA

RelB forward: TGTGGTGAGGATCTGCTTCCAG

RelB reverse: TCGGCAAATCCGCAGCTCTGAT

TNFa forward: AAGGGTGACCGACTCAGCG

TNFa reverse: ATCCCAAAGTAGACCTGCCCA

IGFBP4 forward: AGCTTCAGCCCCTGTAGCG

IGFBP4 reverse: TCATCTTGCCCCCACTGGT

5. HIGH AFFINITY STAPLED PEPTIDES TARGETING ESTROGEN RECEPTOR MUTANTS Y537S AND D538G.

5.1 Introduction

Somatic mutations to the estrogen receptor alpha (ERα) ligand binding domain were recently discovered in endocrine-resistant metastatic breast cancer.[19, 21-24] To better understand the prevalence and influence of these mutations in drug resistance and disease progression, post-hoc analysis of circulating tumor DNA (ctDNA) from the FERGI,[141] SOFEA,[142] PALOMA,[142] and BOLERO[143] clinical trials was performed. The frequency of ligand binding domain mutation detection in cfDNA was found to range from 28.8-39.1% with Y537S and D538G showing the highest occurence.[144] The major findings from these studies were that ERα mutations are associated with prior exposure to AI treatment and worse progression-free survival. The phenotype observed in cell lines expressing these mutations has been reported using CRISPR-generated MCF-7 and T47D cell lines that are heterozygous for either the Y537S or D538G mutations.[24] The mutant cell lines show estradiol-independent growth and varying levels of resistance to 4-hydroxytamoxifen, raloxifene, fulvestrant, and AZD 9496. Mechanistic studies implicate that Y537S and D538G mutations shift the folding dynamics of helix 12 into a stabilized conformation to recruit coactivator proteins.[25]

5.2 R4K1 inhibits mutant estrogen receptor/coactivator interaction

Our hypothesis was that stapled peptide coactivator binding inhibitors could be developed with high binding affinity to estrogen receptor mutants and would disrupt cancer cell growth mediated through coactivator recruitment to these receptor isoforms. To test this hypothesis ERY537S and D538G ligand binding domain isoforms were

recombinantly expressed to be used in SPR binding assays and a TR-FRET assay as previously described (Figure 5.4).[72] To determine if stapled peptides SP4 and R4K1 had general differences in binding affinity between receptor isoforms, we screened SRC2-SP4 and R4K1 using SPR and TR-FRET (Figures 5.1, 5.2, and 5.3, Table XVIII). Results from SPR analysis showed that peptide binding to the mutant receptors followed a similar affinity trend as previously found for the wild-type receptor, R4K1 > SRC2-SP4 > SRC2-WT. The K_D values of R4K1 for ERα-wt, ERα-D538G, or ERα-Y537S were 19 nM, 16 nM, and 8 nM respectively. These K_D measurements for the stapled peptides were confirmed using a TR-FRET which showed IC_{50} for inhibiting ER interactions with a fluorescein labeled coactivator peptide to be 69 nM, 75 nM, and 18 nM for ERα-wt, ERα-D538G, or ERα-Y537S respectively. This result suggested that stapled peptides may have enhanced affinity for the Y537S isoform relative to wildtype receptor. This is in good agreement with previous findings that coactivator proteins are recruited with higher affinity to Y537S. [25]

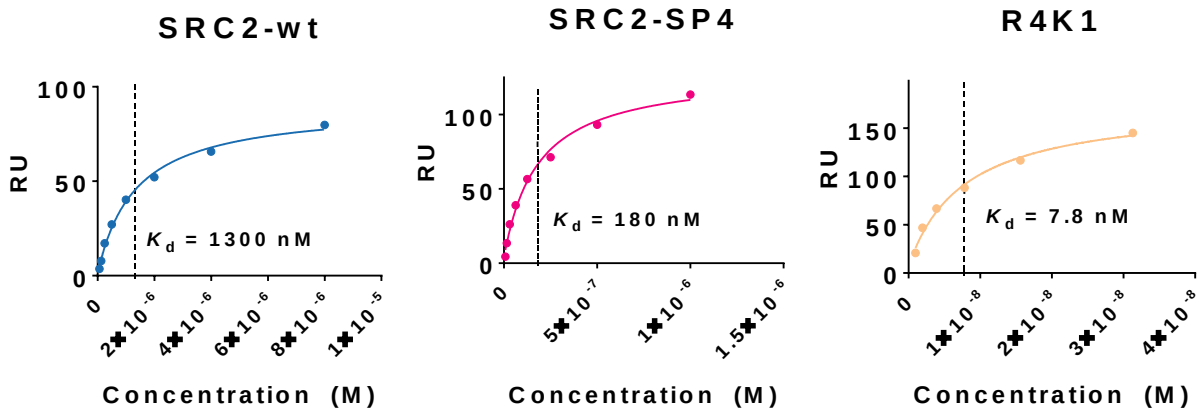

Figure 5.1. SPR steady state binding of peptides to ERY537S

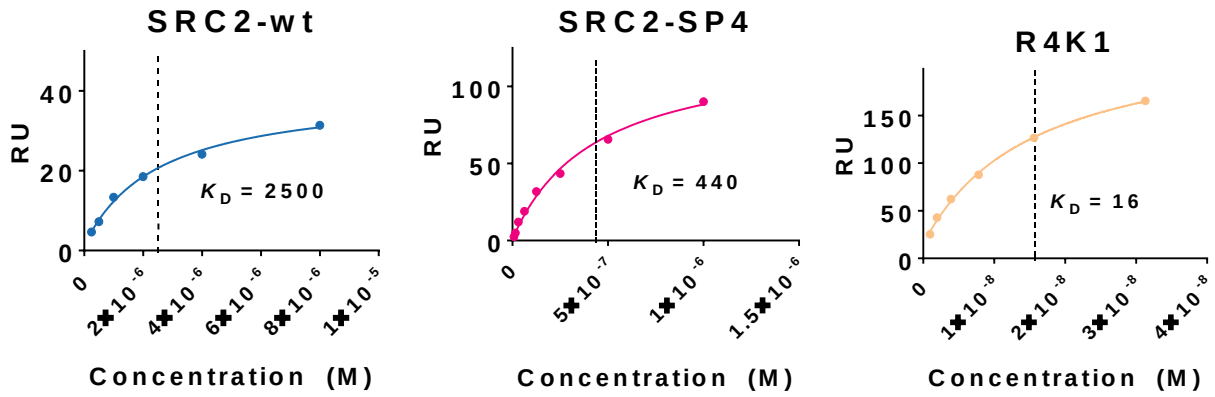

Figure 5.2. SPR steady state binding of peptides to ERD538G

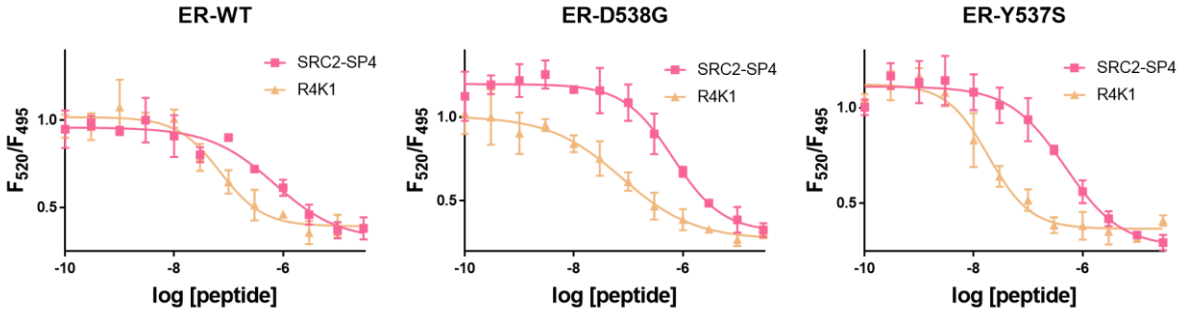

Figure 5.3. Stapled peptides inhibit wild-type and mutant ER/SRC interactions as measured by TR-FRET.

TABLE XVIII. STAPLED PEPTIDE BINDING AFFINITY TO RECEPTORS AS MEASURED BY SPR AND TR-FRET

Assay	Peptide	ERα-wt	ERα-D538G	ERα-Y537S
SPR	**SP4** K_D nM (±se)	420 ±79	440 ±85	180 ±37
SPR	**R4K1** K_D nM (±se)	19 ±3	16 ±2	8 ±2
TR-FRET	**SP4** IC_{50} nM (95% CI)	690 (330-3000)	660 (420-1200)	480 (290-900)
TR-FRET	**R4K1** IC_{50} nM (95% CI)	69 (43-120)	75 (37-160)	18 (13-27)

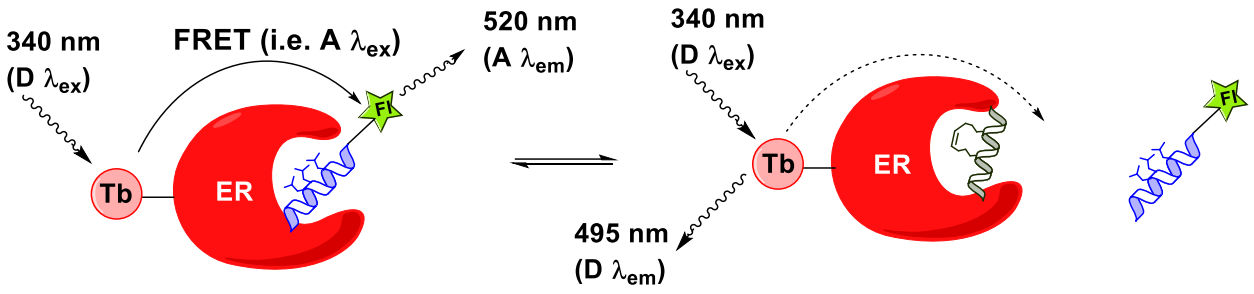

Figure 5.4. Diagram of TR-FRET assay depicting Tb-chelated estrogen receptor and FITC-LxxLL peptide motif.

R4K1, one of the highest affinity stapled peptides prepared, has a K_D of 19 nM for wild-type ERα, but requires concentrations up to 15 μM for moderate activity in MCF-7 cells; our hypothesis is that only a small fraction of the stapled peptide is taken up by breast cancer cells, so that a compound with a lower K_D value that is taken up similarly may show greater activity in cellular models. A rudimentary analysis of other protein-protein interactions suggests that compounds tend to show a level of cellular activity 2-3 orders of magnitude greater than their observed biochemical binding. For instance, the small molecule ABT-199 has an experimental K_i of <0.01 nM for Bcl-2 but an EC_{50} of ~3-10 nM in cell-based assays.[145] Likewise, the stapled peptide $SAHB_A$ has an experimental K_D of 48 nM for BCL-2 and shows cellular EC_{50} values ranging from 5-25 μM.[146] One difficulty associated with inhibiting protein-protein interactions is that the inhibitor has to compete with a natural high-affinity binder, which in some forms of disease may be overexpressed, as is the case with SRC-3 in breast cancer.[16]

5.3 Stapled peptides with non-natural amino acids for enhanced binding affinity to estrogen receptor

One established strategy for enhancing binding affinity for coactivator-mimicking peptides involves mutating the leucine amino acids in the $IL^1xxL^2L^3$ recognition motif (Figure 5.5). In one example, conversion of L^1 to *tert*-leucine resulted in a 156-fold increase in binding affinity for ER.[32] Furthermore, conversion of either L^1 or L^3 to neopentylglycine resulted in a 28-fold increase in binding affinity. In a separate study, 37 non-natural hydrophobic amino acid substitutions were carried out for each L^1, L^2, and L^3, showing that in addition to increasing binding affinity, leucine substitutions can also instill selectivity for homologous receptors such as the thyroid receptor and ERβ.[42]

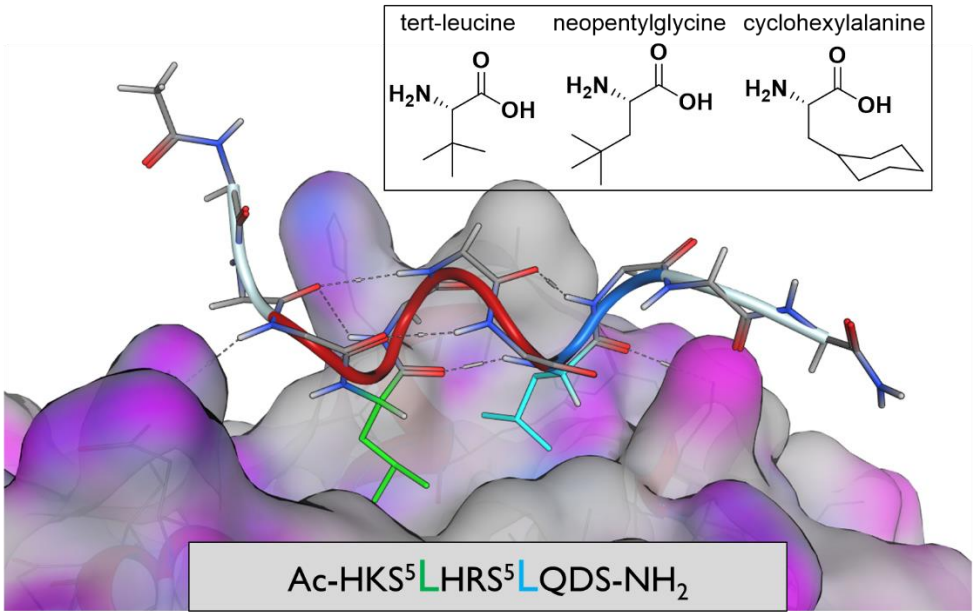

Figure 5.5. Surface of estrogen receptor indicating L_1 (green) and L_3 (blue) position of $L_1xxL_2L_3$ binding motif. Replacement of these residues with non-natural amino acids like tert-leucine, neopentylglycine, and cyclohexylalanine has previously been shown to have effects on affinity and selectivity.[32, 42]

Using SP4 as a model peptide, substitutions of non-natural amino acids *tert*-leucine (*t*-Leu), neopentylglycine (NPG), or cyclohexylalanine (CHA) were made at either the L^1 or L^3 position and binding affinity for ERα was measured using a TR-FRET assay (Figure 5.6, TABLE XVIX). Substitution of cyclohexylalanine at L3 resulted in ~6 fold improvement in binding affinity across each receptor isoform. A simple computational analysis of hydrophobic surface area of SP4 and SP4-$L3^{CHA}$ computed an addition of 35 $Å^2$ when incorporating the non-natural amino acid. An analysis of PPI hotspots suggests that hydrophobic amino acids can contribute upwards of 33 cal $Å^{-2}$ mol^{-1} of binding energy;[147] thus a reasonable estimate of increased binding energy is then calculated to be 1.15 kcal, which agrees with the observed 6-fold increase in binding affinity. In general, amino acid substitutions were better tolerated by ERα-wt and ERα-Y537S compared with ERα-D538G. Regarding selectivity, neopentylglycine substitution at L^1 established a 12-fold selectivity for the ERα-Y537S mutant relative to wildtype. Preparing additional peptides with substitutions at L^1 may be a method for preparing selective inhibitors of ERα-Y537S. In general, the amino acid substitutions had a minor impact on the helicity of the stapled peptides. All six peptides remained helical, and the overall CD spectrum looked very similar to SP4, with a less negative minima at 220 nM indicating a minor decrease in helicity (Figures 5.7 and 5.8).

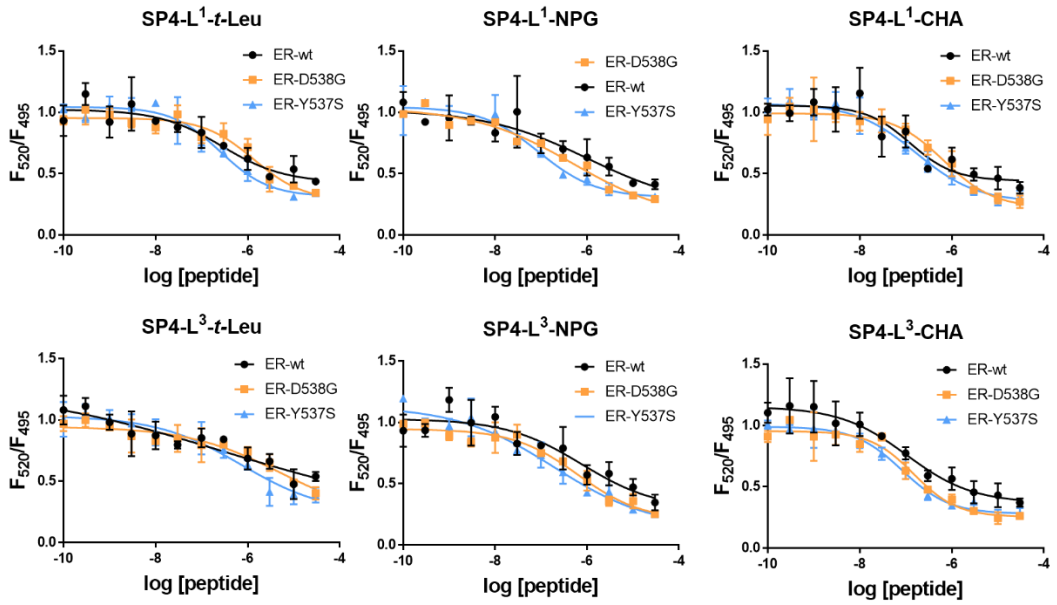

Figure 5.6. TR-FRET binding curves for SP4 peptide with L1 and L3 substitutions

TABLE XIX. IC_{50} VALUES DERIVED FROM TR-FRET BINDING CURVES FOR SP4 PEPTIDE WITH L^1 AND L^3 SUBSTITUTIONS

Peptide	**ERα-wt** IC_{50} nM (95% CI)	**ERα-D538G** IC_{50} nM (95% CI)	**ERα-Y537S** IC_{50} nM (95% CI)
SP4	690 (330-3000)	660 (420-1200)	480 (290-900)
SP4-L^1 t-Leu	270 (74-2600)	1400 (670-15000)	260 (140-510)
SP4-L^1 NPG	1100 (N/A)	510 (N/A)	90 (49-180)
SP4-L^1 CHA	120 (48-750)	670 (330-2500)	170 (89-370)
SP4-L^3 t-Leu	330 (N/A)	5000 (1100-10000)	740 (200-1800)
SP4-L^3 NPG	770 (N/A)	640 (310-7900)	190 (N/A)
SP4-L^3 CHA	100 (37-560)	150 (90-270)	83 (53-130)

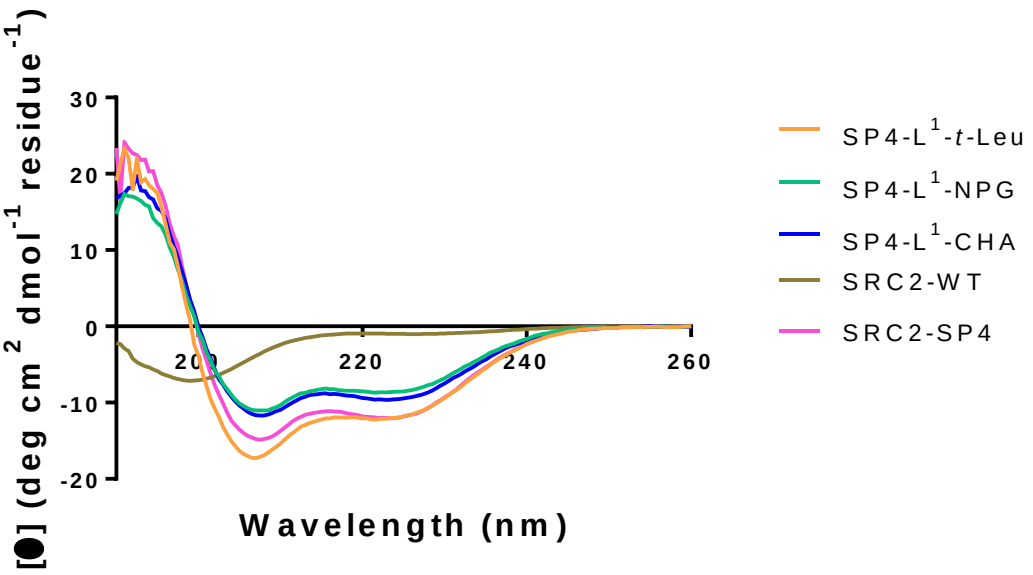

Figure 5.7. Circular dichroism spectra of SP4 with L^1 substitutions

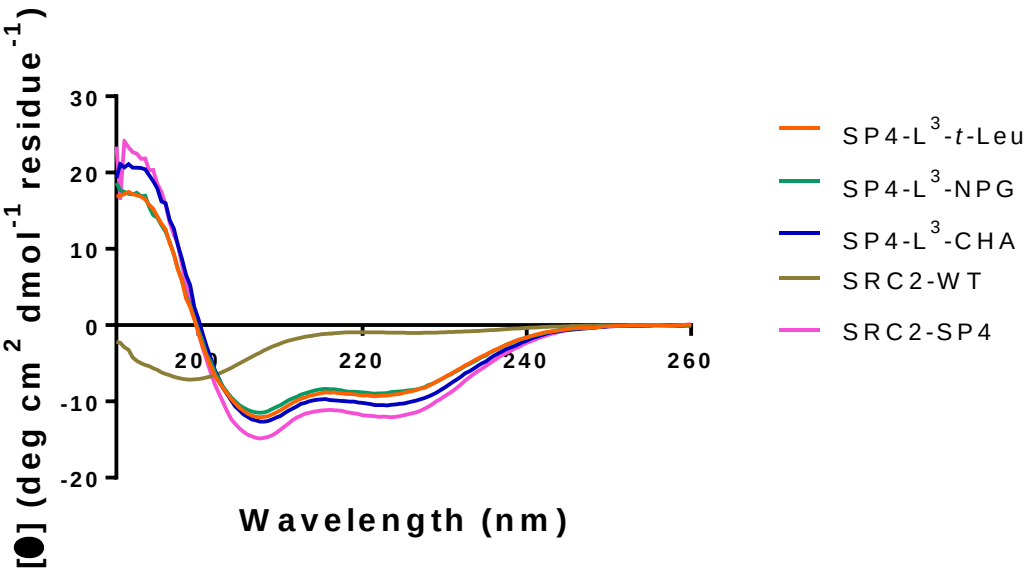

Figure 5.8. Circular dichroism spectra of SP4 peptide with L^3 substitutions

5.4 Design and synthesis of gamma-functionalized stapled peptides to selectively target estrogen receptor with D538G multination

An objective in further developing stapled peptides was to prepare a selective inhibitor of ERα-D538G to probe the function of this receptor isoform within a cellular context. From crystal structure analysis, the gamma methyl groups of **SRC2-SP3** and **SRC2-SP2** are < 4 Å from and point directly toward ER residue D538 (Figure 5.12). The vacancy produced by this D538G mutation results in an open groove on the surface of the mutant that can be filled by a functionalized stapled peptide, whereas the functionalized peptide may be sterically repelled by D538 in the wild-type isoform. In a communication in *Angewandte Chemie* (Chapter 2) [71], gamma-methyl substituted stapling amino acids at the *i* position of *i*, *i*+4 stapled peptides (**SRC2-SP2** and **-SP3**) were shown to increase binding affinity relative to unmodified staple (**SRC2-SP4**) through a combination of stabilizing the bioactive conformation and increasing van der Waals contacts. Using molecular dynamics simulations and X-ray crystallography, it was shown that minimization of 1,5-interactions between the alpha- and gamma-methyl groups dictated the conformations taken up by peptides when in solution and when bound to estrogen receptor. Our solved crystal structures (PDB 5HYR and 5DX3) showed that a gamma-methyl group in the *R* (**SRC2-SP2**) and *S* (**SRC2-SP3**) configuration are both directed towards estrogen receptor amino acid position 538. Simple chemical intuition would suggest that the strain-enforced conformation of gamma-functionalized stapling amino acids could be leveraged to prepare selective binding for the D538G mutant isoform. To test this hypothesis, an expanded series of gamma-functionalized stapling amino acids with extended branching groups were prepared to sterically impede binding

to wild-type receptor (Figures 5.9, 5.10, 5.11, and 5.12). To establish selectivity, non-substituted aromatic groups with multiple linker lengths and stereochemical configurations were prepared to determine the most effective conformation for D538G selective binding. Additionally, the C_α-H bond of glycine can form weak cation-pi interaction with aromatic rings, which could be leveraged to enhance binging to the D538G mutant.[148] The ease of synthesis would also allow for substituting the aromatic ring of second generation gamma-functionalized stapled peptides.

The chemical synthesis of the functionalized stapling amino acids was performed as previously reported, with a modification to the final step; instead of isolating the amino methyl ester intermediate, better yields were obtained via a three-step, one-pot reaction sequence consisting of TFA-mediated bislactim ether hydrolysis, sodium hydroxide-catalyzed ester hydrolysis, and sodium carbonate facilitated Fmoc protection. The Fmoc protected stapling amino acids were incorporated into the SP4 sequence with functionalization at the *i* position of the staple.

Circular dichroism showed that the larger substituents had similar effects on helicity as did the previously reported gamma-methyl groups. In general, substituents in the same configuration as the *S*-methyl of SRC2-SP3 showed only a slight decrease in helicity relative to the unfunctionalized SRC2-SP4 (Figure 5.15). Substituents in the same configuration as the *R*-methyl of SRC2-SP2 led to a larger decrease in helicity relative to unfunctionalized SRC2-SP4 (Figure 5.14). The CD spectra confirm that the secondary structure of the functionalized peptides is helical and that larger substituents likely have a similar structural influence as the gamma-methyl groups of SRC2-SP2 and SRC3-SP3.

A TR-FRET binding assay was used to measure inhibition of ER-wt and ERD538G interactions with an LxxLL coactivator peptide (Figure 5.13, Table XX). Contrary to our hypothesis, the functional groups substituted in the configuration of the gamma-methyl of SRC2-SP3 all showed slightly enhanced binding to the wild-type receptor, albeit a ~3-fold preference for the ER-D538G was found for the *S*-phenethyl substituted peptide. The opposite configuration was less tolerated by both receptors, but the benzyl group produced a 6-fold selectivity for ER-D538G over the wildtype receptor. Towards achieving a goal to reduce affinity to the wild-type receptor, it appears that a continued SAR could be built around the benzyl-substituted peptide SP4-SBZ as a way to diminish binding to ER-wt.

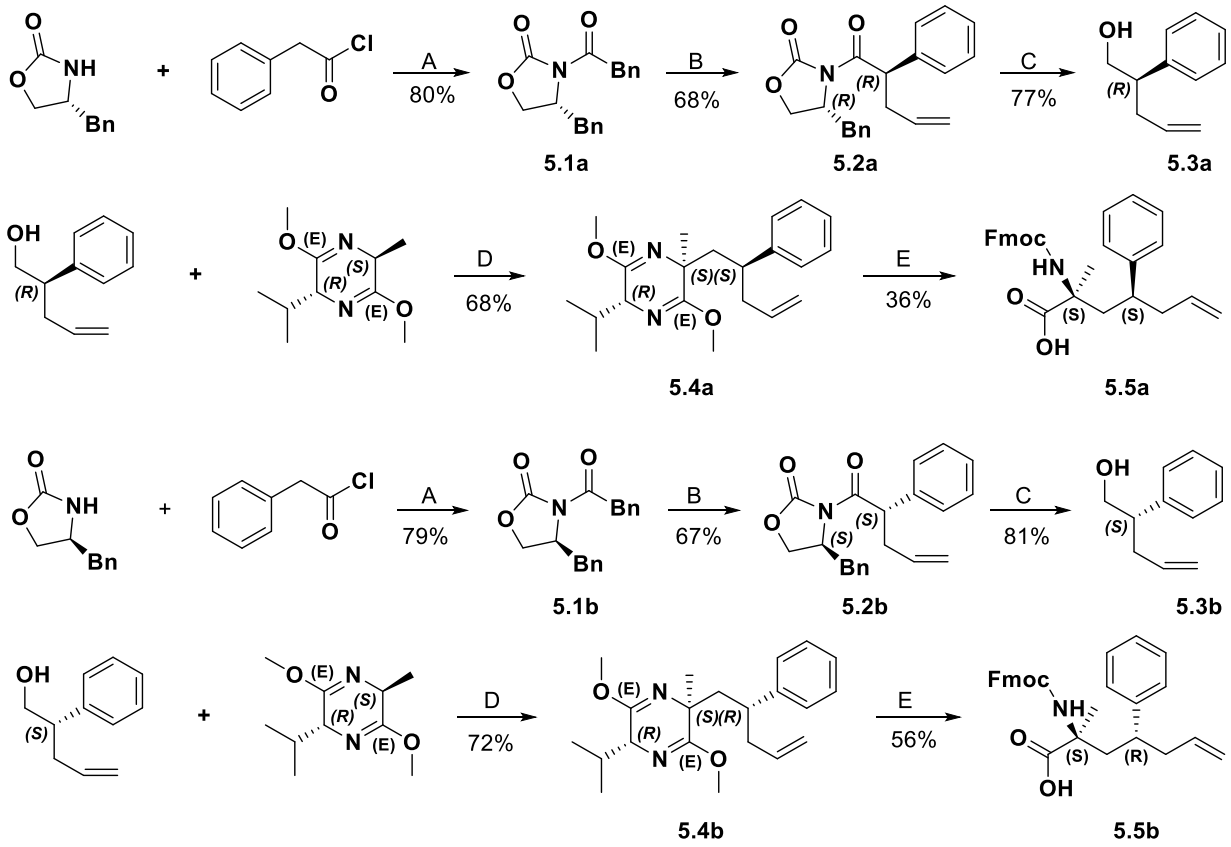

Figure 5.9. Synthesis of gamma-phenyl stapling amino acids. A) *n*-BuLi B) $Li^{+}[N\text{-}iPr_2]^{-}$ C) $LiBH_4$ D) $(F_3CSO_2)_2O$; *n*-BuLi E) TFA; NaOH; Fmoc-Cl, Na_2CO_3

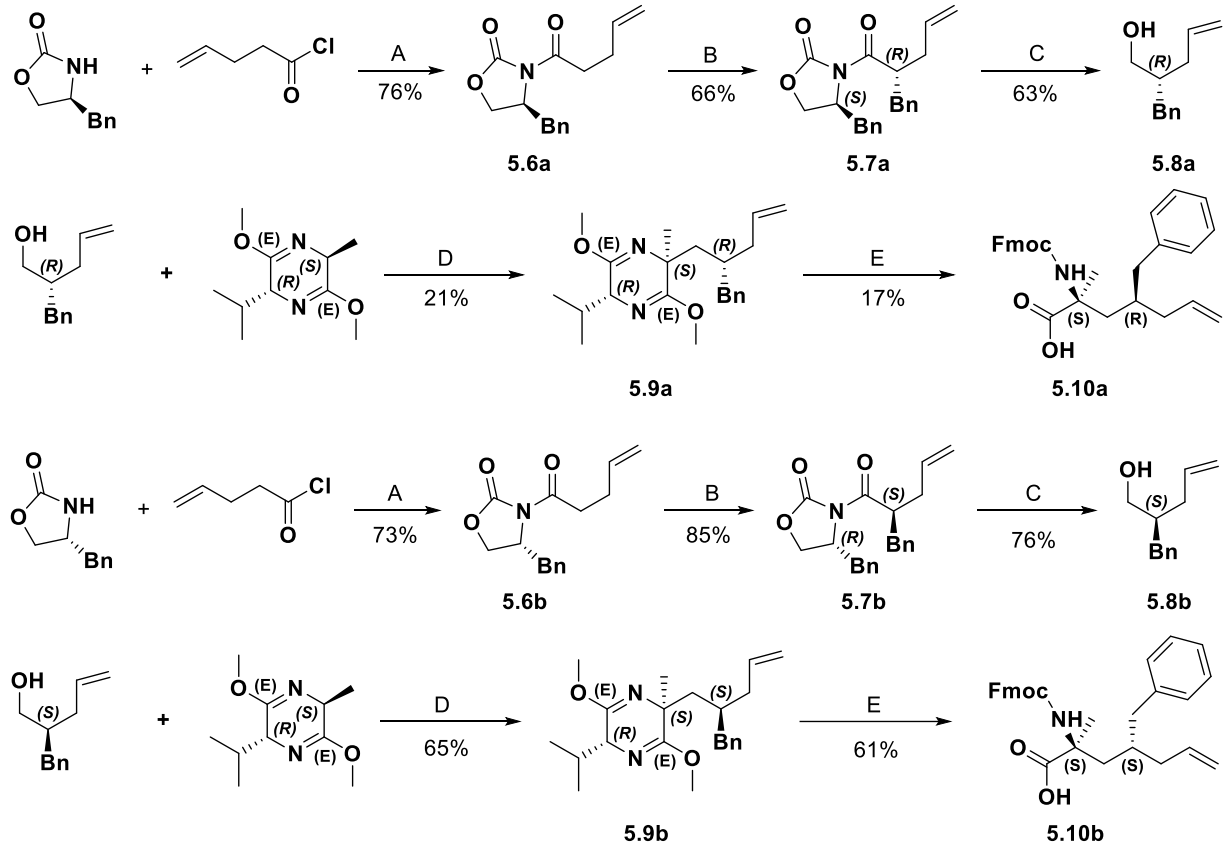

Figure 5.10. Synthesis of gamma-benzyl stapling amino acids. A) *n*-BuLi B) $Li^{+}[N\text{-}iPr_2]^{-}$ C) $LiBH_4$ D) $(F_3CSO_2)_2O$; *n*-BuLi E) TFA; NaOH; Fmoc-Cl, Na_2CO_3

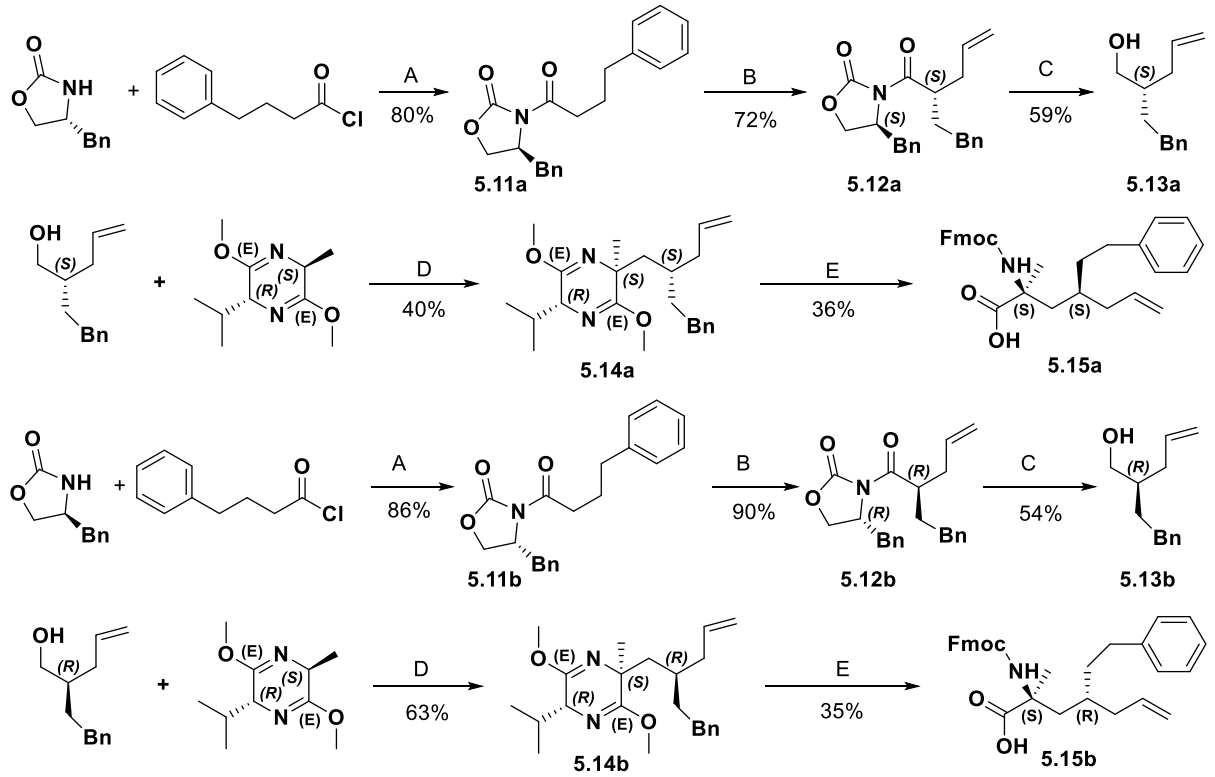

Figure 5.11. Synthesis of gamma-phenethyl stapling amino acids. A) *n*-BuLi B) $Li^{+}[N\text{-}iPr_2]^{-}$ C) $LiBH_4$ D) $(F_3CSO_2)_2O$; *n*-BuLi E) TFA; NaOH; Fmoc-Cl, Na_2CO_3

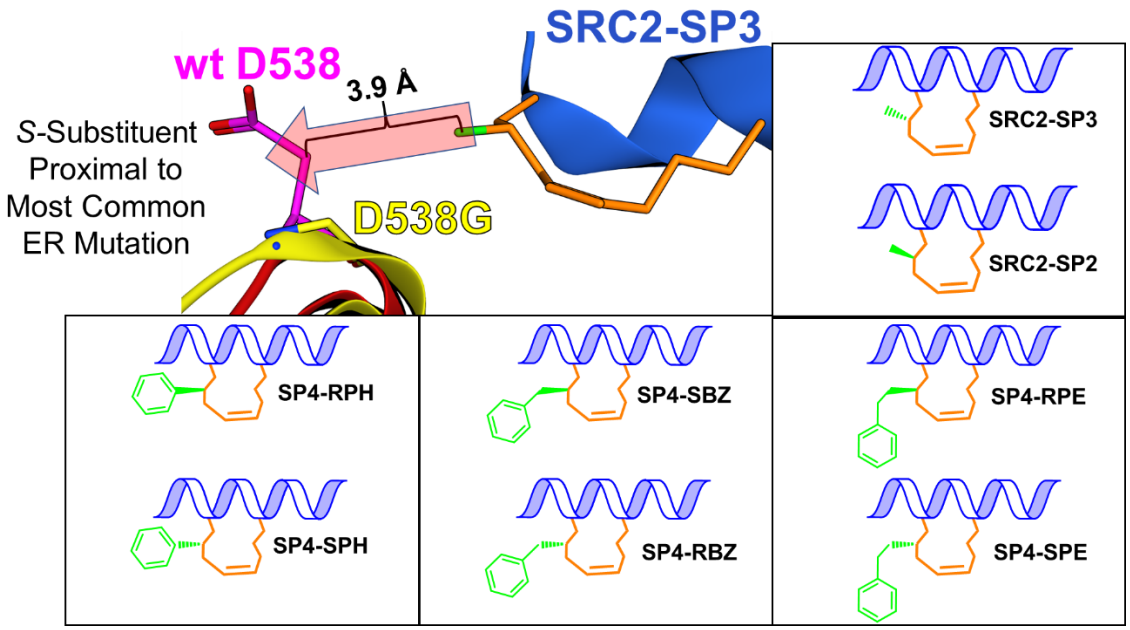

Figure 5.12 Interaction of gamma-methyl of SP3 with estrogen receptor residue 538. Structure and configuration nomenclature indicated for gamma-substituted peptides.

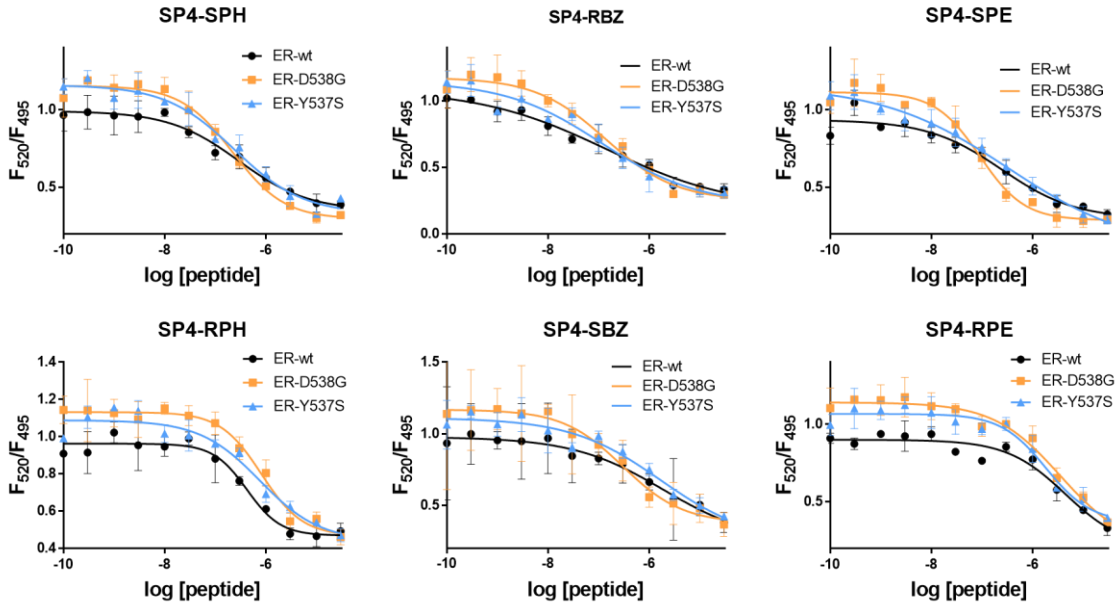

Figure 5.13. TR-FRET IC_{50} curves measured for SP4 peptide substituted with *R* or *S*-phenyl, -benzyl, or -phenethyl branching groups.

TABLE XXI. IC_{50} VALUES DERIVED FROM TR-FRET BINDING CURVES FOR R4K1 PEPTIDE WITH ADDITIONAL MODIFICATIONS

Peptide	**ERα-wt** IC_{50} nM (95% CI)	**ERα-D538G** IC_{50} nM (95% CI)	**ERα-Y537S** IC_{50} nM (95% CI)
SP4	690 (330-3000)	660 (420-1200)	480 (290-900)
SP4-SPH	290 (130-990)	220 (150-350)	240 (130-480)
SP4-RBZ	140 (n.d.)	140 (71-290)	110 (36-800)
SP4-SPE	250 (110-780)	91 (62-130)	330 (n.d.)
SP4-RPH	420 (260-710)	820 (510-1500)	760 (410-2300)
SP4-SBZ	1900 (n.d.)	300 (160-800)	1700 (n.d.)
SP4-RPE	4500 (2000-6500)	3500 (1600-5000)	1800 (n.d.)

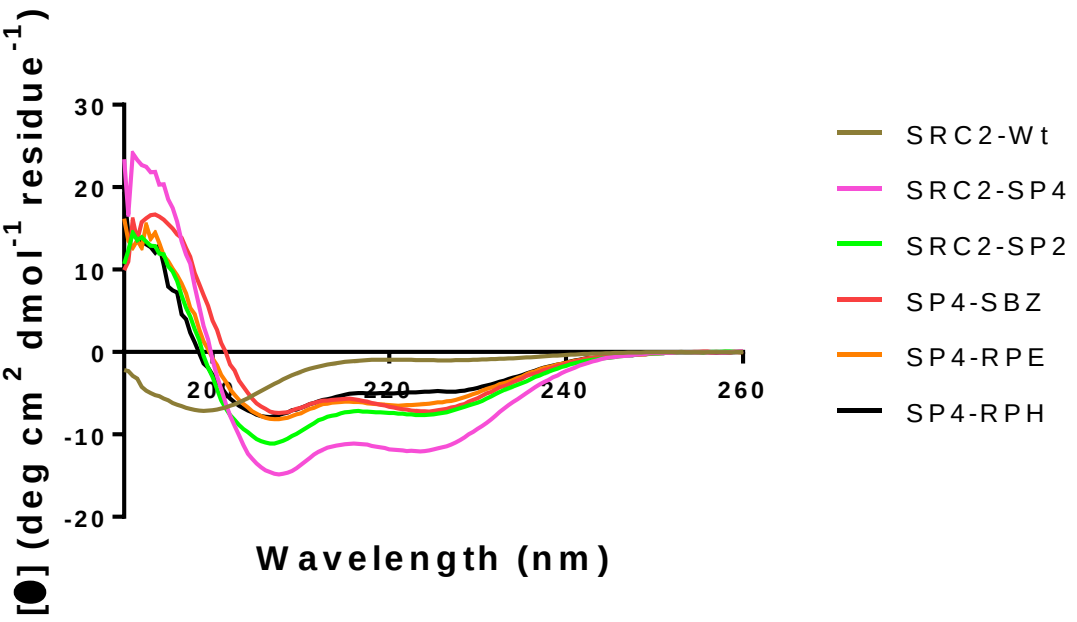

Figure 5.14. Circular dichroism spectra of gamma-substituted stapled peptide (substituent in the configuration corresponding to the SRC2-SP2 peptide (i.e., *R*-methyl))

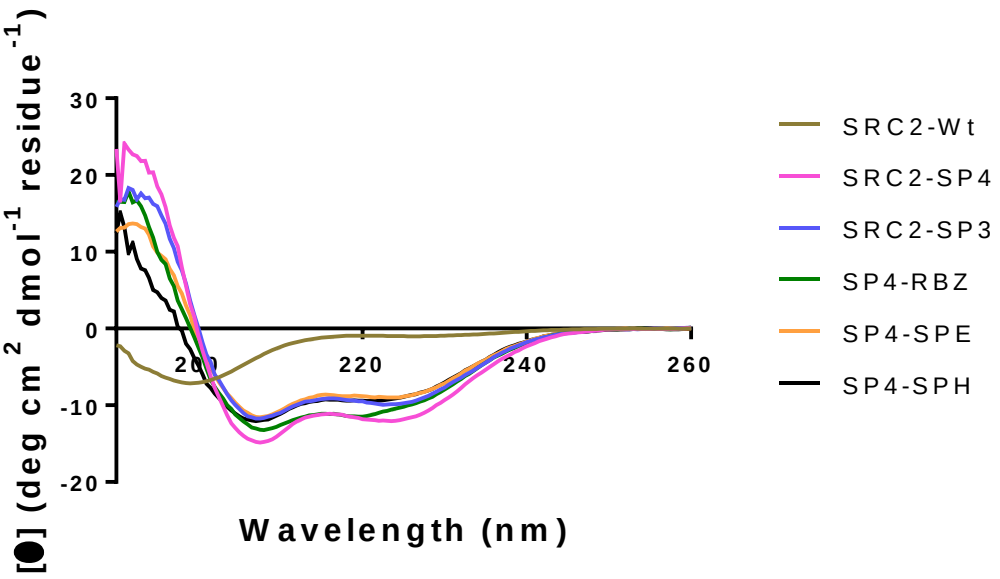

Figure 5.15. Circular dichroism analysis of gamma-substituted stapled peptide (substituent in the configuration corresponding to the SRC2-SP3 peptide (i.e., *S*-methyl))

5.5 Multi-functionalized stapled peptides with enhanced binding affinity to estrogen receptor

To determine if gamma-functionalization, lactam bicyclization, or amino acid substitution would be compatible with binding enhancement achieved with the Arg_4, a series of multi-functionalized peptides was prepared. The structure-activity relationship built around SRC2-SP4 suggests that the explored modifications could be complimentary in preparing extremely high-affinity peptides for ER. A significant binding enhancement could be feasible by incorporating an R4 tail to promote charge-mediated hydrogen bonds (10-20x), installing a gamma-methyl substituent at the *i*-position to increase van der Waals interactions (4x), and replacing L_3 with cyclohexylalanine to increase van der Waals interactions (4-6x). Additionally, we converted the Arg692→D696 salt bridge to a

lactam to promote helicity and proteolytic stability, even though this has relatively little impact on the binding affinity (Figure 5.16).

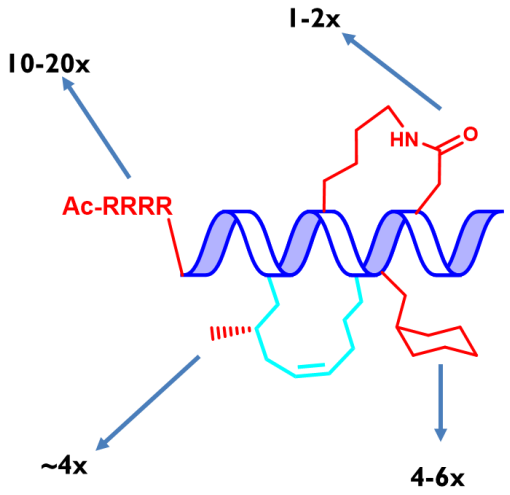

Figure 5.16. Summary of chemical modifications to SP4 peptide

Multi-functionalized peptides incorporating the design elements mentioned above (Figure 5.17) were prepared and assayed against ER-wt, ERD538G, and ERY537S using TR-FRET (Figure 5.18, Table XXI). The peptides were functionalized with the arginine-rich sequence from R4K1, and they also included the following design features: R4K1-SM, featured an S-configured methyl at the *i*-position; R4K1-BC featured an Arg692→D696 salt bridge-to-lactam replacement; and R4K1-CHA featured an L_3→cyclohexylalanine replacement. Each of these peptides showed enhanced affinities relative to R4K1 across all receptor isoforms. The bifunctional peptide R4K1-SPH contained an *S*-configured phenyl at the *i*-position, and it a large increase in binding relative to individual modifications, achieving a 130-fold binding enhancement relative to SP4. Interestingly, each individual modification of R4K1-SPH enhanced binding affinity only 2.4-fold (SP4-SPH) or 10-fold (R4K1) alone. The highest affinity peptide across each

receptor was R4K1-MBC, which incorporates the R4 modification, an *S*-configured gamma-methyl stapling amino acid, a lactam bridge, and an $L^3 \rightarrow$CHA substitution. The fold increase for this peptide relative to SP4 was 223-fold (ERα-wt), 116-fold (ERα-D538G), and 253-fold (ERα-Y537S).

Aside from the R4K1 modification, a general approach to increasing binding affinity in this SAR relied on enhancing hydrophobic interactions. A close inspection of the binding curves reveals an increase in TR-FRET at high concentrations of peptide inhibitor. Shoichet and coworkers have shown that unusual dose-response curves may be suggestive of aggregation or insolubility. Applied to our own data, this may suggest that some of these hydrophobic peptides may aggregate at concentrations exceeding 1 μM. This is most strongly observed with the peptide R4K1-MCB (Figure 5.18). Perhaps unsurprising, the structure activity relationship indicates that additional hydrophobic surface can lead to enhanced binding affinity. This finding agrees with the general notion that protein-protein interactions are mediated via large hydrophobic surface areas, such as the “LxxLL” motif that orchestrates ER/SRC interactions.

One of the next objectives for the development of these peptides will be to determine how the combination of charged residues and additional hydrophobicity effect interactions with the cell membrane, cellular uptake, and target engagement. Recent studies indicate that positive charge can facilitate permeability of stapled peptides and an increase in hydrophobic moment of amphipathic peptides was also shown to enhance cell permeability. [52] [149] We are currently working in collaboration with the Frasor lab at UIC to determine the biological activity of the modified R4K1 peptides. Cytotoxicity assays are being used to determine potential toxic liabilities and qPCR assays are being carried out

to validate the proposed mechanism of action. In conclusion, the peptide R4K1-MCB has extremely high affinity for estrogen receptor, perhaps even exceeding the single digit nanomolar affinity that has been reported for some coactivator complexes.[88] Verification of desirable biophysical properties and target engagement of these peptides will be an important step in continuing to develop these valuable chemical probes.

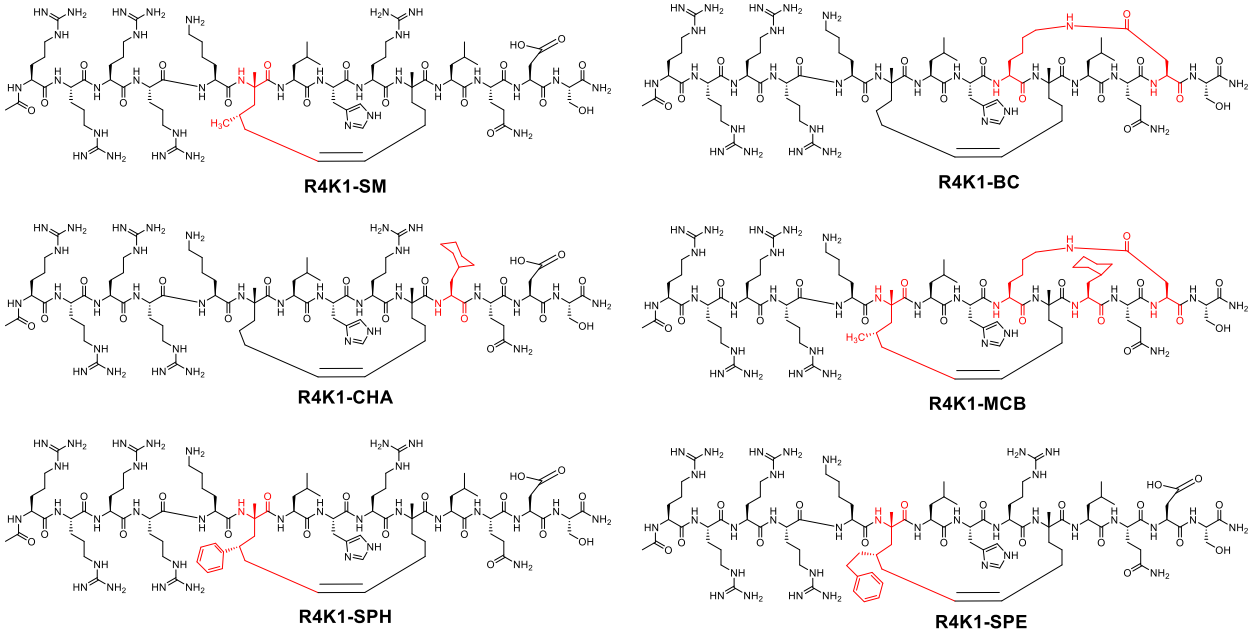

Figure 5.17. Chemical structures of R4K1 derived stapled peptides with additional modifications

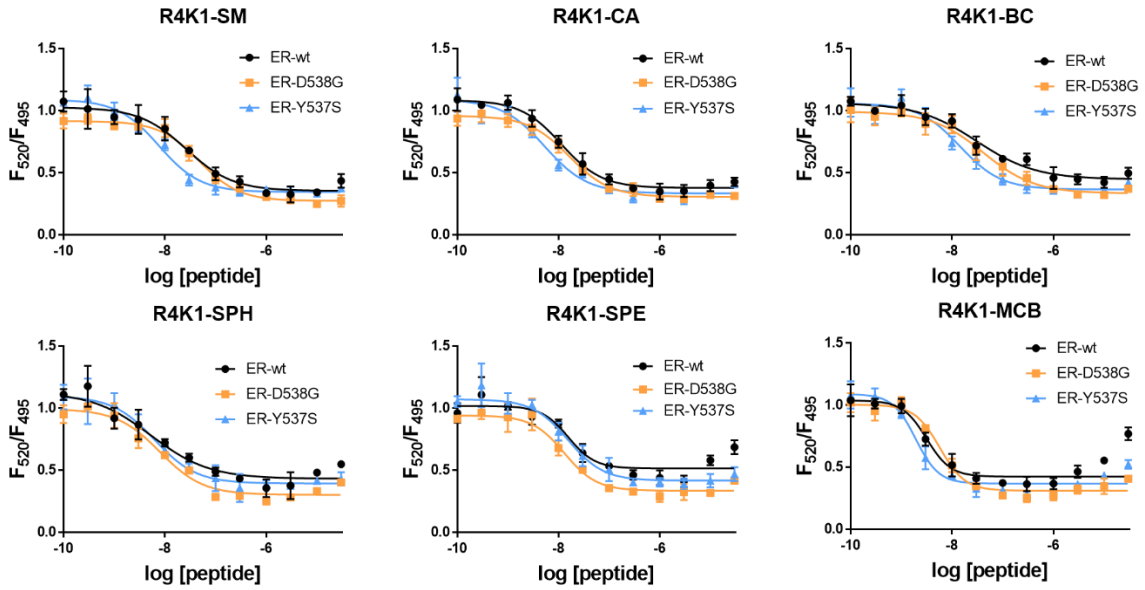

Figure 5.18. TR-FRET binding curves for modified R4K1 peptides.

TABLE XX. IC_{50} values derived from TR-FRET binding curves for R4K1 peptide with additional modifications. 95% CI = 95% confidence interval

Peptide	**ERα-wt** IC_{50} nM (95% CI)	**ERα-D538G** IC_{50} nM (95% CI)	**ERα-Y537S** IC_{50} nM (95% CI)
R4K1-SM	26 (15-43)	48 (37-62)	7.6 (5.4-11)
R4K1-CA	11 (8.2-15)	16 (13-21)	5.4 (3.4-7.8)
R4K1-BC	31 (17-54)	41 (27-64)	14 (9.6-22)
R4K1-SPH	5.3 (1.7-11)	8.0 (5.1-12)	6.3 (3.7-10)
R4K1-SPE	16 (8.1-27)	13 (9.6-18)	15 (11-21)
R4K1-MCB	3.1 (2.2-4.6)	5.7 (4.4-7.4)	1.9 (1.4-2.6)

5.6 General methods

Peptide synthesis, circular dichroism, and SPR binding analysis were carried out as described in chapter 4. HPLC retention times for peptides were measured as previously described, except 0.1% formic acid was used in place of 0.1% TFA. The TR-FRET assay was carried out as previously described, except a coactivator peptide with the sequence

FITC-EARRPSLLKKLLLAPANTQ (ThermoFisher PV4421), was used in place of the steroid receptor coactivator fragment.

TABLE XXII. STAPLED PEPTIDE SEQUENCE AND PURITY CHARACTERIZATION

Peptide	Sequence	Exact Mass ($M+H^+$)	Observed Mass ($M+H^+$)	RT (min)
SP4-L^1-*t*-Leu	Ac-HK<u>XB^1HRX</u>LQDS-NH_2	1424.812	1424.828	5.71
SP4-L^1-NPG	Ac-HK<u>XB^2HRX</u>LQDS-NH_2	1438.828	1438.805	6.02
SP4-L^1-CHA	Ac-HK<u>XB^3HRX</u>LQDS-NH_2	1464.843	1464.823	6.19
SP4-L^3- *t*-Leu	Ac-HK<u>XLHRX</u>B^1QDS-NH_2	1424.812	1424.818	5.82
SP4-L^3-NPG	Ac-HK<u>XLHRX</u>B^2QDS-NH_2	1438.828	1438.827	5.97
SP4-L^3-CHA	Ac-HK<u>XLHRX</u>B^3QDS-NH_2	1464.843	1464.819	6.18
SP4-SPH	Ac-HK<u>X^1HRX</u>LQDS-NH_2	1500.843	1500.804	6.53
SP4-SBZ	Ac-HK<u>X^2HRX</u>LQDS-NH_2	1514.859	1514.869	6.47
SP4-SPE	Ac-HK<u>X^3HRX</u>LQDS-NH_2	1528.875	1528.887	6.77
SP4-RPH	Ac-HK<u>X^4HRX</u>LQDS-NH_2	1500.843	1500.819	6.15
SP4-RBZ	Ac-HK<u>X^5HRX</u>LQDS-NH_2	1514.859	1514.838	6.61
SP4-SPE	Ac-HK<u>X^6HRX</u>LQDS-NH_2	1528.875	1528.887	6.63
R4K1-SM	Ac-RRRRK<u>X^7HRX</u>LQDS-NH_2	1926.173	1926.171	4.97
R4K1-CA	Ac-RRRRK<u>XHRXB^3</u>QDS-NH_2	1952.189	1952.179	5.07
R4K1-BC	Ac-RRRRK<u>XH[KX</u>LQD]S-NH_2	1866.141	1866.130	5.05
R4K1-SPH	Ac-RRRRK<u>X^1HRX</u>LQDS-NH_2	1988.189	1988.186	5.39
R4K1-SPE	Ac-RRRRK<u>X^3HRX</u>LQDS-NH_2	2016.220	2016.225	5.56
R4K1-MCB	Ac-RRRRK<u>X^7H[KXB^3</u>QD]S-NH_2	1920.188	1920.183	5.546

B^1 tert-lecuine; B^2 neopentylglycine; B^3 cyclohexylalanine; X (*S*)-2-amino-2-methylhept-6-enoic acid; X^1 (2*S*,4*S*)-2-amino-2-methyl-4-phenylhept-6-enoic acid; X^2 (2*S*,4*S*)-2-amino-4-benzyl-2-methylhept-6-enoic acid; X^3 (2*S*,4*S*)-2-amino-2-methyl-4-phenethylhept-6-enoic acid; X^4 (2*S*,4*R*)-2-amino-2-methyl-4-phenylhept-6-enoic acid; X^5 (2*S*,4*R*)-2-amino-4-benzyl-2-methylhept-6-enoic acid; X^6 (2*S*,4*R*)-2-amino-2-methyl-4-phenethylhept-6-enoic acid; X^7 (2*S*,4*S*)-2-amino-2,4-dimethylhept-6-enoic acid.

5.7 Synthesis of gamma-functionalized amino acids

General method A: *N*-Acylation of oxazolidinones.

Oxazolidinone (1.00 eq) was dissolved in THF (5 mL/mmol) and cooled to -78 °C. *n*-BuLi (~1.8 M in hexanes; 1.05 eq) was added dropwise over 30 minutes and the reaction was stirred for an additional 30 minutes at -78 °C. Acid chloride (1.00 eq) was dissolved in THF (2 mL/g) and added dropwise over 30 minutes. The reaction mixture was stirred for an additional 2 hrs at -78 °C and then allowed to come to room temperature and stirred for an additional 30 minutes at room temperature. The reaction was quenched with saturated ammonium chloride (1.5 mL/mmol) and the THF/hexanes were removed by rotary evaporation. The reaction mixture was dissolved in dichloromethane and washed with water (1.5 mL/mmol), 10% sodium hydroxide (1.5 mL/mmol), and brine (1.5 mL/mmol). The organic layer was dried with $MgSO_4$, and the solvent was removed. The product was purified using flash column chromatography (hexanes/ethyl acetate), typical eluting between 15-25% ethyl acetate.

5.1a (*R*)-4-benzyl-3-(2-phenylacetyl)oxazolidin-2-one. Compound **5.1a** was prepared on 20 mmol scale using general method A with a yield of 4.70 g (79.7%).

^{1}H NMR (CHLOROFORM-d, 400 MHz): δ = 7.26-7.43 (m, 8H), 7.14-7.19 (m, 2H), 4.66-4.75 (m, 1H), 4.34 (q, *J* = 15.7 Hz, 2H), 4.17-4.26 (m, 2H), 3.30 (dd, *J* = 13.4, 3.3 Hz, 1H), 2.79 ppm (dd, *J* = 13.4, 9.3 Hz, 1H)

^{13}C NMR (CHLOROFORM-d, 101 MHz): δ = 171.2, 153.4, 135.1, 133.5, 129.8, 129.4, 128.9, 128.6, 127.3, 127.2, 66.1, 55.3, 41.6, 37.7 ppm

$[\alpha]_D^{20}$ -71 (*c* 1.75, $CHCl_3$)

HRMS $[M+H]^+$ calcd for $C_{18}H_{18}NO_3$, 296.1281; found 296.1278

5.1b (*S*)-4-benzyl-3-(2-phenylacetyl)oxazolidin-2-one. Compound **5.1b** was prepared on 20 mmol scale using general method A with a yield of 4.74 g (79.1%).

^{1}H NMR (CHLOROFORM-d, 400 MHz): δ = 7.83-7.85 (m, 1H), 7.36-7.42 (m, 1H), 7.26-7.36 (m, 1H), 7.14-7.20 (m, 2H), 4.71 (ddt, *J* = 9.6, 7.1, 3.3 Hz, 1H), 4.34 (q, *J* = 15.7 Hz, 2H), 4.16-4.25 (m, 2H), 3.29 (dd, *J* = 13.4, 3.3 Hz, 1H), 2.80 ppm (dd, *J* = 13.4, 9.6 Hz, 1H)

^{13}C NMR (CHLOROFORM-d, 101 MHz): δ = 171.1, 153.3, 135.1, 133.5, 129.7, 129.4, 128.9, 128.5, 127.3, 127.2, 66.0, 55.2, 41.5, 37.6 ppm

$[\alpha]_D^{20}$ 65 (*c* 3.75, $CHCl_3$)

HRMS $[M+H]^+$ calcd for $C_{18}H_{18}NO_3$, 296.1281; found 296.1283

5.6a (*S*)-4-benzyl-3-(pent-4-enoyl)oxazolidin-2-one. Compound **5.6a** was prepared on 20 mmol scale using general method A with a yield of 3.95 g (76.2%).

^{1}H NMR (CHLOROFORM-d, 400 MHz): δ = 7.32-7.37 (m, 2H), 7.25-7.32 (m, 1H), 7.20-7.25 (m, 2H), 5.90 (ddt, *J* = 17.0, 10.3, 6.5 Hz, 1H), 5.13 (dq, *J* = 17.2, 1.6 Hz, 1H), 5.05 (dd, *J* = 10.1, 1.5 Hz, 1H), 4.63-4.75 (m, 1H), 4.14-4.25 (m, 2H), 3.31 (dd, *J* = 13.3, 3.2 Hz, 1H), 2.98-3.16 (m, 2H), 2.78 (dd, *J* = 13.4, 9.6 Hz, 1H), 2.42-2.53 ppm (m, 2H)

^{13}C NMR (CHLOROFORM-d, 101 MHz) δ ppm 172.51 (s, 1 C), 153.44 (s, 1 C), 136.69 (s, 1 C), 135.28 (s, 1 C), 129.41 (s, 1 C), 128.93 (s, 1 C), 127.33 (s, 1 C), 115.70 (s, 1 C), 66.20 (s, 1 C), 55.12 (s, 1 C), 37.89 (s, 1 C), 34.79 (s, 1 C), 28.16 (s, 1 C)

$[\alpha]_D^{20}$ 65 (*c* 3.00, $CHCl_3$)

HRMS $[M+H]^+$ calcd for $C_{15}H_{18}NO_3$, 260.1281; found 260.1268

5.6b (*R*)-4-benzyl-3-(pent-4-enoyl)oxazolidin-2-one. Compound **5.6b** was prepared on 20 mmol scale using general method A with a yield of 3.77 g (72.7%).

^{1}H NMR (CHLOROFORM-d, 400 MHz): δ = 7.32-7.38 (m, 2H), 7.26-7.32 (m, 1H), 7.21-7.26 (m, 2H), 5.90 (ddt, *J* = 17.1, 10.4, 6.5 Hz, 1H), 5.13 (dq, *J* = 17.1, 1.5 Hz, 1H), 5.05 (dd, *J* = 10.2, 1.4 Hz, 1H), 4.69 (s, 1H), 4.15-4.25 (m, 2H), 3.31 (dd, *J* = 13.4, 3.3 Hz, 1H), 2.99-3.16 (m, 2H), 2.78 (dd, *J* = 13.4, 9.6 Hz, 1H), 2.43-2.53 ppm (m, 2H)

^{13}C NMR (CHLOROFORM-d, 101 MHz): δ = 172.5, 153.4, 136.6, 135.2, 129.4, 128.9, 127.3, 115.7, 66.2, 55.1, 37.9, 34.8, 28.1 ppm

$[\alpha]_D^{20}$ -63 (*c* 1.65, $CHCl_3$)

HRMS $[M+H]^+$ calcd for $C_{15}H_{18}NO_3$, 260.1281; found 260.1277

5.11a (*S*)-4-benzyl-3-(4-phenylbutanoyl)oxazolidin-2-one. Compound **5.11a** was prepared on 20 mmol scale using general method A with a yield of 5.20 g (80.4%).

^{1}H NMR (CHLOROFORM-d, 400 MHz): δ = 7.29-7.40 (m, 5H), 7.21-7.29 (m, 5H), 4.68 (ddt, *J* = 9.9, 7.1, 3.5 Hz, 1H), 4.15-4.23 (m, 2H), 3.31 (dd, *J* = 13.4, 3.3 Hz, 1H), 2.94-3.10 (m, 2H), 2.68-2.85 (m, 3H), 1.97-2.16 ppm (m, 2H)

^{13}C NMR (CHLOROFORM-d, 101 MHz): δ = 172.9, 153.3, 141.4, 135.2, 129.3, 128.9, 128.4, 128.3, 127.3, 125.9, 66.1, 55.0, 37.8, 35.1, 34.9, 25.8 ppm

$[\alpha]_D^{20}$ 45 (*c* 2.55, $CHCl_3$)

HRMS $[M+H]^+$ calcd for $C_{20}H_{23}NO_3$, 324.1594; found 324.1586

5.11b (*R*)-4-benzyl-3-(4-phenylbutanoyl)oxazolidin-2-one. Compound **5.11b** was prepared on 20 mmol scale using general method A with a yield of 5.55 g (90.0%).

^{1}H NMR (CHLOROFORM-d, 400 MHz): δ = 7.30-7.40 (m, 5H), 7.21-7.30 (m, 5H), 4.68 (ddt, *J* = 9.9, 7.1, 3.5 Hz, 1H), 4.15-4.22 (m, 2H), 3.31 (dd, *J* = 13.4, 3.3 Hz, 1H), 2.94-3.10 (m, 2H), 2.73-2.83 (m, 3H), 2.08 ppm (quind, *J* = 7.5, 2.7 Hz, 2H)

^{13}C NMR (CHLOROFORM-d, 101 MHz): δ = 172.9, 153.3, 141.4, 135.2, 129.3, 128.9, 128.4, 128.3, 127.2, 125.9, 66.1, 55.0, 37.8, 35.1, 34.9, 25.8 ppm

$[\alpha]_D^{20}$ -47 (*c* 2.60, $CHCl_3$)

HRMS $[M+H]^+$ calcd for $C_{20}H_{23}NO_3$, 324.1594; found 324.1584

General method B: Stereoselective alkylation of oxazolidinones.

The previously prepared *N*-acyl oxazolidinone (1.0 eq) was dissolved in THF (1 mL/mmol) and added dropwise over 30 minutes to a solution of 0.85 M lithium diisopropyl amide (1.1 eq; 1:1 THF:hexane) at -78 °C. After stirring for an additional 30 minutes, the alkyl halide (3.0 eq) was added dropwise over 30 minutes. The reaction was stirred for 30 minutes at -78 °C, followed by 2.5 hrs at 0 °C. After the reaction was complete (monitored by TLC), the mixture was warmed to room temperature and quenched with saturated ammonium chloride (1 mL/mmol). Volatile reaction components were removed by vacuum, the mixture was dissolved in dichloromethane (3 mL/mmol), washed with water (2 × 3 mL/mmol), washed with brine (3 mL/mmol), dried with $MgSO_4$, and concentrated. The crude product was purified by flash column chromatography (hexane:ethyl acetate) eluting between 10-20% ethyl acetate.

5.2a (*R*)-4-benzyl-3-((*R*)-2-phenylpent-4-enoyl)oxazolidin-2-one. Compound **5.2a** was prepared on 15.6 mmol scale using general method B with a yield of 3.55 g (67.8%).

^{1}H NMR (CHLOROFORM-d, 400 MHz): δ = 7.41-7.45 (m, 2H), 7.23-7.39 (m, 8H), 5.82 (ddt, *J* = 17.2, 10.4, 6.8 Hz, 1H), 5.23 (dd, *J* = 8.7, 6.4 Hz, 1H), 5.11-5.19 (m, 1H), 5.02-5.10 (m, 1H), 4.58-4.67 (m, 1H), 4.03-4.23 (m, 2H), 3.36 (dd, *J* = 13.4, 3.3 Hz, 1H), 2.93-3.04 (m, 1H), 2.79 (dd, *J* = 13.4, 9.9 Hz, 1H), 2.53-2.63 ppm (m, 1H)

^{13}C NMR (CHLOROFORM-d, 101 MHz): δ = 173.4, 152.9, 138.2, 135.3, 135.2, 129.4, 128.9, 128.6, 127.4, 127.3, 117.2, 65.7, 55.7, 48.1, 38.3, 38.0 ppm

$[\alpha]_D^{20}$ -111 (*c* 1.00, $CHCl_3$)

HRMS $[M+H]^+$ calcd for $C_{21}H_{22}NO_3$, 336.1594; found 336.1604

5.2b (*S*)-4-benzyl-3-((*S*)-2-phenylpent-4-enoyl)oxazolidin-2-one. Compound **5.2b** was prepared on 15.6 mmol scale using general method B with a yield of 3.52 g (67.3%).

^{1}H NMR (CHLOROFORM-d, 400 MHz): δ = 7.40-7.46 (m, 2H), 7.22-7.40 (m, 8H), 5.82 (ddt, *J* = 17.1, 10.3, 6.7 Hz, 1H), 5.22 (dd, *J* = 8.7, 6.4 Hz, 1H), 5.15 (dd, *J* = 17.1, 1.4 Hz, 1H), 5.07 (d, *J* = 10.1 Hz, 1H), 4.62 (ddt, *J* = 9.9, 7.3, 2.9 Hz, 1H), 4.03-4.16 (m, 2H), 3.36 (dd, *J* = 13.4, 3.0 Hz, 1H), 2.90-3.03 (m, 1H), 2.79 (dd, *J* = 13.3, 9.7 Hz, 1H), 2.58 ppm (dt, *J* = 14.1, 6.4 Hz, 1H)

^{13}C NMR (CHLOROFORM-d, 101 MHz): δ = 173.4, 152.9, 138.2, 135.3, 135.3, 129.4, 128.9, 128.6, 127.4, 127.3, 117.2, 65.8, 55.8, 48.2, 38.3, 38.0 ppm

$[\alpha]_D^{20}$ 116 (*c* 0.80, $CHCl_3$)

HRMS $[M+H]^+$ calcd for $C_{21}H_{22}NO_3$, 336.1594; found 336.1591

5.7a (*S*)-4-benzyl-3-((*R*)-2-benzylpent-4-enoyl)oxazolidin-2-one. Compound **5.7a** was prepared on 15.8 mmol scale using general method B with a yield of 3.50 g (66.0%).

^{1}H NMR (CHLOROFORM-d, 400 MHz): δ = 7.19-7.41 (m, 8H), 7.00-7.10 (m, 2H), 5.85 (ddt, *J* = 17.1, 10.0, 7.2 Hz, 1H), 5.02-5.19 (m, 2H), 4.62-4.72 (m, 1H), 4.34-4.46 (m, 1H), 4.06-4.17 (m, 2H), 3.12 (dd, *J* = 13.4, 8.6 Hz, 1H), 3.03 (dd, *J* = 13.6, 3.3 Hz, 1H), 2.87 (dd, *J* = 13.4, 6.6 Hz, 1H), 2.45-2.58 (m, 2H), 2.30-2.41 ppm (m, 1H)

^{13}C NMR (CHLOROFORM-d, 101 MHz): δ = 175.2, 153.1, 139.0, 135.2, 135.2, 129.4, 129.4, 128.9, 128.4, 127.3, 126.5, 117.3, 65.8, 55.1, 44.3, 38.2, 37.6, 36.4 ppm

$[\alpha]_D^{20}$ 25 (*c* 2.75, $CHCl_3$)

HRMS $[M+H]^+$ calcd for $C_{22}H_{24}NO_3$, 350.1751; found 350.1738

5.7b (*R*)-4-benzyl-3-((*S*)-2-benzylpent-4-enoyl)oxazolidin-2-one. Compound **5.7b** was prepared on 13.4 mmol scale using general method B with a yield of 4.00 g (85%).

^{1}H NMR (CHLOROFORM-d, 400 MHz): δ = 7.20-7.34 (m, 8H), 7.04 (dd, *J* = 7.3, 1.5 Hz, 2H), 5.83 (ddt, *J* = 17.0, 10.0, 7.1 Hz, 1H), 5.04-5.14 (m, 2H), 4.62-4.69 (m, 1H), 4.38 (tt, *J* = 8.3, 6.3 Hz, 1H), 4.11-4.17 (m, 1H), 4.08 (dd, *J* = 3304.1, 2.8 Hz, 1H), 3.10 (dd, *J* = 13.4, 8.6 Hz, 1H), 3.03 (dd, *J* = 13.6, 3.3 Hz, 1H), 2.86 (dd, *J* = 13.4, 6.6 Hz, 1H), 2.44-2.55 (m, 2H), 2.32 ppm (dt, *J* = 13.7, 6.2 Hz, 1H)

^{13}C NMR (CHLOROFORM-d, 101 MHz): δ = 175.2, 153.1, 138.9, 135.2, 129.4, 129.4, 128.9, 128.4, 127.2, 126.5, 117.3, 65.8, 55.0, 44.3, 38.1, 37.6, 36.3 ppm

$[\alpha]_D^{20}$ -27 (*c* 1.70, $CHCl_3$)

HRMS $[M+H]^+$ calcd for $C_{22}H_{24}NO_3$, 350.1751; found 350.1745

5.12a (*S*)-4-benzyl-3-((*S*)-2-phenethylpent-4-enoyl)oxazolidin-2-one. Compound **5.12a** was prepared on 15.9 mmol scale using general method B with a yield of 4.18 g (72.2%).

^{1}H NMR (CHLOROFORM-d, 400 MHz): δ = 7.33-7.39 (m, 2H), 7.27-7.32 (m, 3H), 7.17-7.26 (m, 5H), 5.86 (ddt, *J* = 17.1, 10.1, 7.1 Hz, 1H), 5.04-5.17 (m, 2H), 4.55 (ddt, *J* = 10.1, 6.8, 3.4 Hz, 1H), 4.06-4.18 (m, 2H), 4.00 (dddd, *J* = 8.6, 7.3, 6.1, 4.9 Hz, 1H), 3.29 (dd, *J* = 13.3, 3.3 Hz, 1H), 2.60-2.75 (m, 3H), 2.53 (dt, *J* = 14.1, 7.2 Hz, 1H), 2.34-2.44 (m, 1H), 2.17 (dtd, *J* = 13.7, 9.1, 6.7 Hz, 1H), 1.87 ppm (dddd, *J* = 13.9, 9.5, 5.9, 4.6 Hz, 1H)

^{13}C NMR (CHLOROFORM-d, 101 MHz): δ = 175.6, 153.1, 141.5, 135.4, 135.0, 129.4, 128.9, 128.5, 128.3, 127.3, 125.9, 117.4, 65.9, 55.4, 42.1, 38.1, 37.2, 33.8, 33.0 ppm

$[\alpha]_D^{20}$ 43 (*c* 1.85, $CHCl_3$)

HRMS $[M+H]^+$ calcd for $C_{23}H_{26}NO_3$, 364.1907; found 364.1902

5.12b (*R*)-4-benzyl-3-((*R*)-2-phenethylpent-4-enoyl)oxazolidin-2-one. Compound **5.12b** was prepared on 15.9 mmol scale using general method B with a yield of 5.20 g (90.0%).

^{1}H NMR (CHLOROFORM-d, 400 MHz): δ = 7.29-7.39 (m, 5H), 7.19-7.27 (m, 5H), 5.85 (ddt, *J* = 17.1, 10.1, 7.2 Hz, 1H), 5.05-5.16 (m, 2H), 4.55 (ddt, *J* = 10.1, 6.8, 3.4 Hz, 1H), 4.07-4.16 (m, 2H), 4.00 (ddd, *J* = 13.3, 7.3, 6.2 Hz, 1H), 3.29 (dd, *J* = 13.3, 3.3 Hz, 1H), 2.60-2.74 (m, 3H), 2.53 (dt, *J* = 14.1, 7.2 Hz, 1H), 2.33-2.43 (m, 1H), 2.17 (dtd, *J* = 13.8, 9.1, 6.7 Hz, 1H), 1.87 ppm (dddd, *J* = 14.2, 9.8, 5.9, 4.9 Hz, 1H)

^{13}C NMR (CHLOROFORM-d, 101 MHz): δ = 175.7, 153.1, 141.5, 135.4, 135.0, 129.4, 128.9, 128.5, 128.3, 127.3, 125.9, 117.4, 65.9, 55.4, 42.1, 38.1, 37.2, 33.8, 33.0 ppm

$[\alpha]_D^{20}$ -38 (*c* 1.65, $CHCl_3$)

HRMS $[M+H]^+$ calcd for $C_{23}H_{26}NO_3$, 364.1907; found 364.1908

General method C: Reductive cleavage of *N*-acyl oxazolidinones.

N-acyl oxazolidinone (1.0 eq) and ethanol (1.5 mL/eq) were dissolved in diethylether (10 mL/mmol) and cooled to 0 °C in an ice/salt bath. $LiBH_4$ (1.5 eq, divided and added in 4 portions) was added, and stirring was continued for 2 hrs as the reaction mixture warmed to room temperature. When the reaction was complete, as monitored by TLC, the mixture was cooled back to 0 °C and quenched with 1 M NaOH (7.5 mL/mmol). The aqueous phase was extracted with ether (2 × 5 mL/mmol), and the combined organic phase was washed with saturated ammonium chloride (7.5 mL/mmol), water (7.5 mL/mmol), and brine (7.5 mL/mmol). The ether phase was dried with $MgSO_4$, concentrated, and purified by flash chromatography (hexanes/ethyl acetate). The product alcohol elutes between 10-30% ethyl acetate.

5.3a (*R*)-2-phenylpent-4-en-1-ol. Compound **5.3a** was prepared on 10.4 mmol scale using general method C with a yield of 1.30 g (77.1%).

^{1}H NMR (CHLOROFORM-d, 400 MHz): δ = 7.21-7.39 (m, 5H), 5.72 (dddd, *J* = 16.9, 10.1, 7.3, 6.3 Hz, 1H), 4.95-5.11 (m, 2H), 3.79 (qd, *J* = 12.0, 5.6 Hz, 2H), 2.91 (quin, *J* = 7.0 Hz, 1H), 2.37-2.56 (m, 2H), 1.46 ppm (br s, 1H)

^{13}C NMR (CHLOROFORM-d, 101 MHz): δ = 141.8, 136.3, 128.6, 128.0, 126.8, 116.4, 66.9, 48.2, 36.6 ppm

$[\alpha]_D^{20}$ -16 (*c* 0.55, $CHCl_3$)

5.3b (*S*)-2-phenylpent-4-en-1-ol. Compound **5.3b** was prepared on 10.4 mmol scale using general method C with a yield of 1.36 g (80.5%).

^{1}H NMR (CHLOROFORM-d, 400 MHz): δ = 7.31-7.38 (m, 2H), 7.19-7.31 (m, 3H), 5.75 (ddt, *J* = 17.1, 10.0, 7.0 Hz, 1H), 4.96-5.11 (m, 2H), 3.80 (qd, *J* = 11.7, 6.0 Hz, 2H), 2.91 (quin, *J* = 7.0 Hz, 1H), 2.37-2.57 (m, 2H), 1.47 ppm (br s, 1H)

^{13}C NMR (CHLOROFORM-d, 101 MHz): δ = 141.9, 136.3, 128.6, 128.0, 126.8, 116.4, 66.9, 48.2, 36.6 ppm

$[\alpha]_D^{20}$ 18 (*c* 0.30, $CHCl_3$)

5.8a (*R*)-2-benzylpent-4-en-1-ol. Compound **5.8a** was prepared on 8.9 mmol scale using general method C with a yield of 0.980 g (62.7%).

^{1}H NMR (CHLOROFORM-d, 400 MHz): δ = 7.29-7.36 (m, 2H), 7.19-7.25 (m, 3H), 5.86 (ddt, *J* = 17.1, 10.1, 7.2 Hz, 1H), 5.02-5.17 (m, 2H), 3.60 (dd, *J* = 11.0, 5.4 Hz, 1H), 3.56 (dd, *J* = 11.0, 5.6 Hz, 1H), 2.62-2.72 (m, 2H), 2.14-2.21 (m, 2H), 1.90-2.01 ppm (m, 1H)

^{13}C NMR (CHLOROFORM-d, 101 MHz): δ = 140.5, 136.8, 129.2, 128.3, 125.9, 116.6, 64.7, 42.4, 37.2, 35.5 ppm

$[\alpha]_D^{20}$ 7.2 (*c* 2.30, $CHCl_3$)

5.8b (*S*)-2-benzylpent-4-en-1-ol. Compound **5.8b** was prepared using general method C with a yield of 1.40 g (75.6%).

^{1}H NMR (CHLOROFORM-d, 400 MHz): δ = 7.30 (s, 2H), 7.16-7.25 (m, 3H), 5.86 (ddt, *J* = 17.1, 10.1, 7.1 Hz, 1H), 5.01-5.18 (m, 2H), 3.57 (d, *J* = 3114.4 Hz, 2H), 2.67 (dd, *J* = 7.3, 3.0 Hz, 1H), 2.11-2.22 (m, 2H), 1.88-2.01 (m, 1H), 1.37 ppm (t, *J* = 5.6 Hz, 1H)

^{13}C NMR (CHLOROFORM-d, 101 MHz): δ = 140.5, 136.8, 129.2, 128.3, 125.9, 116.6, 64.7, 42.4, 37.2, 35.5 ppm

$[\alpha]_D^{20}$ -12 (*c* 1.75, $CHCl_3$)

5.13a (*S*)-2-phenethylpent-4-en-1-ol. Compound **5.13a** was prepared on 10.5 mmol scale using general method C with a yield of 1.13 g (59.4%).

^{1}H NMR (CHLOROFORM-d, 400 MHz): δ = 7.29-7.36 (m, 2H), 7.18-7.24 (m, 3H), 5.76-5.91 (m, 1H), 5.01-5.17 (m, 2H), 3.60-3.82 (m, 2H), 2.61-2.75 (m, 2H), 2.07-2.26 (m, 2H), 1.56-1.76 ppm (m, 4H)

^{13}C NMR (CHLOROFORM-d, 101 MHz): δ = 142.5, 136.8, 128.3, 128.3, 125.8, 116.5, 65.4, 39.9, 35.7, 33.3, 32.5 ppm

$[\alpha]_D^{20}$ -6.1 (*c* 2.15, $CHCl_3$)

5.13b (*R*)-2-phenethylpent-4-en-1-ol. Compound **5.13b** was prepared on 11.3 mmol scale using general method C with a yield of 1.15 g (53.6%).

^{1}H NMR (CHLOROFORM-d, 400 MHz): δ = 7.29-7.34 (m, 2H), 7.20-7.24 (m, 3H), 5.75-5.94 (m, 1H), 5.00-5.17 (m, 2H), 3.61-3.83 (m, 2H), 2.65-2.72 (m, 2H), 2.15-2.27 (m, 2H), 1.63-1.73 ppm (m, 4H)

^{13}C NMR (CHLOROFORM-d, 101 MHz): δ = 142.4, 136.8, 128.3, 128.3, 125.7, 116.4, 65.3, 39.9, 35.6, 33.2, 32.4 ppm

$[\alpha]_D^{20}$ 6.0 (*c* 2.55, $CHCl_3$)

General method D: Alkylation of Schöllkopf bislactim ethers.

The previously prepared alcohol (2.0 eq) was dissolved in dichloromethane (2 mL/mmol) and cooled to -78 °C. Pyridine (2.2 eq) was added, followed by trifluoromethanesulfonic anhydride (1.05 eq). The reaction mixture was stirred for 10 minutes and warmed by transferring the reaction vessel to an ice bath, where stirring was continued for an additional 30 minutes. Ice-cold hexane (4 mL/mmol) and 1 M sulfuric acid (4 mL/mmol) were added, and the organic phase was collected. The aqueous phase was extracted with dichloromethane (4 mL/mmol) and the combined organic solutions were filtered through a silica plug. An additional volume of dichloromethane (5 mL/mmol) was flushed through the silica plug to collect any remaining product. The combined organic phases were dried with $MgSO_4$, the solvent was removed by vacuum, and the triflate was dissolved in THF (0.25 mL/mmol) for addition to the Schöllkopf enolate. The Schöllkopf bislactim ether ((2*R*,5*S*)-2-isopropyl-3,6-dimethoxy-5-methyl-2,5-dihydropyrazine) (1 eq) was dissolved in THF (4 mL/mmol) and cooled to -78 °C. *n*-BuLi (1.1 eq, 1.6 M in hexane) was added dropwise, the reaction was stirred for 1.5 hrs, and the triflate, dissolved in THF (0.25 mL/mmol), was added dropwise. The reaction was maintained at -78 °C for 6 hrs and then left to warm to room temperature overnight. The next day the reaction was quenched with saturated ammonium chloride and the solvents were removed by vacuum. The mixture was extracted with dichloromethane (3 × 2 mL/mmol), washed with water (3 × 2 mL/mmol), dried with $MgSO_4$, concentrated under vacuum, and purified by flash column chromatography (hexanes: ethyl acetate).

5.4a (2*S*,5*R*)-5-isopropyl-3,6-dimethoxy-2-methyl-2-((*S*)-2-phenylpent-4-en-1-yl)-2,5-dihydropyrazine. Compound **5.4a** was prepared on 4 mmol scale using general method D with a yield of 0.933 g (68.1% yield).

^{1}H NMR (CHLOROFORM-d, 400 MHz): δ = 7.18-7.25 (m, 2H), 7.09-7.18 (m, 1H), 6.99-7.06 (m, 2H), 5.59 (dddd, *J* = 16.9, 10.1, 7.3, 6.6 Hz, 1H), 4.88-4.97 (m, 2H), 3.75 (s, 3H), 3.68 (d, *J* = 3.0 Hz, 1H), 3.10 (s, 3H), 2.51-2.58 (m, 1H), 2.23-2.42 (m, 3H), 2.18 (dtd, *J* = 13.8, 6.9, 3.3 Hz, 1H), 1.93 (dd, *J* = 13.6, 3.5 Hz, 1H), 1.30 (s, 3H), 0.94 (d, *J* = 6.8 Hz, 3H), 0.67 ppm (d, *J* = 6.8 Hz, 3H)

^{13}C NMR (CHLOROFORM-d, 400 MHz): δ = 164.0, 162.0, 144.3, 137.1, 128.0, 127.9, 127.7, 127.6, 126.0, 115.7, 77.3, 77.0, 76.7, 61.2, 57.2, 52.2, 51.4, 46.3, 42.8, 42.4, 31.1, 30.1, 19.3, 19.2, 17.4 ppm

$[\alpha]_D^{20}$ 72 (*c* 1.15, $CHCl_3$)

HRMS $[M+H]^+$ calcd for $C_{21}H_{31}N_2O_2$, 343.2380; found 343.2335

5.4b (2*S*,5*R*)-5-isopropyl-3,6-dimethoxy-2-methyl-2-((*R*)-2-phenylpent-4-en-1-yl)-2,5-dihydropyrazine. Compound **5.4b** was prepared on 4 mmol scale using general method D with a yield of 0.986 g (72.0%).

^{1}H NMR (CHLOROFORM-d, 400 MHz): δ = 7.18-7.25 (m, 2H), 7.09-7.14 (m, 1H), 7.04 (d, *J* = 7.3 Hz, 2H), 5.58 (ddt, *J* = 17.0, 10.1, 7.0 Hz, 1H), 4.89-4.96 (m, 2H), 3.77 (d, *J* = 3.3 Hz, 1H), 3.73-3.75 (m, 3H), 3.00 (s, 3H), 2.33-2.43 (m, 1H), 2.21-2.30 (m, 3H), 2.17

(dtd, *J* = 13.7, 6.8, 3.4 Hz, 1H), 2.03 (br dd, *J* = 13.5, 10.0 Hz, 1H), 1.28 (s, 3H), 1.07 (d, *J* = 6.8 Hz, 3H), 0.60 ppm (d, *J* = 6.8 Hz, 3H)

^{13}C NMR (CHLOROFORM-d, 101 MHz): δ = 164.4, 160.4, 146.2, 136.9, 128.0, 127.6, 125.5, 115.8, 61.3, 58.9, 52.1, 51.5, 46.7, 43.5, 42.9, 30.8, 29.4, 19.3, 16.8 ppm

$[\alpha]_D^{20}$ 33 (*c* 0.70, $CHCl_3$)

HRMS $[M+H]^+$ calcd for $C_{21}H_{31}N_2O_2$, 343.2380; found 343.2349

5.9a (2*S*,5*R*)-2-((*R*)-2-benzylpent-4-en-1-yl)-5-isopropyl-3,6-dimethoxy-2-methyl-2,5-dihydropyrazine. Compound **5.9a** was prepared on 3 mmol scale using general method D with a yield of 0.226 g (21.1%).

^{1}H NMR (CHLOROFORM-d, 400 MHz): δ = 7.26-7.34 (m, 2H), 7.16-7.22 (m, 1H), 7.10 (d, *J* = 6.8 Hz, 2H), 5.70-5.84 (m, 1H), 4.96-5.08 (m, 2H), 4.04 (d, *J* = 3.3 Hz, 1H), 3.70 (s, 3H), 3.55 (s, 3H), 2.47-2.56 (m, 1H), 2.36-2.44 (m, 1H), 2.32 (td, *J* = 6.9, 3.4 Hz, 1H), 2.00 (q, *J* = 7.0 Hz, 2H), 1.88 (dd, *J* = 13.9, 5.6 Hz, 1H), 1.67 (dd, *J* = 13.9, 5.3 Hz, 1H), 1.50-1.61 (m, 1H), 1.33 (s, 3H), 1.11 (d, *J* = 6.8 Hz, 3H), 0.71 ppm (d, *J* = 6.8 Hz, 3H)

^{13}C NMR (CHLOROFORM-d, 101 MHz): δ = 165.5, 161.4, 141.4, 137.0, 129.3, 128.2, 128.1, 125.6, 116.3, 61.1, 58.4, 52.1, 51.9, 43.8, 40.4, 38.3, 36.6, 31.0, 29.6, 19.4, 16.9 ppm

$[\alpha]_D^{20}$ 46 (*c* 1.20, $CHCl_3$)

HRMS $[M+H]^+$ calcd for $C_{22}H_{33}N_2O_2$, 357.2537; found 357.2484

5.9b (2*S*,5*R*)-2-((*S*)-2-benzylpent-4-en-1-yl)-5-isopropyl-3,6-dimethoxy-2-methyl-2,5-dihydropyrazine. Compound **5.9b** was prepared on 4 mmol scale using general method D with a yield of 0.932 g (65.4%).

^{1}H NMR (CHLOROFORM-d, 400 MHz): δ = 7.23-7.32 (m, 2H), 7.15-7.22 (m, 1H), 7.10 (d, *J* = 7.1 Hz, 2H), 5.64-5.77 (m, 1H), 4.94-5.06 (m, 2H), 4.07 (d, *J* = 3.3 Hz, 1H), 3.64-3.69 (m, 6H), 2.77 (dd, *J* = 13.6, 4.8 Hz, 1H), 2.27-2.48 (m, 2H), 1.91-2.05 (m, 2H), 1.81-1.91 (m, 1H), 1.47-1.61 (m, 2H), 1.34 (s, 3H), 1.12 (d, *J* = 6.8 Hz, 3H), 0.72 ppm (d, *J* = 6.8 Hz, 3H)

^{13}C NMR (CHLOROFORM-d, 400 MHz): δ = 165.5, 161.4, 141.4, 136.8, 129.2, 128.1, 125.6, 116.3, 77.3, 77.0, 76.7, 61.1, 58.8, 52.1, 52.0, 43.7, 41.3, 37.5, 36.6, 31.0, 29.5, 19.4, 16.8 ppm

$[\alpha]_D^{20}$ 36 (*c* 1.75, $CHCl_3$)

HRMS $[M+H]^+$ calcd for $C_{22}H_{33}N_2O_2$, 357.2537; found 357.2487

5.14a (2*S*,5*R*)-5-isopropyl-3,6-dimethoxy-2-methyl-2-((*S*)-2-phenethylpent-4-en-1-yl)-2,5-dihydropyrazine. Compound **5.14a** was prepared on 3 mmol scale using general method D with a yield of 0.445 g (40.0%).

^{1}H NMR (CHLOROFORM-d, 400 MHz): δ = 7.27 (t, *J* = 6.9 Hz, 2H), 7.14-7.20 (m, 3H), 5.74 (ddt, *J* = 17.7, 9.3, 7.1 Hz, 1H), 5.00-5.05 (m, 2H), 3.92 (d, *J* = 3.3 Hz, 1H), 3.68 (s, 3H), 3.65 (s, 3H), 2.57 (t, *J* = 8.2 Hz, 2H), 2.29 (dtd, *J* = 13.6, 6.8, 3.3 Hz, 1H), 1.99-2.07

(m, 2H), 1.95 (dd, *J* = 13.9, 5.6 Hz, 1H), 1.52-1.65 (m, 3H), 1.35 (s, 3H), 1.24-1.34 (m, 1H), 1.10 (d, *J* = 6.8 Hz, 3H), 0.70 ppm (d, *J* = 6.8 Hz, 3H)

^{13}C NMR (CHLOROFORM-d, 101 MHz): δ = 165.5, 161.4, 142.9, 136.9, 128.3, 128.2, 125.5, 116.0, 61.0, 58.5, 52.1, 51.9, 44.6, 38.2, 36.7, 33.9, 33.1, 30.9, 29.6, 19.4, 16.8 ppm

$[\alpha]_D^{20}$ 12 (*c* 1.20, $CHCl_3$)

HRMS $[M+H]^+$ calcd for $C_{23}H_{35}N_2O_2$, 371.2693; found 371.2665

5.14b (2*S*,5*R*)-5-isopropyl-3,6-dimethoxy-2-methyl-2-((*R*)-2-phenethylpent-4-en-1-yl)-2,5-dihydropyrazine. Compound **5.14b** was prepared on 3 mmol scale using general method D with a yield of 0.695 g (62.5%).

^{1}H NMR (CHLOROFORM-d, 400 MHz): δ = 7.28 (t, *J* = 6.9 Hz, 2H), 7.14-7.21 (m, 3H), 5.78 (ddt, *J* = 16.3, 10.8, 7.1 Hz, 1H), 5.00-5.06 (m, 2H), 3.93 (d, *J* = 3.3 Hz, 1H), 3.67 (s, 3H), 3.67 (s, 3H), 2.47-2.65 (m, 2H), 2.30 (td, *J* = 6.8, 3.3 Hz, 1H), 2.14-2.23 (m, 1H), 1.99-2.10 (m, 1H), 1.93 (dd, *J* = 13.9, 5.1 Hz, 1H), 1.62 (dd, *J* = 13.9, 5.8 Hz, 1H), 1.43-1.59 (m, 2H), 1.35 (s, 3H), 1.30 (dt, *J* = 11.4, 5.8 Hz, 1H), 1.11 (d, *J* = 6.8 Hz, 3H), 0.71 ppm (d, *J* = 6.8 Hz, 3H)

^{13}C NMR (CHLOROFORM-d, 101 MHz): δ = 165.5, 161.4, 143.0, 137.1, 128.3, 128.2, 125.5, 115.9, 61.0, 58.6, 52.1, 52.0, 44.5, 39.1, 35.7, 34.1, 32.8, 30.9, 29.6, 19.4, 16.9 ppm

$[\alpha]_D^{20}$ 55 (*c* 2.00, $CHCl_3$)

HRMS $[M+H]^+$ calcd for $C_{23}H_{35}N_2O_2$, 371.2693; found 371.2661

General method E: Hydrolysis of bislactim ethers and Fmoc protection.

The bislactim ether (1.0 eq) was added to a solution of MeCN:H_2O:TFA (3.3:1.1:0.52 mL/mmol) and stirred at room temperature for 7 days. The pH was adjusted to > 7 and the solvent and valine methyl ester were removed by vacuum. NaOH (4.0 eq), water (0.5 mL/mmol), and methanol (20 mL/mmol) were added to the remaining mixture and the reaction was heated to reflux for 6 hrs. Upon cooling, the reaction was neutralized to pH 7 with 2 M HCl and the solvents were evaporated. The flask with the dried material was charged with 10% sodium carbonate (4 mL/mmol) and dioxane (6 mL/mmol) and cooled to 0 °C. Fmoc-Cl (1.0 eq) was dissolved in dioxane (4 mL/mmol) and added dropwise, and the reaction mixture was stirred for 3 hrs. Upon completion, as monitored by TLC, the reaction was acidified to pH 3 and the solvent was removed by vacuum. The mixture was dissolved in dichloromethane (10 mL/mmol), washed with water (3 × 10 mL/mmol), washed with brine (10 mL/mmol), and dried with $MgSO_4$. The crude product was purified by flash column chromatography (CH_2Cl_2:MeOH, 0-5%).

5.5a (2*S*,4*S*)-2-((((9H-fluoren-9-yl)methoxy)carbonyl)amino)-2-methyl-4-phenylhept-6-enoic acid. Compound **5.5a** was prepared on 2.44 mmol scale using general method E with a yield of 0.400 g (36.0%)

^{1}H NMR (CHLOROFORM-d, 400 MHz): δ = 8.20 (br s, 1H), 7.80 (d, *J* = 7.6 Hz, 2H), 7.57 (d, *J* = 7.3 Hz, 2H), 7.39-7.50 (m, 2H), 7.30-7.39 (m, 2H), 7.06-7.26 (m, 5H), 5.46-5.66 (m, 1H), 5.33 (br s, 1H), 4.85-5.02 (m, 2H), 4.38-4.51 (m, 1H), 4.23-4.35 (m, 1H), 4.15-4.21 (m, 1H), 2.61-2.72 (m, 1H), 2.55 (br d, *J* = 13.9 Hz, 1H), 2.26-2.42 (m, 3H), 1.57 ppm (br s, 3H)

^{13}C NMR (CHLOROFORM-d, 101 MHz): δ = 178.9, 154.5, 143.9, 143.8, 143.3, 141.4, 136.2, 128.3, 127.8, 127.1, 126.8, 125.1, 120.0, 116.7, 66.4, 59.0, 47.2, 42.3, 41.8, 41.8, 23.8 ppm

$[\alpha]_D^{20}$ 12 (*c* 16.05, $CHCl_3$)

HRMS $[M-H]^-$ calcd for $C_{29}H_{28}NO_4$, 454.2024; found, 454.2020

5.5b (2*S*,4*R*)-2-((((9H-fluoren-9-yl)methoxy)carbonyl)amino)-2-methyl-4-phenylhept-6-enoic acid. Compound **5.5b** was prepared on 2.21 mmol scale using general method E with a yield of 0.540 g (55.9%)

^{1}H NMR (CHLOROFORM-d, 400 MHz): δ = 10.04 (br s, 1H), 7.81 (br d, *J* = 7.6 Hz, 2H), 7.51-7.62 (m, 2H), 7.21-7.49 (m, 7H), 7.11-7.19 (m, 1H), 5.45-5.78 (m, 1H), 5.34 (br s, 1H), 4.93-5.10 (m, 2H), 4.02 -4.40 (m, 3H), 2.71 (br s, 2H), 2.05-2.50 (m, 3H), 1.66 ppm (br s, 3H)

^{13}C NMR (CHLOROFORM-d, 101 MHz): δ = 179.2, 154.5, 144.5, 144.1, 143.9, 141.3, 136.2, 128.5, 127.8, 127.1, 126.5, 125.3, 120.0, 116.8, 66.6, 60.2, 47.1, 42.8, 41.7, 24.6 ppm

$[\alpha]_D^{20}$ -4.2 (*c* 11.0, $CHCl_3$)

HRMS $[M-H]^-$ calcd for $C_{29}H_{28}NO_4$, 454.2024; found, 454.2025

5.10a (2*S*,4*R*)-2-((((9H-fluoren-9-yl)methoxy)carbonyl)amino)-4-benzyl-2-methylhept-6-enoic acid. Compound **5.10a** was prepared on 0.561 mmol scale using general method E with a yield of 0.045 g (17%).

^{1}H NMR (CHLOROFORM-d, 400 MHz): δ = 7.76-7.82 (m, 2H), 7.56-7.63 (m, 2H), 7.39-7.46 (m, 2H), 7.29-7.36 (m, 2H), 7.22-7.29 (m, 2H), 7.11 (br s, 3H), 5.65-5.84 (m, 1H), 4.94-5.14 (m, 2H), 4.38 (br s, 2H), 4.22 (br t, *J* = 6.3 Hz, 1H), 2.51 (br s, 2H), 2.20 (br s, 1H), 1.95-2.12 (m, 2H), 1.83 (br s, 2H), 1.60 ppm (br s, 3H)

^{13}C NMR (CHLOROFORM-d, 101 MHz): δ = 179.1, 179.0, 154.7, 143.9, 143.8, 141.3, 140.4, 136.0, 129.3, 128.4, 128.3, 128.3, 127.7, 127.1, 126.1, 125.0, 120.0, 117.4, 77.2, 66.6, 59.3, 59.2, 53.4, 47.2, 40.7, 39.8, 38.6, 35.9, 31.9, 29.7, 29.7, 29.4, 23.7, 22.7, 14.1 ppm

$[\alpha]_D^{20}$ 4.1 (*c* 2.25, $CHCl_3$)

HRMS $[M-H]^-$ calcd for $C_{30}H_{30}NO_4$, 468.2180; found, 454.2186

5.10b (2*S*,4*S*)-2-((((9H-fluoren-9-yl)methoxy)carbonyl)amino)-4-benzyl-2-methylhept-6-enoic acid. Compound **5.10b** was prepared on 2.49 mmol scale using general method E with a yield of 0.704 g (60.5%)

^{1}H NMR (CHLOROFORM-d, 400 MHz): δ = 10.90 (br s, 1H), 7.80 (dd, *J* = 7.6, 3.2 Hz, 2H), 7.59 (br d, *J* = 7.3 Hz, 2H), 7.44 (td, *J* = 7.3, 4.4 Hz, 2H), 7.10-7.37 (m, 7H), 5.55-5.83 (m, 1H), 5.38 (br s, 1H), 4.94-5.13 (m, 2H), 4.38 (br s, 2H), 4.17-4.26 (m, 1H), 2.43-2.80 (m, 2H), 1.71-2.26 (m, 5H), 1.58 ppm (br s, 3H)

^{13}C NMR (CHLOROFORM-d, 101 MHz): δ = 179.7, 154.8, 143.8, 143.7, 141.3, 140.3, 135.8, 129.2, 128.4, 127.7, 127.0, 126.1, 125.0, 120.0, 117.5, 66.6, 59.3, 47.1, 41.0, 39.8, 38.5, 35.8, 23.7 ppm

$[\alpha]_D^{20}$ 9.7 (*c* 18.7, $CHCl_3$)

HRMS $[M-H]^-$ calcd for $C_{30}H_{30}NO_4$, 468.2180; found, 454.2181

5.15a (2*S*,4*S*)-2-((((9H-fluoren-9-yl)methoxy)carbonyl)amino)-2-methyl-4-phenethylhept-6-enoic acid. Compound **5.15a** was prepared on 1.73 mmol scale using general method E with a yield of 0.303 g (36.3%)

^{1}H NMR (CHLOROFORM-d, 400 MHz): δ = 10.82 (br s, 1H), 7.80 (d, *J* = 7.6 Hz, 2H), 7.62 (br d, *J* = 6.8 Hz, 2H), 7.43 (br t, *J* = 7.3 Hz, 2H), 7.32-7.37 (m, 2H), 7.22-7.28 (m, 2H), 7.10-7.19 (m, 3H), 5.76 (br d, *J* = 0.5 Hz, 1H), 5.06 (br d, *J* = 10.1 Hz, 2H), 4.42 (br s, 2H), 4.24 (br t, *J* = 6.2 Hz, 1H), 2.57 (br s, 2H), 2.06-2.35 (m, 3H), 1.94 (br d, *J* = 11.9 Hz, 1H), 1.64 (br s, 3H), 1.58 (br s, 2H), 1.25 ppm (br s, 1H)

^{13}C NMR (CHLOROFORM-d, 101 MHz): δ = 179.6, 154.6, 143.8, 142.3, 141.3, 136.1, 128.3, 128.3, 127.7, 127.1, 125.7, 125.0, 120.0, 117.0, 77.3, 77.0, 76.7, 66.5, 59.5, 47.2, 39.8, 38.5, 35.8, 33.4, 32.5, 24.3 ppm

$[\alpha]_D^{20}$ 29 (*c* 1.15, $CHCl_3$)

HRMS $[M-H]^-$ calcd for $C_{31}H_{32}NO_4$, 482.2387; found, 482.2336

5.15b (2*S*,4*R*)-2-((((9H-fluoren-9-yl)methoxy)carbonyl)amino)-2-methyl-4-phenethylhept-6-enoic acid. Compound **5.15b** was prepared on 1.11 mmol scale using general method E with a yield of 0.212 g (34.6%)

^{1}H NMR (CHLOROFORM-d, 400 MHz): δ = 11.45 (br s, 1H), 7.81 (br d, *J* = 7.6 Hz, 2H), 7.63 (br d, *J* = 6.6 Hz, 2H), 7.45 (br t, *J* = 7.2 Hz, 2H), 7.35 (br t, *J* = 7.2 Hz, 2H), 7.22-7.31 (m, 2H), 7.11-7.20 (m, 3H), 5.75 (br s, 2H), 5.08 (br d, *J* = 11.1 Hz, 2H), 4.42 (br s, 2H), 4.23 (br t, *J* = 6.3 Hz, 1H), 2.61 (br s, 2H), 2.32 (br d, *J* = 12.4 Hz, 1H), 2.12 (br s, 2H), 1.91-2.04 (m, 1H), 1.68 (br s, 5H), 1.33 ppm (s, 1H)

^{13}C NMR (CHLOROFORM-d, 101 MHz): δ = 180.0, 154.5, 143.7, 142.3, 141.3, 136.0, 128.2, 128.2, 127.7, 127.0, 125.6, 125.0, 119.9, 117.0, 66.5, 59.5, 47.1, 39.8, 38.1, 36.1, 33.3, 32.5, 29.7, 23.9 ppm

$[\alpha]_D^{20}$ 3.5 (*c* 3.35, $CHCl_3$)

HRMS $[M-H]^-$ calcd for $C_{31}H_{32}NO_4$, 482.2387; found, 482.2342

Figure 5.19. ^{1}H NMR spectrum (400 MHz) of **5.1a** in $CDCl_3$

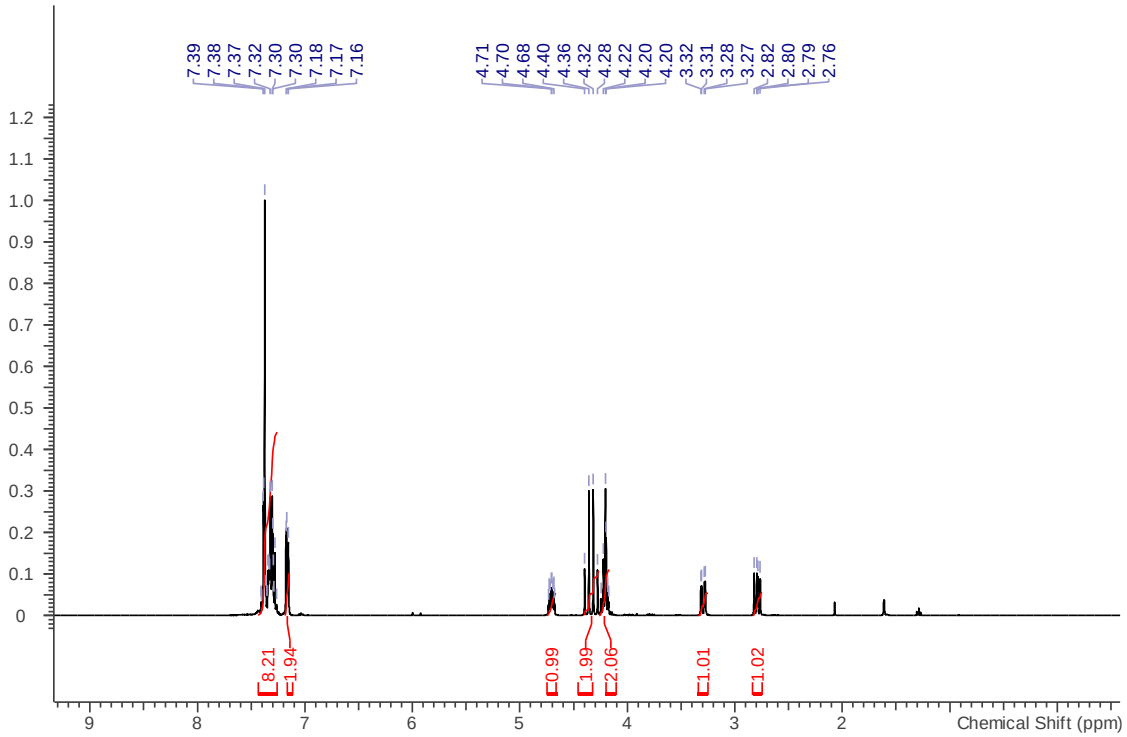

Figure 5.20. ^{13}C NMR spectrum (101 MHz) of **5.1a** in $CDCl_3$

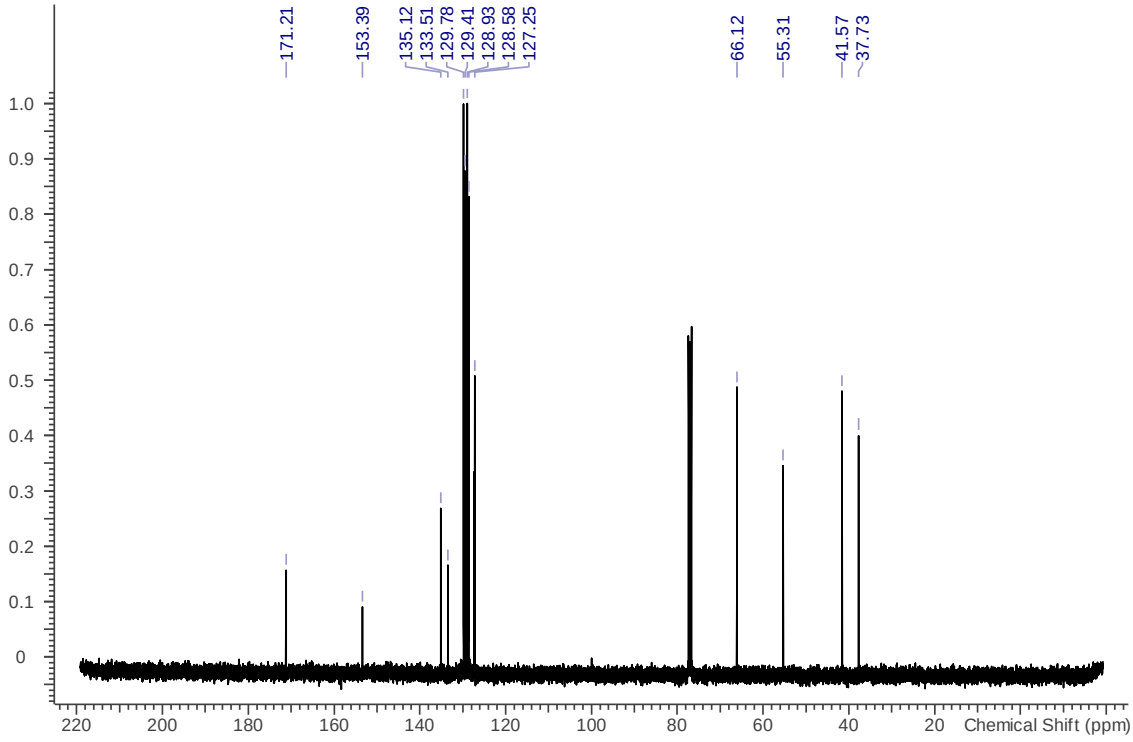

Figure 5.21. ^{1}H NMR spectrum (400 MHz) of **5.2a** in $CDCl_3$

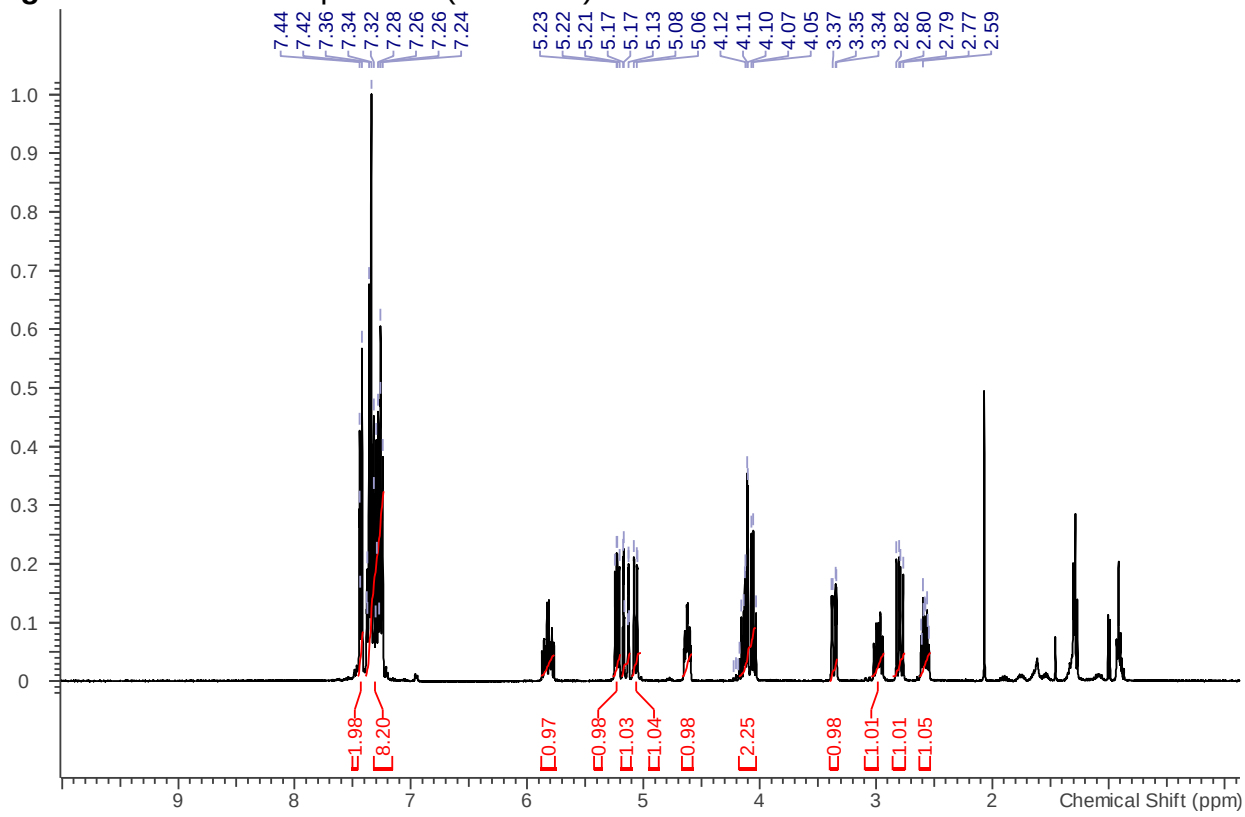

Figure 5.22. ^{13}C NMR spectrum (101 MHz) of **5.2a** in $CDCl_3$

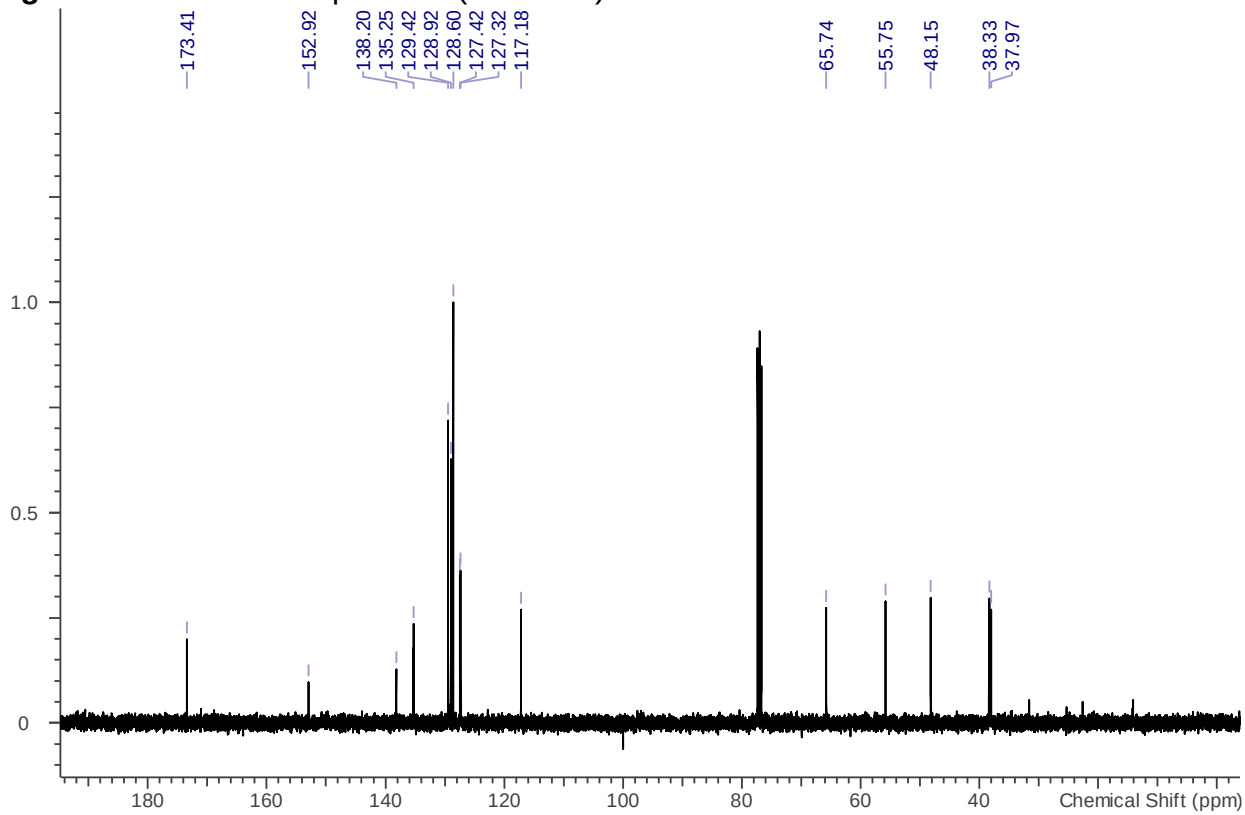

Figure 5.23. ^{1}H NMR spectrum (400 MHz) of **5.3a** in $CDCl_3$

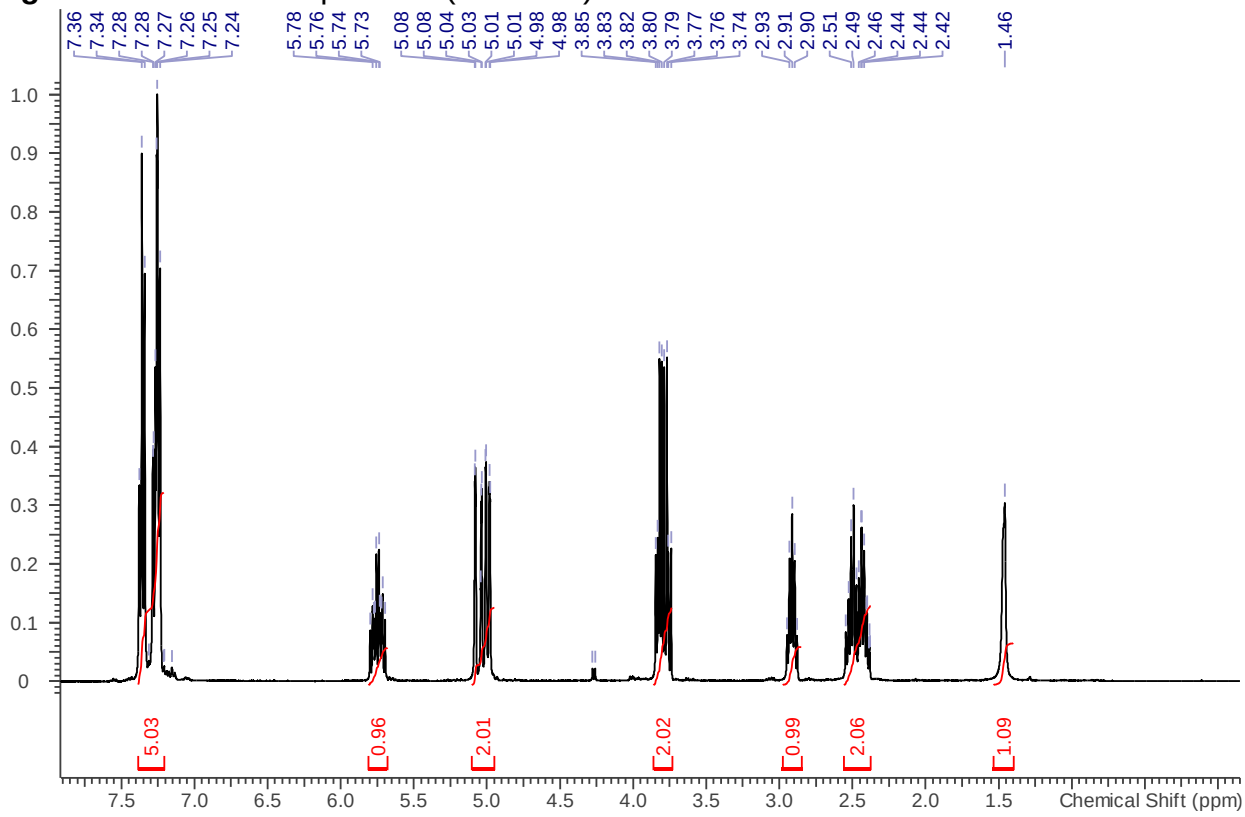

Figure 5.24. ^{13}C NMR spectrum (101 MHz) of **5.3a** in $CDCl_3$

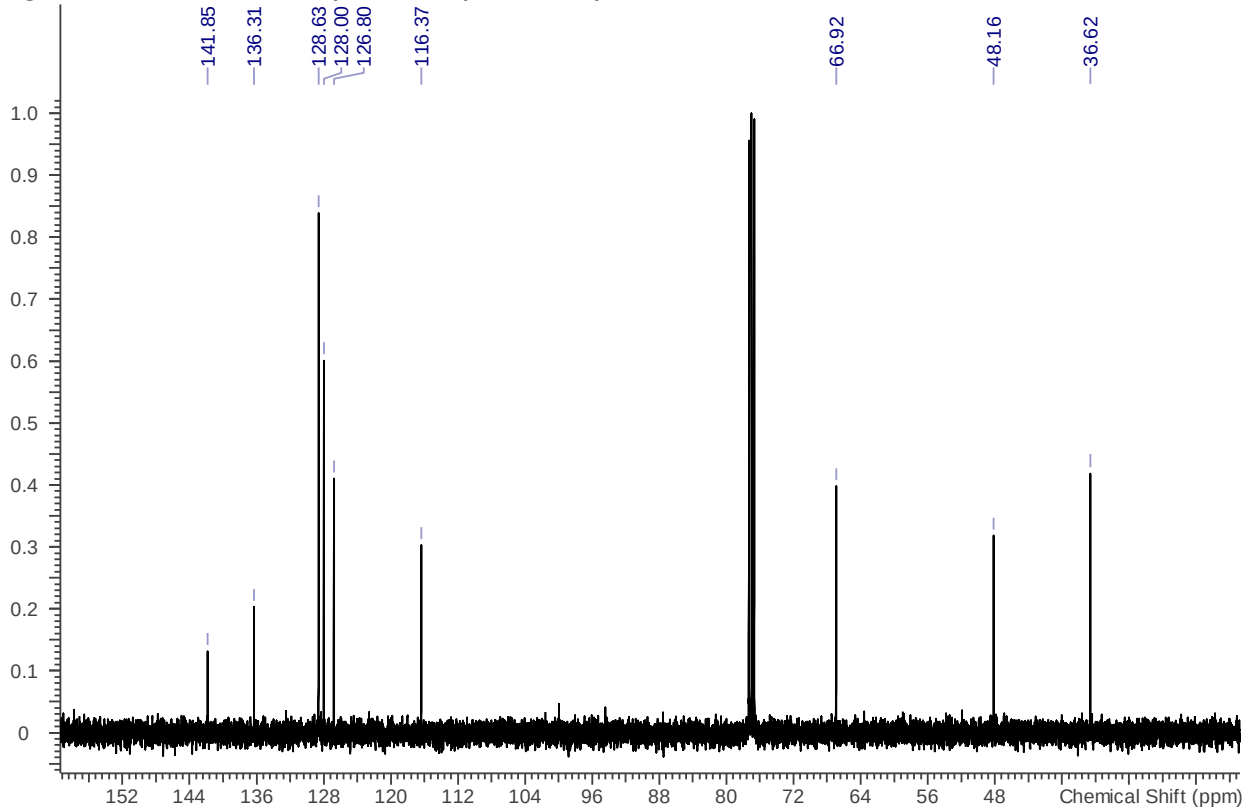

Figure 5.25. ^{1}H NMR spectrum (400 MHz) of **5.4a** in $CDCl_3$

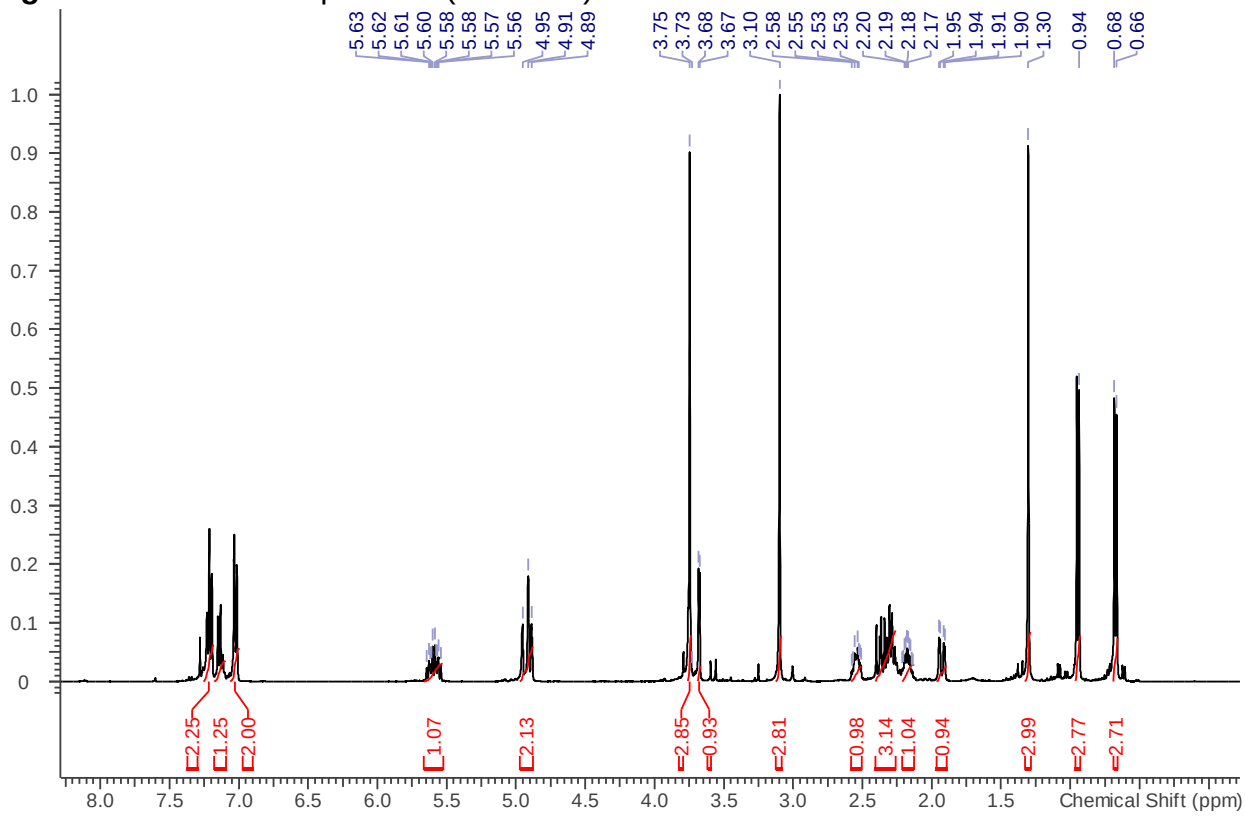

Figure 5.26. ^{13}C NMR spectrum (101 MHz) of **5.4a** in $CDCl_3$

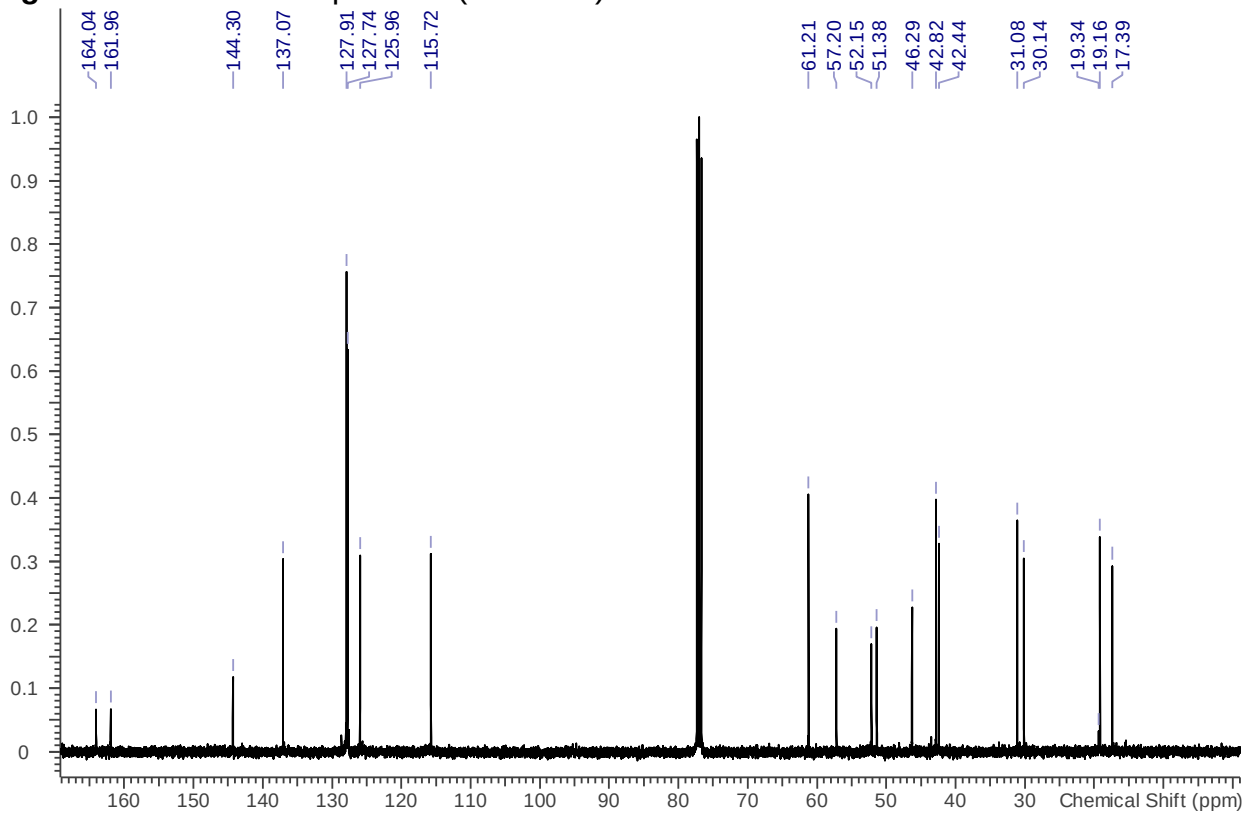

Figure 5.27. ^{1}H NMR spectrum (400 MHz) of **5.5a** in $CDCl_3$

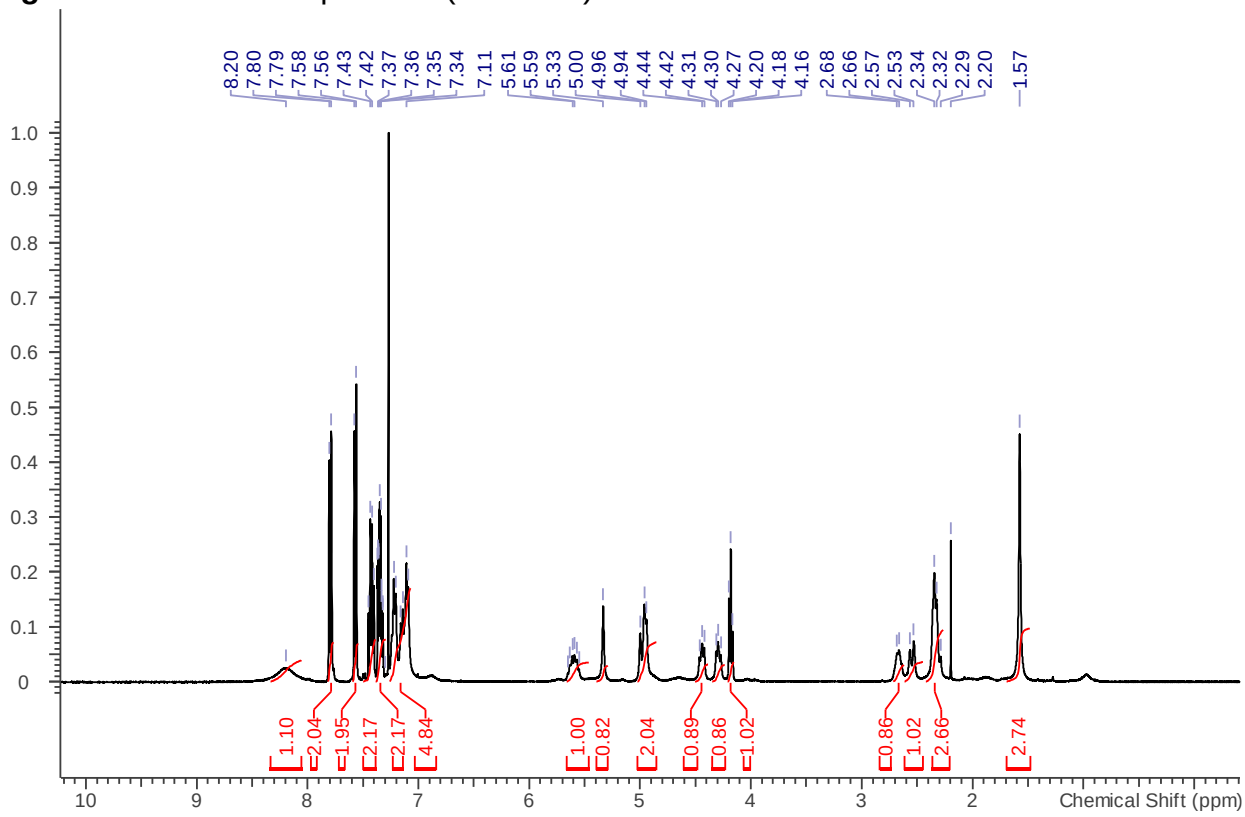

Figure 5.28. ^{13}C NMR spectrum (101 MHz) of **5.5a** in $CDCl_3$

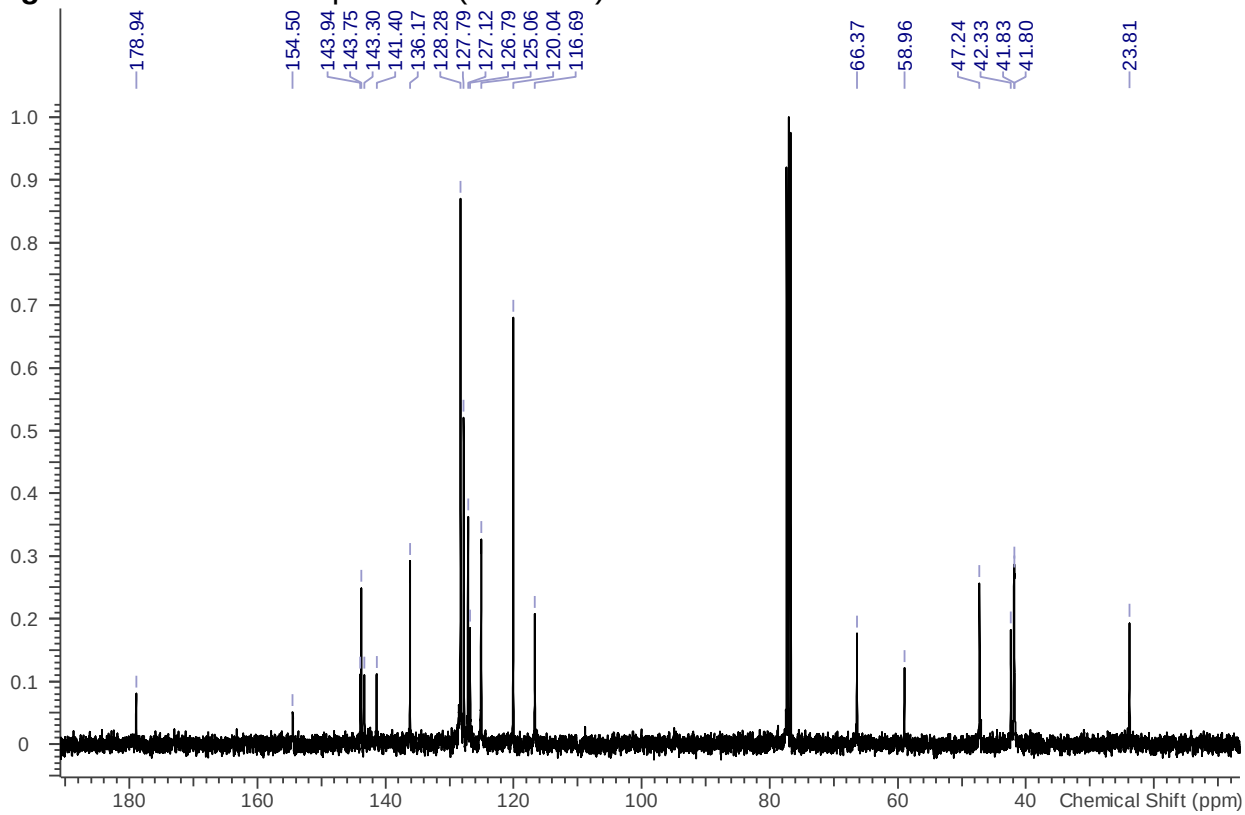

Figure 5.29. ^{1}H NMR spectrum (400 MHz) of **5.1b** in $CDCl_3$

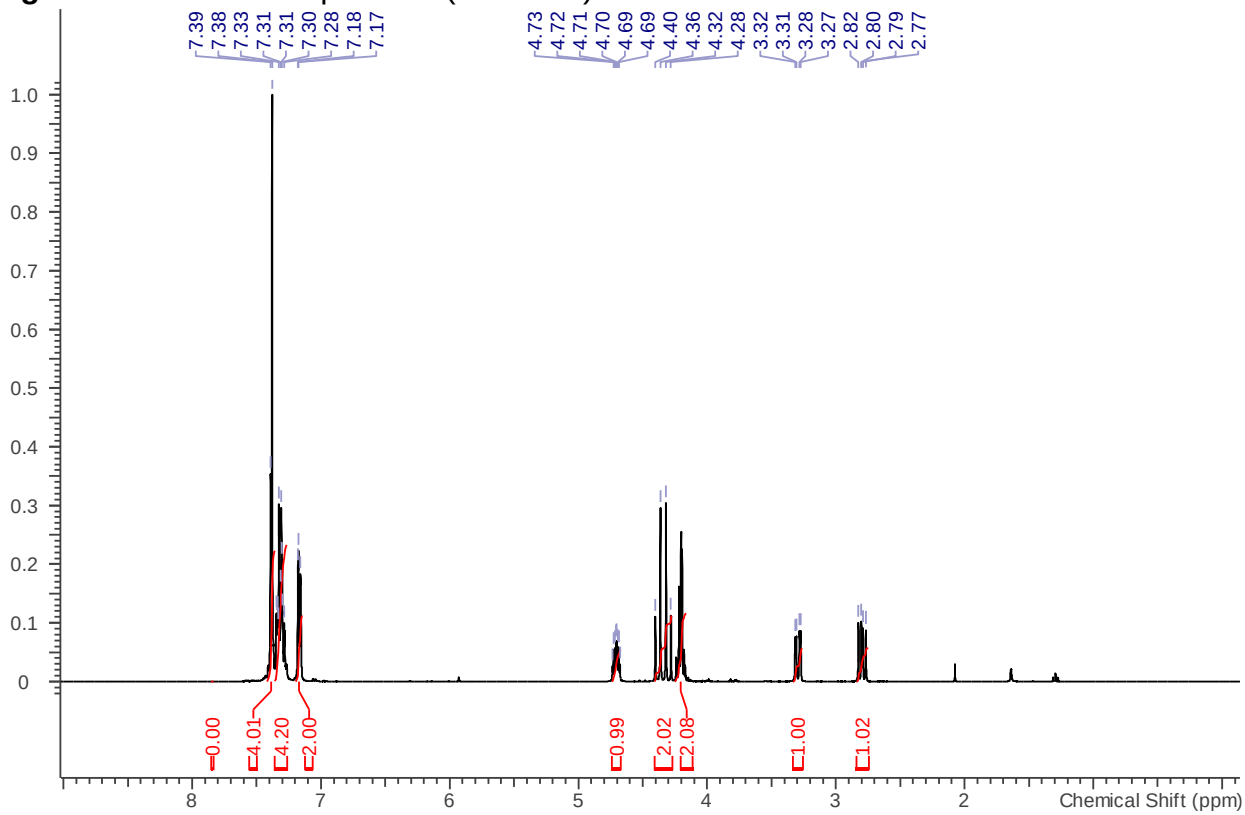

Figure 5.30. ^{13}C NMR spectrum (101 MHz) of **5.1b** in $CDCl_3$

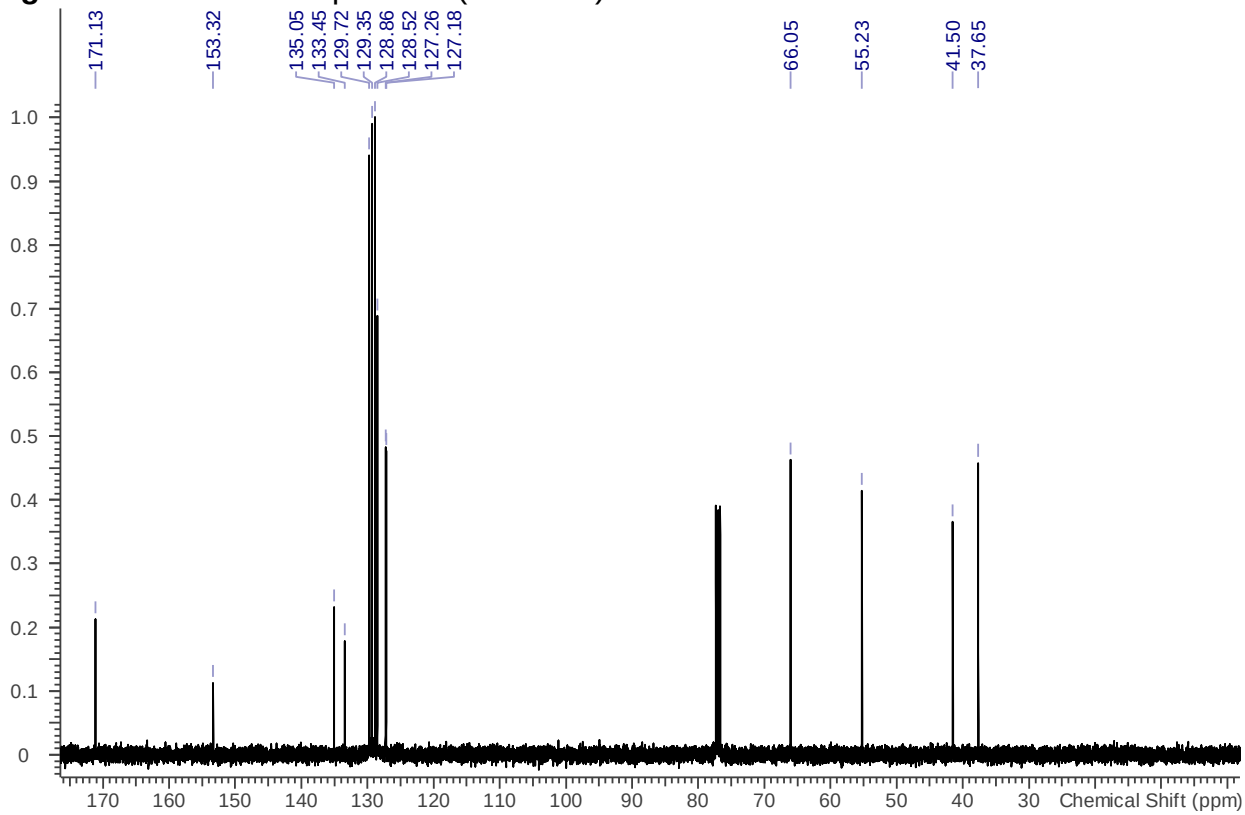

Figure 5.31. ^{1}H NMR spectrum (400 MHz) of **5.2b** in $CDCl_3$

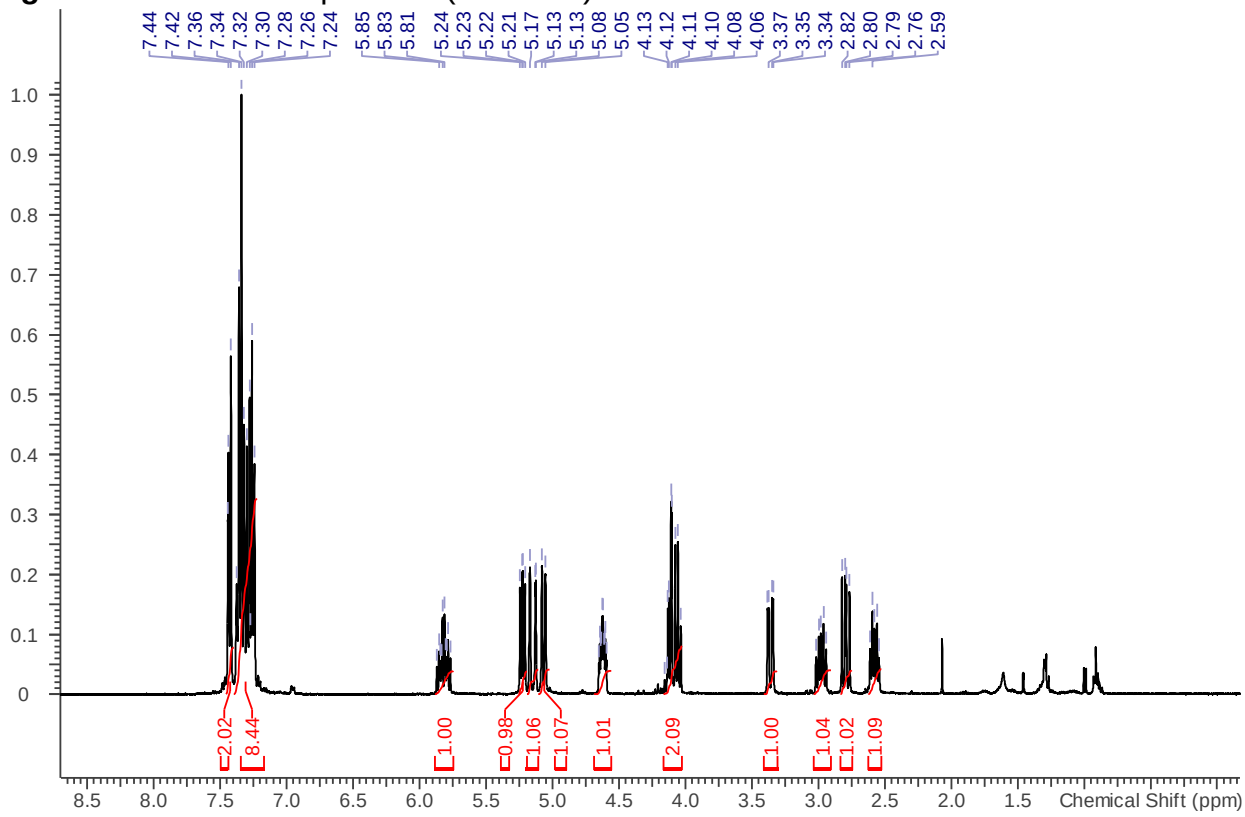

Figure 5.32. ^{13}C NMR spectrum (101 MHz) of **5.2b** in $CDCl_3$

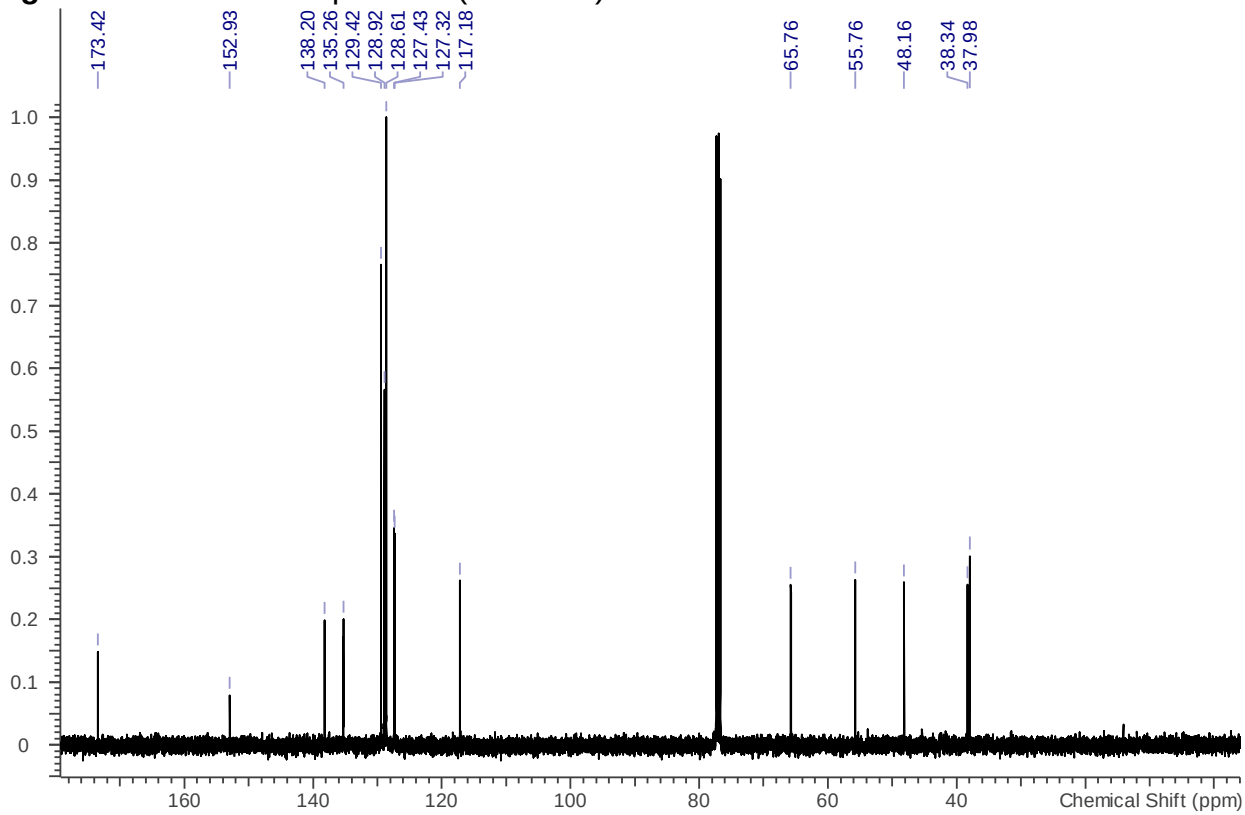

Figure 5.33. ^{1}H NMR spectrum (400 MHz) of **5.3b** in $CDCl_3$

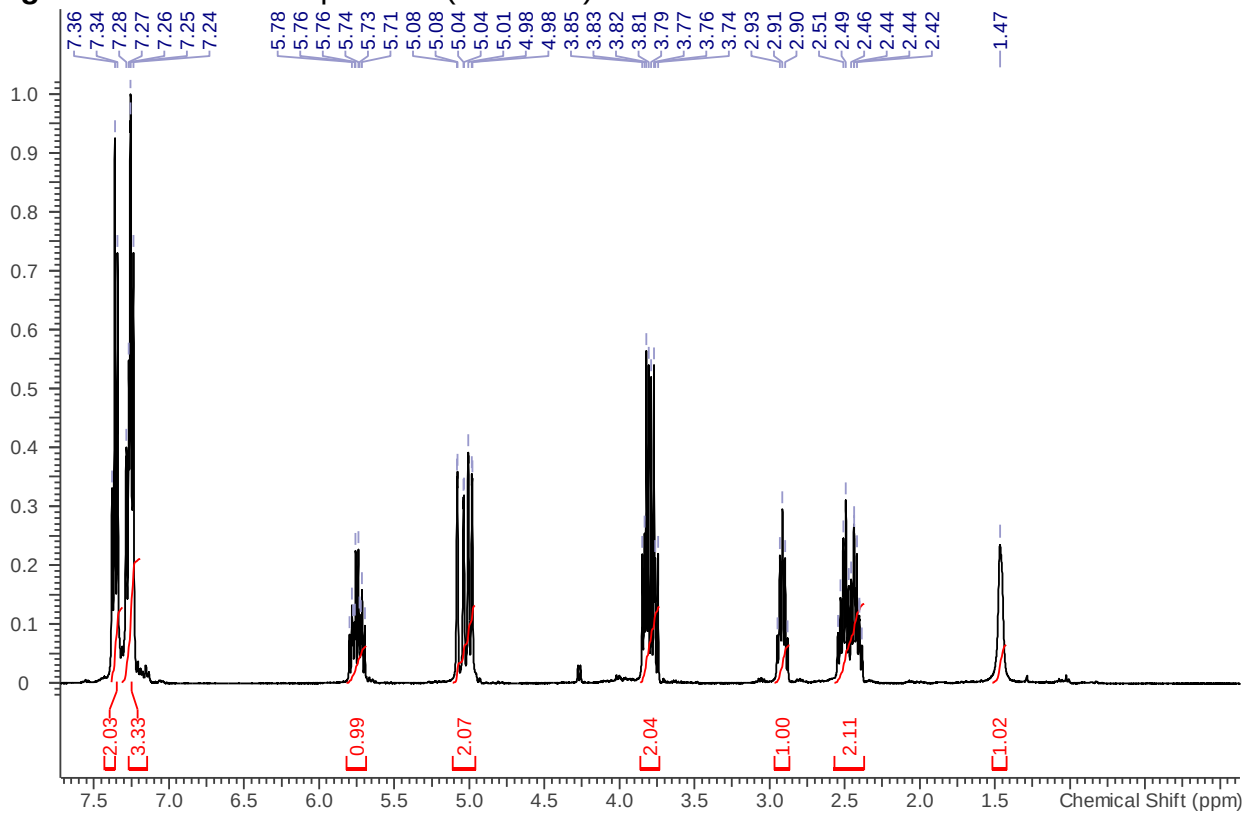

Figure 5.34. ^{13}C NMR spectrum (101 MHz) of **5.3b** in $CDCl_3$

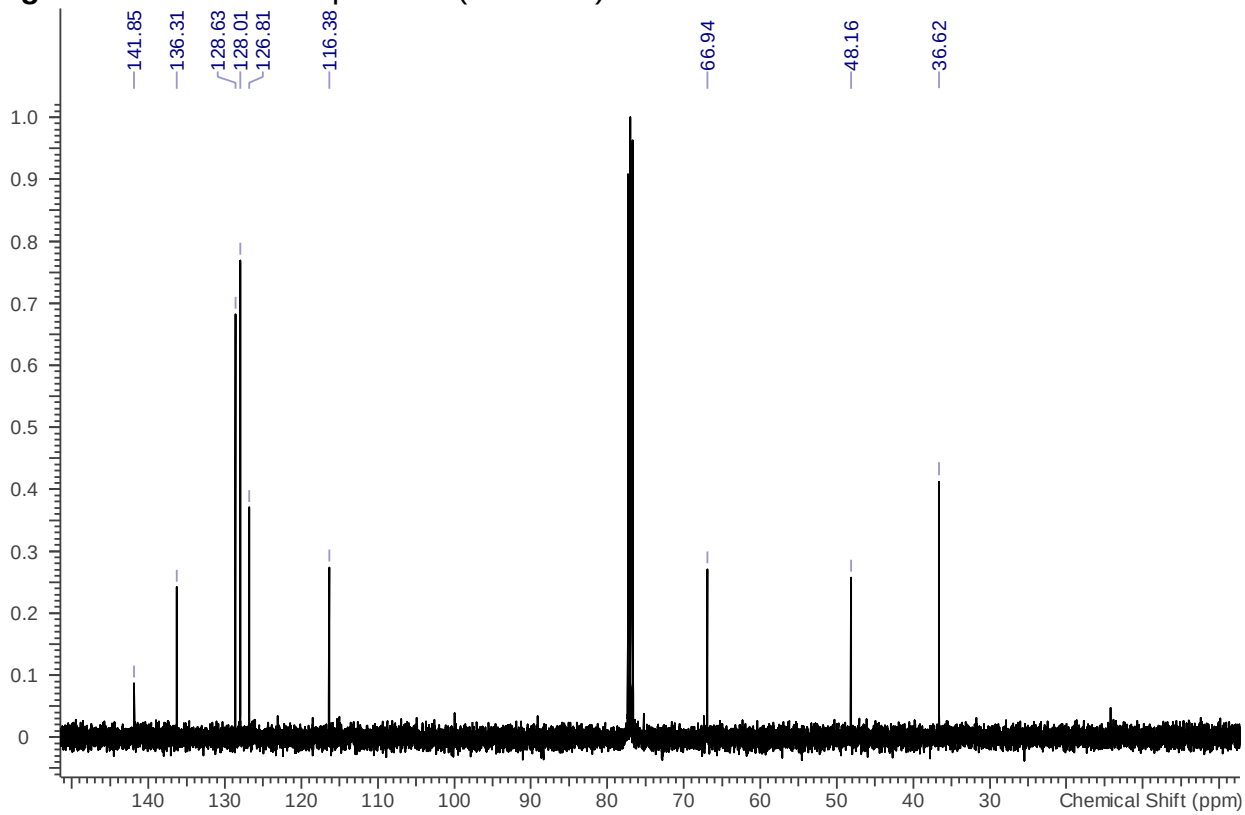

Figure 5.35. ^{1}H NMR spectrum (400 MHz) of **5.4b** in $CDCl_3$

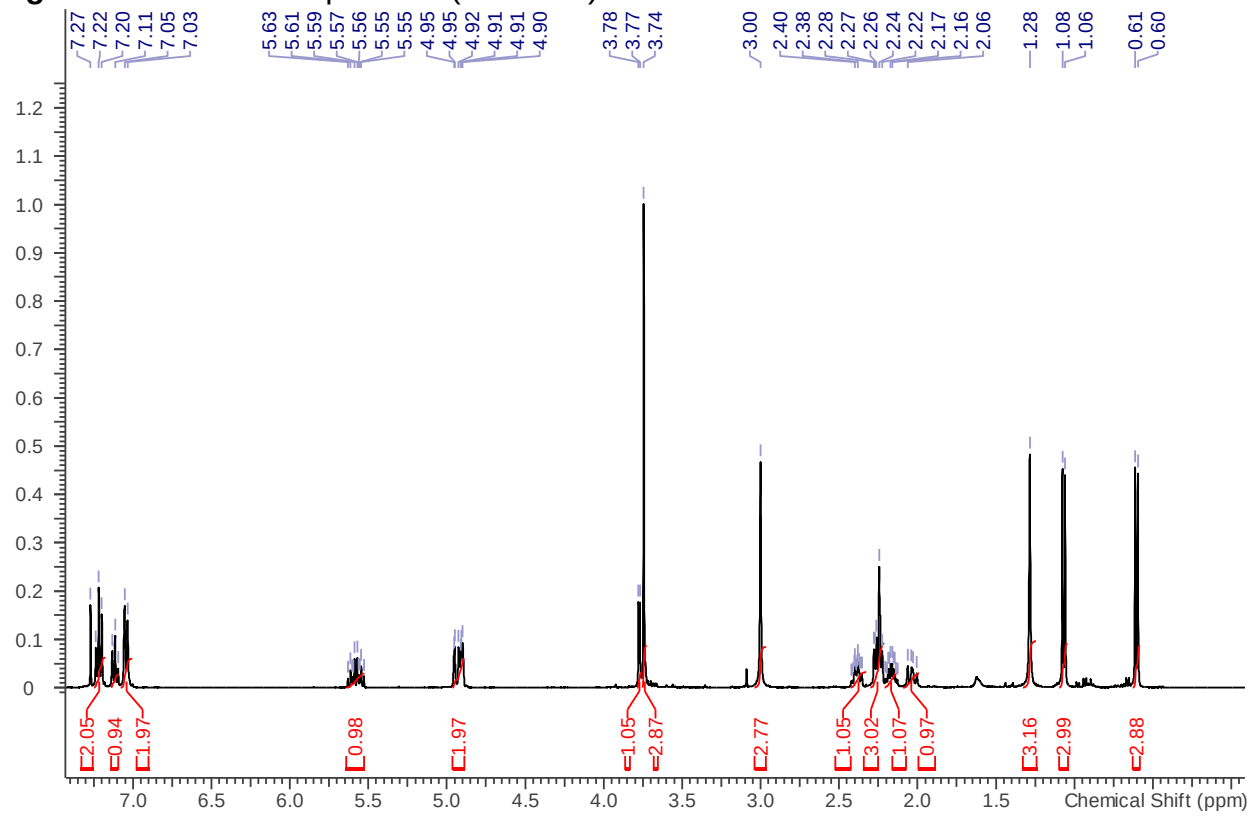

Figure 5.36. ^{13}C NMR spectrum (101 MHz) of **5.4b** in $CDCl_3$

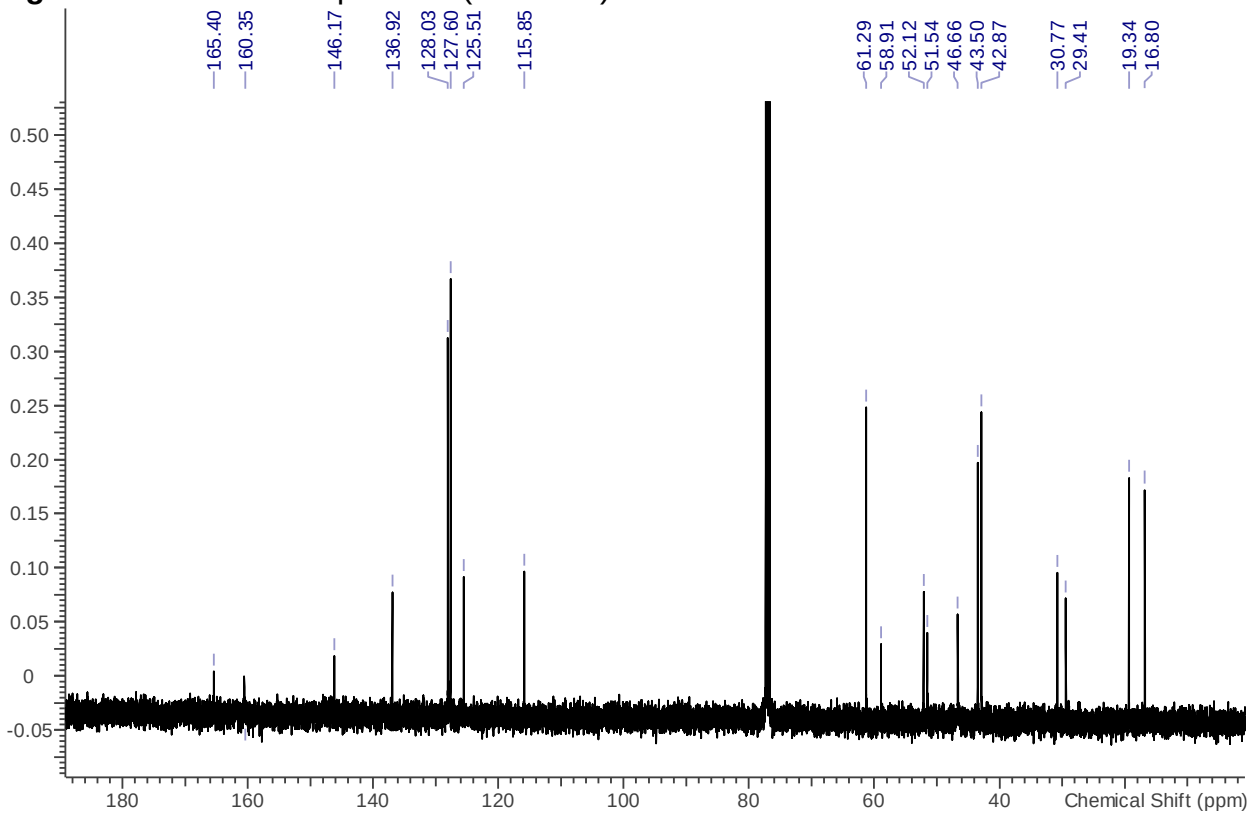

Figure 5.37. ^{1}H NMR spectrum (400 MHz) of **5.5b** in $CDCl_3$

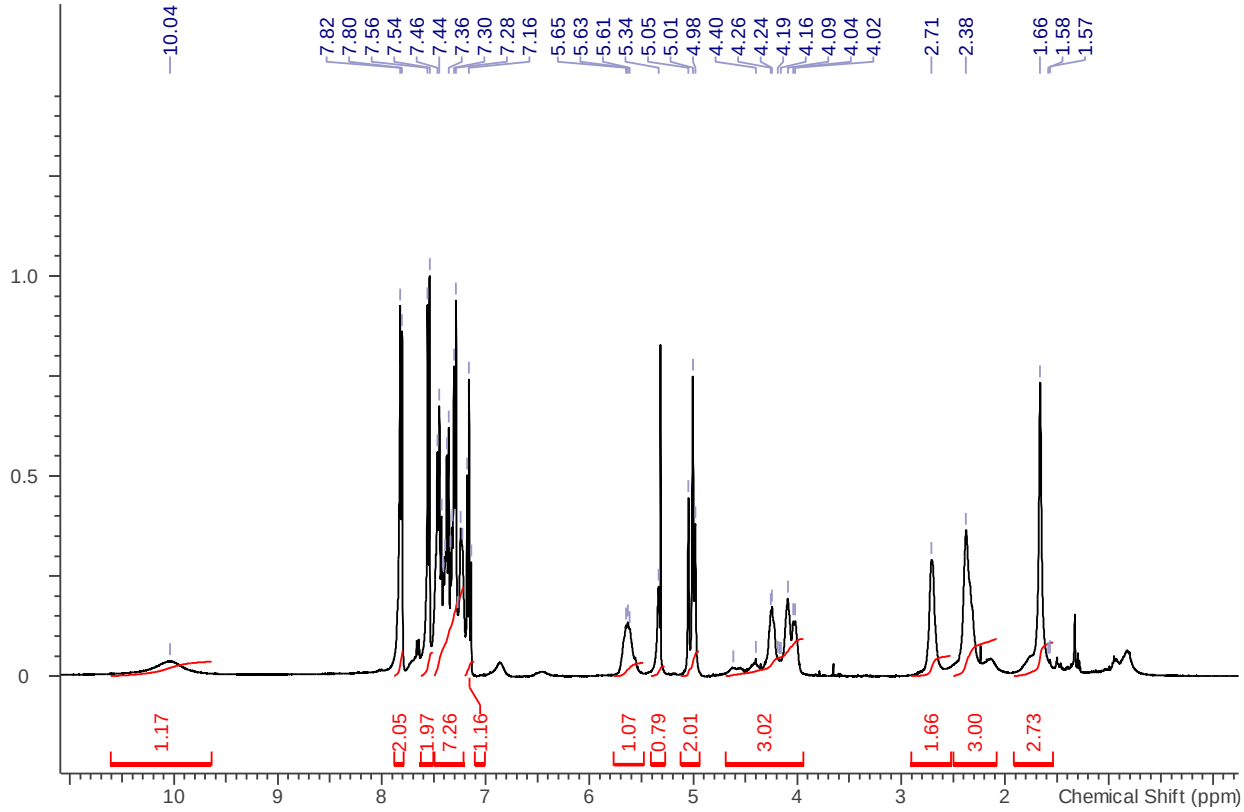

Figure 5.38. ^{13}C NMR spectrum (101 MHz) of **5.5b** in $CDCl_3$

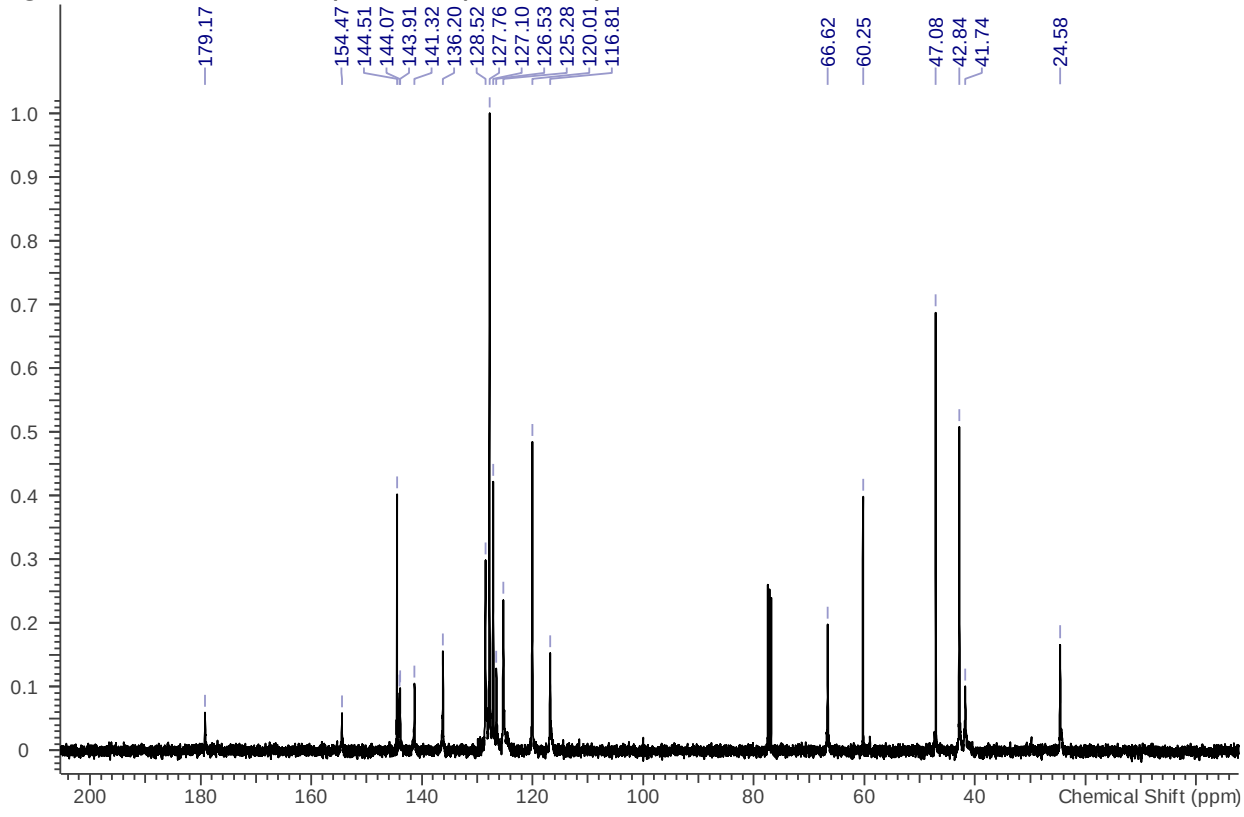

Figure 5.39. ^{1}H NMR spectrum (400 MHz) of **5.6a** in $CDCl_3$

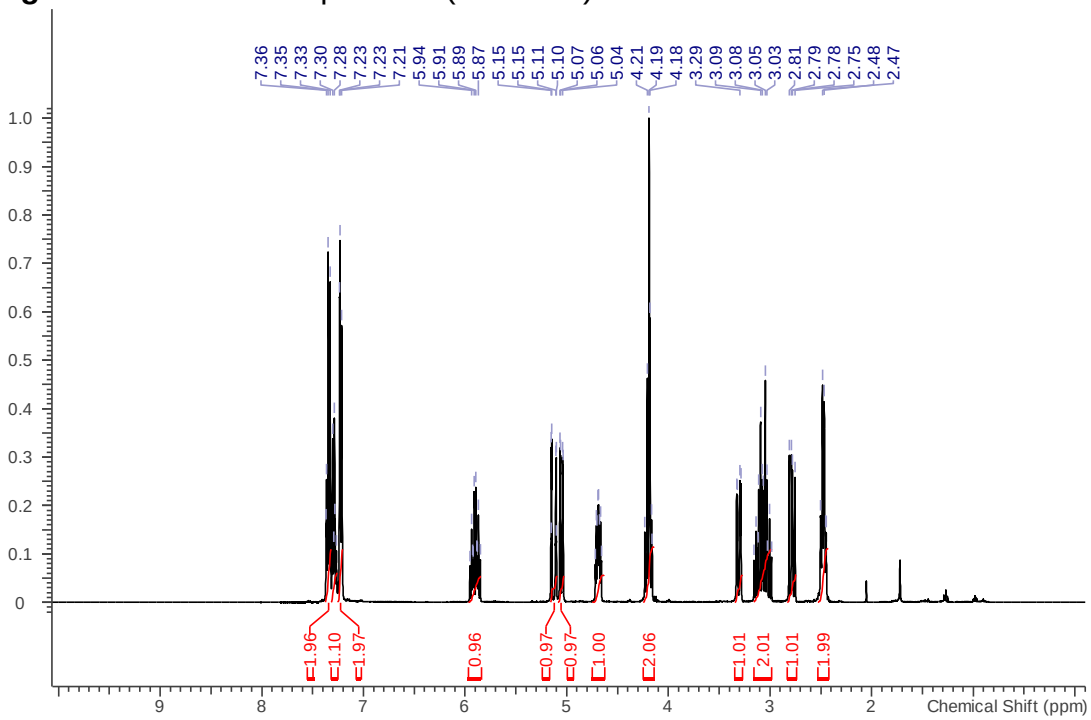

Figure 5.40. ^{13}C NMR spectrum (101 MHz) of **5.6a** in $CDCl_3$

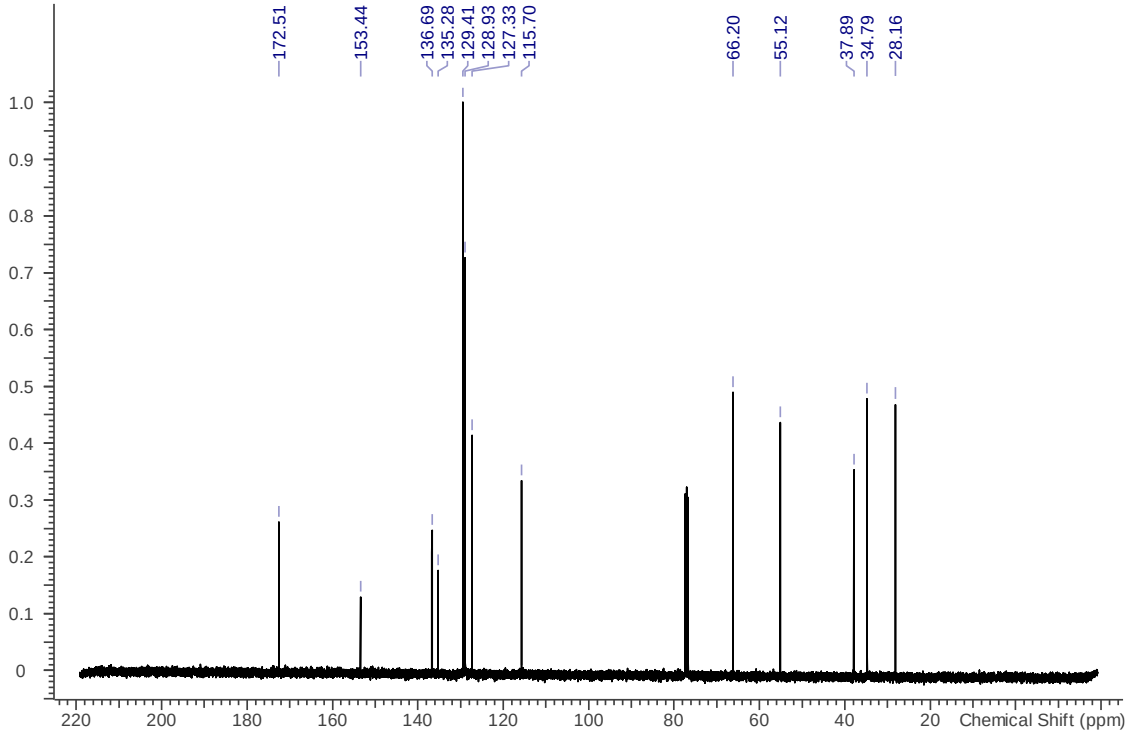

Figure 5.41. ^{1}H NMR spectrum (400 MHz) of **5.7a** in $CDCl_3$

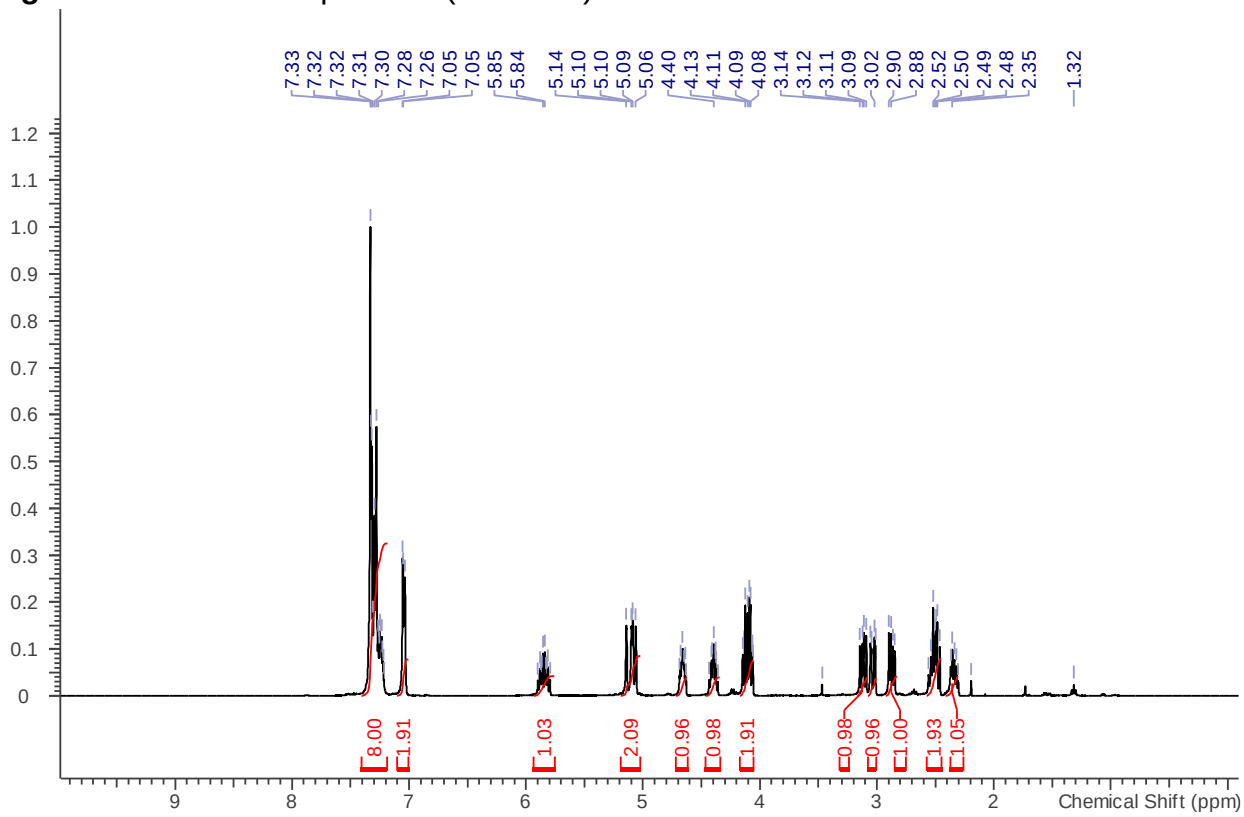

Figure 5.42. ^{13}C NMR spectrum (101 MHz) of **5.7a** in $CDCl_3$

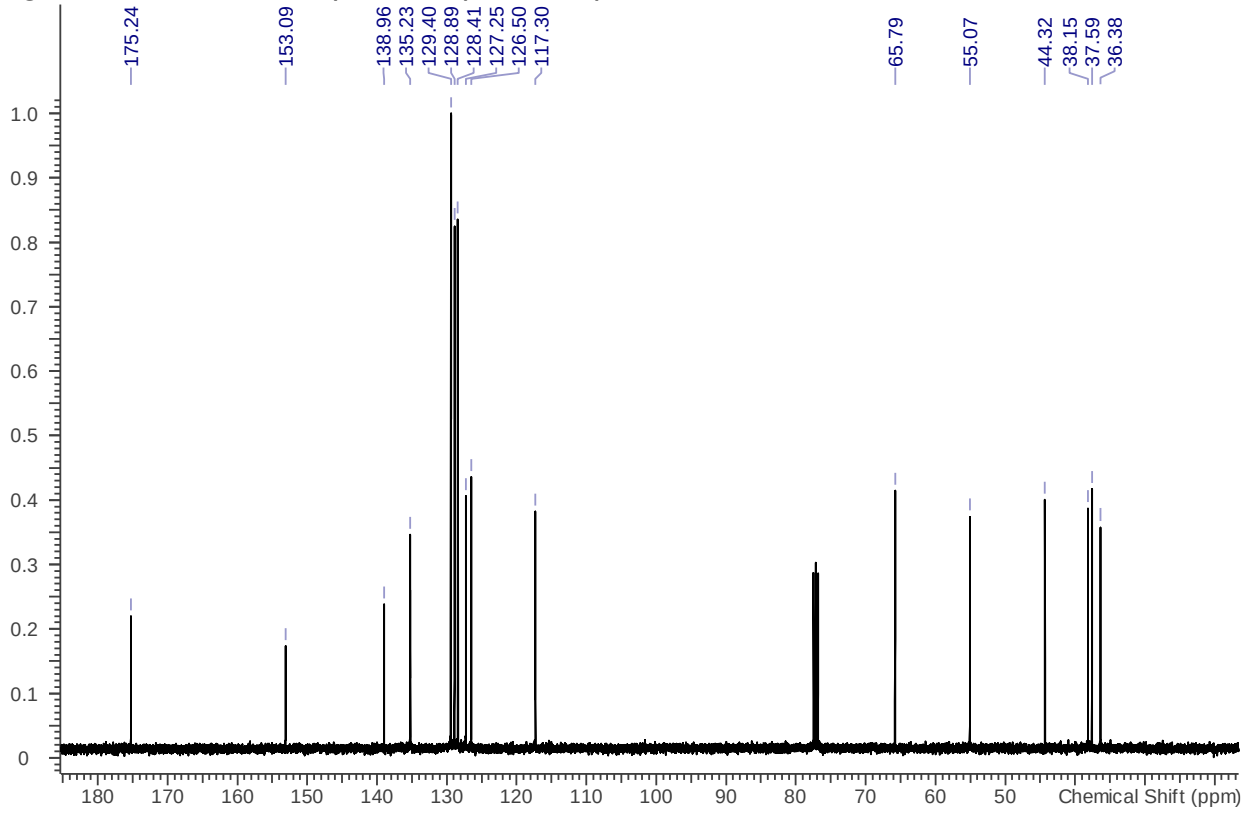

Figure 5.43. ^{1}H NMR spectrum (400 MHz) of **5.8a** in $CDCl_3$

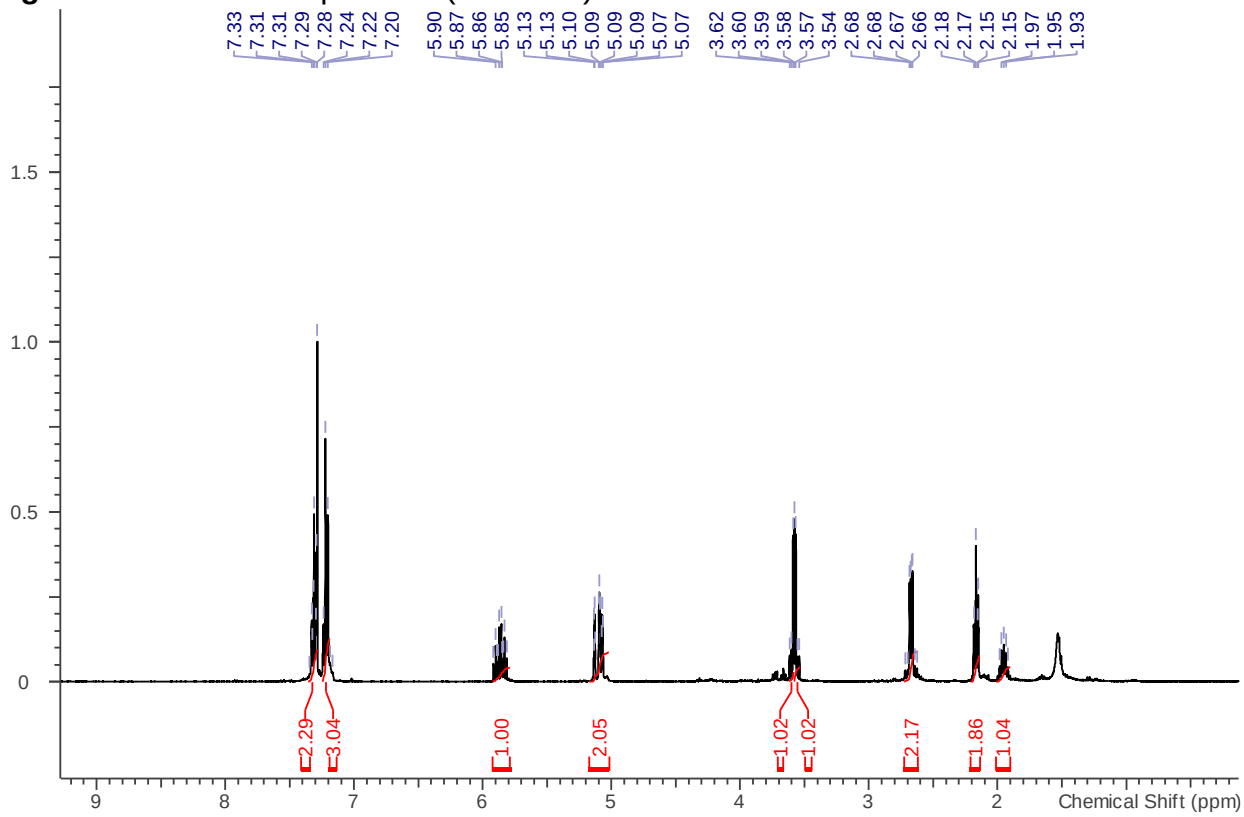

Figure 5.44. ^{13}C NMR spectrum (101 MHz) of **5.8a** in $CDCl_3$

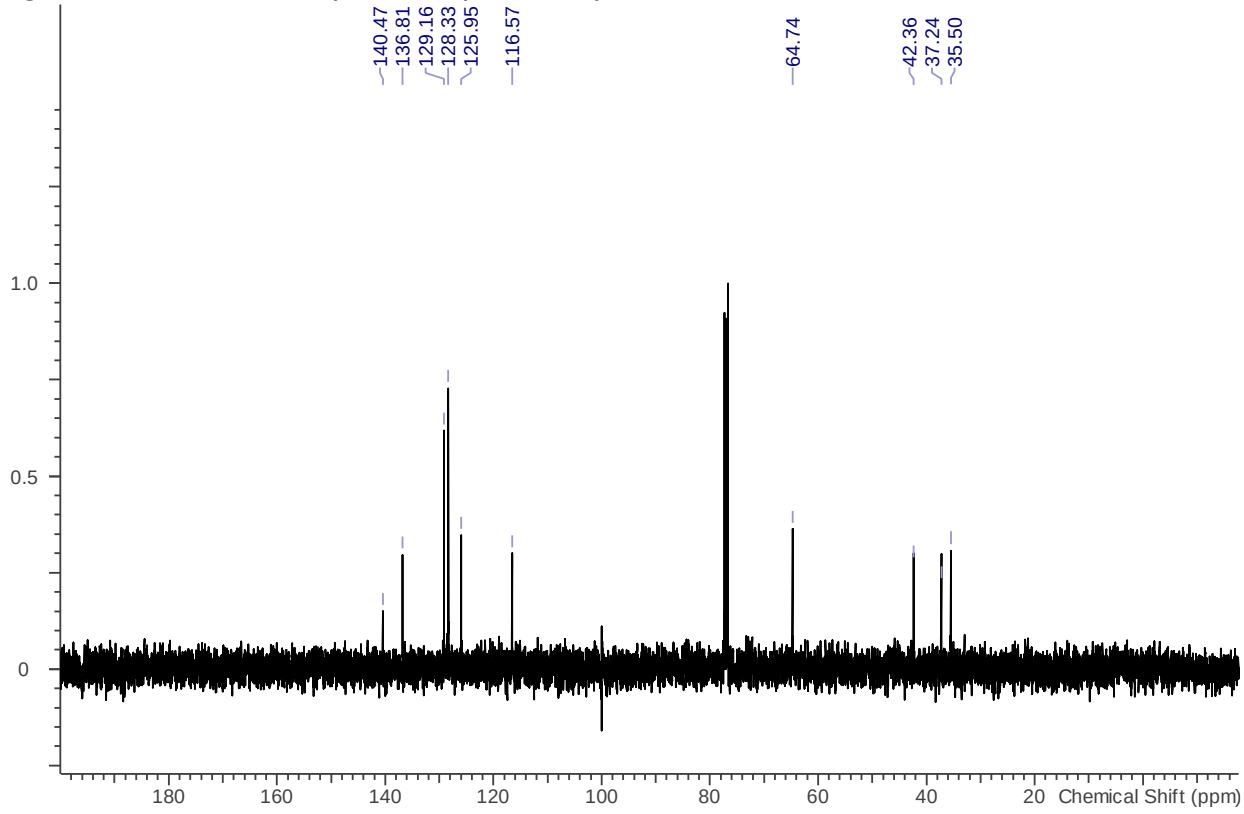

Figure 5.45. ^{1}H NMR spectrum (400 MHz) of **5.9a** in $CDCl_3$

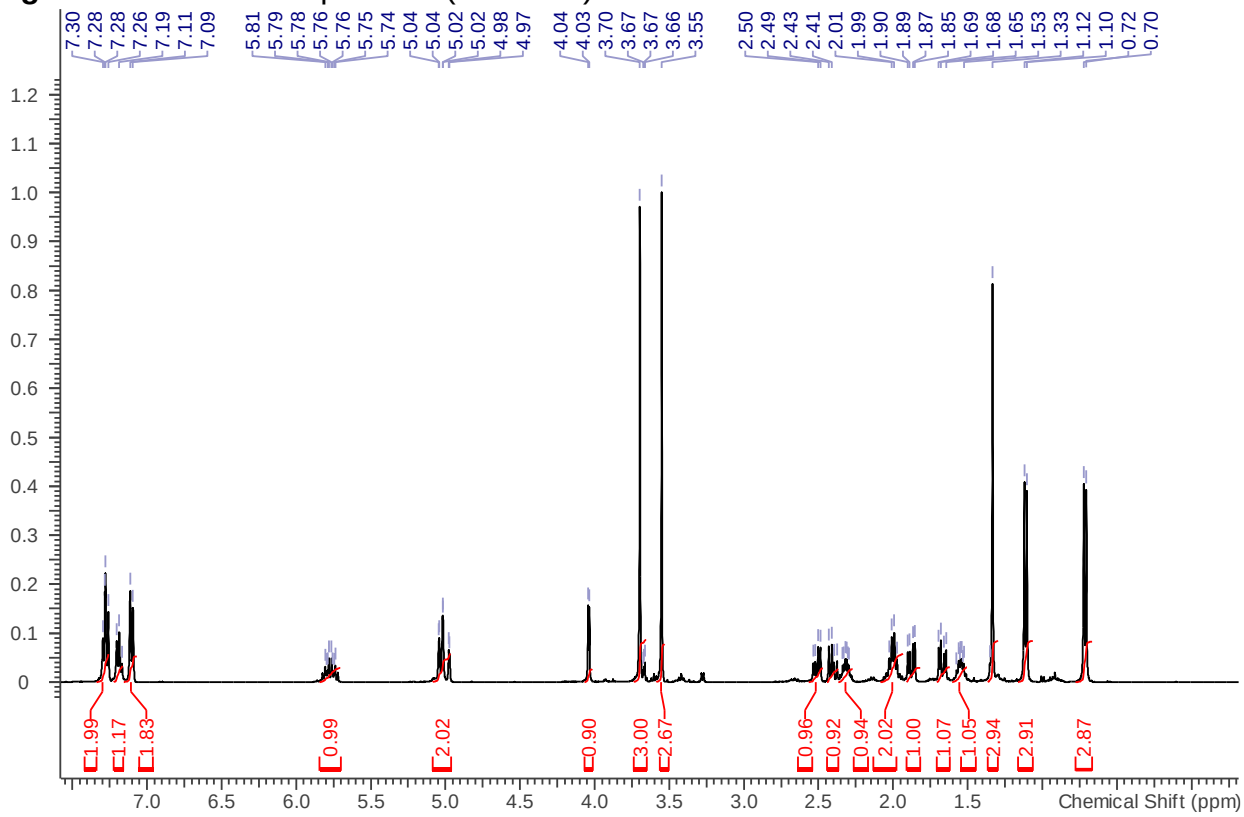

Figure 5.46. ^{13}C NMR spectrum (101 MHz) of **5.9a** in $CDCl_3$

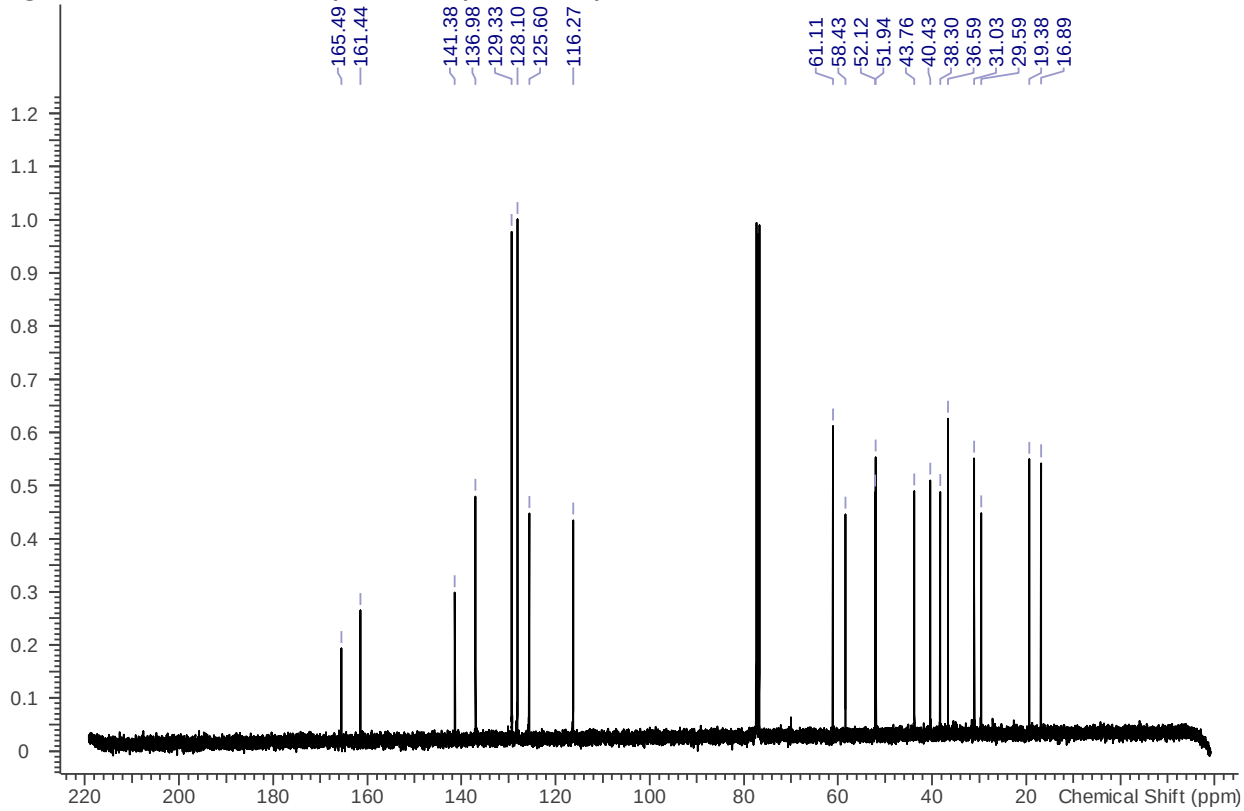

Figure 5.47. ^{1}H NMR spectrum (400 MHz) of **5.10a** in $CDCl_3$

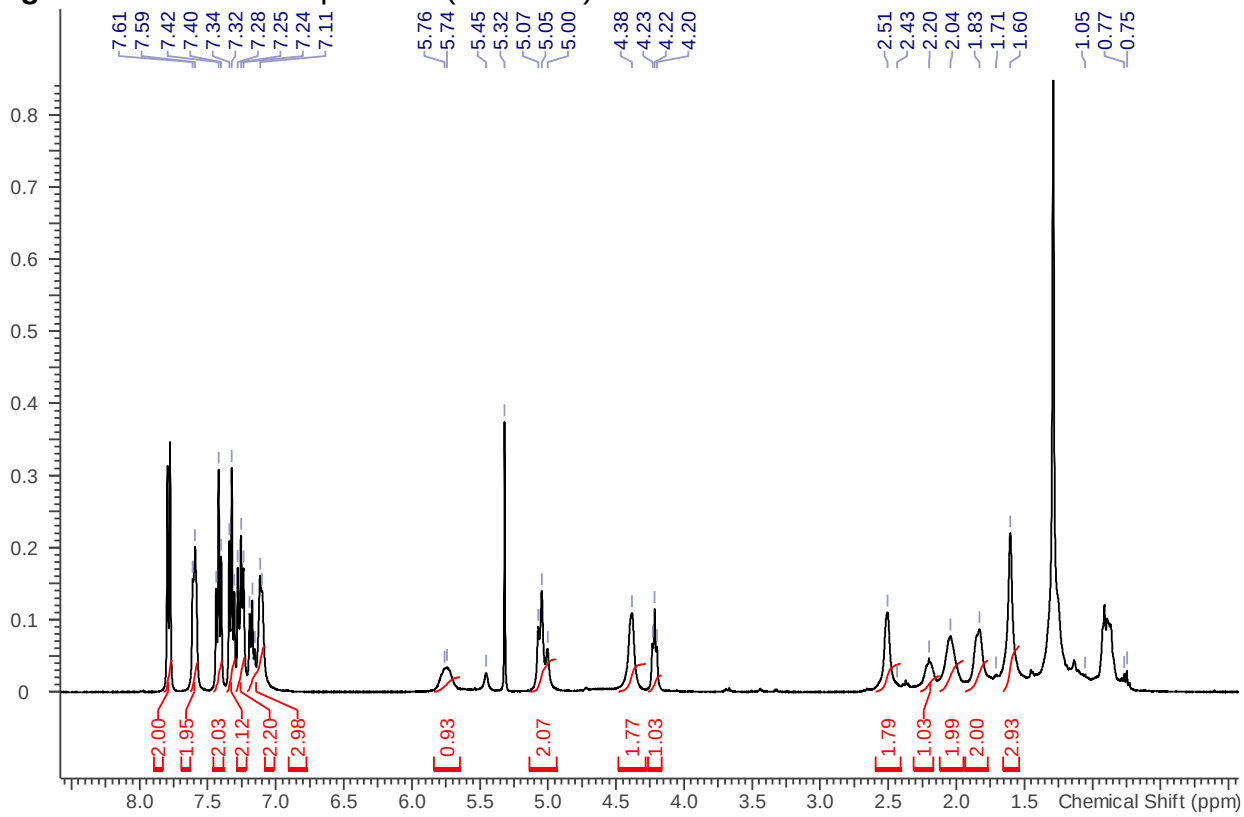

Figure 5.48. ^{13}C NMR spectrum (101 MHz) of **5.10a** in $CDCl_3$

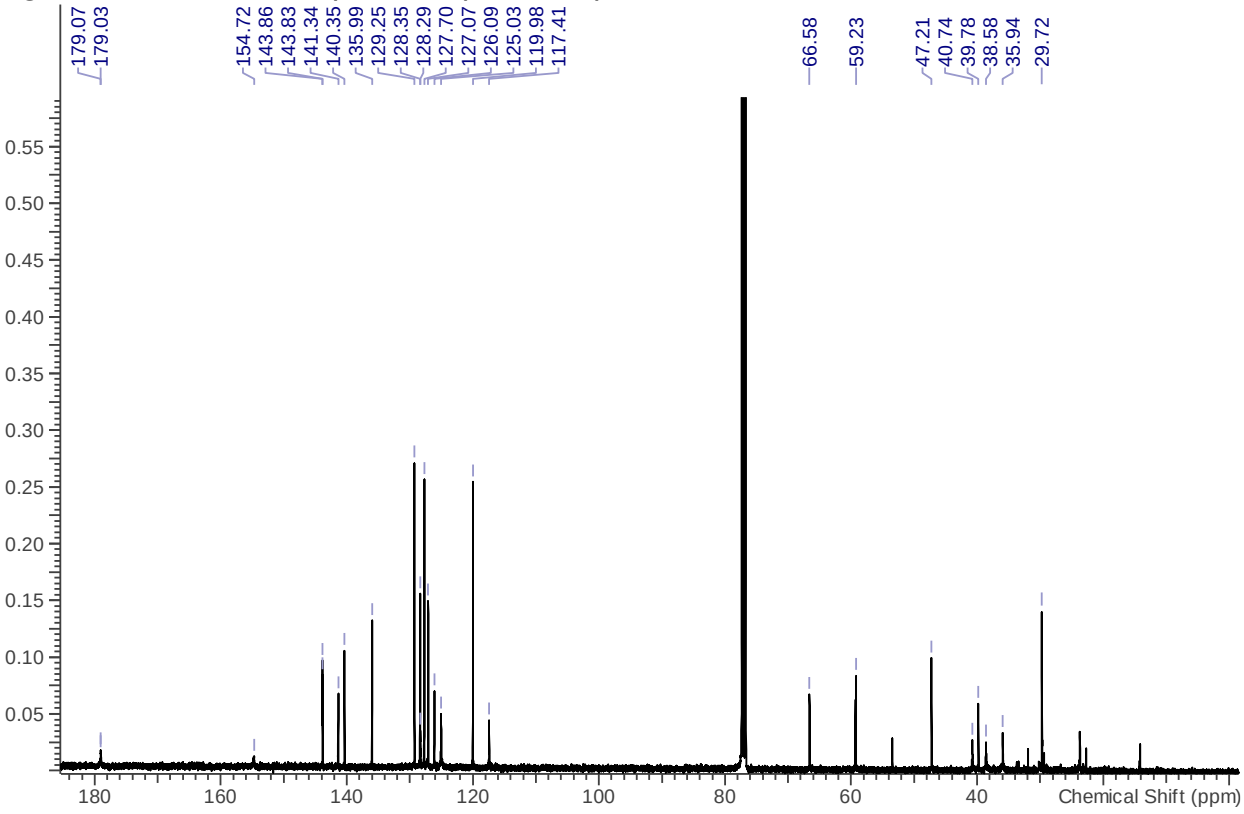

Figure 5.49. ^{1}H NMR spectrum (400 MHz) of **5.6b** in $CDCl_3$

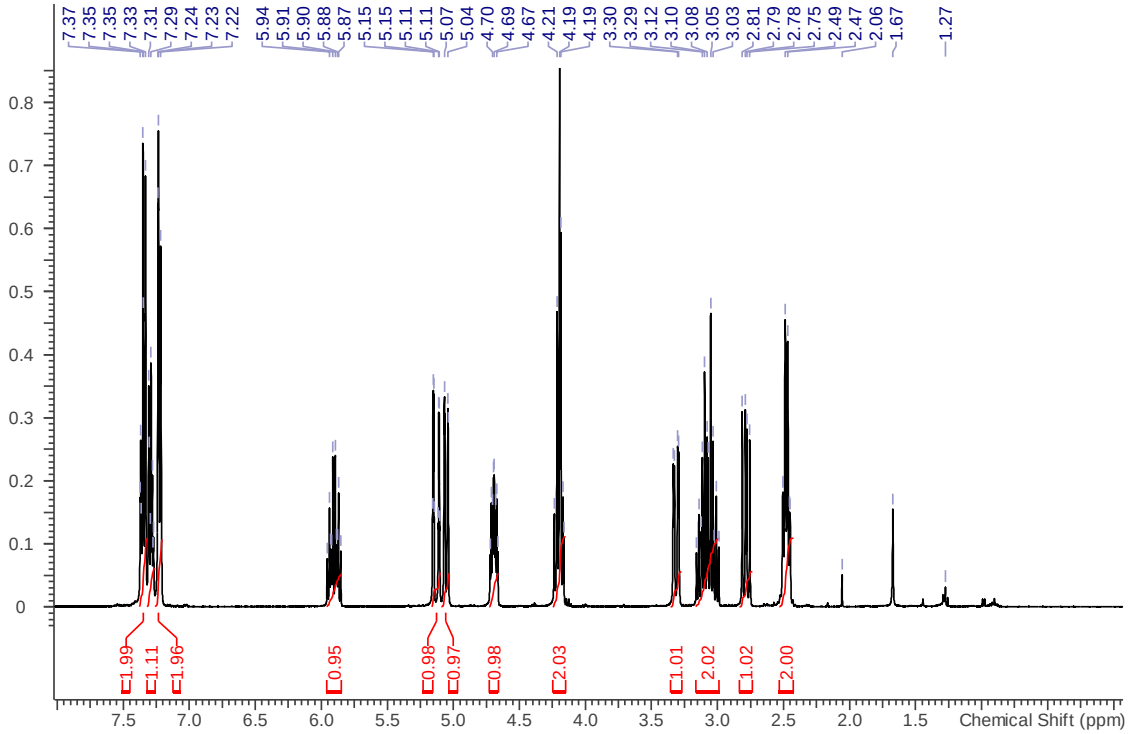

Figure 5.50. ^{13}C NMR spectrum (101 MHz) of **5.6b** in $CDCl_3$

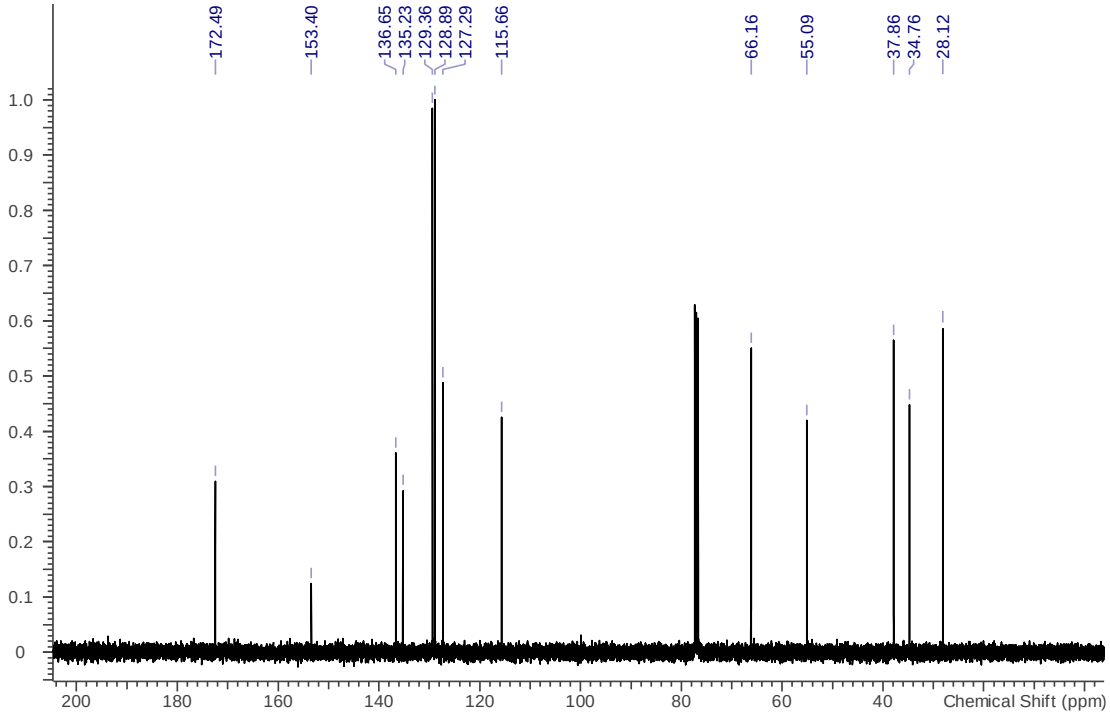

Figure 5.51. ^{1}H NMR spectrum (400 MHz) of **5.7b** in $CDCl_3$

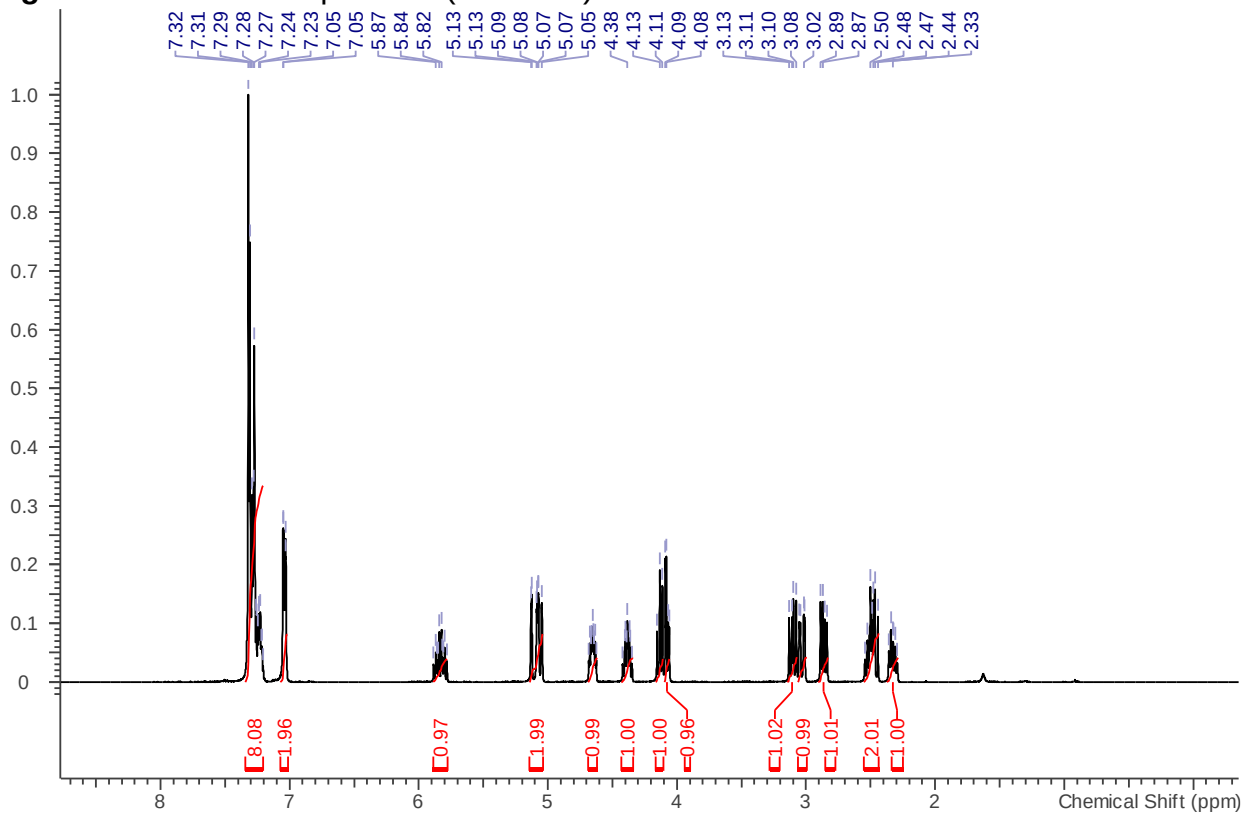

Figure 5.52. ^{13}C NMR spectrum (101 MHz) of **5.7b** in $CDCl_3$

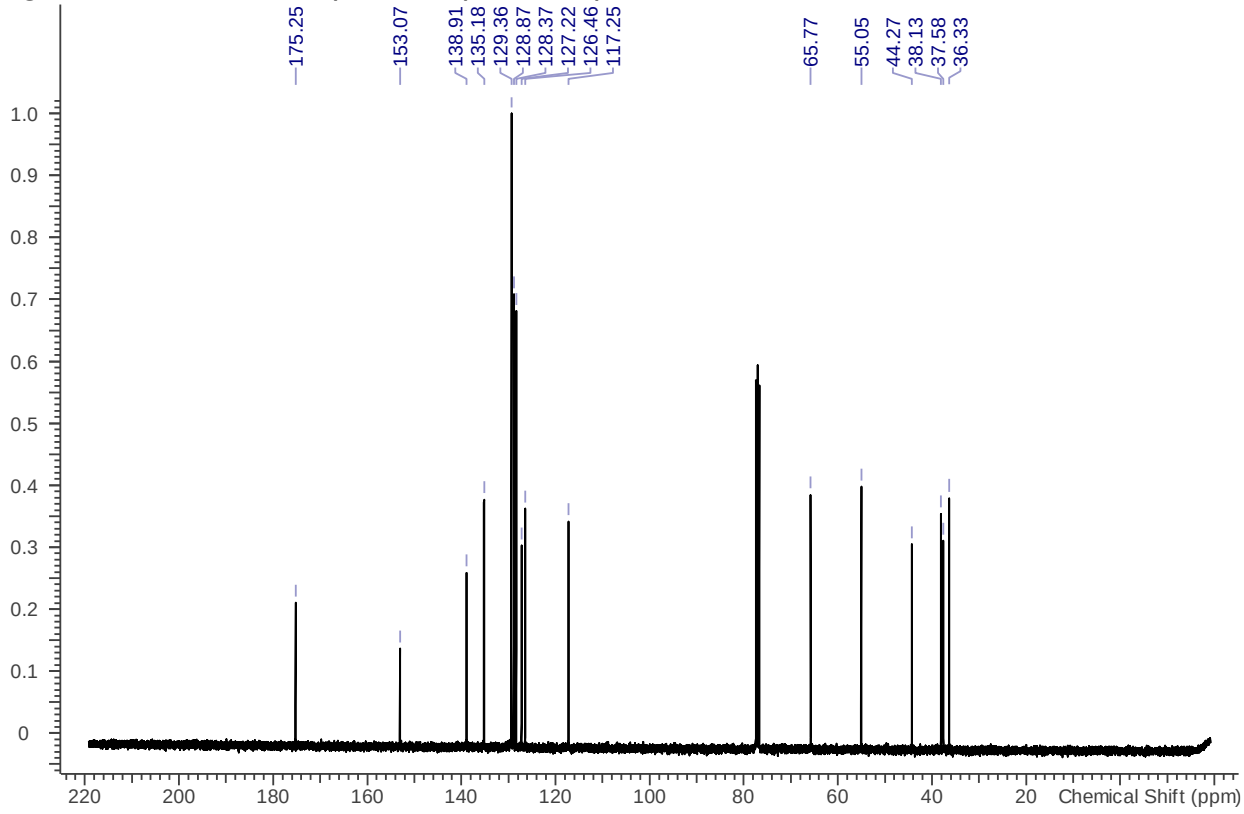

Figure 5.53. ^{1}H NMR spectrum (400 MHz) of **5.8b** in $CDCl_3$

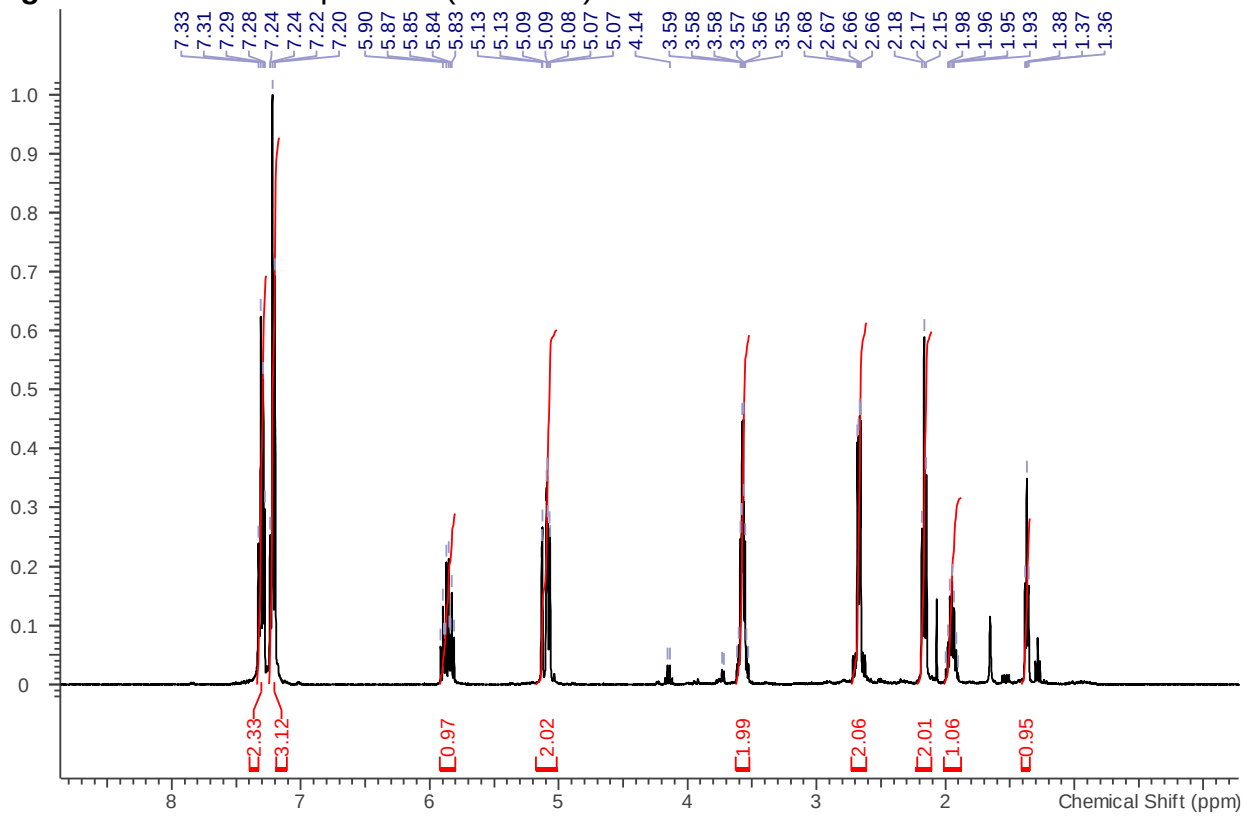

Figure 5.54. ^{13}C NMR spectrum (101 MHz) of **5.8b** in $CDCl_3$

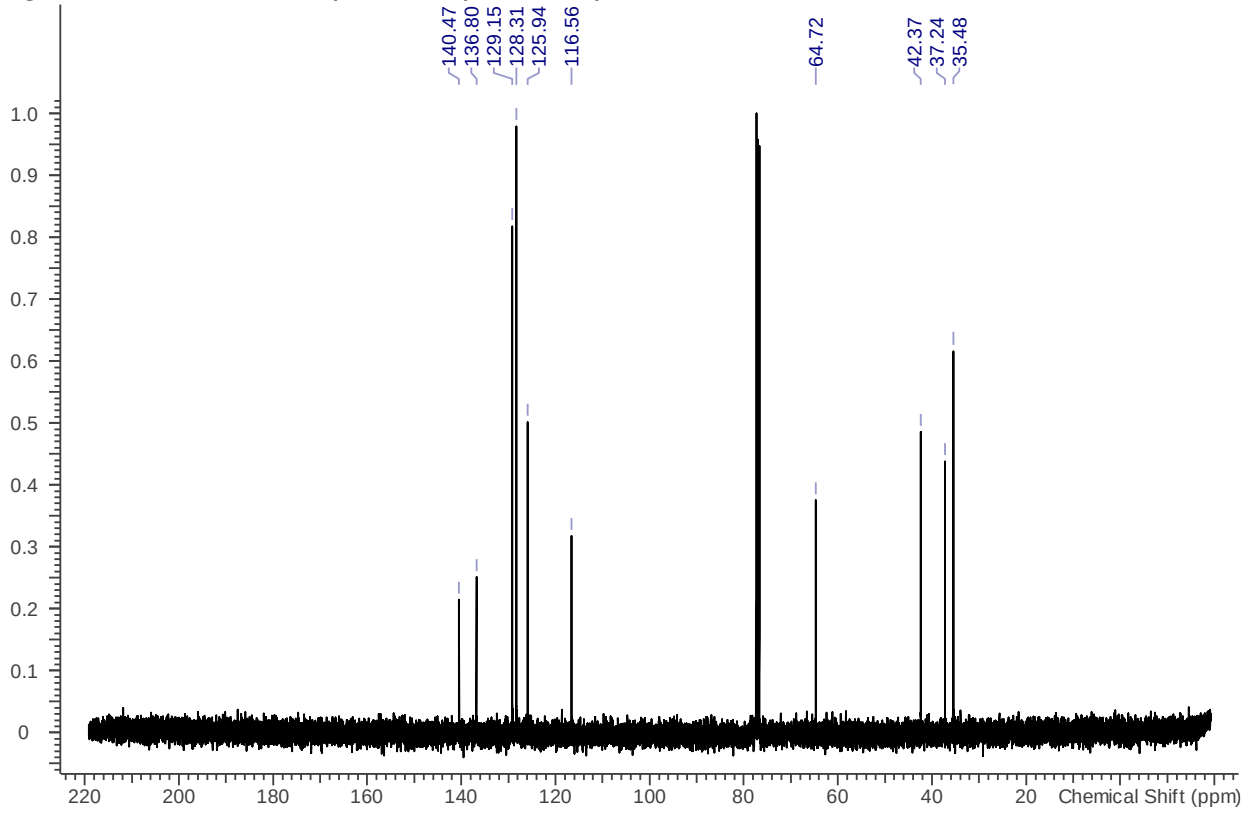

Figure 5.55. ^{1}H NMR spectrum (400 MHz) of **5.9b** in $CDCl_3$

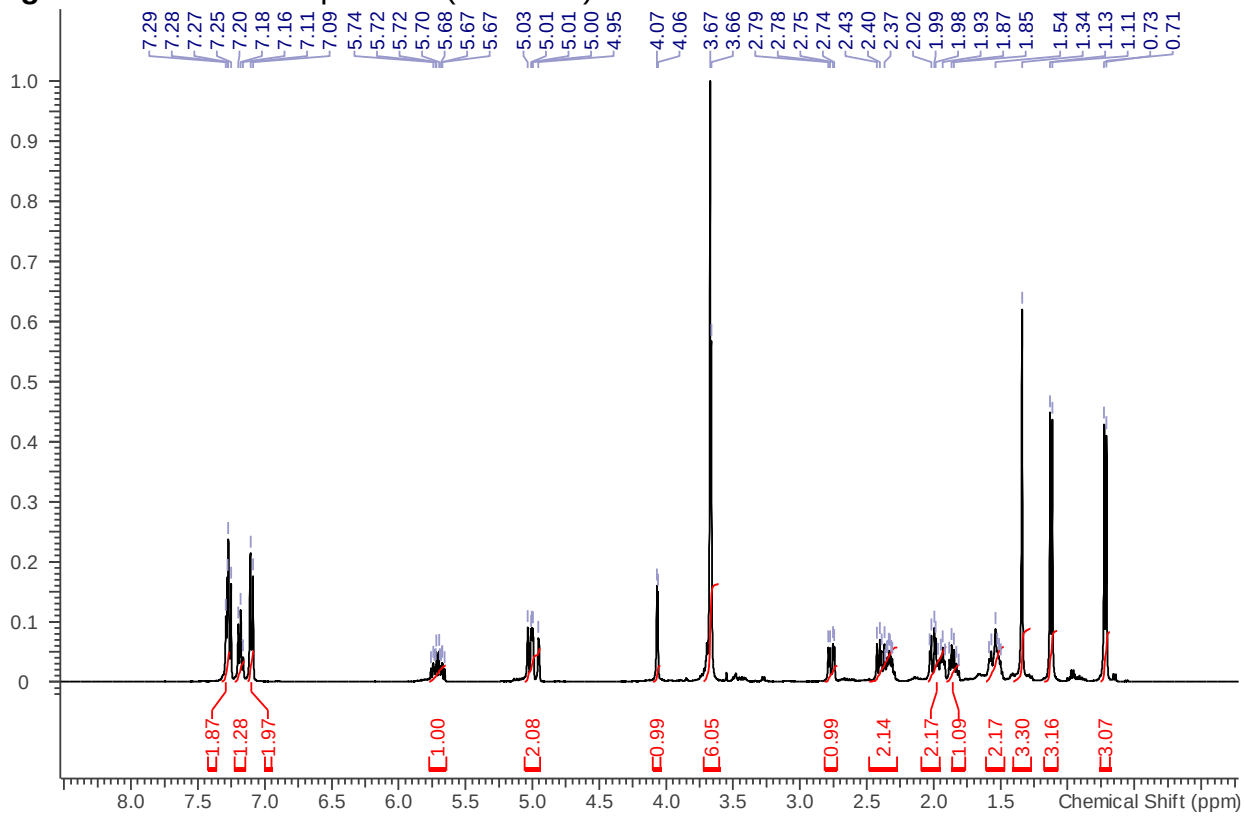

Figure 5.56. ^{13}C NMR spectrum (101 MHz) of **5.9b** in $CDCl_3$

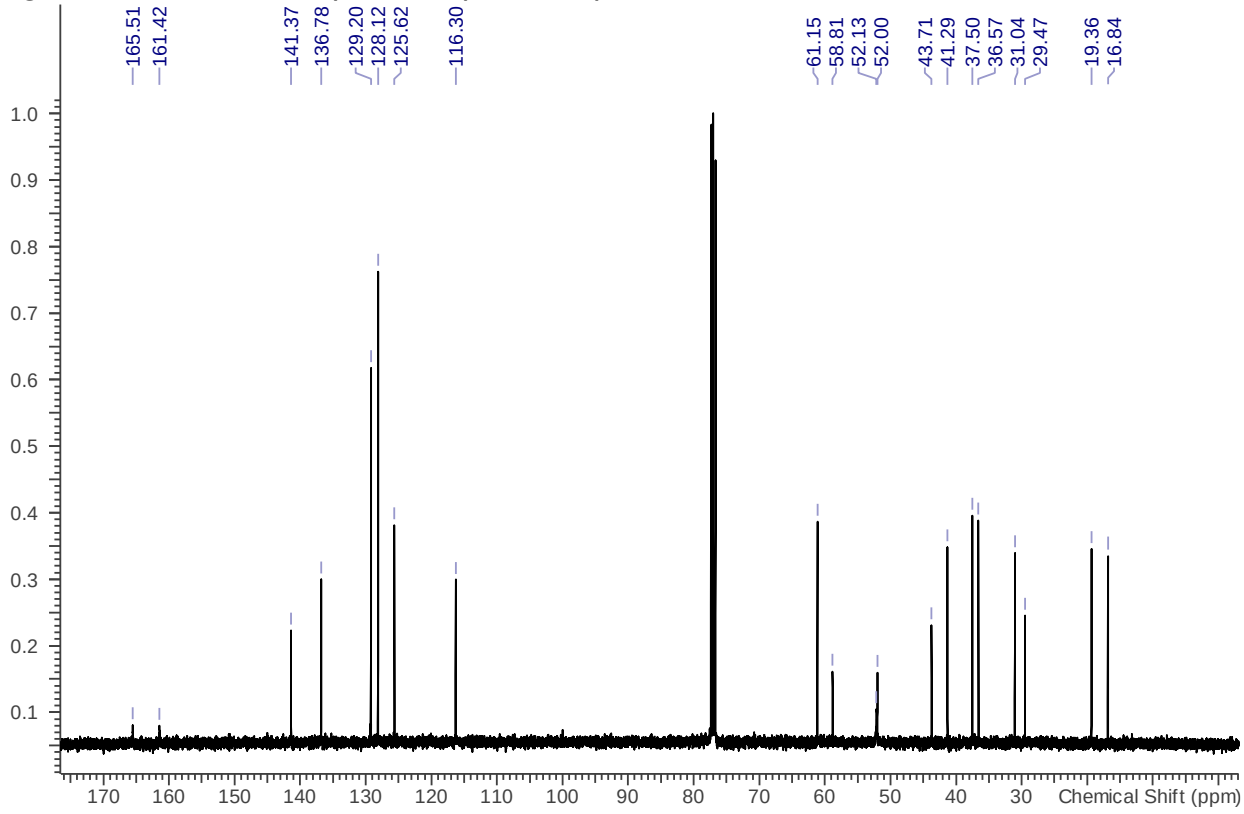

Figure 5.57. ^{1}H NMR spectrum (400 MHz) of **5.10b** in $CDCl_3$

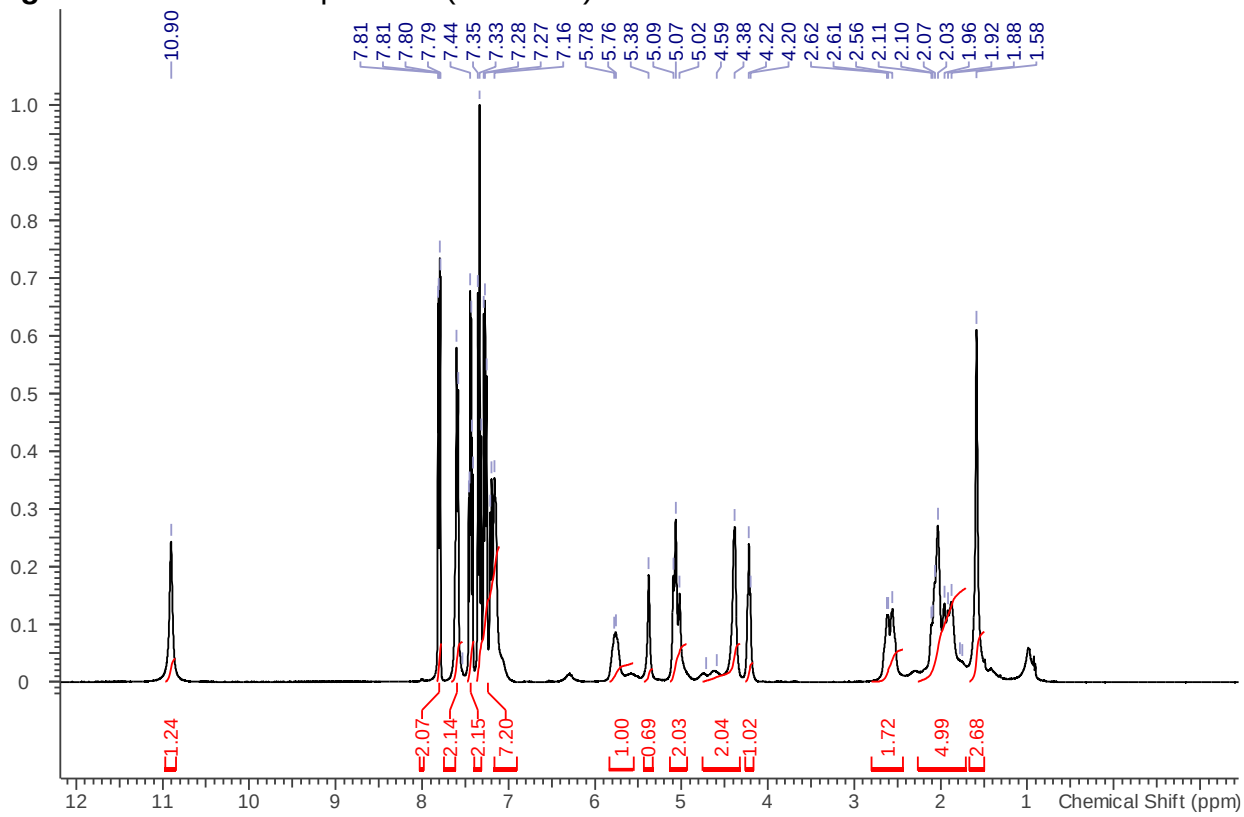

Figure 5.58. ^{13}C NMR spectrum (101 MHz) of **5.10b** in $CDCl_3$

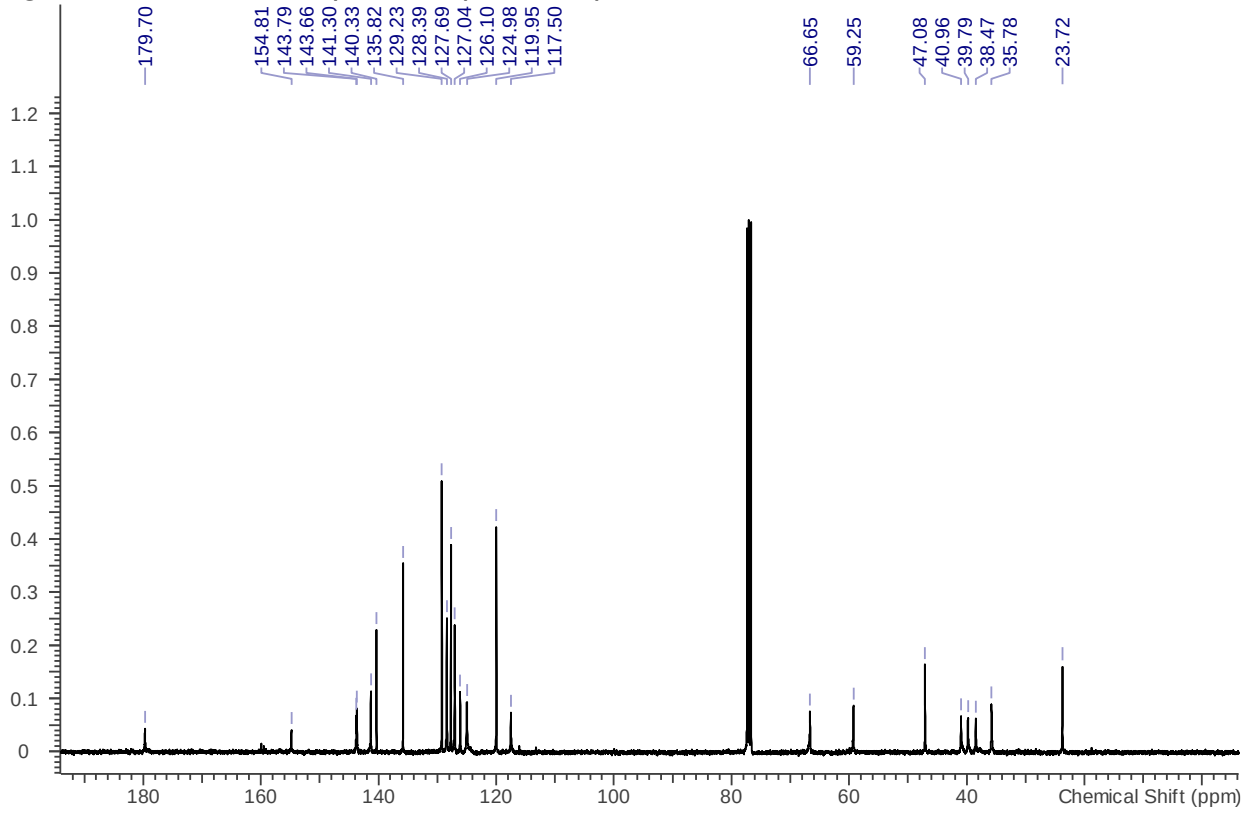

Figure 5.59. ^{1}H NMR spectrum (400 MHz) of **5.11a** in $CDCl_3$

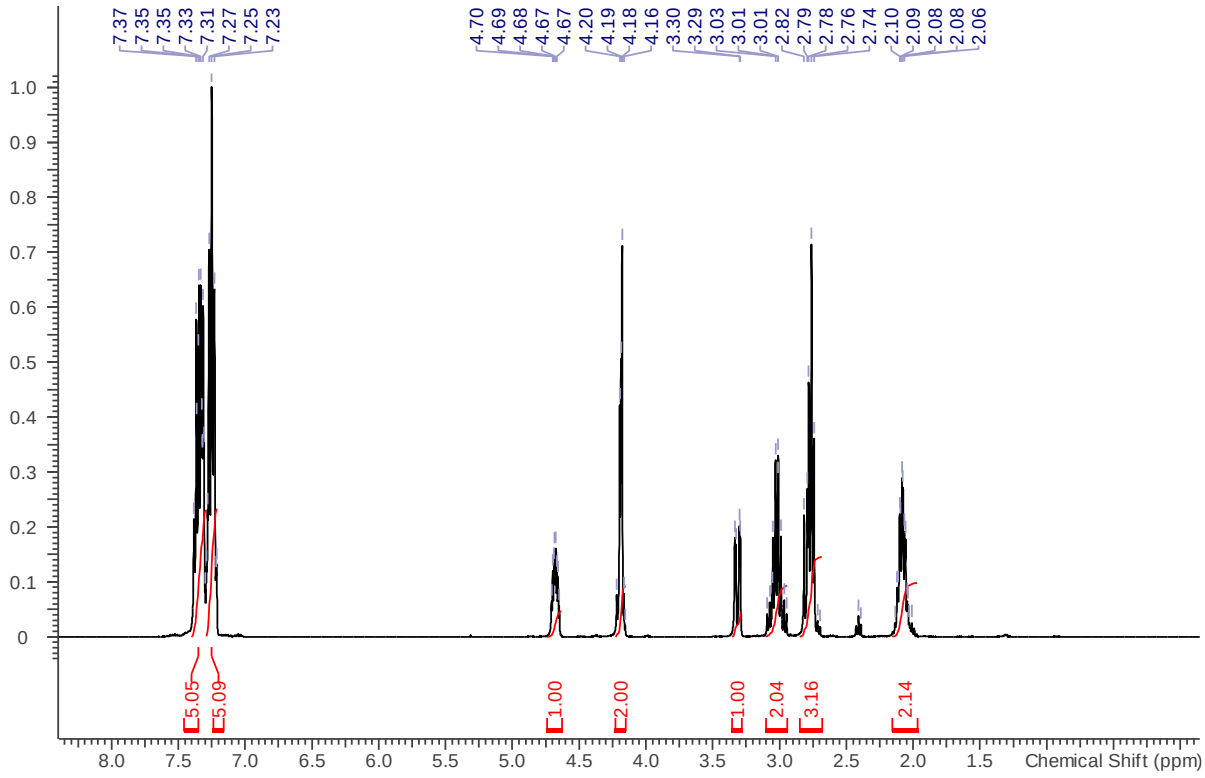

Figure 5.60. ^{13}C NMR spectrum (101 MHz) of **5.11a** in $CDCl_3$

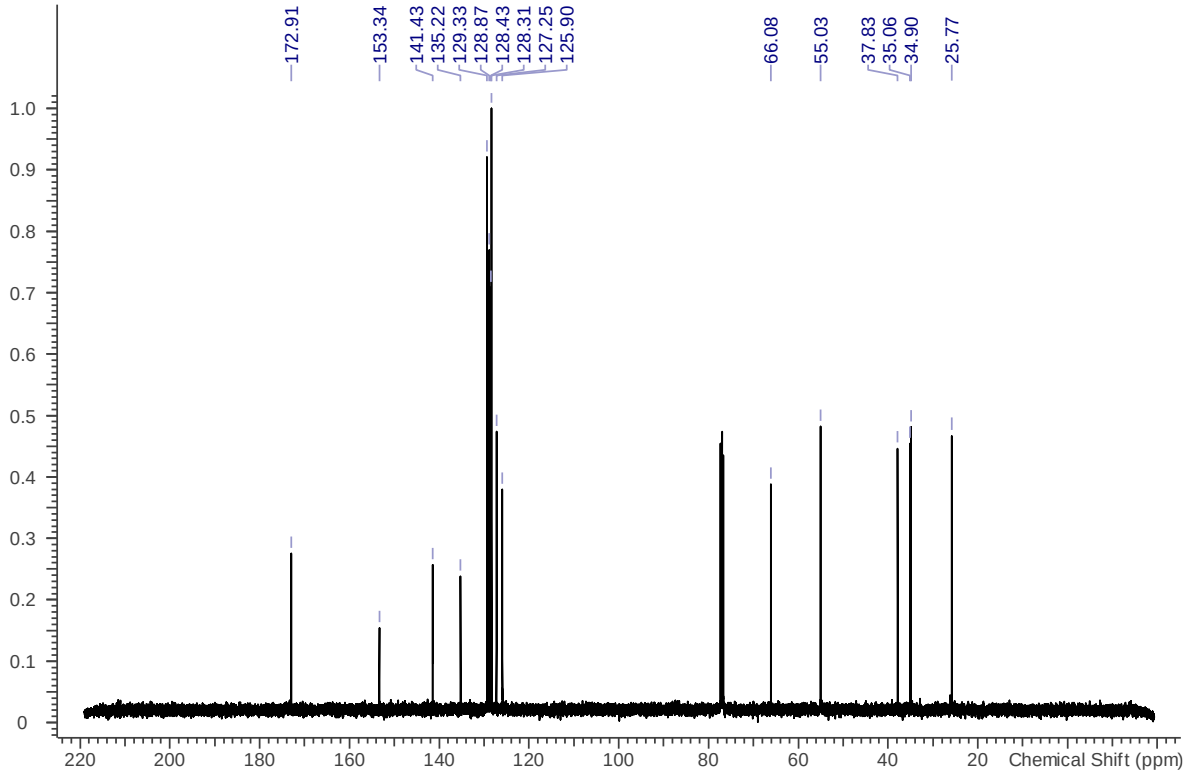

Figure 5.61. ^{1}H NMR spectrum (400 MHz) of **5.12a** in $CDCl_3$

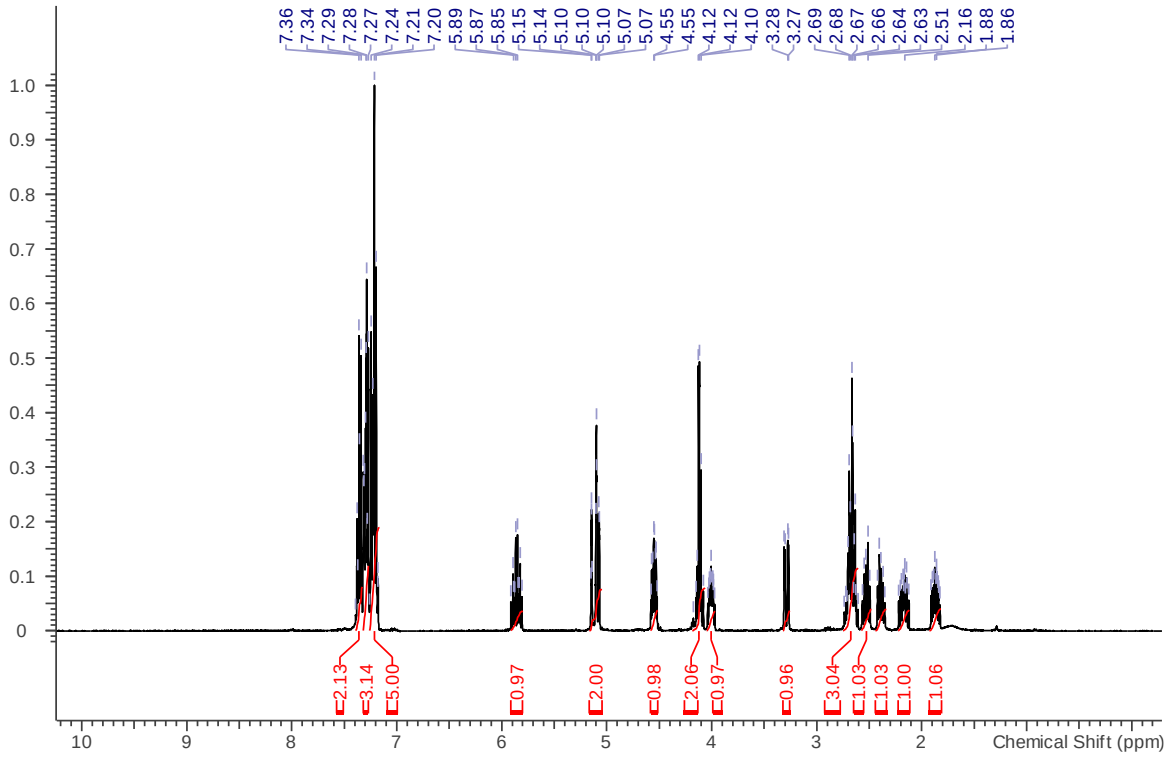

Figure 5.62. ^{13}C NMR spectrum (101 MHz) of **5.12a** in $CDCl_3$

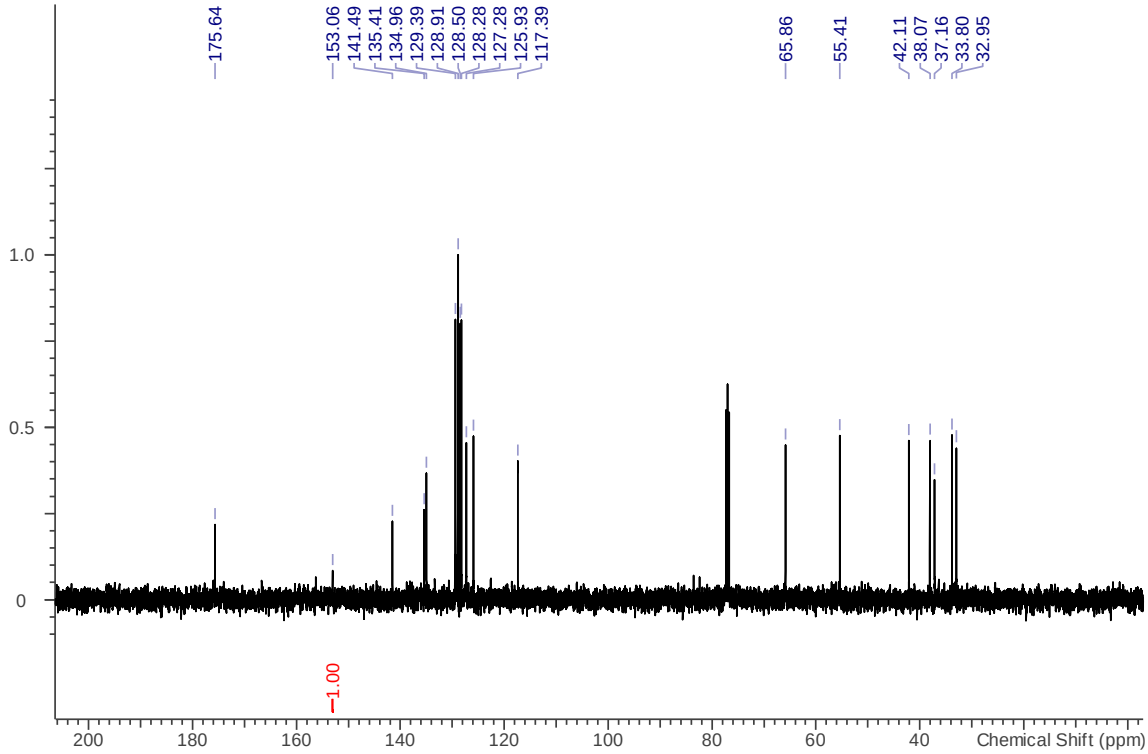

Figure 5.63. ^{1}H NMR spectrum (400 MHz) of **5.13a** in $CDCl_3$

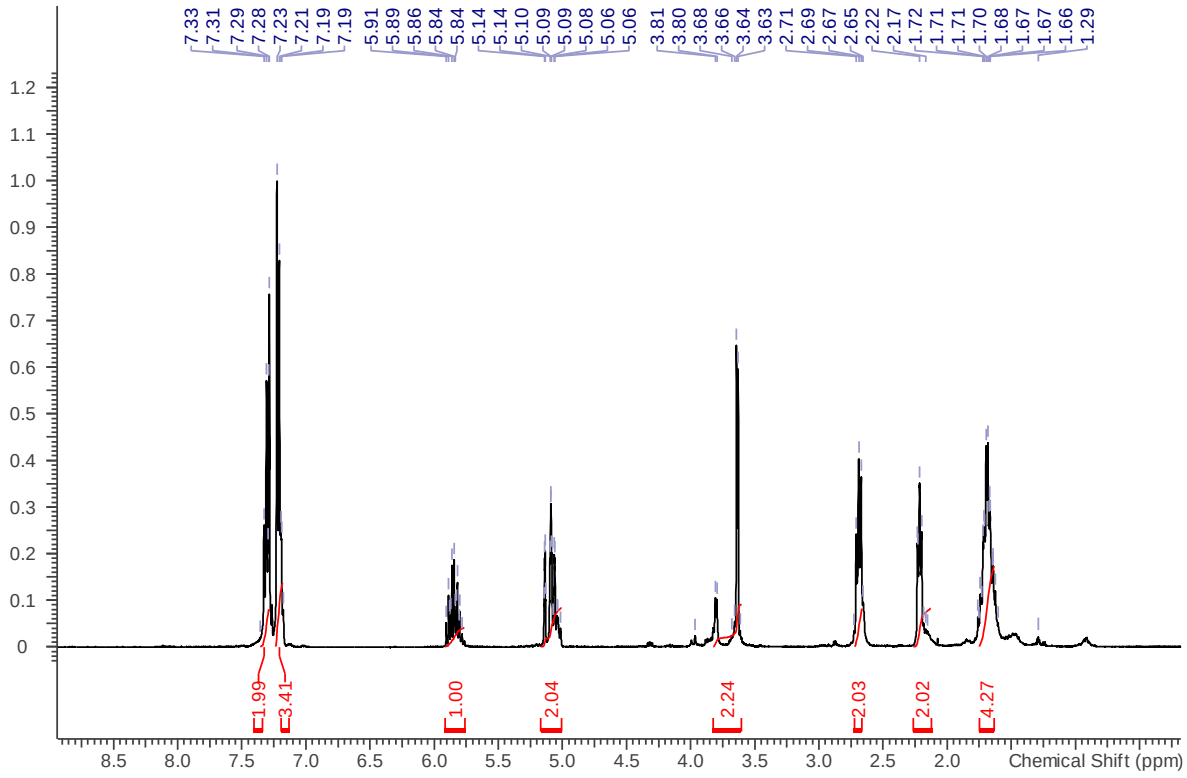

Figure 5.64. ^{13}C NMR spectrum (101 MHz) of **5.13a** in $CDCl_3$

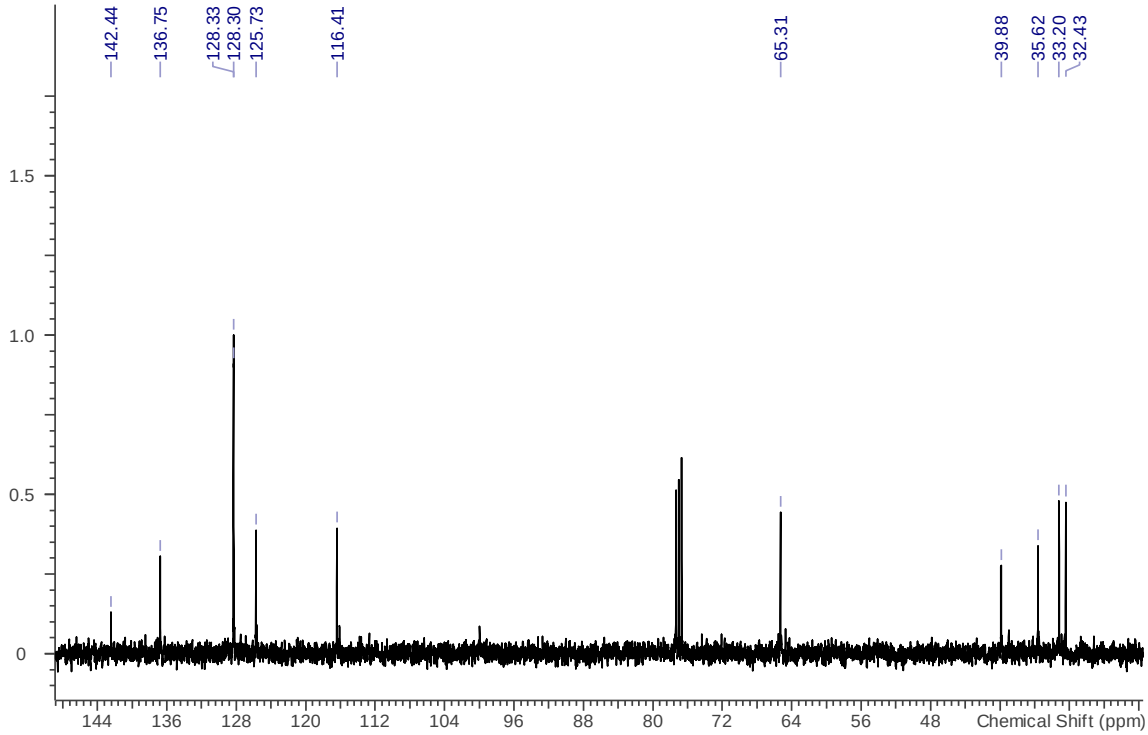

Figure 5.65. ^{1}H NMR spectrum (400 MHz) of **5.14a** in $CDCl_3$

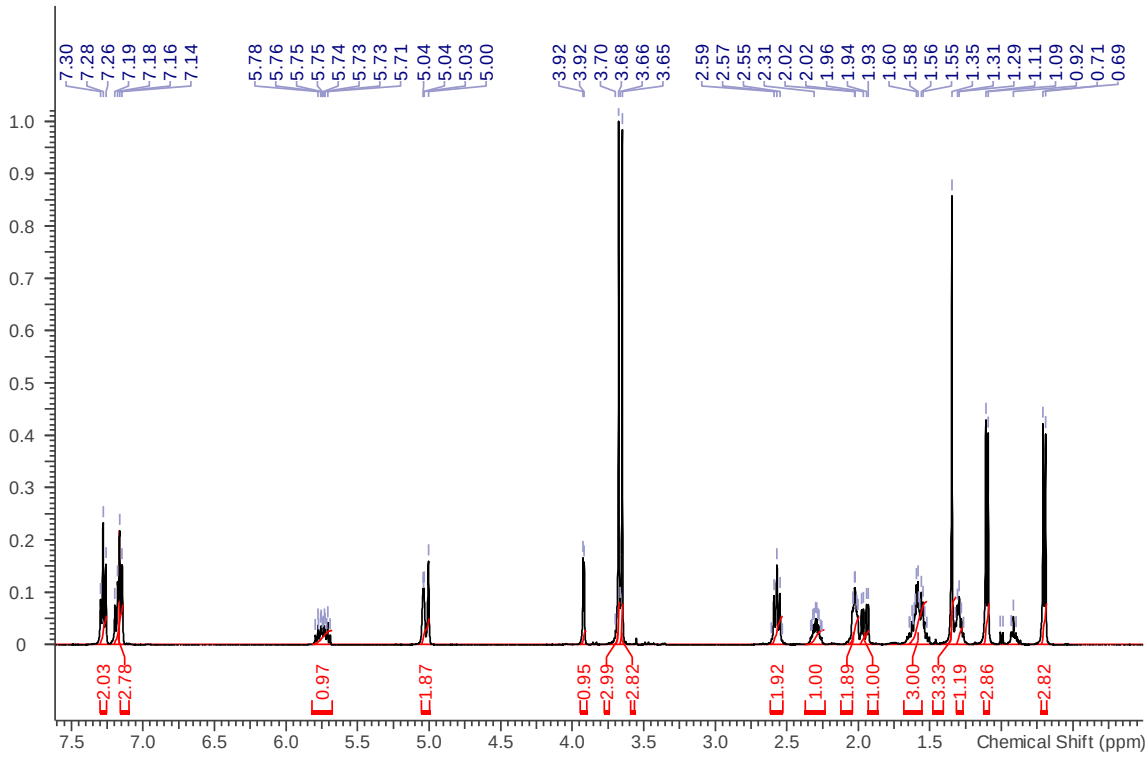

Figure 5.66. ^{13}C NMR spectrum (101 MHz) of **5.14a** in $CDCl_3$

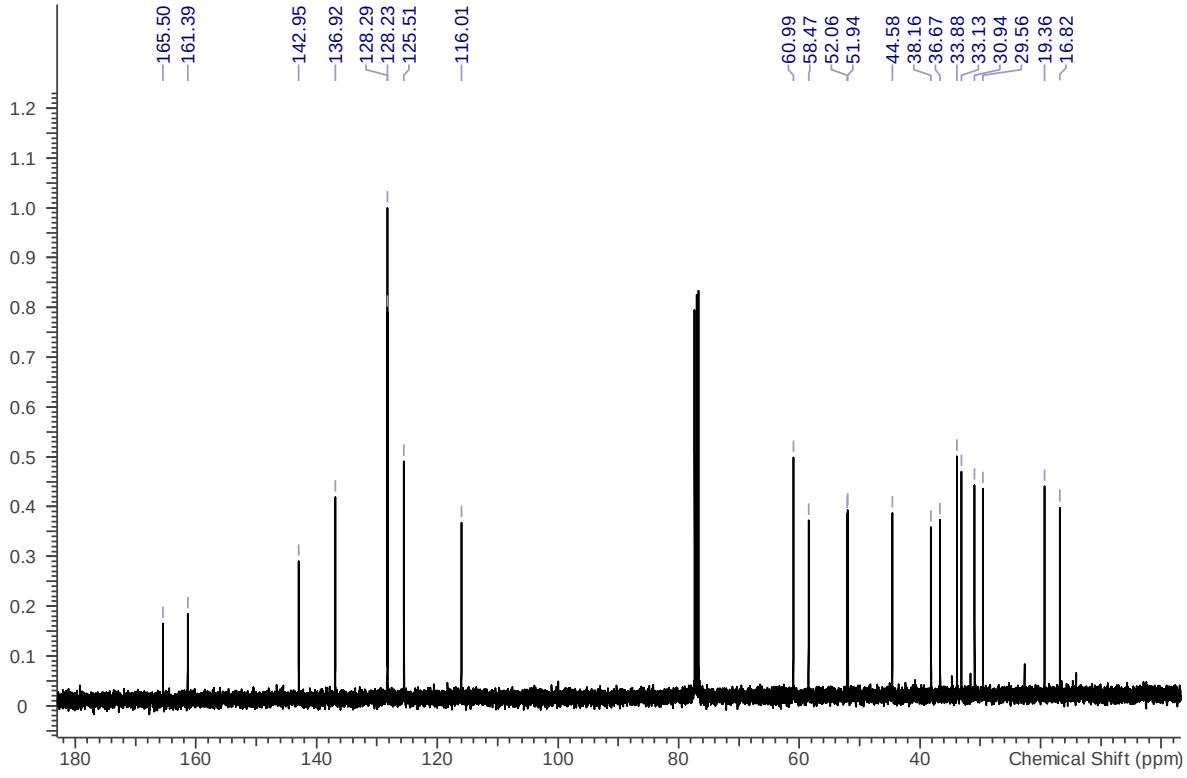

Figure 5.67. ^{1}H NMR spectrum (400 MHz) of **5.15a** in $CDCl_3$

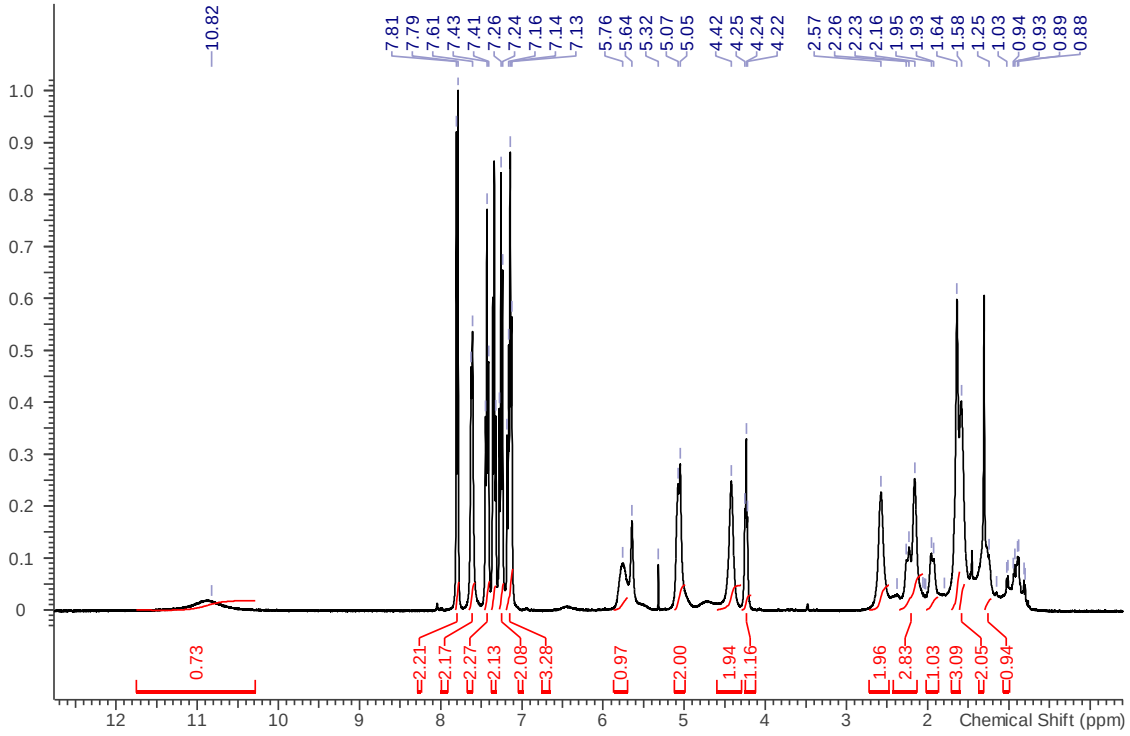

Figure 5.68. ^{13}C NMR spectrum (101 MHz) of **5.15a** in $CDCl_3$

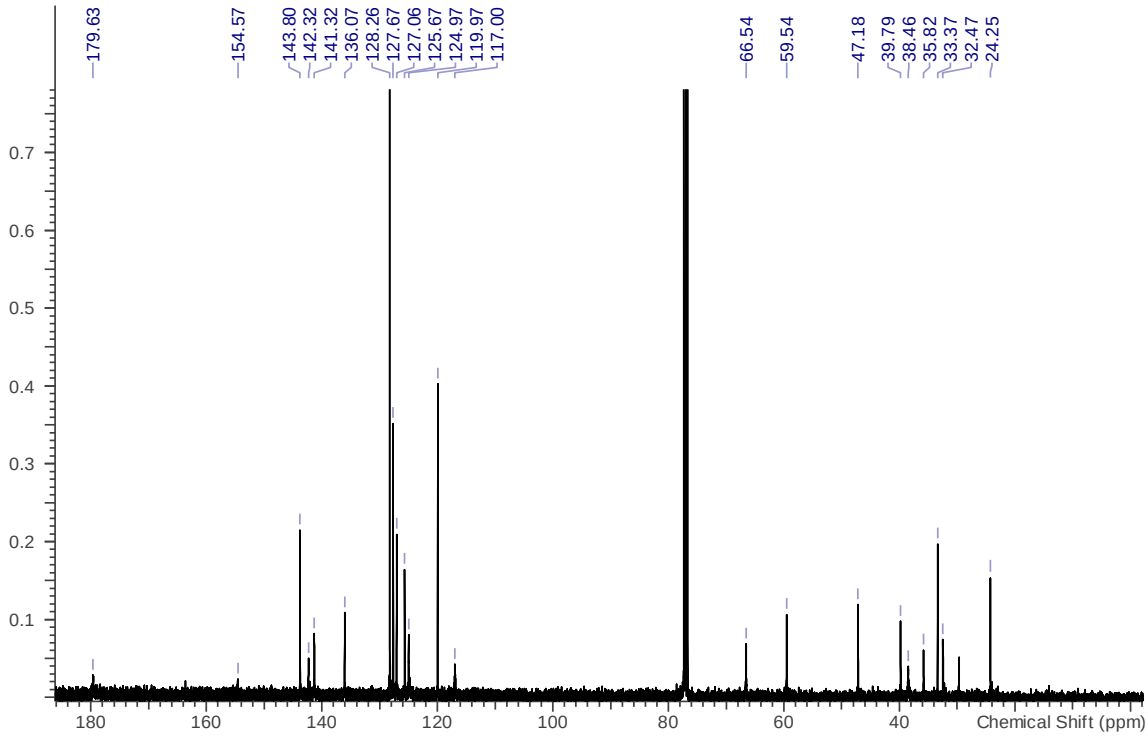

Figure 5.69. ^{1}H NMR spectrum (400 MHz) of **5.11b** in $CDCl_3$

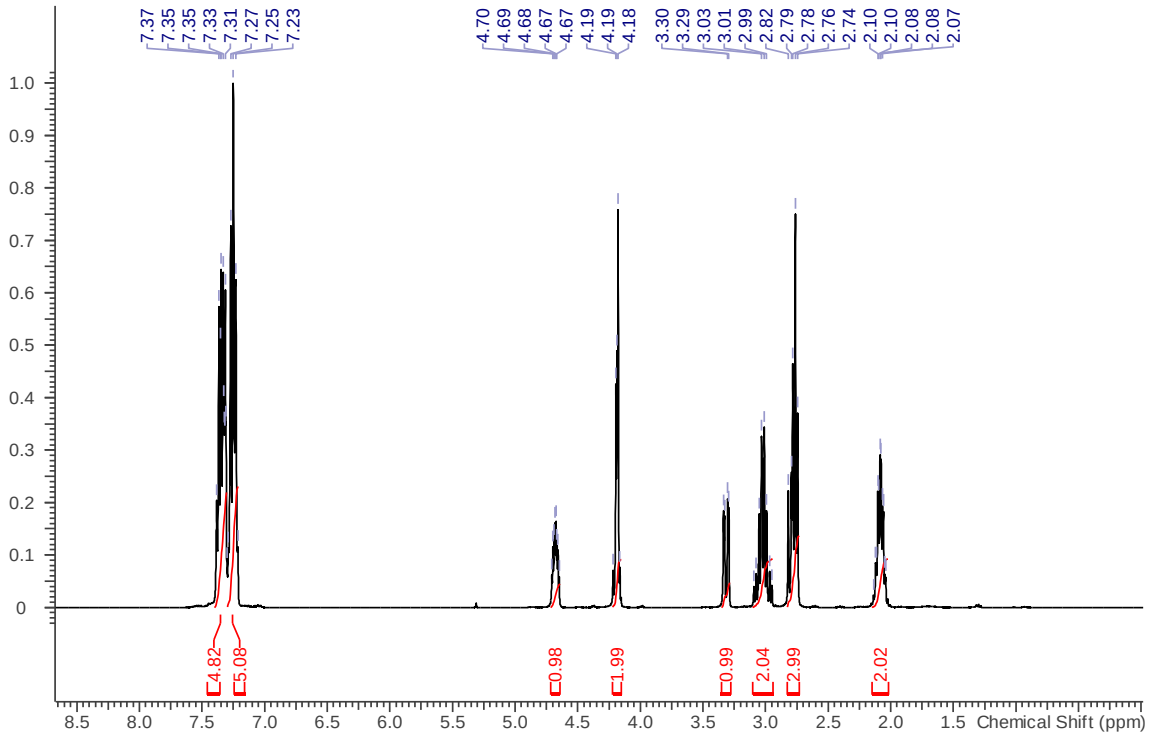

Figure 5.70. ^{13}C NMR spectrum (101 MHz) of **5.11b** in $CDCl_3$

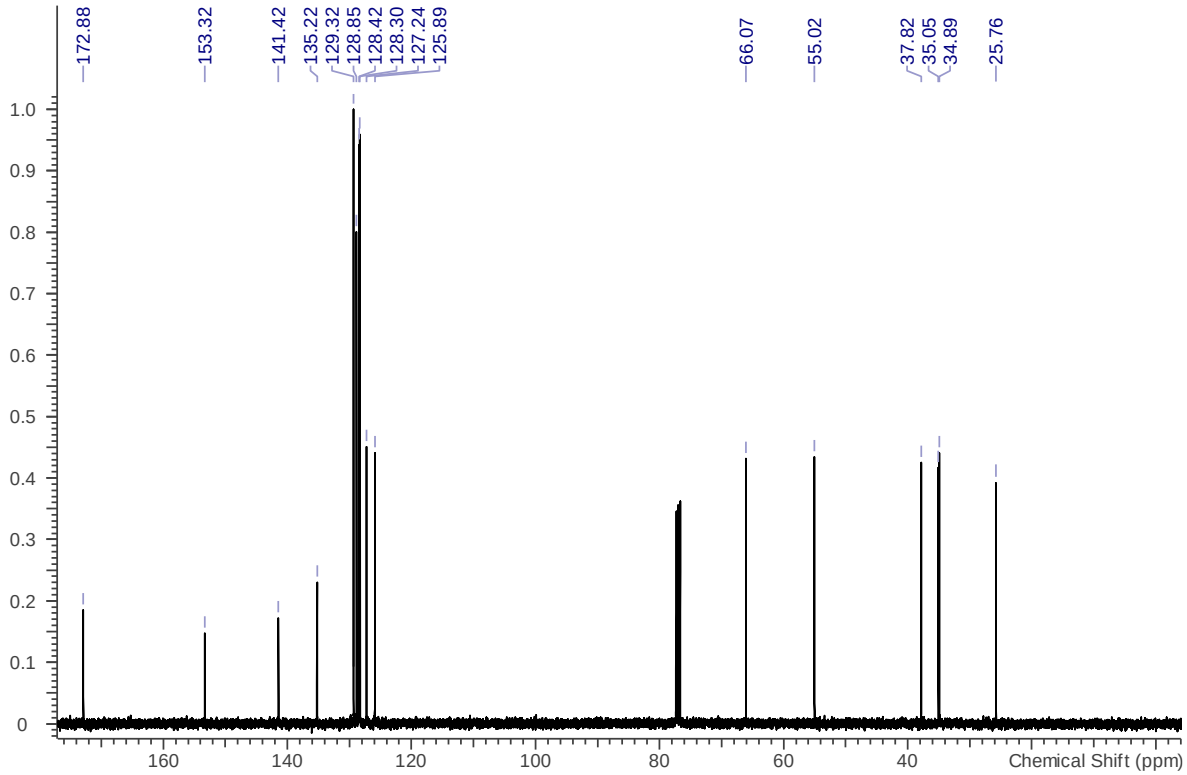

Figure 5.71. ^{1}H NMR spectrum (400 MHz) of **5.12b** in $CDCl_3$

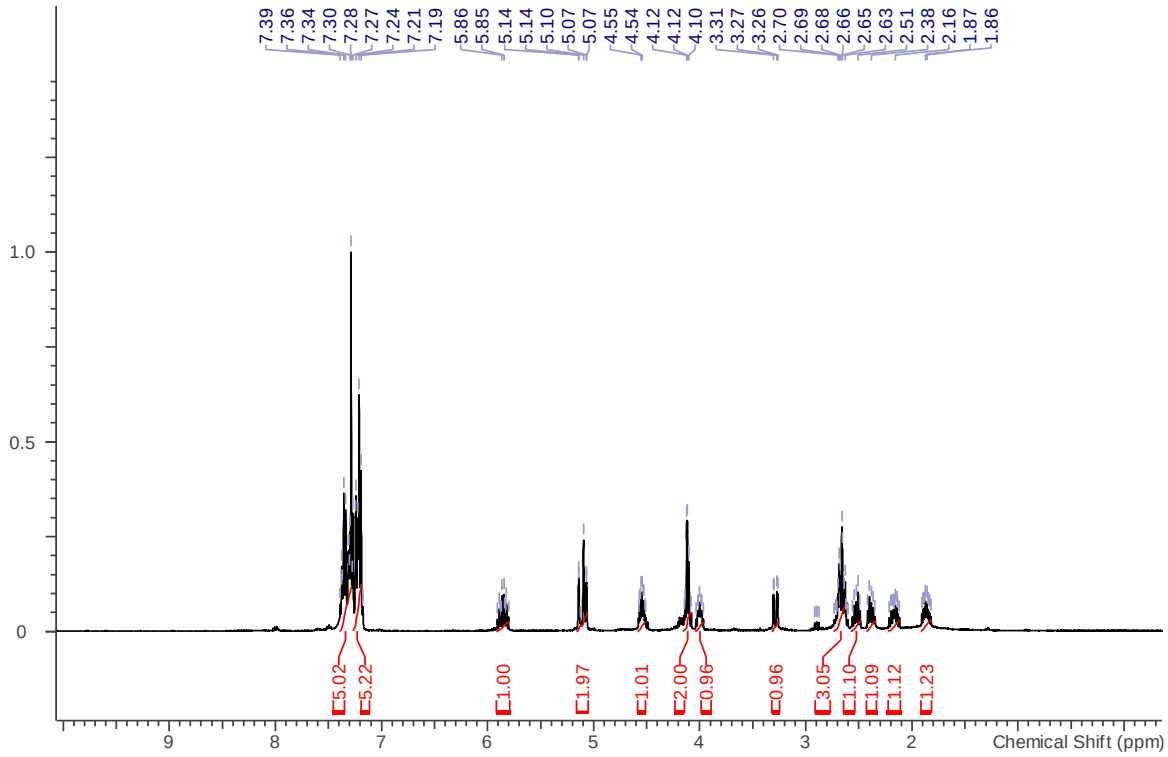

Figure 5.72. ^{13}C NMR spectrum (101 MHz) of **5.12b** in $CDCl_3$

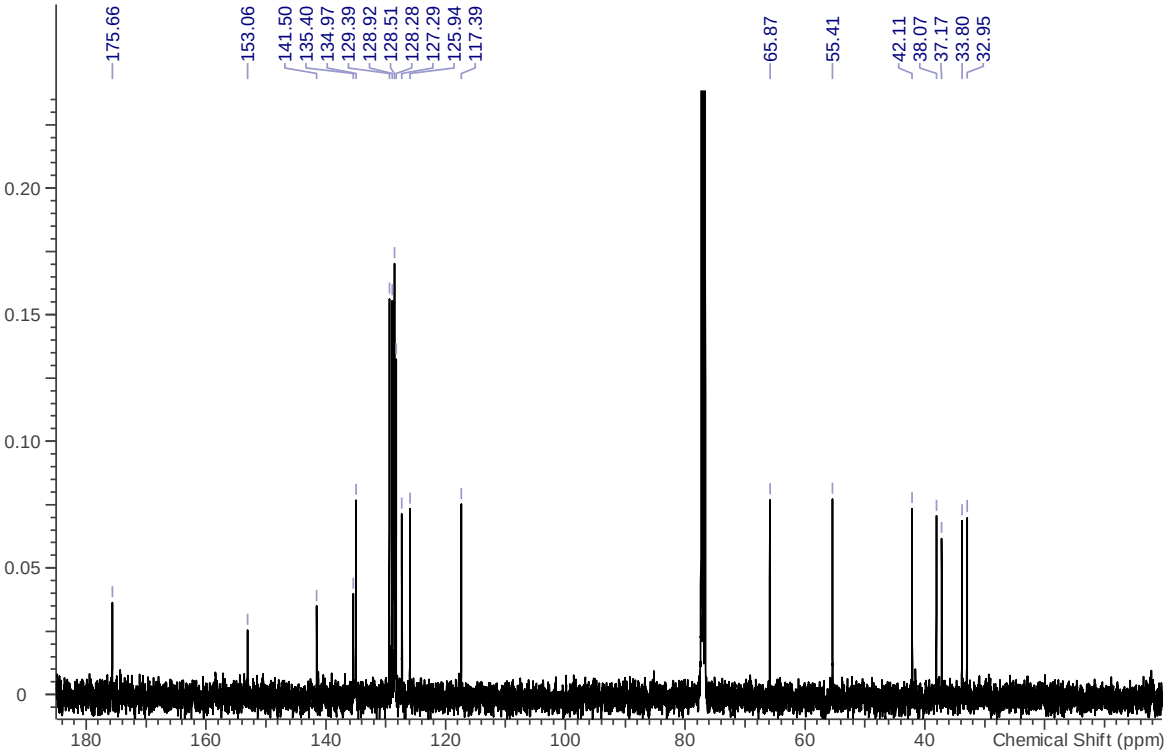

Figure 5.73. ^{1}H NMR spectrum (400 MHz) of **5.13b** in $CDCl_3$

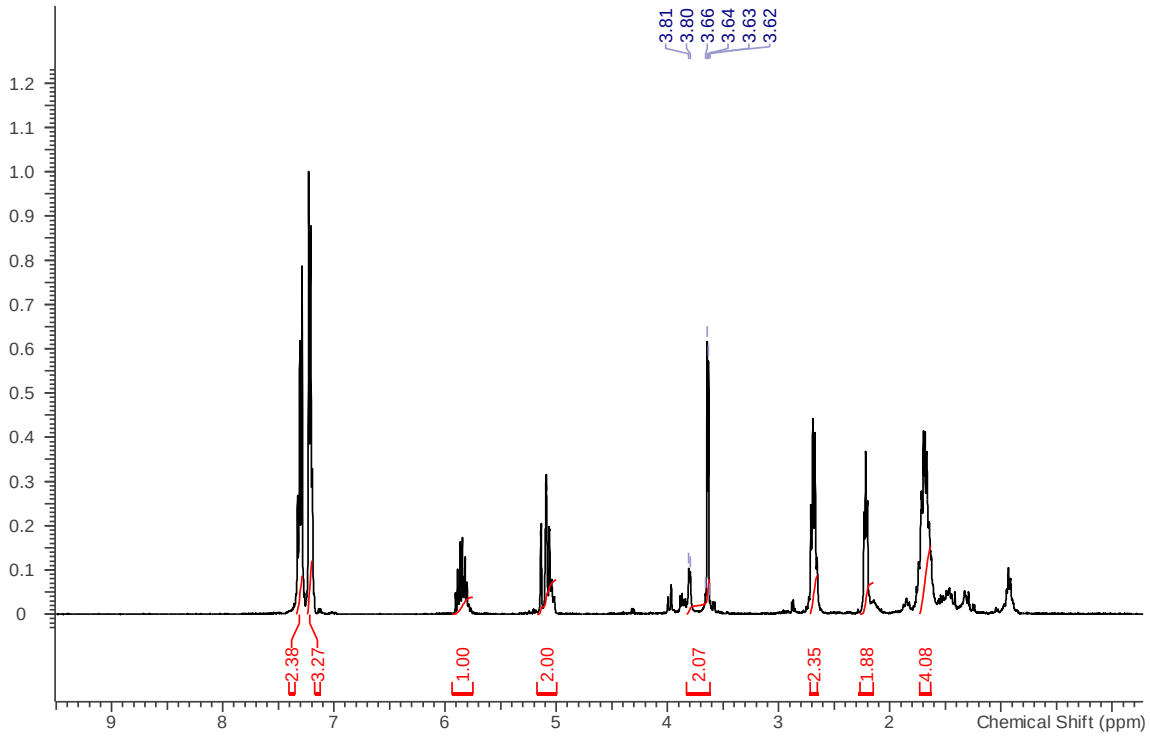

Figure 5.74. ^{13}C NMR spectrum (101 MHz) of **5.13b** in $CDCl_3$

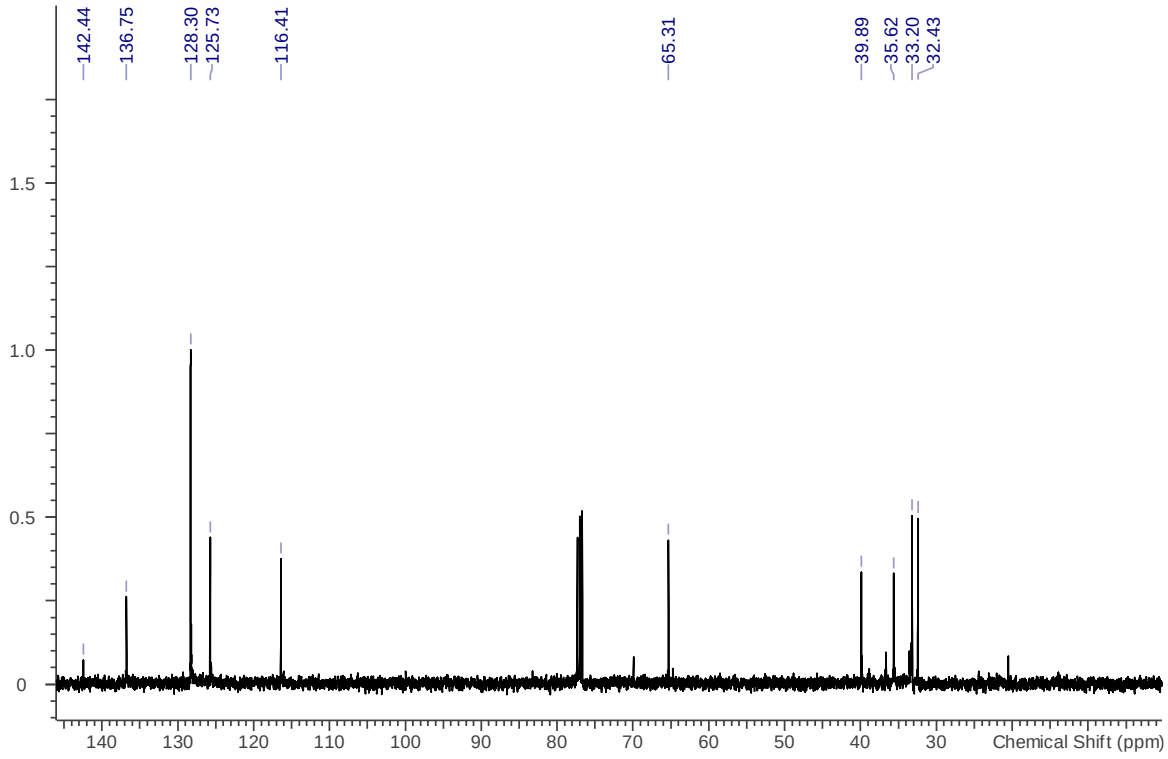

Figure 5.75. ^{1}H NMR spectrum (400 MHz) of **5.14b** in $CDCl_3$

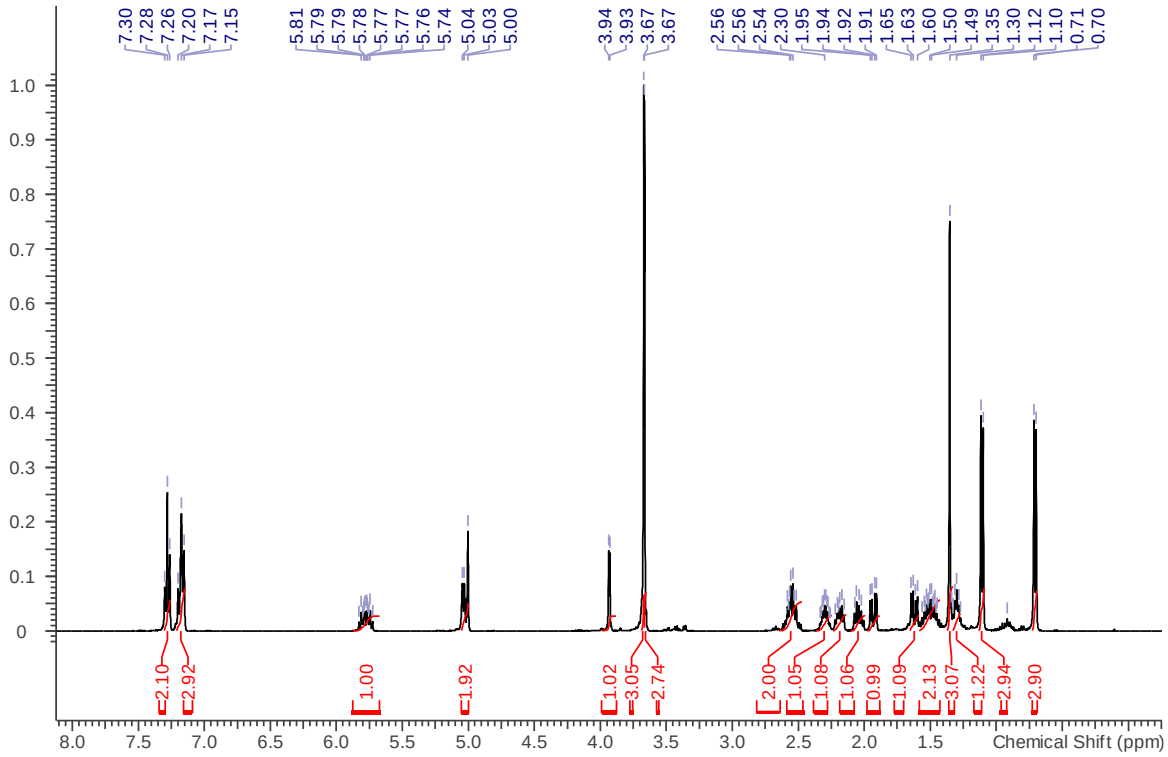

Figure 5.76. ^{13}C NMR spectrum (101 MHz) of **5.14b** in $CDCl_3$

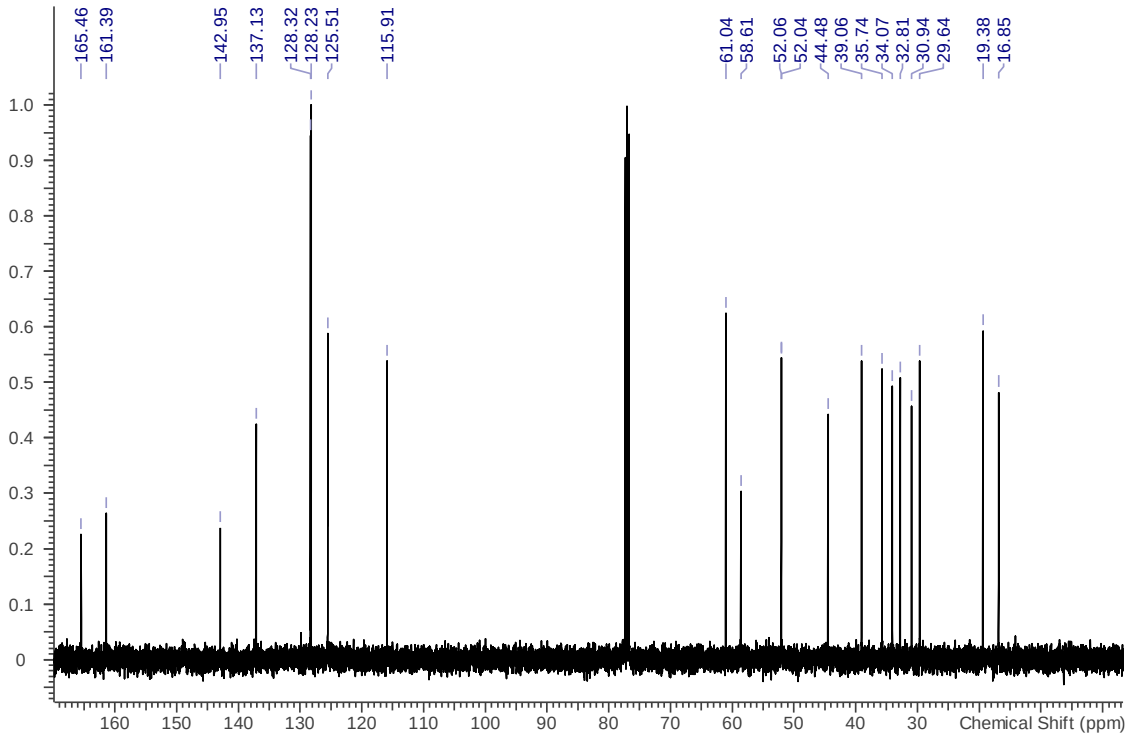

Figure 5.77. ^{1}H NMR spectrum (400 MHz) of **5.15b** in $CDCl_3$

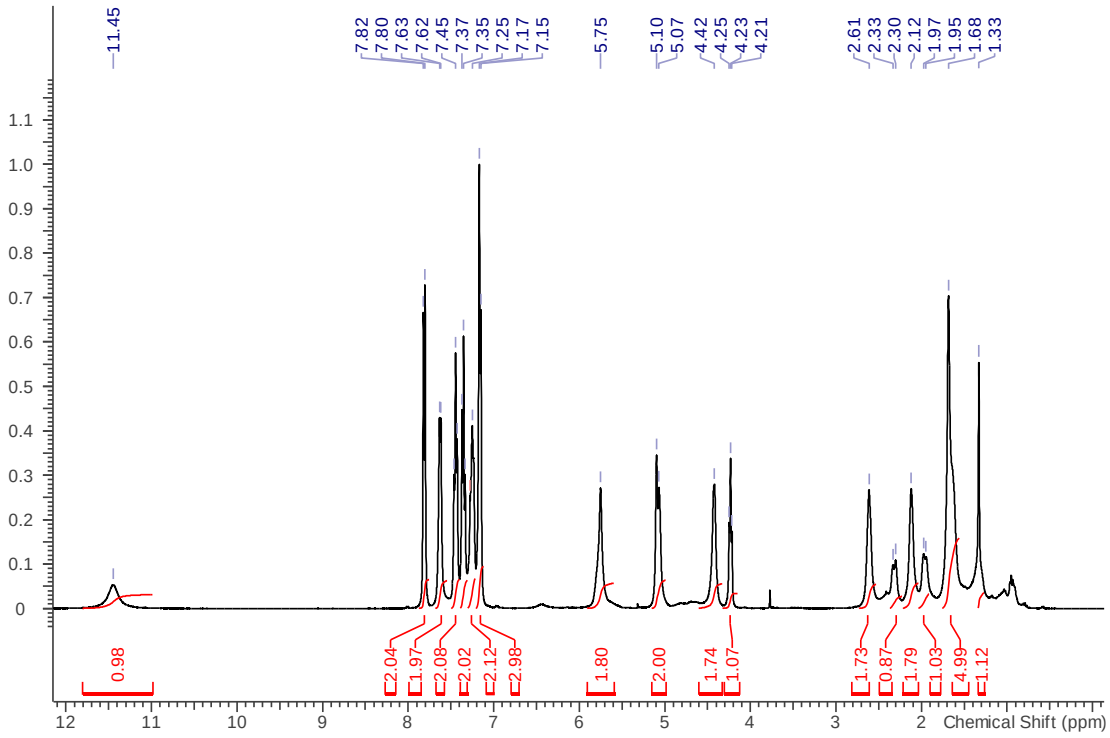

Figure 5.78. ^{13}C NMR spectrum (101 MHz) of **5.15b** in $CDCl_3$

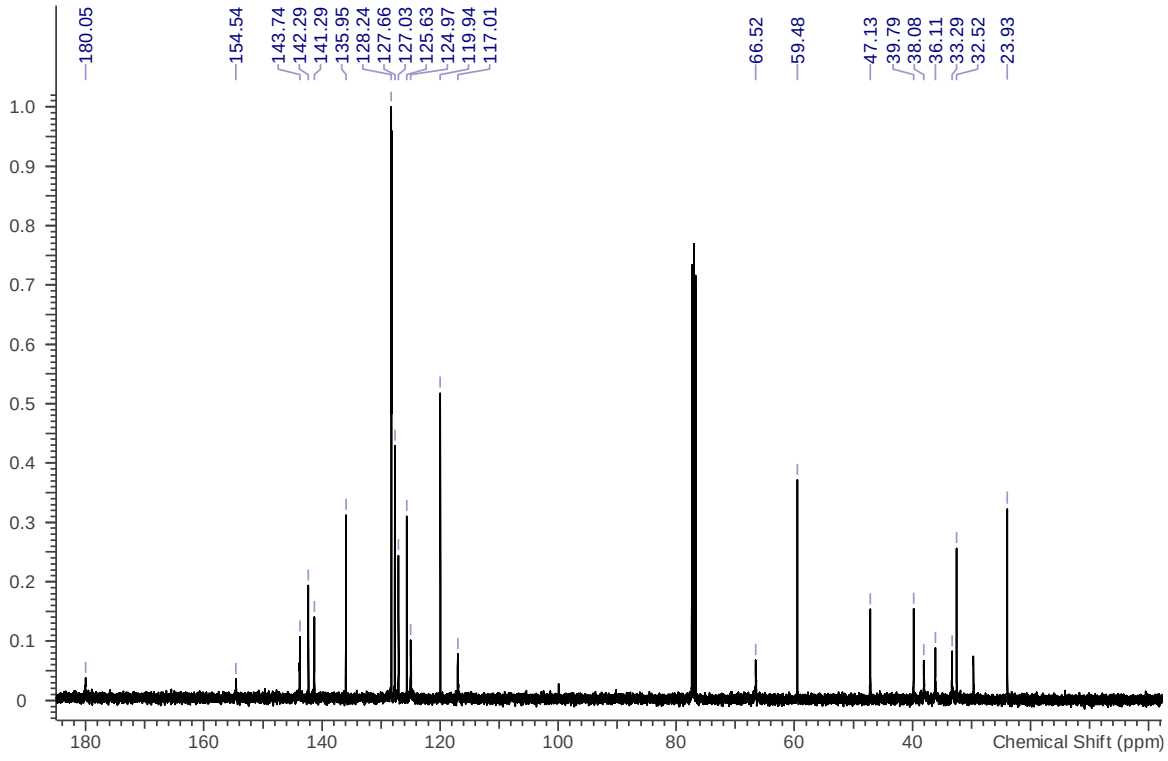

6. Design of a high-throughput screen for natural product inhibitors of estrogen receptor/steroid receptor coactivator interaction.

6.1 Introduction to natural product TR-FRET screen

Gunther et al. previously described a high-throughput time-resolved fluorescence resonance energy transfer (TR-FRET) screening assay for discovery of coactivator binding inhibitors of estrogen receptor/steroid receptor coactivator interactions.[88] TR-FRET uses a time-gated energy transfer step to alleviate assay interference that can be observed in fluorescence-based readouts. The assay requires covalently labeling estrogen receptor with biotin and a steroid receptor coactivator fragment with fluorescein (SRC3-FITC). Incubating the biotinylated estrogen receptor with a streptavidin/Terbium-chelate, estradiol, and SRC3-FITC generates an intact protein complex that, when excited at 340 nm, emits light at the fluorescein emission wavelength (520 nm). Disruption of the complex results in emission at the donor emission wavelength (495 nm). The purpose of incorporating the lanthanide (Tb^{3+}) is because it exhibits a long-lifetime fluorescence to allow for a 100 μs delay before fluorescent signal transfer measurement, at which point fluorescence from potentially interfering screening molecules will be negligible. The original assay was used to screen roughly 86,000 small molecules. In our interest to identify new chemical scaffolds to function as coactivator binding inhibitors (CBIs) we sought to implement this screening approach using natural product libraries.

Within the department of Medicinal Chemistry and Pharmacognosy at UIC, the Orjala and Murphy labs have isolated natural product extracts for use in high throughput screens. The cyanobacteria and actinomycetes used to prepare these libraries are known to produce secondary metabolites, peptides, and polyketides. [150-151] It has been observed

that such large molecular scaffolds are well-suited to inhibit protein-protein interactions that occur over large surface areas.[152] Previously reported protein-protein interaction inhibitors with affinities <1 μM typically have molecular weights over 500 Dalton.[153] In addition, a correlation between number of heavy atoms and binding affinity to protein surface sites has been observed.[153]

Natural product extracts may harbor leads to discover protein-protein interaction inhibitors because the molecules produced by bacteria have been selected to interact with protein targets.[154] For example, salvianolic acid is proposed to bind to the Lck SH2 domain in a structural motif similar to the naturally binding proteins bearing the sequence pYEEI. [155] Previous screens of microbial extracts identified the macrocyclic peptide chlorofusin as a low μM inhibitor of MDM2-p53 and the natural product Emblin was found to bind X-linked inhibitor of apoptosis (XIAP) BIR3 domain and inhibit interactions with Smac and caspase-9.[156] Additionally, many natural products have been selected to be cell permeable.[157-158]

6.2 Development and implementation of TR-FRET screen

ERα and SRC3 fragment were recombinantly expressed and chemically labeled as previously described (Figure 6.1).[71] The binding of the coactivator fragment to ERα was confirmed by measuring TR-FRET signal while SRC3-FITC was titrated into a solution of streptavidin-Tb with or without ERα (Figure 6.2). The K_d for the ERα/SRC3 complex was found to be 11.2 ± 1.5 nM. An 11-residue peptide (Ac-HKILHRLLQDS-NH_2) derived from an “LxxLL” interacting motif of SRC-2 was used as a control peptide to inhibit the protein complex (Figure 6.3). The IC_{50} for the control peptide was 1.05 μM (95% CI

0.78-1.4 μM), which agrees with previously reported findings. [30, 88] Using this control peptide, the assay z-factor was calculated to be 0.91 (Equation 6.1, where μ_p,μ_n and σ_p,σ_n are the means and standard deviations for positive (SP4 peptide, 30 μM) and negative (uninhibited ER/SRC complex) controls).

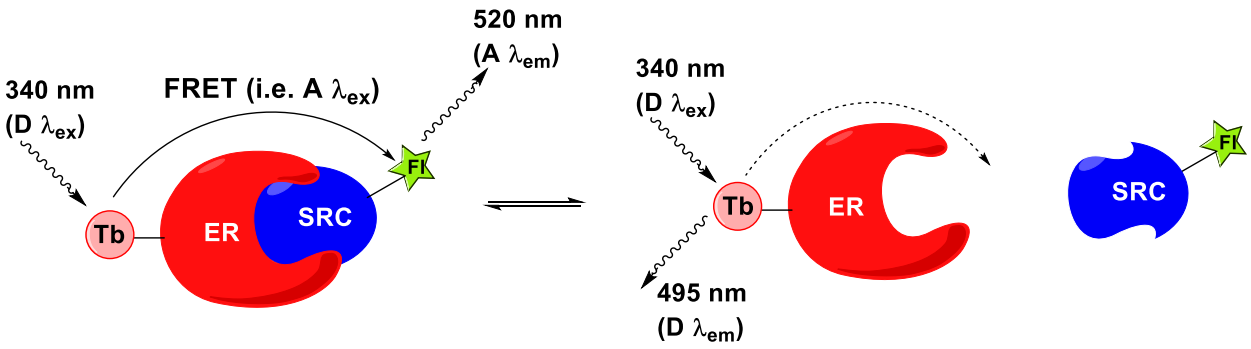

Figure 6.1 TR-FRET assay design. Biotinylated estrogen receptor forms a complex with a streptavidin-terbium chelate. Excitation of Tb at 340 nm will result in fluorescence at 495 nm that can be absorbed and emitted at 520 nm by fluorescein tagged SRC3 fragment if the protein complex is formed.

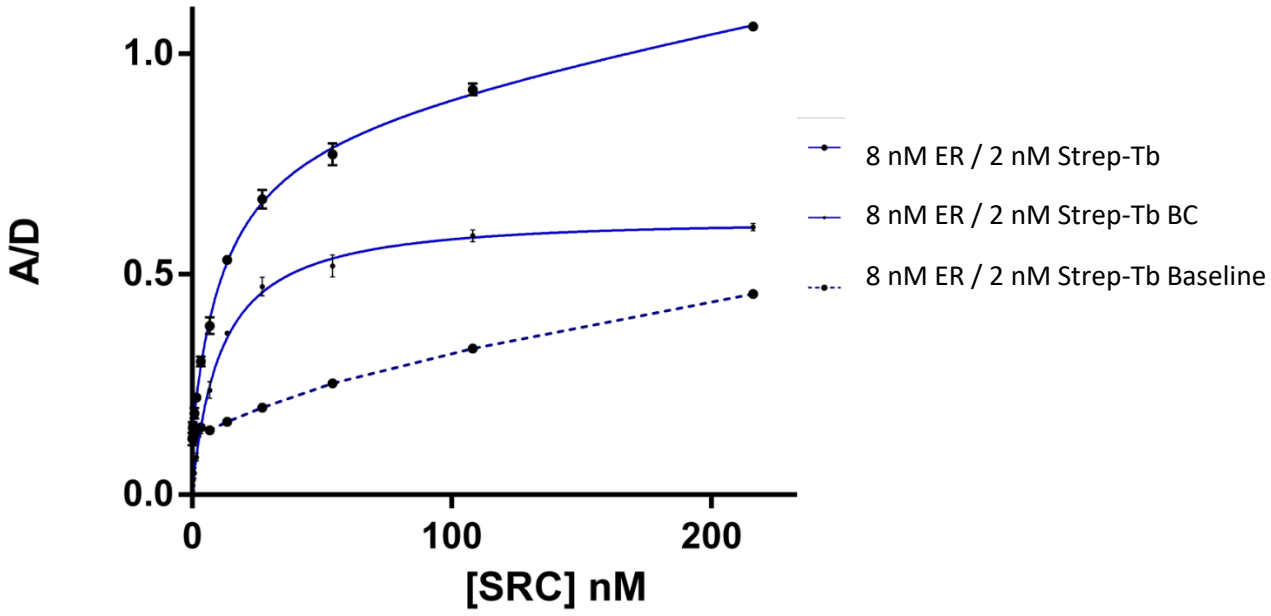

Figure 6.2 Binding affinity of SRC3-FITC to estrogen receptor alpha ligand binding domain. Increasing concentration of SRC3-FITC with 8 nM ERα and 2 nM Streptavidin-Tb with 1 µM estradiol. The dashed line was run with no ERα. The K_d for the baseline corrected (BC) binding curve is 11.2 +/- 1.5 nM.

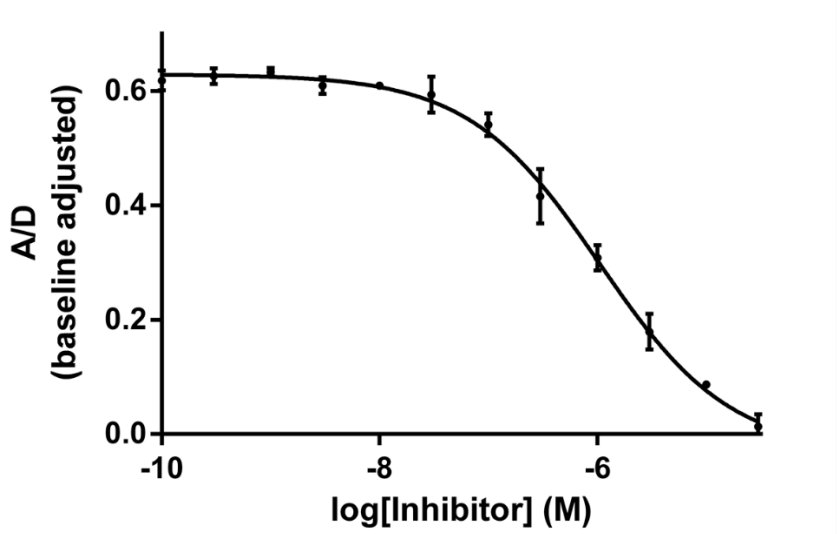

	WT 60 min
Sigmoidal, 4PL, X is log(concentration)	
Best-fit values	
Top	0.6290
Bottom	-0.03221
LogIC50	-5.980
HillSlope	-0.7224
IC50	1.047e-006
Span	0.6612
Std. Error	
Top	0.006955
Bottom	0.02482
LogIC50	0.06400
HillSlope	0.05948
Span	0.02809
95% Confidence Intervals	
Top	0.6148 to 0.6432
Bottom	-0.08280 to 0.01837
LogIC50	-6.110 to -5.849
HillSlope	-0.8437 to -0.6012
IC50	7.757e-007 to 1.414e-006
Span	0.6040 to 0.7185
Goodness of Fit	
Degrees of Freedom	32
R square	0.9906

Figure 6.3 TR-FRET binding curve for competition of ERα/SRC3 interaction with LxxLL peptide. This competition assay shows a dose response decrease in TR-FRET signal of ERα/SRC3 interaction when treated with increasing concentration of peptide inhibitor. The IC_{50} for the LxxLL peptide was measured to be 1 µM. Assay conditions: 25 nM SRC3-FITC, 8 nM ERα, 2 nM Streptavidin-Tb, 1 µM estradiol, 3% DMSO, 60 min incubation, reading at 25 ^{o}C.

Equation 1:

$$Z - factor = 1 - \frac{3(\sigma_p + \sigma_n)}{|\mu_p - \mu_n|}$$

$$Z - factor = 1 - \frac{3(0.008 + 0.01)}{0.455 - 1.08}$$

$$Z - factor = 0.91$$

The TR-FRET assay was used to screen ~3600 natural product extracts obtained from 42 96-well plates (OJ20-43 and BM1-18; Figure 6.4). The extracts were screened at a concentration of 0.05 mg/ml. The extracts from OJ20-43 resulted in 44 hits with inhibition > 50% resulting in a hit-rate of ~1%. The wells showing inhibition over 50% were

rescreened in triplicate and 9 extracts reproduced inhibition > 50%. The Taxon and known chemistry of the producing organisms is listed in Table XXIII. The extracts from BM1-18 resulted in 56 hits with inhibition > 50%, resulting in a hit-rate of ~3% (Table XXIV). The hits from BM1-18 were not confirmed in a triplicate follow-up screen.

The results of the initial screen suggest that the natural product extracts tested may contain chemical matter with high affinity for estrogen receptor coactivator binding groove. To rapidly identify the potential hit compounds, the MagMASS affinity assay may be helpful to bypass traditional approaches such as activity-guided fractionation.[159] The MagMASS assay would rely on immobilizing biotinylated estrogen receptor to streptavidin-coated magnetic beads followed by incubation of lead fractions. Unbound compounds in the incubation mixture can be washed and the bound compounds can be eluted by denaturing the protein. The molecular weights of bound components can be identified using mass spectrometry. In conclusion, a combined effort of TR-FRET screening and MagMASS target identification could prove effective for rapidly identifying natural product leads for inhibiting ER/SRC interactions.

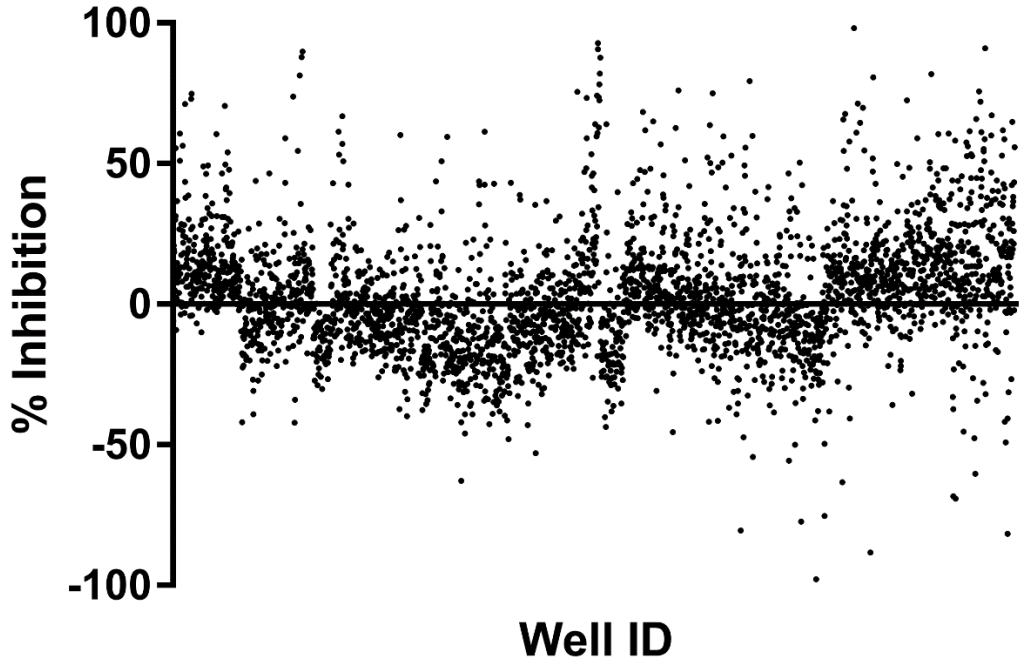

Figure 6.4 TR-FRET screen of OJ43-20 and BM1-18. 3610 microbial natural product extracts were screened at 0.05 mg/mL for inhibition of the ERα/SRC3 interaction. 100% inhibition was set as the TR-FRET reading obtained in the absence of the agonist estradiol. The % inhibition was calculated as a ratio of observed TR-FRET response to the response observed when no interaction is observed.

TABLE XXIII HITS GREATER THAN 50% INHIBITION FROM ORJALA LIBRARY

% Inhibition (triplicate)	% Inhibition (screen)	Well ID	Strain	Fraction Number	Taxon	Known Chemistry
80 ± 3	51	OJ45-C4	10449	F4	Oscillatoriales	Assemblage
71 ± 5	61	OJ45-C5	10449	F3	Oscillatoriales	Assemblage
82 ± 1	72	OJ45-E3	10230	F3	Chroococcales	None
50 ± 3	73	OJ45-E4	10230	F4	Chroococcales	None
62 ± 1	71	OJ43-C4	10250	F3	Nostoc	Merocyclophanes
54 ± 5	54	OJ43-D4	10250	F4	Nostoc	Merocyclophanes
70 ± 3	60	OJ27-G9	10231	F7	Nostoc	None
55 ± 5	74	OJ27-G10	10232	F7	Nostoc	None
56 ± 2	78	OJ27-H9	10231	F8	Nostoc	None

TABLE XXIII. HITS GREATER THAN 50% INHIBITION FROM MURPHY LIBRARY

Well ID	% Inhibition	**Well ID**	% Inhibition	**Well ID**	% Inhibition
BM8-H12	61.99	**BM10-H8**	67.61	**BM17-B7**	70.66
BM8-H3	68.38	**BM11-B5**	57.37	**BM17-C7**	80.91
BM1-C10	65.11	**BM11-D3**	96.96	**BM17-D2**	77.17
BM1-F7	56.84	**BM11-E7**	70.56	**BM17-D7**	65.6
BM2-C11	62.72	**BM11-E2**	60.4	**BM17-D5**	51.49
BM2-D11	76.16	**BM11-F7**	63.89	**BM17-E9**	63.07
BM2-H3	51.27	**BM11-G7**	69.11	**BM17-E5**	59.31
BM3-G12	63.71	**BM11-H3**	98.78	**BM17-E6**	58.4
BM3-H12	75.14	**BM18-C6**	80.88	**BM17-E7**	54.86
BM3-G2	52.25	**BM18-C4**	53.86	**BM17-E10**	54.27
BM3-H2	50.18	**BM12-H3**	70.19	**BM17-E12**	97.15
BM4-D6	50.48	**BM15-D3**	58.76	**BM17-H5**	71.98
BM4-D11	59.69	**BM14-A6**	80.05	**BM17-H2**	64.43
BM4-G8	52.86	**BM17-D3**	57.12	**BM17-H3**	50.63
BM5-D9	55.7	**BM17-B7**	59.03	**BM13-D5**	51.06
BM5-F3	79.42	**BM17-F12**	58.37	**BM13-D8**	60.01
BM5-G3	59.86	**BM17-G5**	56.99	**BM13-H3**	62.97
BM6-H1	50.36	**BM17-H6**	54.41	**BM13-E4**	54.07
BM10-H2	54.96	**BM17-H12**	53.72		

7. CONCLUSIONS

Hormone-activated and constitutively active mutant isoforms of estrogen receptor play a fundamental role in breast cancer disease progression.[160] The genomic response mediated by estrogen receptor is intrinsically tied to coregulator interactions. [15, 161] Biologically active chemical probes that directly block this binding interface continue to remain elusive. Hydrocarbon stapled peptides mimicking steroid receptor coactivators were previously shown to bind to estrogen receptor [30], but no evidence was shown that they could inhibit coactivator binding and disrupt transcriptional activation in cellular assays. Reported within this dissertation are novel strategies to prepare biologically active coactivator binding inhibitors through the enhancement of binding affinity and cellular permeability.[72]

A novel strategy used to enhance binding affinity of stapled peptides to estrogen receptor was realized through the preparation of gamma-methylated stapling amino acids.[71] The inspiration for preparing functionalized stapling amino acids was to replicate naturally occurring amino acids at protein-binding interfaces, specifically the hydrocarbon branching of leucine and isoleucine sidechains. From this work, the ability to enhance target engagement by modifying the structure of stapling amino acids was conclusively established, and the method developed here is currently being expanded to prepare selective inhibitors of mutant estrogen receptor isoforms. Although the peptide modifications reported in this thesis focus on gamma-functionalization, modifications at the beta or delta position could also prove effective. A limitation in the current design strategy is low synthetic throughput which limits facile preparation of high structural

diversity. Approaches to install amine, alkyne, or azide handles on the staple may be useful towards rapidly producing libraries of functionalized stapled peptides.

An array of different cyclizing constraints have been designed to enhance peptide helicity[98]; however, the inclusion of orthogonally prepared macrocycles into a single peptide is less well studied. The development of a computational method to quantify the energetics of helix folding and the design of a new class of “cross-stitched” peptides are reported in chapter 3. The peptide SRC2-BCP1 was prepared with two helical enhancing macrocycles using orthogonal olefin and lactam chemistry. Peptides requiring large amounts of energy to unfold were, in general, more stable to proteolysis. The reported method may find use in developing short peptides with greatly enhanced proteolytic stability. In some examples, stapled peptides have been shown to be taken up by endosomes and reach the cytoplasm through lysosomal escape.[55] Although no studies were performed to measure cellular uptake of bicyclic peptides, the bicyclic peptide SRC2-BCP1 is more stable to degradation, which could result in an enhanced ability to resist lysosomal degradation and accumulate in the cytoplasm. In the future, this bicyclic approach to stabilize peptide helicity could be applied in studying the effect of greatly stabilizing secondary structure on cellular uptake.

Optimizing cell permeability is perhaps the greatest challenge in developing stapled peptides for intracellular targets. In chapter 4, a structure-based computational approach was used to incorporate an Arg_4 sequence into the peptide SP4 to greatly enhance binding affinity and cell permeability. R4K1 is shown to inhibit transcription of ER-regulated native genes by qPCR and reverse estradiol-stimulated proliferation in MCF-7 cells. To confirm the findings, RNA-Seq was used to show that R4K1 globally

reduces E2 gene regulation in MCF-7 cells. An LDH assay was used to asses the cytotoxicity of R4K1 on MCF-7 cells. R4K1 was not significantly toxic at efficacious concentrations; however, toxicity became observable at treatments above 30 μM. The mechanism of toxicity has not been fully elucidated. Moving forward, cellular assays should be designed to determine if the toxicity is mechanism/pathway-dependent or non-specifically mediated through destabilizing membrane integrity.[55] Alternatively, off-target interactions may include other nuclear receptors that are mediated by LxxLL binding motifs.[119] Biotinylated analogs of R4K1 could be used to perform affinity pull-down mass spectrometry on cellular lysates to identify additional binding targets.

Mutant forms of ER have recently been discovered in drug-resistant forms of ER+ breast cancer.[21-22] The most common mutants, D538G and Y537S, provide tumor cells significant resistance to traditional endocrine therapies.[143] In chapter 5, the coactivator binding inhibitor R4K1 was shown to bind with high affinity to the mutant estrogen receptors, and new stapled peptides with even higher affinity are reported. Gamma-substituted stapling amino acids with phenyl, benzyl, and phenethyl substituents were prepared to enhance binding selectivity for mutant receptor D538G. The peptide SP4-SBZ shows the greatest selectivity for D538G at ~6-fold. Additionally, a structure-activity relationship of modifications to R4K1 shows that binding affinity can be enhanced >10-fold by including a gamma-methyl group, lactam bicyclization, and substitution of leucine to cyclohexylalanine within the LxxLL binding pocket. The biological activity of the functionalized peptide R4K1-MCB is currently being investigated. Initial experiments show that the peptides with higher affinity for ER (R4K1-MCB and R4K1-SPE) also induce the highest level of toxicity. An additional correlation is that peptides with higher affinity

are also more hydrophobic. Previous reports suggest hydrophobicity and high positive charge may be correlated with non-specific disruption of membrane integrity.[55] One important approach moving forward will be to develop higher affinity analogs of R4K1 that cause no appreciable toxicity so that the biological effects of higher doses can be characterized in cellular assays. A starting point for generating these peptides may be to perform alanine and aspartic acid scans of R4K1. The peptide library developed from this approach could be tested for affinity and non-specific cell lysis to identify amino acid sites that can be modified to obtain peptides with lower hydrophobicity and decreased positive charge.

Estrogen receptor and steroid receptor coactivators are expressed at elevated levels in breast cancer. Therapies targeting estrogen receptor are often initially effective; however, clinically approved modulators of this protein-protein interaction network lose efficacy in some cases of metastatic cancer. Our hope is that coactivator binding inhibitors such as R4K1 will be more effective at inhibiting the function of ER/SRC interactions in these cases of resistant disease. If proven effective in metastatic models, these chemical probes will validate a mechanistic pathway for inhibiting the growth of ER-positive metastatic breast cancer and serve as a starting point to translate coactivator binding inhibitors towards clinical application.

CITED LITERATURE

1. Howlader, N.; Krapcho, A. N. M.; Miller, D.; Bishop, K.; Altekruse, S. F.; Kosary, C. L.; Yu, M.; Ruhl, J.; Tatalovich, Z.; Mariotto, A.; Lewis, D. R.; Chen, H. S.; Feuer, E. J.; Cronin K. A. SEER Cancer Statistics Review. http://seer.cancer.gov/csr/1975_2013/.

2. Siegel, R. L.; Miller, K. D.; Jemal, A., Cancer statistics, 2016. *CA: Cancer J. Clin.* **2016,** *66*, 7-30.

3. Fan , C.; Oh , D. S.; Wessels , L.; Weigelt , B.; Nuyten , D. S. A.; Nobel , A. B.; van't Veer , L. J.; Perou , C. M., Concordance among Gene-Expression–Based Predictors for Breast Cancer. *N. Engl. J. Med.* **2006,** *355*, 560-569.

4. NCI Drugs Approved for Breast Cancer. https://www.cancer.gov/about-cancer/treatment/drugs/breast (accessed April 15, 2018).

5. Board, P. A. T. E. PDQ Breast Cancer Treatment. http://www.cancer.gov/types/breast/patient/breast-treatment-pdq. (accessed 10/26/2018).

6. Musgrove, E. A.; Sutherland, R. L., Biological determinants of endocrine resistance in breast cancer. *Nat. Rev. Cancer.* **2009,** *9*, 631-643.

7. BreastCancerTrials.org. www.breastcancertrials.org (accessed March 15, 2018).

8. Frasor, J.; Danes, J. M.; Komm, B.; Chang, K. C. N.; Lyttle, C. R.; Katzenellenbogen, B. S., Profiling of Estrogen Up- and Down-Regulated Gene Expression in Human Breast Cancer Cells: Insights into Gene Networks and Pathways Underlying Estrogenic Control of Proliferation and Cell Phenotype. *Endocrinology.* **2003,** *144*, 4562-4574.

9. Carroll, J. S.; Meyer, C. A.; Song, J.; Li, W.; Geistlinger, T. R.; Eeckhoute, J.; Brodsky, A. S.; Keeton, E. K.; Fertuck, K. C.; Hall, G. F.; Wang, Q.; Bekiranov, S.; Sementchenko, V.; Fox, E. A.; Silver, P. A.; Gingeras, T. R.; Liu, X. S.; Brown, M., Genome-wide analysis of estrogen receptor binding sites. *Nature Genet.* **2006,** *38*, 1289.

10. Couse, J. F.; Korach, K. S., Estrogen Receptor Null Mice: What Have We Learned and Where Will They Lead Us? *Endocr. Rev.* **1999,** *20*, 358-417.

11. Shiau, A. K.; Barstad, D.; Loria, P. M.; Cheng, L.; Kushner, P. J.; Agard, D. A.; Greene, G. L., The Structural Basis of Estrogen Receptor/Coactivator Recognition and the Antagonism of This Interaction by Tamoxifen. *Cell.* **1998,** *95*, 927-937.

12. Björnström, L.; Sjöberg, M., Mechanisms of Estrogen Receptor Signaling: Convergence of Genomic and Nongenomic Actions on Target Genes. *Mol. Endocrinol.* **2005,** *19*, 833-842.

13. Osborne, C. K.; Schiff, R., MECHANISMS OF ENDOCRINE RESISTANCE IN BREAST CANCER. *Annu. Rev. Med.* **2011,** *62*, 233-247.

14. De Marchi, T.; Foekens, J. A.; Umar, A.; Martens, J. W. M., Endocrine therapy resistance in estrogen receptor (ER)-positive breast cancer. *Drug Discov. Today.* **2016,** *21*, 1181-1188.

15. Osborne, C. K.; Bardou, V.; Hopp, T. A.; Chamness, G. C.; Hilsenbeck, S. G.; Fuqua, S. A. W.; Wong, J.; Allred, D. C.; Clark, G. M.; Schiff, R., Role of the Estrogen Receptor Coactivator AIB1 (SRC-3) and HER-2/neu in Tamoxifen Resistance in Breast Cancer. *J. Natl. Cancer Inst.* **2003,** *95*, 353-361.

16. Anzick, S. L.; Kononen, J.; Walker, R. L.; Azorsa, D. O.; Tanner, M. M.; Guan, X.-Y.; Sauter, G.; Kallioniemi, O.-P.; Trent, J. M.; Meltzer, P. S., AIB1, a Steroid Receptor Coactivator Amplified in Breast and Ovarian Cancer. *Science.* **1997,** *277*, 965.

17. Shou, J.; Massarweh, S.; Osborne, C. K.; Wakeling, A. E.; Ali, S.; Weiss, H.; Schiff, R., Mechanisms of Tamoxifen Resistance: Increased Estrogen Receptor-HER2/neu Cross-Talk in ER/HER2–Positive Breast Cancer. *J. Natl. Cancer Inst.* **2004,** *96*, 926-935.

18. Lavinsky, R. M.; Jepsen, K.; Heinzel, T.; Torchia, J.; Mullen, T.-M.; Schiff, R.; Del-Rio, A. L.; Ricote, M.; Ngo, S.; Gemsch, J.; Hilsenbeck, S. G.; Osborne, C. K.; Glass, C. K.; Rosenfeld, M. G.; Rose, D. W., Diverse signaling pathways modulate nuclear receptor recruitment of N-CoR and SMRT complexes. *Proc. Natl. Acad. Sci. USA.* **1998,** *95*, 2920-2925.

19. Li, S.; Shen, D.; Shao, J.; Crowder, R.; Liu, W.; Prat, A.; He, X.; Liu, S.; Hoog, J.; Lu, C.; Ding, L.; Griffith, O. L.; Miller, C.; Larson, D.; Fulton, R. S.; Harrison, M.; Mooney, T.; McMichael, J. F.; Luo, J.; Tao, Y.; Goncalves, R.; Schlosberg, C.; Hiken, J. F.; Saied, L.; Sanchez, C.; Giuntoli, T.; Bumb, C.; Cooper, C.; Kitchens, R. T.; Lin, A.; Phommaly, C.; Davies, S. R.; Zhang, J.; Kavuri, M. S.; McEachern, D.; Dong, Y. Y.; Ma, C.; Pluard, T.; Naughton, M.; Bose, R.; Suresh, R.; McDowell, R.; Michel, L.; Aft, R.; Gillanders, W.; DeSchryver, K.; Wilson, R. K.; Wang, S.; Mills, G. B.; Gonzalez-Angulo, A.; Edwards, J. R.; Maher, C.; Perou, C. M.; Mardis, E. R.; Ellis, M. J., Endocrine-therapy-resistant ESR1 variants revealed by genomic characterization of breast-cancer-derived xenografts. *Cell Rep.* **2013,** *4*, 1116-30.

20. Merenbakh-Lamin, K.; Ben-Baruch, N.; Yeheskel, A.; Dvir, A.; Soussan-Gutman, L.; Jeselsohn, R.; Yelensky, R.; Brown, M.; Miller, V. A.; Sarid, D.; Rizel, S.; Klein, B.; Rubinek, T.; Wolf, I., D538G mutation in estrogen receptor-alpha: A novel mechanism for acquired endocrine resistance in breast cancer. *Cancer Res.* **2013,** *73*, 6856-64.

21. Robinson, D. R.; Wu, Y. M.; Vats, P.; Su, F.; Lonigro, R. J.; Cao, X.; Kalyana-Sundaram, S.; Wang, R.; Ning, Y.; Hodges, L.; Gursky, A.; Siddiqui, J.; Tomlins, S. A.; Roychowdhury, S.; Pienta, K. J.; Kim, S. Y.; Roberts, J. S.; Rae, J. M.; Van Poznak, C. H.; Hayes, D. F.; Chugh, R.; Kunju, L. P.; Talpaz, M.; Schott, A. F.; Chinnaiyan, A. M., Activating ESR1 mutations in hormone-resistant metastatic breast cancer. *Nature Genet.* **2013,** *45*, 1446-51.

22. Toy, W.; Shen, Y.; Won, H.; Green, B.; Sakr, R. A.; Will, M.; Li, Z.; Gala, K.; Fanning, S.; King, T. A.; Hudis, C.; Chen, D.; Taran, T.; Hortobagyi, G.; Greene, G.; Berger, M.; Baselga, J.; Chandarlapaty, S., ESR1 ligand-binding domain mutations in hormone-resistant breast cancer. *Nature Genet.* **2013,** *45*, 1439-45.

23. Harrod, A.; Fulton, J.; Nguyen, V. T. M.; Periyasamy, M.; Ramos-Garcia, L.; Lai, C. F.; Metodieva, G.; de Giorgio, A.; Williams, R. L.; Santos, D. B.; Gomez, P. J.; Lin, M. L.; Metodiev, M. V.; Stebbing, J.; Castellano, L.; Magnani, L.; Coombes, R. C.; Buluwela, L.; Ali, S., Genomic modelling of the ESR1 Y537S mutation for evaluating function and new therapeutic approaches for metastatic breast cancer. *Oncogene.* **2016,** *36*, 2286.

24. Bahreini, A.; Li, Z.; Wang, P.; Levine, K. M.; Tasdemir, N.; Cao, L.; Weir, H. M.; Puhalla, S. L.; Davidson, N. E.; Stern, A. M.; Chu, D.; Park, B. H.; Lee, A. V.; Oesterreich, S., Mutation site and context dependent effects of ESR1 mutation in genome-edited breast cancer cell models. *Breast Cancer Res.* **2017,** *19*, 60.

25. Fanning, S. W.; Mayne, C. G.; Dharmarajan, V.; Carlson, K. E.; Martin, T. A.; Novick, S. J.; Toy, W.; Green, B.; Panchamukhi, S.; Katzenellenbogen, B. S.; Tajkhorshid, E.; Griffin, P. R.; Shen, Y.; Chandarlapaty, S.; Katzenellenbogen, J. A.; Greene, G. L., Estrogen receptor alpha somatic mutations Y537S and D538G confer breast cancer endocrine resistance by stabilizing the activating function-2 binding conformation. *eLife.* **2016,** *5*, e12792.

26. Moore, T. W.; Mayne, C. G.; Katzenellenbogen, J. A., Minireview: Not Picking Pockets: Nuclear Receptor Alternate-Site Modulators (NRAMs). *Mol. Endocrinol.* **2010,** *24*, 683-695.

27. LaFrate, A. L.; Gunther, J. R.; Carlson, K. E.; Katzenellenbogen, J. A., Synthesis and biological evaluation of guanylhydrazone coactivator binding inhibitors for the estrogen receptor. *Bioorg. Med. Chem.* **2008,** *16*, 10075-10084.

28. Weiser, P. T.; Williams, A. B.; Chang, C.-Y.; McDonnell, D. P.; Hanson, R. N., 3,3′-Disubstituted bipolar biphenyls as inhibitors of nuclear receptor coactivator binding. *Bioorg. Med. Chem. Lett.* **2012,** *22*, 6587-6590.

29. Rodriguez, A. L.; Tamrazi, A.; Collins, M. L.; Katzenellenbogen, J. A., Design, Synthesis, and in Vitro Biological Evaluation of Small Molecule Inhibitors of Estrogen Receptor α Coactivator Binding. *J. Med. Chem.* **2004,** *47*, 600-611.

30. Phillips, C.; Roberts, L. R.; Schade, M.; Bazin, R.; Bent, A.; Davies, N. L.; Moore, R.; Pannifer, A. D.; Pickford, A. R.; Prior, S. H.; Read, C. M.; Scott, A.; Brown, D. G.; Xu, B.; Irving, S. L., Design and structure of stapled peptides binding to estrogen receptors. *J. Am. Chem. Soc.* **2011,** *133*, 9696.

31. Carraz, M.; Zwart, W.; Phan, T.; Michalides, R.; Brunsveld, L., Perturbation of estrogen receptor alpha localization with synthetic nona-arginine LXXLL-peptide coactivator binding inhibitors. *Chem. Biol.* **2009,** *16*, 702-11.

32. Galande, A. K.; Bramlett, K. S.; Trent, J. O.; Burris, T. P.; Wittliff, J. L.; Spatola, A. F., Potent Inhibitors of LXXLL-Based Protein–Protein Interactions. *ChemBioChem.* **2005,** *6*, 1991-1998.

33. Johnson, A. B.; O'Malley, B. W., Steroid receptor coactivators 1, 2, and 3: critical regulators of nuclear receptor activity and steroid receptor modulator (SRM)-based cancer therapy. *Mol. Cell. Endocrinol.* **2012,** *348*, 430-9.

34. Yi, P.; Wang, Z.; Feng, Q.; Pintilie, G. D.; Foulds, C. E.; Lanz, R. B.; Ludtke, S. J.; Schmid, M. F.; Chiu, W.; O'Malley, B. W., The Structure of A Biologically Active Estrogen Receptor-Coactivator Complex on DNA. *Mol. Cell.* **2015,** *57*, 1047-1058.

35. Chang, C.-y.; Norris, J. D.; Grøn, H.; Paige, L. A.; Hamilton, P. T.; Kenan, D. J.; Fowlkes, D.; McDonnell, D. P., Dissection of the LXXLL Nuclear Receptor-Coactivator Interaction Motif Using Combinatorial Peptide Libraries: Discovery of Peptide Antagonists of Estrogen Receptors α and β. *Mol. Cell. Biol.* **1999,** *19*, 8226-8239.

36. Sheppard, H. M.; Harries, J. C.; Hussain, S.; Bevan, C.; Heery, D. M., Analysis of the steroid receptor coactivator 1 (SRC1)-CREB binding protein interaction interface and its importance for the function of SRC1. *Mol. Cell. Biol.* **2001,** *21*, 39-50.

37. Raj, G. V.; Sareddy, G. R.; Ma, S.; Lee, T.-K.; Viswanadhapalli, S.; Li, R.; Liu, X.; Murakami, S.; Chen, C.-C.; Lee, W.-R.; Mann, M.; Krishnan, S. R.; Manandhar, B.; Gonugunta, V. K.; Strand, D.; Tekmal, R. R.; Ahn, J.-M.; Vadlamudi, R. K., Estrogen receptor coregulator binding modulators (ERXs) effectively target estrogen receptor positive human breast cancers. *eLife.* **2017,** *6*, e26857.

38. Sun, A.; Moore, T. W.; Gunther, J. R.; Kim, M.-S.; Rhoden, E.; Du, Y.; Fu, H.; Snyder, J. P.; Katzenellenbogen, J. A., Discovering Small-Molecule Estrogen Receptor α/Coactivator Binding Inhibitors: High-Throughput Screening, Ligand Development, and Models for Enhanced Potency. *ChemMedChem.* **2011,** *6*, 654-666.

39. Heery, D. M.; Kalkhoven, E.; Hoare, S.; Parker, M. G., A signature motif in transcriptional co-activators mediates binding to nuclear receptors. *Nature.* **1997,** *387*, 733-736.

40. Leduc, A.-M.; Trent, J. O.; Wittliff, J. L.; Bramlett, K. S.; Briggs, S. L.; Chirgadze, N. Y.; Wang, Y.; Burris, T. P.; Spatola, A. F., Helix-stabilized cyclic peptides as selective inhibitors of steroid receptor–coactivator interactions. *Proc. Natl. Acad. Sci. USA.* **2003,** *100*, 11273.

41. Galande, A. K.; Bramlett, K. S.; Burris, T. P.; Wittliff, J. L.; Spatola, A. F., Thioether side chain cyclization for helical peptide formation: inhibitors of estrogen receptor–coactivator interactions. *J. Peptide Res.* **2004,** *63*, 297-302.

42. Geistlinger, T. R.; Guy, R. K., Novel Selective Inhibitors of the Interaction of Individual Nuclear Hormone Receptors with a Mutually Shared Steroid Receptor Coactivator 2. *J. Am. Chem. Soc.* **2003,** *125*, 6852-6853.

43. Schafmeister, C. E.; Po, J.; Verdine, G. L., An All-Hydrocarbon Cross-Linking System for Enhancing the Helicity and Metabolic Stability of Peptides. *J. Am. Chem. Soc.* **2000,** *122*, 5891-5892.

44. Walensky, L. D.; Kung, A. L.; Escher, I.; Malia, T. J.; Barbuto, S.; Wright, R. D.; Wagner, G.; Verdine, G. L.; Korsmeyer, S. J., Activation of apoptosis in vivo by a hydrocarbon-stapled BH3 helix. *Science.* **2004,** *305*, 1466-70.

45. Moellering, R. E.; Cornejo, M.; Davis, T. N.; Del Bianco, C.; Aster, J. C.; Blacklow, S. C.; Kung, A. L.; Gilliland, D. G.; Verdine, G. L.; Bradner, J. E., Direct inhibition of the NOTCH transcription factor complex. *Nature.* **2009,** *462*, 182-8.

46. Sinclair, J. K.; Schepartz, A., Influence of macrocyclization on allosteric, juxtamembrane-derived, stapled peptide inhibitors of the epidermal growth factor receptor (EGFR). *Org. Lett.* **2014,** *16*, 4916.

47. Wang, Y.; Ho, T. G.; Bertinetti, D.; Neddermann, M.; Franz, E.; Mo, G. C.; Schendowich, L. P.; Sukhu, A.; Spelts, R. C.; Zhang, J.; Herberg, F. W.; Kennedy, E. J., Isoform-selective disruption of AKAP-localized PKA using hydrocarbon stapled peptides. *ACS Chem. Biol.* **2014,** *9*, 635.

48. Leshchiner, E. S.; Parkhitko, A.; Bird, G. H.; Luccarelli, J.; Bellairs, J. A.; Escudero, S.; Opoku-Nsiah, K.; Godes, M.; Perrimon, N.; Walensky, L. D., Direct inhibition of oncogenic KRAS by hydrocarbon-stapled SOS1 helices. *Proc. Natl. Acad. Sci. USA.* **2015,** *112*, 1761-6.

49. Wachter, F.; Morgan, A. M.; Godes, M.; Mourtada, R.; Bird, G. H.; Walensky, L. D., Mechanistic validation of a clinical lead stapled peptide that reactivates p53 by dual HDM2 and HDMX targeting. *Oncogene.* **2016**.

50. McGrath, S.; Tortorici, M.; Drouin, L.; Solanki, S.; Vidler, L.; Westwood, I.; Gimeson, P.; Van Montfort, R.; Hoelder, S., Structure-Enabled Discovery of a Stapled Peptide Inhibitor to Target the Oncogenic Transcriptional Repressor TLE1. *Chem. Euro. J.* **2017,** *23*, 9577.

51. Mitra, S.; Montgomery, J. E.; Kolar, M. J.; Li, G.; Jeong, K. J.; Peng, B.; Verdine, G. L.; Mills, G. B.; Moellering, R. E., Stapled peptide inhibitors of RAB25 target context-specific phenotypes in cancer. *Nat. Commun.* **2017,** *8*, 660.

52. Dietrich, L.; Rathmer, B.; Ewan, K.; Bange, T.; Heinrichs, S.; Dale, T. C.; Schade, D.; Grossmann, T. N., Cell Permeable Stapled Peptide Inhibitor of Wnt Signaling that Targets β-Catenin Protein-Protein Interactions. *Cell Chem. Biol.* **2017,** *24*, 958-968.

53. Walensky, L. D.; Bird, G. H., Hydrocarbon-stapled peptides: principles, practice, and progress. *J. Med. Chem.* **2014,** *57*, 6275-88.

54. All-hydrocarbon stapled peptides as Synthetic Cell-Accessible Mini-Proteins. *Drug Discov. Today. Technol.* **2012,** *9*, e1-e70.

55. Bird, G. H.; Mazzola, E.; Opoku-Nsiah, K.; Lammert, M. A.; Godes, M.; Neuberg, D. S.; Walensky, L. D., Biophysical determinants for cellular uptake of hydrocarbon-stapled peptide helices. *Nat. Chem. Biol.* **2016,** *12*, 845-852.

56. Verdine, G. L.; Hilinski, G. J., Stapled peptides for intracellular drug targets. *Methods Enzymol.* **2012,** *503*, 3-33.

57. Bernal, F.; Katz, S. G., Synthesis of Stabilized Alpha-Helical Peptides. In *Cancer Genomics and Proteomics: Methods and Protocols*, Wajapeyee, N., Ed. Springer New York: New York, NY, 2014; pp 107-114.

58. Bird, G. H.; Crannell, W. C.; Walensky, L. D., Chemical Synthesis of Hydrocarbon-Stapled Peptides for Protein Interaction Research and Therapeutic Targeting. *Curr. Protoc. Chem. Biol.* **2011,** *3*, 99-117.

59. Kim, Y.-W.; Grossmann, T. N.; Verdine, G. L., Synthesis of all-hydrocarbon stapled α-helical peptides by ring-closing olefin metathesis. *Nature Protocols* **2011,** *6*, 761.

60. Yeo, D. J.; Warriner, S. L.; Wilson, A. J., Monosubstituted alkenyl amino acids for peptide "stapling". *Chem. Commun.* **2013,** *49*, 9131-3.

61. Hilinski, G. J.; Kim, Y.-W.; Hong, J.; Kutchukian, P. S.; Crenshaw, C. M.; Berkovitch, S. S.; Chang, A.; Ham, S.; Verdine, G. L., Stitched α-Helical Peptides via Bis Ring-Closing Metathesis. *J. Am. Chem. Soc.* **2014,** *136*, 12314-12322.

62. Li, Y.-C.; Rodewald, Luo W.; Hoppmann, C.; Wong, Ee T.; Lebreton, S.; Safar, P.; Patek, M.; Wang, L.; Wertman, Kenneth F.; Wahl, Geoffrey M., A Versatile Platform to Analyze Low-Affinity and Transient Protein-Protein Interactions in Living Cells in Real Time. *Cell Rep.* **2014,** *9*, 1946-1958.

63. Chu, Q.; Moellering, R. E.; Hilinski, G. J.; Kim, Y.-W.; Grossmann, T. N.; Yeh, J. T. H.; Verdine, G. L., Towards understanding cell penetration by stapled peptides. *Med. Chem. Commun.* **2015,** *6*, 111-119.

64. Gaillard, V.; Galloux, M.; Garcin, D.; Eléouët, J.-F.; Le Goffic, R.; Larcher, T.; Rameix-Welti, M.-A.; Boukadiri, A.; Héritier, J.; Segura, J.-M.; Baechler, E.; Arrell, M.; Mottet-Osman, G.; Nyanguile, O., A Short Double-Stapled Peptide Inhibits Respiratory Syncytial Virus Entry and Spreading. *Antimicrob. Agents Chemother.* **2017,** *61*.

65. Wang, C.; Xia, S.; Zhang, P.; Zhang, T.; Wang, W.; Tian, Y.; Meng, G.; Jiang, S.; Liu, K., Discovery of Hydrocarbon-Stapled Short α-Helical Peptides as Promising Middle East Respiratory Syndrome Coronavirus (MERS-CoV) Fusion Inhibitors. *J. Med. Chem.* **2018,** *61*, 2018-2026.

66. Luong, H. X.; Kim, D.-H.; Lee, B.-J.; Kim, Y.-W., Antimicrobial activity and stability of stapled helices of polybia-MP1. *Archives Pharma. Res.* **2017,** *40*, 1414-1419.

67. KleinJan, A.; Tindemans, I.; Montgomery, J. E.; Lukkes, M.; de Bruijn, M. J. W.; van Nimwegen, M.; Bergen, I.; Moellering, R. E.; Hoogsteden, H. C.; Boon, L.; Amsen, D.; Hendriks, R. W., The Notch pathway inhibitor stapled α-helical peptide derived from mastermind-like 1 (SAHM1) abrogates the hallmarks of allergic asthma. *J. Allergy Clin. Immunol.* **2017**.

68. Yang, P.; Zou, H.; Lee, C.; Muppidi, A.; Chao, E.; Fu, Q.; Luo, X.; Wang, D.; Schultz, P. G.; Shen, W., A Stapled, Long-Acting Glucagon-like Peptide 2 Analog with Efficacy in Dextran Sodium Sulfate-Induced Mouse Colitis Models. *J. Med. Chem.* **2018**. DOI: 10.1021/acs.jmedchem.7b00768.

69. Rezaei Araghi, R.; Bird, G. H.; Ryan, J. A.; Jenson, J. M.; Godes, M.; Pritz, J. R.; Grant, R. A.; Letai, A.; Walensky, L. D.; Keating, A. E., Iterative optimization yields Mcl-1–targeting stapled peptides with selective cytotoxicity to Mcl-1–dependent cancer cells. *Proc. Natl. Acad. Sci. USA.* **2018,** *115*, E886-E895.

70. Wu, Y.; Villa, F.; Maman, J.; Lau, Y. H.; Dobnikar, L.; Simon, A. C.; Labib, K.; Spring, D. R.; Pellegrini, L., Targeting the Genome-Stability Hub Ctf4 by Stapled-Peptide Design. *Angew. Chem.* **2017,** *129*, 13046-13052.

71. Speltz, T. E.; Fanning, S. W.; Mayne, C. G.; Fowler, C.; Tajkhorshid, E.; Greene, G. L.; Moore, T. W., Stapled Peptides with γ-Methylated Hydrocarbon Chains for the Estrogen Receptor/Coactivator Interaction. *Angew. Chem. Int. Ed.* **2016**, *55*, 4252-4255.

72. Speltz, T. E.; Danes, J. M.; Stender, J. D.; Frasor, J.; Moore, T. W., A Cell-Permeable Stapled Peptide Inhibitor of the Estrogen Receptor/Coactivator Interaction. *ACS Chem. Biol.* **2018,** *13*, 676-684.

73. John, K. C.; Yong, T.; Bendzunas, N. G.; Roxan, A.; Ali, S. A.; Eileen, J. K., Suppression of Breast Cancer Metastasis Using Stapled Peptides Targeting the WASF Regulatory Complex. *Cancer Growth Metastasis.* **2017,** *10*, 1-9.

74. Yoshimaru, T.; Aihara, K.; Komatsu, M.; Matsushita, Y.; Okazaki, Y.; Toyokuni, S.; Honda, J.; Sasa, M.; Miyoshi, Y.; Otaka, A.; Katagiri, T., Stapled BIG3 helical peptide ERAP potentiates anti-tumour activity for breast cancer therapeutics. *Sci. Rep.* **2017,** *7*, 1821.

75. Kim, Y.-W.; Grossmann, T. N.; Verdine, G. L., Synthesis of all-hydrocarbon stapled [alpha]-helical peptides by ring-closing olefin metathesis. *Nat. Protoc.* **2011,** *6*, 761-771.

76. Douse, C. H.; Maas, S. J.; Thomas, J. C.; Garnett, J. A.; Sun, Y.; Cota, E.; Tate, E. W., Crystal Structures of Stapled and Hydrogen Bond Surrogate Peptides Targeting a Fully Buried Protein–Helix Interaction. *ACS Chem. Biol.* **2014,** *9*, 2204-2209.

77. Chang, Y. S.; Graves, B.; Guerlavais, V.; Tovar, C.; Packman, K.; To, K.-H.; Olson, K. A.; Kesavan, K.; Gangurde, P.; Mukherjee, A.; Baker, T.; Darlak, K.; Elkin, C.; Filipovic, Z.; Qureshi, F. Z.; Cai, H.; Berry, P.; Feyfant, E.; Shi, X. E.; Horstick, J.; Annis, D. A.; Manning, A. M.; Fotouhi, N.; Nash, H.; Vassilev, L. T.; Sawyer, T. K., Stapled α−helical peptide drug development: A potent dual inhibitor of MDM2 and MDMX for p53-dependent cancer therapy. *Proc. Natl. Acad. Sci. USA.* **2013,** *110*, E3445-E3454.

78. Glas, A.; Bier, D.; Hahne, G.; Rademacher, C.; Ottmann, C.; Grossmann, T. N., Constrained Peptides with Target-Adapted Cross-Links as Inhibitors of a Pathogenic Protein–Protein Interaction. *Angew. Chem. Int. Ed.* **2014,** *53*, 2489-2493.

79. Baek, S.; Kutchukian, P. S.; Verdine, G. L.; Huber, R.; Holak, T. A.; Lee, K. W.; Popowicz, G. M., Structure of the Stapled p53 Peptide Bound to Mdm2. *J. Am. Chem. Soc.* **2012,** *134*, 103-106.

80. Stewart, M. L.; Fire, E.; Keating, A. E.; Walensky, L. D., The MCL-1 BH3 helix is an exclusive MCL-1 inhibitor and apoptosis sensitizer. *Nat. Chem. Biol.* **2010,** *6*, 595-601.

81. Fuchs, S.; Nguyen, H. D.; Phan, T. T. P.; Burton, M. F.; Nieto, L.; de Vries-van Leeuwen, I. J.; Schmidt, A.; Goodarzifard, M.; Agten, S. M.; Rose, R.; Ottmann, C.; Milroy, L.-G.; Brunsveld, L., Proline Primed Helix Length as a Modulator of the Nuclear Receptor–Coactivator Interaction. *J. Am. Chem. Soc.* **2013,** *135*, 4364-4371.

82. Caboni, L.; Lloyd, D. G., Beyond the Ligand-Binding Pocket: Targeting Alternate Sites in Nuclear Receptors. *Medicinal Research Reviews* **2013,** *33* (5), 1081-1118.

83. Schöllkopf, U., Enantioselective synthesis of non-proteinogenic amino acids via metallated bis-lactim ethers of 2,5-diketopiperazines. *Tetrahedron.* **1983,** *39*, 2085-2091.

84. Evans, D. A.; Ennis, M. D.; Mathre, D. J., Asymmetric alkylation reactions of chiral imide enolates. A practical approach to the enantioselective synthesis of .alpha.-substituted carboxylic acid derivatives. *J. Am. Chem. Soc.* **1982,** *104*, 1737-1739.

85. Shapiro, G.; Buechler, D.; Marzi, M.; Schmidt, K.; Gomez-Lor, B., A Versatile Asymmetric Synthesis of .beta.-Branched .alpha.-Amino Acids. *J. Org. Chem.* **1995,** *60*, 4978-4979.

86. Brown, A. C.; Carpino, L. A., Magnesium in methanol: substitute for sodium amalgam in desulfonylation reactions. *J. Org. Chem.* **1985,** *50*, 1749-1750.

87. Nájera, C.; Yus, M., Desulfonylation reactions: Recent developments. *Tetrahedron.* **1999,** *55*, 10547-10658.

88. Gunther, J. R.; Du, Y.; Rhoden, E.; Lewis, I.; Revennaugh, B.; Moore, T. W.; Kim, S. H.; Dingledine, R.; Fu, H.; Katzenellenbogen, J. A., A set of time-resolved fluorescence resonance energy transfer assays for the discovery of inhibitors of estrogen receptor-coactivator binding. *J. Biomol. Screen.* **2009,** *14*, 181-93.

89. Nettles, K. W.; Bruning, J. B.; Gil, G.; Nowak, J.; Sharma, S. K.; Hahm, J. B.; Kulp, K.; Hochberg, R. B.; Zhou, H.; Katzenellenbogen, J. A.; Katzenellenbogen, B. S.; Kim, Y.; Joachmiak, A.; Greene, G. L., NFκB selectivity of estrogen receptor ligands revealed by comparative crystallographic analyses. *Nat. Chem. Biol.* **2008,** *4*, 241-247.

90. Phillips, J. C.; Braun, R.; Wang, W.; Gumbart, J.; Tajkhorshid, E.; Villa, E.; Chipot, C.; Skeel, R. D.; Kalé, L.; Schulten, K., Scalable molecular dynamics with NAMD. *J. Comput. Chem.* **2005,** *26*, 1781-1802.

91. Humphrey, W.; Dalke, A.; Schulten, K., VMD: Visual molecular dynamics. *J. Mol. Graphics.* **1996,** *14*, 33-38.

92. Kim, Y. W.; Grossmann, T. N.; Verdine, G. L., Synthesis of all-hydrocarbon stapled alpha-helical peptides by ring-closing olefin metathesis. *Nat. Protoc.* **2011,** *6*, 761-71.

93. Evans, D. A.; DiMare, M., Asymmetric synthesis of premonensin, a potential intermediate in the biosynthesis of monensin. *J. Am. Chem. Soc.* **1986,** *108*, 2476-2478.

94. Schöllkopf, U.; Groth, U.; Deng, C., Enantioselective Syntheses of (R)-Amino Acids Using L-Valine as Chiral Agent. *Angew. Chem. Int. Ed.* **1981,** *20*, 798-799.

95. Bird, G. H.; Madani, N.; Perry, A. F.; Princiotto, A. M.; Supko, J. G.; He, X.; Gavathiotis, E.; Sodroski, J. G.; Walensky, L. D., Hydrocarbon double-stapling remedies the proteolytic instability of a lengthy peptide therapeutic. *Proc. Natl. Acad. Sci. USA.* **2010,** *107*, 14093-8.

96. Gaillard, V.; Galloux, M.; Garcin, D.; Eléouët, J.-F.; Le Goffic, R.; Larcher, T.; Rameix-Welti, M.-A.; Boukadiri, A.; Héritier, J.; Segura, J.-M., A short double-stapled peptide inhibits respiratory syncytial virus entry and spreading. *Antimicrob. Agents Chemother.* **2017,** *61*, e02241-16.

97. Cromm, P. M.; Spiegel, J.; Küchler, P.; Dietrich, L.; Kriegesmann, J.; Wendt, M.; Goody, R. S.; Waldmann, H.; Grossmann, T. N., Protease-Resistant and Cell-Permeable Double-Stapled Peptides Targeting the Rab8a GTPase. *ACS Chem. Biol.* **2016,** *11*, 2375-2382.

98. Lau, Y. H.; de Andrade, P.; Wu, Y.; Spring, D. R., Peptide stapling techniques based on different macrocyclisation chemistries. *Chem. Soc. Rev.* **2015,** *44*, 91-102.

99. Norris, J. D.; Paige, L. A.; Christensen, D. J.; Chang, C.-Y.; Huacani, M. R.; Fan, D.; Hamilton, P. T.; Fowlkes, D. M.; McDonnell, D. P., Peptide Antagonists of the Human Estrogen Receptor. *Science.* **1999,** *285*, 744-746.

100. Xie, M.; Zhao, H.; Liu, Q.; Zhu, Y.; Yin, F.; Liang, Y.; Jiang, Y.; Wang, D.; Hu, K.; Qin, X.; Wang, Z.; Wu, Y.; Xu, N.; Ye, X.; Wang, T.; Li, Z., Structural Basis of Inhibition of ERα-Coactivator Interaction by High-Affinity N-Terminus Isoaspartic Acid Tethered Helical Peptides. *J. Med. Chem.* **2017,** *60*, 8731-8740.

101. Marqusee, S.; Baldwin, R. L., Helix stabilization by Glu-... Lys+ salt bridges in short peptides of de novo design. *Proc. Natl. Acad. Sci.* **1987,** *84*, 8898-8902.

102. Lyu, P. C.; Gans, P. J.; Kallenbach, N. R., Energetic contribution of solvent-exposed ion pairs to alpha-helix structure. *J. Mol. Biol.* **1992,** *223*, 343-350.

103. Moradi, M.; Tajkhorshid, E., Computational Recipe for Efficient Description of Large-Scale Conformational Changes in Biomolecular Systems. *J. Chem. Theo. Comput.* **2014,** *10*, 2866-2880.

104. de Araujo, A. D.; Hoang, H. N.; Kok, W. M.; Diness, F.; Gupta, P.; Hill, T. A.; Driver, R. W.; Price, D. A.; Liras, S.; Fairlie, D. P., Comparative α-Helicity of Cyclic Pentapeptides in Water. *Angew. Chem.* **2014,** *126*, 7085-7089.

105. Luo, P.; Baldwin, R. L., Mechanism of Helix Induction by Trifluoroethanol: A Framework for Extrapolating the Helix-Forming Properties of Peptides from Trifluoroethanol/Water Mixtures Back to Water. *Biochemistry.* **1997,** *36*, 8413-8421.

106. Morihara, K.; Tsuzuki, H., Specificity of Proteinase K from Tritirachium album Limber for Synthetic Peptides. *Agricult. Biol. Chem.* **1975,** *39*, 1489-1492.

107. MacKerell, A. D.; Bashford, D.; Bellott, M.; Dunbrack, R. L.; Evanseck, J. D.; Field, M. J.; Fischer, S.; Gao, J.; Guo, H.; Ha, S.; Joseph-McCarthy, D.; Kuchnir, L.; Kuczera, K.; Lau, F. T. K.; Mattos, C.; Michnick, S.; Ngo, T.; Nguyen, D. T.; Prodhom, B.; Reiher, W. E.; Roux, B.; Schlenkrich, M.; Smith, J. C.; Stote, R.; Straub, J.; Watanabe, M.; Wiórkiewicz-Kuczera, J.; Yin, D.; Karplus, M., All-Atom Empirical Potential for Molecular Modeling and Dynamics Studies of Proteins. *J. Phys. Chem. B.* **1998,** *102*, 3586-3616.

108. Mackerell, A. D.; Feig, M.; Brooks, C. L., Extending the treatment of backbone energetics in protein force fields: Limitations of gas-phase quantum mechanics in reproducing protein conformational distributions in molecular dynamics simulations. *J. Comput. Chem.* **2004,** *25*, 1400-1415.

109. Jorgensen, W. L.; Chandrasekhar, J.; Madura, J. D.; Impey, R. W.; Klein, M. L., Comparison of simple potential functions for simulating liquid water. *J. Chem. Phys.* **1983,** *79*, 926-935.

110. Darden, T.; York, D.; Pedersen, L., Particle mesh Ewald: An N·log(N) method for Ewald sums in large systems. *J. Chem. Phys.* **1993,** *98*, 10089-10092.

111. Martyna, G. J.; Tobias, D. J.; Klein, M. L., Constant pressure molecular dynamics algorithms. *J. Chem. Phys.* **1994,** *101*, 4177-4189.

112. Fiorin, G.; Klein, M. L.; Hénin, J., Using collective variables to drive molecular dynamics simulations. *Mol. Phys.* **2013,** *111*, 3345-3362.

113. Bartels, C., Analyzing biased Monte Carlo and molecular dynamics simulations. *Chem. Phys. Lett.* **2000,** *331*, 446-454.

114. Scholtz, J. M.; Qian, H.; York, E. J.; Stewart, J. M.; Baldwin, R. L., Parameters of helix–coil transition theory for alanine-based peptides of varying chain lengths in water. *Biopolymers.* **1991,** *31*, 1463-1470.

115. Evans, D. L.; Taylor, S. L.; Leary, J. H., 3rd; Bishop, G. R.; Eldar, A.; Jaso-Friedmann, L., In vivo activation of tilapia nonspecific cytotoxic cells by Streptococcus iniae and amplification with apoptosis regulatory factor(s). *Fish Shellfish Immunol.* **2000,** *10*, 419-34.

116. Minor, W.; Cymborowski, M.; Otwinowski, Z.; Chruszcz, M., HKL-3000: the integration of data reduction and structure solution–from diffraction images to an initial model in minutes. *Acta Crystallogr. D.* **2006,** *62*, 859-866.

117. Adams, P. D.; Afonine, P. V.; Bunkóczi, G.; Chen, V. B.; Davis, I. W.; Echols, N.; Headd, J. J.; Hung, L.-W.; Kapral, G. J.; Grosse-Kunstleve, R. W., PHENIX: a comprehensive Python-based system for macromolecular structure solution. *Acta Crystallogr. D.* **2010,** *66*, 213-221.

118. Emsley, P.; Lohkamp, B.; Scott, W. G.; Cowtan, K., Features and development of Coot. *Acta Crystallogr. D.* **2010,** *66*, 486-501.

119. Savkur, R. S.; Burris, T. P., The coactivator LXXLL nuclear receptor recognition motif. *J. Peptide Res.* **2004,** *63*, 207-212.

120. Nagakubo, T.; Demizu, Y.; Kanda, Y.; Misawa, T.; Shoda, T.; Okuhira, K.; Sekino, Y.; Naito, M.; Kurihara, M., Development of Cell-Penetrating R7 Fragment-Conjugated Helical Peptides as Inhibitors of Estrogen Receptor-Mediated Transcription. *Bioconjugate Chem.* **2014,** *25*, 1921-1924.

121. Jiang, Y.; Hu, K.; Shi, X.; Tang, Q.; Wang, Z.; Ye, X.; Li, Z., Switching substitution groups on the in-tether chiral centre influences backbone peptides' permeability and target binding affinity. *Org. Biomol. Chem.* **2017,** *15*, 541-544.

122. Ziegler, A., Thermodynamic studies and binding mechanisms of cell-penetrating peptides with lipids and glycosaminoglycans. *Advan. Drug Deliv. Rev.* **2008,** *60*, 580-597.

123. Boulikas, T., Putative nuclear localization signals (NLS) in protein transcription factors. *J. Cell. Biochem.* **1994,** *55*, 32-58.

124. Tang, H.; Yin, L.; Kim, K. H.; Cheng, J., Helical Poly(arginine) Mimics with Superior Cell-Penetrating and Molecular Transporting Properties. *Chem. Sci.* **2013,** *4*, 3839-3844.

125. Bechinger, B., Structure and Functions of Channel-Forming Peptides: Magainins, Cecropins, Melittin and Alamethicin. *J. Membrane Biol.* **1997,** *156*, 197-211.

126. Herce, H. D.; Garcia, A. E.; Litt, J.; Kane, R. S.; Martin, P.; Enrique, N.; Rebolledo, A.; Milesi, V., Arginine-Rich Peptides Destabilize the Plasma Membrane, Consistent with a Pore Formation Translocation Mechanism of Cell-Penetrating Peptides. *Biophys. J.* **2009,** *97*, 1917-1925.

127. Li, Y.-C.; Rodewald, Luo W.; Hoppmann, C.; Wong, Ee T.; Lebreton, S.; Safar, P.; Patek, M.; Wang, L.; Wertman, Kenneth F.; Wahl, Geoffrey M., A Versatile Platform to Analyze Low-Affinity and Transient Protein-Protein Interactions in Living Cells in Real Time. *Cell Rep. 9*, 1946-1958.

128. Wu, R.-C.; Qin, J.; Hashimoto, Y.; Wong, J.; Xu, J.; Tsai, S. Y.; Tsai, M.-J.; O'Malley, B. W., Regulation of SRC-3 (pCIP/ACTR/AIB-1/RAC-3/TRAM-1) coactivator activity by IκB kinase. *Mol. Cell. Biol.* **2002,** *22*, 3549-3561.

129. Weiser, P. T.; Chang, C.-Y.; McDonnell, D. P.; Hanson, R. N., 4, 4′-Unsymmetrically substituted 3, 3′-biphenyl alpha helical proteomimetics as potential coactivator binding inhibitors. *Bioorg. Med. Chem.* **2014,** *22*, 917-926.

130. Gunther, J. R.; Moore, T. W.; Collins, M. L.; Katzenellenbogen, J. A., Amphipathic benzenes are designed inhibitors of the estrogen receptor α/steroid receptor coactivator interaction. *ACS Chem. Biol.* **2008,** *3*, 282-286.

131. Choi, Y. B.; Ko, J. K.; Shin, J., The transcriptional corepressor, PELP1, recruits HDAC2 and masks histones using two separate domains. *J. Biol. Chem.* **2004,** *279*, 50930-50941.

132. Wei, L.-N.; Hu, X.; Chandra, D.; Seto, E.; Farooqui, M., Receptor-interacting protein 140 directly recruits histone deacetylases for gene silencing. *J. Biol. Chem.* **2000,** *275*, 40782-40787.

133. Min, G.; Kim, H.; Bae, Y.; Petz, L.; Kemper, J. K., Inhibitory cross-talk between estrogen receptor (ER) and constitutively activated androstane receptor (CAR) CAR inhibits ER-mediated signaling pathway by squelching p160 coactivators. *J. Biol. Chem.* **2002,** *277*, 34626-34633.

134. Guertin, M. J.; Zhang, X.; Coonrod, S. A.; Hager, G. L., Transient Estrogen Receptor Binding and p300 Redistribution Support a Squelching Mechanism for Estradiol-Repressed Genes. *Mol. Endocrinol.* **2014,** *28*, 1522-1533.

135. Towns, J.; Cockerill, T.; Dahan, M.; Foster, I.; Gaither, K.; Grimshaw, A.; Hazlewood, V.; Lathrop, S.; Lifka, D.; Peterson, G. D., XSEDE: accelerating scientific discovery. *Comput. Sci. Engineer.* **2014,** *16*, 62-74.

136. Huang, J.; Rauscher, S.; Nawrocki, G.; Ran, T.; Feig, M.; de Groot, B. L.; Grubmüller, H.; MacKerell, A., CHARMM36m: an improved force field for folded and intrinsically disordered proteins. *Nat. Meth.* **2017,** *14*, 71-73.

137. Vanommeslaeghe, K.; Hatcher, E.; Acharya, C.; Kundu, S.; Zhong, S.; Shim, J.; Darian, E.; Guvench, O.; Lopes, P.; Vorobyov, I., CHARMM general force field: A force field for drug-like molecules compatible with the CHARMM all-atom additive biological force fields. *J. Comput. Chem.* **2010,** *31*, 671-690.

138. Feller, S. E.; Zhang, Y.; Pastor, R. W.; Brooks, B. R., Constant pressure molecular dynamics simulation: The Langevin piston method. *J. Chem. Phys.* **1995,** *103*, 4613-4621.

139. Kastrati, I.; Canestrari, E.; Frasor, J., PHLDA1 expression is controlled by an estrogen receptor-NFκB-miR-181 regulatory loop and is essential for formation of ER+ mammospheres. *Oncogene.* **2015,** *34*, 2309-2316.

140. Saldanha, A. J., Java Treeview—extensible visualization of microarray data. *Bioinformatics.* **2004,** *20*, 3246-3248.

141. Spoerke, J. M.; Gendreau, S.; Walter, K.; Qiu, J.; Wilson, T. R.; Savage, H.; Aimi, J.; Derynck, M. K.; Chen, M.; Chan, I. T.; Amler, L. C.; Hampton, G. M.; Johnston, S.; Krop, I.; Schmid, P.; Lackner, M. R., Heterogeneity and clinical significance of ESR1 mutations in ER-positive metastatic breast cancer patients receiving fulvestrant. *Nat. Commun.* **2016,** *7*, 11579.

142. Fribbens, C.; O'Leary, B.; Kilburn, L.; Hrebien, S.; Garcia-Murillas, I.; Beaney, M.; Cristofanilli, M.; Andre, F.; Loi, S.; Loibl, S.; Jiang, J.; Bartlett, C. H.; Koehler, M.; Dowsett, M.; Bliss, J. M.; Johnston, S. R. D.; Turner, N. C., Plasma ESR1 Mutations and the Treatment of Estrogen Receptor–Positive Advanced Breast Cancer. *J. Clin. Oncol.* **2016,** *34*, 2961-2968.

143. Chandarlapaty, S.; Chen, D.; He, W.; et al., Prevalence of esr1 mutations in cell-free dna and outcomes in metastatic breast cancer: A secondary analysis of the bolero-2 clinical trial. *JAMA Oncol.* **2016,** *2*, 1310-1315.

144. Jeselsohn, R.; De Angelis, C.; Brown, M.; Schiff, R., The Evolving Role of the Estrogen Receptor Mutations in Endocrine Therapy-Resistant Breast Cancer. *Curr. Oncol. Rep.* **2017,** *19*, 35.

145. Pan, R.; Hogdal, L. J.; Benito, J. M.; Bucci, D.; Han, L.; Borthakur, G.; Cortes, J.; DeAngelo, D. J.; Debose, L.; Mu, H.; Döhner, H.; Gaidzik, V. I.; Galinsky, I.; Golfman, L. S.; Haferlach, T.; Harutyunyan, K. G.; Hu, J.; Leverson, J. D.; Marcucci, G.; Müschen, M.; Newman, R.; Park, E.; Ruvolo, P. P.; Ruvolo, V.; Ryan, J.; Schindela, S.; Zweidler-McKay, P.; Stone, R. M.; Kantarjian, H.; Andreeff, M.; Konopleva, M.; Letai, A. G., Selective BCL-2 Inhibition by ABT-199 Causes On Target Cell Death in Acute Myeloid Leukemia. *Cancer Discov.* **2014,** *4*, 362-375.

146. Walensky, L. D.; Kung, A. L.; Escher, I.; Malia, T. J.; Barbuto, S.; Wright, R. D.; Wagner, G.; Verdine, G. L.; Korsmeyer, S. J., Activation of Apoptosis in Vivo by a Hydrocarbon-Stapled BH3 Helix. *Science.* **2004,** *305*, 1466-1470.

147. Chen, J.; Sawyer, N.; Regan, L., Protein–protein interactions: General trends in the relationship between binding affinity and interfacial buried surface area. *Prot. Sci.* **2013,** *22*, 510-515.

148. Ibrahim, B. S.; Pattabhi, V., Role of weak interactions in thermal stability of proteins. *Biochem. Biophys. Res. Commun.* **2004,** *325*, 1082-1089.

149. Tian, Y.; Zeng, X.; Li, J.; Jiang, Y.; Zhao, H.; Wang, D.; Huang, X.; Li, Z., Achieving enhanced cell penetration of short conformationally constrained peptides through amphiphilicity tuning. *Chem. Sci.* **2017,** *8*, 7576-7581.

150. Nunnery, J. K.; Mevers, E.; Gerwick, W. H., Biologically active secondary metabolites from marine cyanobacteria. *Curr. Opin. Biotechnol.* **2010,** *21*, 787-793.

151. Solecka, J.; Zajko, J.; Postek, M.; Rajnisz, A., Biologically active secondary metabolites from Actinomycetes. *Cent. Euro. J. Biol.* **2012,** *7*, 373-390.

152. Clark, R. C.; Lee, S. Y.; Searcey, M.; Boger, D. L., The isolation, total synthesis and structure elucidation of chlorofusin, a natural product inhibitor of the p53-MDM2 protein-protein interaction. *Nat. Prod. Rep.* **2009,** *26*, 465-477.

153. Wells, J. A.; McClendon, C. L., Reaching for high-hanging fruit in drug discovery at protein–protein interfaces. *Nature.* **2007,** *450*, 1001.

154. Balamurugan, R.; Dekker, F. J.; Waldmann, H., Design of compound libraries based on natural product scaffolds and protein structure similarity clustering (PSSC). *Mol. BioSystems.* **2005,** *1*, 36-45.

155. Sperl, B.; Seifert, M. H. J.; Berg, T., Natural product inhibitors of protein–protein interactions mediated by Src-family SH2 domains. *Bioorg. Med. Chem. Lett.* **2009,** *19*, 3305-3309.

156. Nikolovska-Coleska, Z.; Xu, L.; Hu, Z.; Tomita, Y.; Li, P.; Roller, P. P.; Wang, R.; Fang, X.; Guo, R.; Zhang, M.; Lippman, M. E.; Yang, D.; Wang, S., Discovery of Embelin as a Cell-Permeable, Small-Molecular Weight Inhibitor of XIAP through Structure-Based Computational Screening of a Traditional Herbal Medicine Three-Dimensional Structure Database. *J. Med. Chem.* **2004,** *47*, 2430-2440.

157. Bockus, A. T.; Lexa, K. W.; Pye, C. R.; Kalgutkar, A. S.; Gardner, J. W.; Hund, K. C. R.; Hewitt, W. M.; Schwochert, J. A.; Glassey, E.; Price, D. A.; Mathiowetz, A. M.; Liras, S.; Jacobson, M. P.; Lokey, R. S., Probing the Physicochemical Boundaries of Cell Permeability and Oral Bioavailability in Lipophilic Macrocycles Inspired by Natural Products. *J. Med. Chem.* **2015,** *58*, 4581-4589.

158. Yudin, A. K., Macrocycles: lessons from the distant past, recent developments, and future directions. *Chem. Sci.* **2015,** *6*, 30-49.

159. Rush, M. D.; Walker, E. M.; Prehna, G.; Burton, T.; van Breemen, R. B., Development of a magnetic microbead affinity selection screen (MagMASS) using mass spectrometry for ligands to the retinoid X receptor-α. *J. Am. Soc. Mass Spectrom.* **2017,** *28*, 479-485.

160. Davies, C.; Pan, H.; Godwin, J.; Gray, R.; Arriagada, R.; Raina, V.; Abraham, M.; Alencar, V. H. M.; Badran, A.; Bonfill, X.; Bradbury, J.; Clarke, M.; Collins, R.; Davis, S. R.; Delmestri, A.; Forbes, J. F.; Haddad, P.; Hou, M.-F.; Inbar, M.; Khaled, H.; Kielanowska, J.; Kwan, W.-H.; Mathew, B. S.; Mittra, I.; Müller, B.; Nicolucci, A.; Peralta, O.; Pernas, F.; Petruzelka, L.; Pienkowski, T.; Radhika, R.; Rajan, B.; Rubach, M. T.; Tort, S.; Urrútia, G.; Valentini, M.; Wang, Y.; Peto, R., Long-term effects of continuing adjuvant tamoxifen to 10 years versus stopping at 5 years after diagnosis of oestrogen receptor-positive breast cancer: ATLAS, a randomised trial. *Lancet.* **2013,** *381*, 805-816.

161. Xu, J.; Wu, R.-C.; O'Malley, B. W., Normal and cancer-related functions of the p160 steroid receptor co-activator (SRC) family. *Nat. Rev. Cancer.* **2009,** *9*, 615-630.

APPENDIX A

APPENDICES

Copyright permission for Chapter 2

This Agreement between Mr. Thomas Speltz ("You") and John Wiley and Sons ("John Wiley and Sons") consists of your license details and the terms and conditions provided by John Wiley and Sons and Copyright Clearance Center.

License Number	4284860114129
License date	Feb 09, 2018
Licensed Content Publisher	John Wiley and Sons
Licensed Content Publication	Angewandte Chemie International Edition
Licensed Content Title	Stapled Peptides with γ-Methylated Hydrocarbon Chains for the Estrogen Receptor/Coactivator Interaction
Licensed Content Author	Thomas E. Speltz,Sean W. Fanning,Christopher G. Mayne,Colin Fowler,Emad Tajkhorshid,Geoffrey L. Greene,Terry W. Moore
Licensed Content Date	Mar 1, 2016
Licensed Content Pages	4
Type of use	Dissertation/Thesis
Requestor type	Author of this Wiley article
Format	Print and electronic
Portion	Full article
Will you be translating?	No
Title of your thesis / dissertation	Functionalized Hydrocarbon Stapled Peptides for Inhibiting Estrogen Receptor/Steroid Receptor Coactivator Interaction
Expected completion date	Apr 2018
Expected size (number of pages)	200
Requestor Location	Mr. Thomas Speltz Department of Medicinal Chemistry 833 S wood Street 539 PHARM MC 781 MIDWEST, IL 60612 United States Attn: Mr. Thom as Speltz
Publisher Tax ID	EU826007151
Total	0.00 USD

APPENDIX A (CONTINUED)

Copyright permission chapter 4

RightsLink®

Home | Create Account | Help

Title:	A Cell-Permeable Stapled Peptide Inhibitor of the Estrogen Receptor/Coactivator Interaction
Author:	Thomas E. Speltz, Jeanne M. Danes, Joshua D. Stender, et al
Publication:	ACS Chemical Biology
Publisher:	American Chemical Society
Date:	Mar 1, 2018

LOGIN

If you're a copyright.com user, you can login to RightsLink using your copyright.com credentials.

Already **a RightsLink user** or want to learn more?

PERMISSION/LICENSE IS GRANTED FOR YOUR ORDER AT NO CHARGE

This type of permission/license, instead of the standard Terms & Conditions, is sent to you because no fee is being charged for your order. Please note the following:

- Permission is granted for your request in both print and electronic formats, and translations.
- If figures and/or tables were requested, they may be adapted or used in part.
- Please print this page for your records and send a copy of it to your publisher/graduate school.
- Appropriate credit for the requested material should be given as follows: "Reprinted (adapted) with permission from (COMPLETE REFERENCE CITATION). Copyright (YEAR) American Chemical Society." Insert appropriate information in place of the capitalized words.
- One-time permission is granted only for the use specified in your request. No additional uses are granted (such as derivative works or other editions). For any other uses, please submit a new request.

BACK | CLOSE WINDOW

VITAE

NAME: Thomas Edward Speltz

EDUCATION:

B.S., Chemistry, DePaul University, Chicago, IL 2010

M.S., Biochemistry, DePaul University, Chicago, IL 2011

Ph.D., Medicinal chemistry, University of Illinois at Chicago, Chicago, IL 2018

HONORS AND AWARDS:

Chemical Computing Group Research Excellence Award 2017

W.E. van Doren Scholarship, University of Illinois at Chicago, 2017

Horizon Pharma Award for Excellence in Research, Scientific Poster Session Award Winner - Chemistry Category, University of Illinois at Chicago, 2016

W.E. van Doren Scholarship, University of Illinois at Chicago, 2016

NIH NCCAM T32 Predoctoral Research Fellow, Department of Medicinal Chemistry and Pharmacognosy, University of Illinois at Chicago, 2015

Walmart Scholar, American Association of Colleges of Pharmacy, 2015

W.E. van Doren Scholarship, University of Illinois at Chicago, 2015

M.S. in Biochemistry with distinction, 2011

Outstanding Graduate Teaching Assistant Award, DePaul University, 2010

Centennial Scholarship, DePaul University, 2006-2010

TRAININGS AND WORKSHOPS:

NCCIH Fellows and Trainees: Building a Successful Research Career Path, NIH, Bethesda, MD, October 16-17, 2017

Computational Biophysics Workshop, University of Illinois Urbana-Champaign, Urbana, IL, October 17-21, 2016

CBC Proteomics & Informatics Workshop, University of Illinois at Chicago, Chicago, IL, August 11-14, 2014

PROFESSIONAL MEMBERSHIP:

American Chemical Society, Division of Medicinal Chemistry

TEACHING EXPERIENCE: Adjunct Faculty, DePaul University, 2011-2015

INVITED PRESENTATIONS:

γ-Functionalized hydrocarbon stapled peptides for inhibiting mutant estrogen receptor/coactivator interaction. **Oral Presentation**. 55th Annual MIKI Meeting. April 9, 2017. University of Minnesota, Minneapolis, MN.

γ-Functionalized hydrocarbon stapled peptides for inhibiting mutant estrogen receptor/coactivator interaction. **Oral Presentation**. 253rd American Chemical Society National Meeting and Exposition. April 4, 2017. San Francisco, CA.

CONFERENCE PRESENTATIONS:

Functionalized Hydrocarbon Stapled Peptides for the Estrogen Receptor/Coactivator Interaction. 8th Chicago Organic Symposium. September 30, 2017. Chicago, IL.

Branching Out: γ-Methylated Hydrocarbon Stapled Peptides for the Estrogen Receptor/Coactivator Interaction. Chicago Organic Chemistry Symposium. October 1, 2016. Chicago, IL.

Branching Out: γ-Methylated Hydrocarbon Stapled Peptides for the Estrogen Receptor/Coactivator Interaction. 35th National Medicinal Chemistry Symposium. June 26-29, 2016. Chicago, IL.

Branching Out: γ-Methylated Hydrocarbon Stapled Peptides for the Estrogen Receptor/Coactivator Interaction. The 8th Yao Yuan Biotech-Pharma Symposium. April 23, 2016. Chicago, IL.

Branching Out: γ-Methylated Hydrocarbon Stapled Peptides for the Estrogen Receptor/Coactivator Interaction. University of Iowa MIKI meeting. April 9, 2016. Iowa City, IA.

“Tucked” Stapled peptide inhibitors of the estrogen receptor/coactivator interaction. Speltz, T. and Moore, T. W. University of Illinois at Chicago Department of Medicinal chemistry and Pharmacognosy, Research Day. February 26, 2016. Chicago, IL.

Engineering Natural Functional Groups from Leucine and Isoleucine into "Stapling" Amino Acids. Oral presentation at Drug Discovery Chemistry, San Diego, CA, April 23, 2015.

Engineering Natural Functional Groups from Leucine and Isoleucine into "Stapling" Amino Acids. Speltz, T. and Moore, T. W. Drug Discovery Chemistry. San Diego, CA, April 24, 2015.

“Tucked” Stapled peptide inhibitors of the estrogen receptor/coactivator interaction. Speltz, T. and Moore, T. W. University of Kansas, MIKI Meeting. March 7, 2014. Chicago, IL.

"Tucked" Stapled peptide inhibitors of the estrogen receptor/coactivator interaction. Speltz, T. and Moore, T. W. University of Illinois at Chicago Department of Medicinal chemistry and Pharmacognosy, Research Day. March 10, 2014. Chicago, IL.

Non-Natural Natural Products. Speltz, T. and Krzeszowiec, M. DePaul University Natural Sciences, Mathematics & Technology Showcase. November 5, 2010. Chicago, IL.

Amyloid β 1-16 Peptide Interaction with Copper Ions. Speltz, T. and Zbyszynski, P. Chicago Area Undergraduate Research Symposium. April 18, 2009. Chicago, IL.

PUBLICATIONS:

Speltz, T. E.; Danes, J. M.; Stender, J. D.; Frasor, J. M.; Moore, T. W. "A Cell-permeable Stapled Peptide Inhibitor of the Estrogen Receptor/Coactivator Interaction." *ACS Chemical Biology*. **2018**, 13 (3), 676-684.

Speltz, T. E.; Fanning, S. W.; Mayne, C. G.; Fowler, C.; Tajkhorshid, E.; Greene, G. L.; Moore, T. W. "Stapled Peptides with γ-Methylated Hydrocarbon Chains for the Estrogen Receptor/Coactivator Interaction." *Angewandte Chemie International Edition.* **2016**, *55*, 4104.

Richardson, B. G.; Jain, A.D.; **Speltz, T.E**.; Moore, T.W. "Non-electrophilic modulators of the canonical Keap1/Nrf2 pathway." *Bioorganic and Medicinal Chemistry Let*ters, **2015**, 25, 2261-2268.

Ralko, A. A.; **Speltz T. E**.; Burke, J. L.; Murphey, C. M.; Gaskell, Z.; Girel, J. K.; Terranova, E.; Richtscheidt, C.; Krzeszowiec, M.; Maresh J.J. "Chemoselective Zinc/HCl Reduction of Halogenated β-Nitrostyrenes: Synthesis of Halogenated Dopaine Analogues." *Synlett*, **2014**, 25, 2891-2894.

Dintzner, M. R.; Maresh, J. J.; Kinzie, C. R.; Arena, A. F.; **Speltz, T**. "A Research-Based Undergraduate Organic Laboratory Project: Investigation of a One-Pot, Multicomponent, Environmentally Friendly Prins-Friedel-Crafts-Type Reaction." *Journal of Chemical Educ*ation, **2012,** *89*, 265–267.